ISSN 1831-9424

European Commission

JRC TECHNICAL REPORT

A European assessment of freshwater availability and nutrient pollution

Historical analysis and scenarios developed in the project Blue2.2

Grizzetti, B., Vigiak, O., Udias, A., Bisselink, B., Pistocchi, A., Bouraoui, F., Malagó, A., Aloe, A., Zanni, M., Weiss, F., Hristov, J., Wilson, J., Pisoni, E., de Meij, A., De Roo, A., Macias, M., Stips, A.

2022

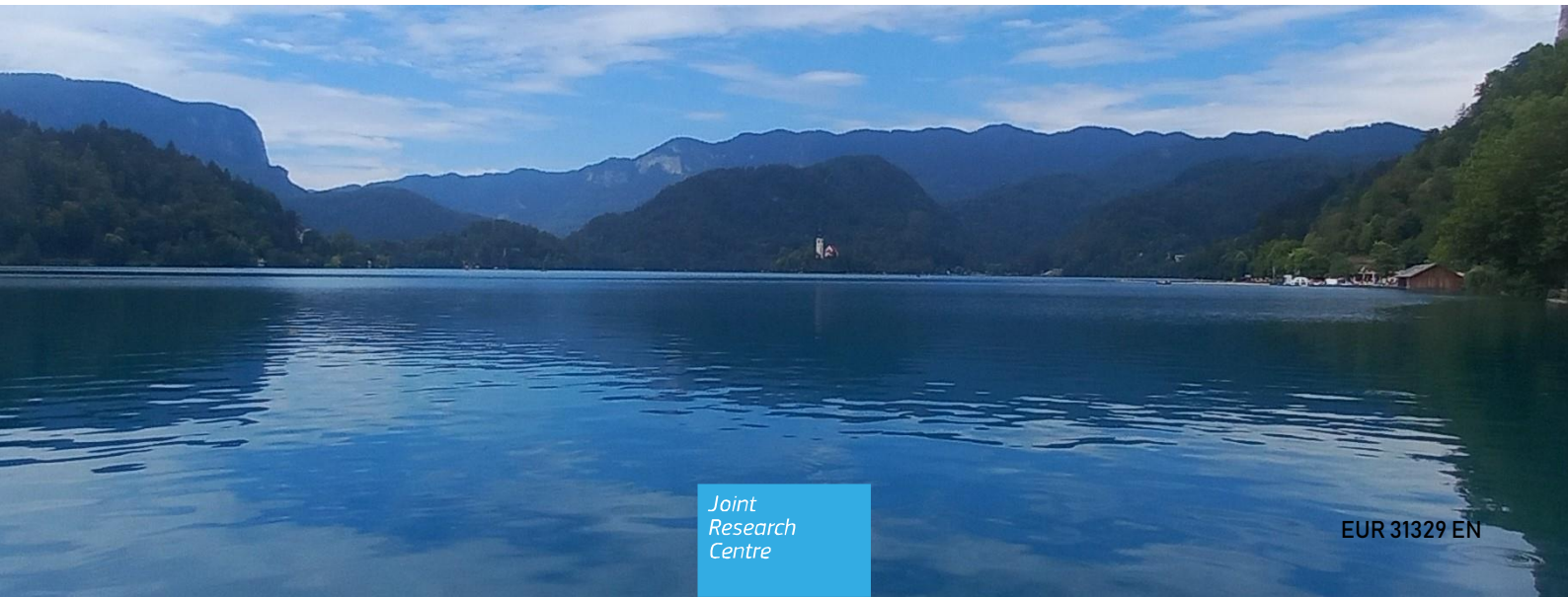

Joint Research Centre

EUR 31329 EN

EU Science Hub
https://joint-research-centre.ec.europa.eu

JRC130025

EUR 31329 EN

PDF ISBN 978-92-76-60057-2 ISSN 1831-9424 doi:10.2760/924432 KJ-NA-31-329-EN-N

Luxembourg: Publications Office of the European Union, 2022

How to cite this report: Grizzetti, B., Vigiak, O., Udias, A., Bisselink, B., Pistocchi, A., Bouraoui, F., Malagó, A., Aloe, A., Zanni, M., Weiss, F., Hristov, J., Wilson, J., Pisoni, E., de Meij, A., Macias, M., Stips, A., *A European assessment of freshwater availability and nutrient pollution - Historical analysis and scenarios developed in the project Blue2.2*, Publications Office of the European Union, Luxembourg, 2022, doi:10.2760/924432, JRC130025.

Contents

Abstract

This report presents an assessment of European freshwater availability and nutrient pollution, including a historical analysis and future scenarios of measures.

The JRC models are evaluated with historical data on water quantity and quality (1990-2018). Two scenarios under future climate (2020-2030) consider the Business As Usual (BAU) and a High Ambition Scenario (HAS) of measures implementation.

The scenario analysis shows that investments planned in BAU are insufficient to compensate for the projected reduction in water availability. The additional measures in HAS might alleviate water scarcity in the Mediterranean countries, but only when desalination is considered. Depending on how fast the global temperature will rise, there might still be time to invest in water saving measures to keep up with the decreasing water availability caused by global warming.

With regard to water quality, measures tackling different sectors and sources (domestic wastewater, air emissions, agriculture) are necessary to reduce nutrient loads in fresh and coastal waters significantly. HAS measures could lower riverine load to European seas by around 30% for nitrogen (N) and 15% for phosphorus (P) compared to BAU. However, the N:P ratio in the receiving waters will change, with impact on their aquatic ecosystems.

Measures need to be targeted to the receiving freshwater and marine environment. The ambitious measures imply drastic changes in several sectors. While the ambitious scenario is realistic, implementing it requires a high political will.

Authors

Grizzetti, B., Vigiak, O., Udias, A., Bisselink, B., Pistocchi, A., Bouraoui, F., Malagó, A., Aloe, A., Zanni, M., Weiss, F., Hristov, J., Wilson, J., Pisoni, E., de Meij, A., De Roo, A., Macias, M., Stips, A.

Executive summary

Policy context

This report presents an assessment of European freshwater availability and nutrient pollution, including and historical analysis and future scenarios of measures to reduce water scarcity and nutrient pollution.

The study was developed in the context of the project Blue2.2 (April 2020 – March 2023), which aims to support the Marine Strategy Framework Directive (MSFD) and other water related EU strategies, by further developing and applying the JRC freshwater and marine modelling framework. The overall objective of freshwater modelling was to assess the impacts of scenarios of measures and climate change on the freshwater environment at pan European scale. (This report presents the work developed in the project Blue2.2 under the Task 2 - Freshwater Modelling, and specifically the Deliverable 2.1, 2.2 and 2.3).

Key conclusions

The ambitious measures imply drastic changes in several sectors, including agriculture with major social and economic impacts on farmers. Even though the ambitious scenario is realistic, implementing it requires a high political will.

Modelling assessments have uncertainties and remain theoretical. Concerning modelling nutrient pollution in waters, a main source of uncertainty is the capacity to take into account the legacy of nitrogen and phosphorus in soils and groundwater, and to estimate the delay in time between the application of measures and the detection of improvements in water quality.

Main findings

Main findings of the freshwater scenario analysis (Section 6) indicate that although the water savings measures have a positive effect on the water resources, planned investments in the BAU scenario are not sufficient to compensate for the projected reduction in water availability. The potential measures in the HAS scenario might improve water scarcity in already water scarce countries around the Mediterranean, but that might only happen when desalination is considered, which is however not much implemented yet. Depending on how fast the global temperature will rise, there might still be time to increase current level of investments or implement one or more additional cycles of investments of increasing irrigation efficiency and other effective water efficiency measures to keep up with the decreasing water availability caused by global warming.

With regard to water quality, the scenario analysis showed that measures tackling different sectors and sources (domestic wastewater, air emissions, agriculture) are necessary to achieve significant reduction in nutrient loads in freshwater and coastal waters. The impact of the measures is specific to the region, its climatic and hydrological characteristics and anthropogenic inputs. Ambitious measures (HAS scenario) could lower the annual riverine load to European seas by around 30% for nitrogen (N) and 15% for phosphorus (P) compared to the measures in the business as usual scenario (BAU). However, it will change the N:P ratio in the aquatic ecosystems, with impact on the biodiversity and condition of the aquatic ecosystem, thus measures need to be targeted to the receiving freshwater and marine environment.

Related and future JRC work

The water flow and nutrient delivery to the European seas simulated by the freshwater modelling for the historical period (1990-2018) and the scenarios of measures under a future climate (2020-2030) described in Section 3, 4 and 5 have been used in the project Blue2.2 as inputs in the marine modelling scenario analysis (Macias et al. 2022). The scenarios modelling described in this report and in Macias et al. (2022) provide the details of the analysis presented in the Zero pollution outlook 2022 (Joint Research Centre 2022).

Quick guide

Section 2 of the report describes the freshwater quantity and quality (nutrients) models developed and implemented by the JRC, complementing the marine models in the freshwater-marine modelling framework, including models parametrisation, calibration and validation, as well as references to

scientific publications. Section 3 and Section 4 illustrate the historical data on water quantity and quality (1990-2018) estimated in the modelling and the construction of the scenarios of measures, respectively. Section 5 shows the results of the scenarios analysis, considering the specific effect of water quantity and quality measures, and coupled scenarios under future climate, with a specific focus on the difference between the Business As Usual (BAU) and an High Ambition Scenario (HAS) of measures implementation.

1 Introduction

Freshwater availability and nutrient pollution are a concern in many EU countries. At present, 11% of the population of the 27 states of the European Union plus the United Kingdom lives in water scarce regions (Bisselink et al., 2020), which means that the demand for freshwater cannot be completely satisfied at least during part of the year. At the same time, nutrient pollution is among the major pressures affecting European freshwater (Grizzetti et al. 2017). Since the '90s, several EU policies have been adopted to reduce nutrient pollution in European waters (Vigiak et al. 2023), with the Water Framework Directive (2000/60/EC) and the Marine Strategy Framework Directive (2008/56/EC) providing the legal framework for protecting and enhancing water resources and aquatic ecosystems.

The aim of the Blue2.2 project (Administrative Arrangement N °110661-070201/2019/818363/AA/ ENV.C.2 between DG ENV and JRC, April 2020 – March 2023) is to support the Marine Strategy Framework Directive (MSFD) and other water related EU strategies, by further developing and applying the JRC freshwater and marine modelling framework.

This report presents the work developed in the project under the Task 2 - Freshwater Modelling, and specifically the Deliverable 2.1, 2.2 and 2.3. The overall objective of freshwater modelling was to assess the impacts of scenarios of measures and climate change on the freshwater environment at a pan European scale, implementing water quantity and quality models (multi-decade simulations), coordinating to the extent possible these activities with work for other relevant European directives, such as the Water Framework Directive (WFD), Urban Waste Water Treatment Directive (UWWTD) and Nitrates Directive (ND).

After this Introduction, Section 2 (Deliverable 2.1) describes the freshwater quantity and quality (nutrients) models developed and implemented by the JRC, complementing the marine models in the freshwater-marine modelling framework, including models parametrisation, calibration and validation, as well as references to scientific publications. Section 3 and Section 4 (Deliverable 2.2) illustrate the historical data on water quantity and quality (1990-2018) estimated in the modelling and the construction of the scenarios of measures, respectively. Section 5 (Deliverable 2.3) shows the results of the scenarios analysis, considering the specific effect of water quantity and quality measures, and coupled scenarios under future climate, with a specific focus on the difference between the Business As Usual (BAU) and an High Ambition Scenario (HAS) of measures implementation. Finally, Section 6 concludes on the main findings of the freshwater scenario analysis.

The water flow and nutrient delivery to the European seas simulated by the freshwater modelling for the historical period (1990-2018) and the scenarios of measures under a future climate (2020-2030) described in Section 3, 4 and 5 have been used as inputs in the marine modelling scenario analysis (Macias et al. 2022).

2 Modelling approach

This Section (Deliverable 2.1) describes the modelling tools developed by the JRC for the analysis of freshwater quantity and quality (nutrients). The model LISFLOOD (Section 2.1) was used for the analysis of measures tackling water scarcity. The model GREEN (Section 2.2) was applied to assess the effects of measures addressing nutrient pollution in water. The model SWAT (Section 2.3) allows to represent both water flow and nutrient pollution. Different models are developed by the JRC to offer flexible tools for the analysis, as each model has its capabilities and limitations, and in view of an ensemble modelling approach. The water and nutrient discharge to European seas estimated by the LISFLOOD and GREEN models for the historical period (1990-2018) and under different scenarios of measures have been used as input in the modelling of the European seas (Macias et al. 2022).

2.1 Water quantity (LISFLOOD-EPIC model)

2.1.1 The LISFLOOD-EPIC model

The water resources calculations are done with the distributed water resources model LISFLOOD (De Roo et al., 2000; Van der Knijff et al., 2010; Burek et al., 2013; Bisselink et al., 2018a) coupled with crop growth processes from the EPIC model (Williams et al., 1989; Williams, 1995; Sharpley and Williams, 1990) and a newly developed irrigation module. Driven by meteorological forcing data, the integrated LISFLOOD-EPIC model simulates dynamically hydrology, crop growth and irrigation, accounting for water abstractions for household, livestock, industry and energy sectors at a daily time step and every grid-cell defined in the model domain (5x5 km for Europe).

Processes simulated for each grid cell include snowmelt, soil freezing, surface runoff, infiltration into the soil, preferential flow, redistribution of soil moisture within the three-layer soil profile, drainage of water to the groundwater system, groundwater storage, and groundwater base flow. Runoff produced for every grid cell is routed through the river network, using a double kinematic wave approach, one for the main channel, and one for the floodplain. Lakes, reservoirs and retention areas or polders are simulated by giving their location, size and in- and outflow boundary conditions and steering parameters. Discharges are calibrated and validated on a regular basis from approximately 1500 gauging stations.

Although LISFLOOD is a regular grid-based model with a constant spatial grid more detailed sub-grid land use classes are used to simulate the main hydrological processes. The model distinguishes for each grid the fraction open water, urban sealed area, forest area, paddy rice irrigated area, crop irrigation area and other land uses. Specific hydrological processes (evapotranspiration, infiltration etc.) are then calculated in a different way for these land use classes. Moreover, sub-gridded elevation information is used to establish detailed altitude zones, which are important for snow accumulation and melting processes, and to correct for surface temperature.

Static maps used by the model are related to topography (i.e., digital elevation model, local drain direction, slope gradient, elevation range), land use (i.e., land use classes, forest fraction, fraction of urban area), soil (i.e., soil texture classes, soil depth), and channel geometry (i.e., channel gradient, Manning's roughness, bank-full channel depth, channel length, bottom width and side slope). Soil texture and depth data were derived from the ISRIC 1km SoilGrids database (Hengl et al., 2014). Elevation data was derived from the Hydrosheds database – using SRTM elevation data - (Lehner et al., 2008, http://www.worldwildlife.org/pages/hydrosheds). The river network was taken from the work by Wu et al. (2012).

LISFLOOD produces a number of outputs, such as daily river discharge, soil moisture conditions, groundwater amounts and water in lakes and reservoirs. In addition, a number of water resources indicators are produced, such as flood and low flow extremes, water scarcity days, Environmental flow (Eflow) breachings, water availability per capita, and the water exploitation index.

The Water Exploitation Index Plus (WEI+) indicator is used to estimate the intensity, duration and the socio-economics impacts of water scarcity. We use here the same method of calculating the WEI+ as the European Environmental Agency (EEA) (ETC/ICM, 2016).

The WEI+ can be calculated for the consumption of water and is defined as the ratio of the total water net consumption divided by the available freshwater resources in a region including upstream inflowing water. The total water net consumption is the difference between the water abstraction and the return

flow. Water abstractions in LISFLOOD-EPIC consists of five components, from which the irrigation water demand is estimated dynamically and crop specific with the coupled EPIC module. The other four sectorial components are used as requirement data. These are (manufacturing) industrial water demand, water demand for energy and cooling, livestock water demand and domestic water demand. The model abstracts the water that is demanded from either surface or groundwater sources. These may include lakes, reservoirs, rivers and groundwater aquifers, depending on local information available on sources of water. The model takes a local Eflow threshold into account – which may be user defined – below which abstraction of water is stopped and flagged as 'shortage'. The WEI+ includes return flow, resulting from drained irrigation water, (warmed up) cooling water returned to the river, and (treated) wastewater returned to surface waters. Per sector, water consumption factors are used and applied to split water abstraction into net consumption and return flow (Bisselink et al., 2018b).

Water abstractions take place at regional level, and also the WEI+ is therefore calculated at this regional level at a monthly timescale to avoid averaging skewed results. WEI+ values have a range between 0 and 1. For distinguishing water scarcity gradations across Europe, we used the water scarcity values as applied by the EEA: values between 0-0.1 denote "low water scarcity", "moderate water scarcity" if the ratio lies in the range 0.1-0.2, "water scarcity" when this ratio is larger than 0.2, and "severe water scarcity" if the ratio exceeds the 0.4 threshold (Feargemann, 2012).

2.1.2 Weather and climate data

For the meteorological forcing of the LISFLOOD-EPIC model – i.e. the weather data used as input – we have been using three sets of data:

- Observed weather data: 1990-2018 (EMO-5)
- Control climate MPI-ESM-LR downscaled with COSMO-CLM (1981-2005)
- Future climate projection MPI-ESM-LR downscaled with COSMO-CLM with a RCP4.5 emission scenario (2005-2030)

Within the LISFLOOD-EPIC reference run, LISFLOOD-EPIC uses gridded observed meteorological data from 1990-2018, the EMO-5 meteo data set. EMO-5 is a pan-European regular 5 km resolution grid meteorological forcing dataset obtained by interpolating the spatially irregular observations from various sources throughout the continent (Thiemig et al., 2021).

Figure 1. (a) Monthly climatology (1981-2005) of the precipitation ensemble for 11 EURO-CORDEX climate models (blue shaded), the ensemble mean and the future climate projection chosen for this study (MPI-M-MPI-ESM-LR_CLMcom-CCLM4-8-17). Only land pixels are considered, (b) the change in precipitation between MPI-M-MPI-ESM-LR_CLMcom-CCLM4-8-17 and the ensemble mean.

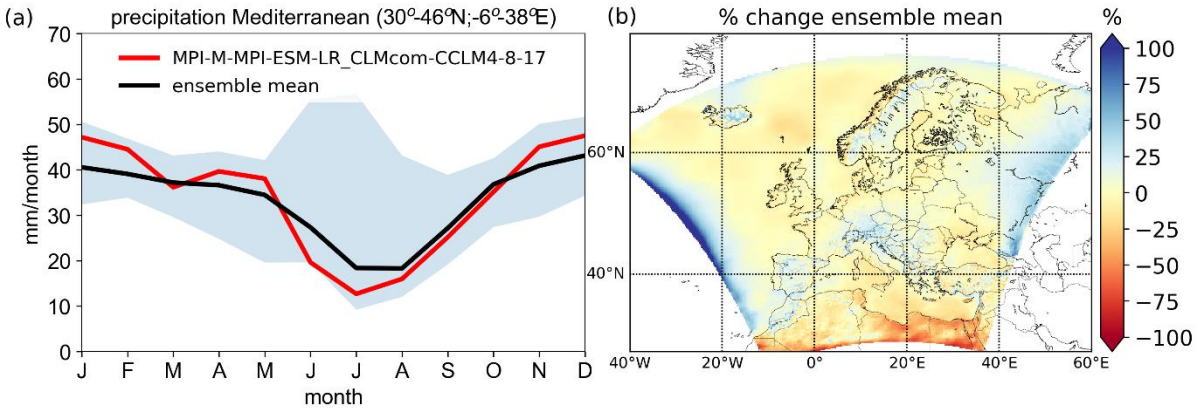

Projections of future climate are available from the EURO-CORDEX initiative (Jacob et al., 2014) and are based on two Representative Concentration Pathways (RCPs): RCP4.5 and RCP8.5. RCP4.5 may be viewed as a moderate-emissions-mitigation-policy scenario and RCP8.5 as a high-end, not plausible, emission scenario. As computational power did not allow to estimate the effects of measures under various climate scenarios, we selected from 11 RCP4.5 climate scenarios the future projection from the

global climate model (GCM), namely: MPI-ESM-LR downscaled with the Regional Climate Model (RCM) COSMO-CLM. In Figure 1 the precipitation (1981-2005) in the Mediterranean of the selected model combination (MPI-M-MPI-ESM-LR_CLMcom-CCLM4-8-17) are presented in relation to the ensemble range and mean of the 11 RCM/GCM model combinations. The projection from MPI-M-MPI-ESM-LR_CLMcom-CCLM4-8-17 is a good representation of the ensemble mean. In the winter months, the amount of precipitation from the MPI-M-MPI-ESM-LR_CLMcom-CCLM4-8-17 is slightly higher and in the summer months slightly lower compared to the ensemble mean (Figure 1a). For Europe, a slight overestimation in average precipitation (1981-2005) is observed for Spain, Balkans, the Alps and Scandinavia (Figure 1b).

2.1.3 Socio-economic and land use projections

We performed the model assessment with static socio-economic conditions in Europe during 1990-2010 with 2010 as the reference year.

The future projections of land use in Europe are derived from the LUISA modelling platform (Jacobs-Crisioni et al., 2017). LUISA translates socio-economic trends and policy scenarios into processes of territorial development. Among other things, LUISA allocates (in space and time) population, economic activities and land use patterns which are constrained by biophysical suitability, policy targets, economic criteria and many other factors. Except from the constraints, LUISA incorporates historical trends, current state and future projections in order to capture the complex interactions between human activities and their determinants. The mechanisms to obtain land-use demands are described in Baranzelli et al. (2014) and Jacobs-Crisioni et al. (2017). Key outputs of the LUISA platform are fine resolution maps (100m) of accessibility, population densities and land-use patterns covering all 27 EU member states including UK, Serbia, Bosnia Herzegovina and Montenegro until 2050. Corine land use maps are used to cover the rest of Europe. Although LISFLOOD normally operates on a substantially coarser resolution, the details of the LUISA output will remain for a large part due to the use of sub-grid fractions in LISFLOOD-EPIC. For a complete description of the LUISA modelling platform and its underlying mechanics we refer to (Batista e Silva et al., 2013; Lavalle et al., 2011).

Water demand in LISFLOOD consists of five components from which the irrigation water demand is estimated dynamically within the model with the EPIC irrigation module. When plant transpiration exceeds a threshold, irrigation is required and is represented by four irrigation methods: drip, sprinkler, and temporary (surface) and permanent (paddy) flooding. It is fully coupled with the hydrologic components through soil moisture, plant water uptake, canopy interception, freshwater availability for irrigation and return flows are taken into account.

The other four sectorial components are based on requirement data. These are (manufacturing) industrial water demand, water demand for energy and cooling, livestock water demand and domestic water demand. Per sector, water consumption factors are used and applied to split water abstraction into net water consumption and return flow (Bisselink at al., 2018b).

In general, water use estimated for these four sectors are derived from mainly country-level data (EUROSTAT, AQUASTAT) with different modelling and downscaling techniques as described in Vandecasteele et al. (2014). Output of the LUISA platform is used for the spatial downscaling of both present and future water use trends to ensure consistency between land use, population and water demand. A brief description of each sectorial component is given below. Livestock water withdrawals are estimated by combining water requirements from literature with livestock density maps for cattle, pigs, poultry, sheep and goats. The methods are described in detail by Mubareka et al. (2013).

For the energy and cooling demand, national water use statistics are downscaled to the locations of large thermal power stations registered in the European Pollutant Release and Transfer Register data base (E-PRTR). Subsequently, the temporal trend of energy water use is simulated based on electricity consumption projections from the POLES model (Prospective Outlook on Long-term Energy Systems).

Industrial water demands are based on country-level figures from national statistics offices for the total water use by manufacturing industries, mining, construction and services. Future industrial water use trends are simulated based on Gross Value Added (GVA) projections for these sub-sectors from the GEM-E3 model to represent industrial activity and an efficiency factor, based on historical trends, to represent improving water efficiency due to technical developments (Bernhard et al. 2018a). Since the GEM-E3

model only provide projections for the EU27+UK, industrial water use projections are assumed constant for countries outside EU27+UK.

Water demands for the household sector are derived from a specific household water usage module (Bernhard et al., 2018b) which simulates water use per capita based on socio-economic, demographic and climate variables. This model was based on data collected at NUTS-3 from 2000-2013 for all EU27 + UK countries on household water use, water price, income, age distribution and number of dry days per year. Subsequently, regression models were fitted to quantify relationships between water use, water price and the other relevant variables for four European clusters of NUTS-3 regions with similar socio-economic and climate conditions. This household water usage module allows us to estimate present and future domestic water use per capita at NUTS3 level using socio-economic, demographic and climate projections. The water use per capita is multiplied with population maps from the LUISA platform from 2010 up to 2050 for every 5 years. For the years in between the 5yr-window a linear growth is assumed. Consumptive use for the domestic sector is assumed at 20% (EEA, 2005) meaning that 80% flows back in the hydrological system as waste water.

Water demands (public water, livestock water, industrial water, cooling water for the energy sector, and irrigation) are abstracted from surface and/or groundwater resources (depending on the region) when available, taking into account the Eflow threshold in rivers, which is a constant (10th percentile of the natural discharge).

2.2 Water quality (GREEN model)

2.2.1 GREEN model

Annual nutrient (total nitrogen TN, and total phosphorus, TP) loads from land to sea were assessed with the conceptual model GREEN (Grizzetti et al., 2012; 2021), as implemented in the R open source package GREENeR (Udias et al. 2022) (Vigiak et al., 2023). Briefly, the model builds on the spatial architecture of the CCM2 hydrological network (Vogt et al. 2007; 2008), which identifies catchments of about 7 km^2 area, each having one main reach with an upstream node and a downstream node to form the network that connects land from headwaters to the seas or internal endorheic lakes. The total land extent considered in the GREEN model application amounts to 6.27M km^2, encompassing all river basins draining in European seas, covering in part or completely 44 countries, namely 27 EU countries and 17 non-EU countries. Figure 2 shows the extent covered by the modelling analysis and attribution to marine regions, defined according to the EU Marine Strategy Framework Directive (MSFD), considered in this study.

The model considers major diffuse nutrient sources to land, which undergo reduction through soil filtering and plant uptake before reaching the stream network, and point sources that are directly emitted to the stream network. Diffuse sources comprise mineral and organic fertilization on agricultural land, and domestic emissions from houses and individual appropriate systems that are disconnected from sewerage systems (termed herein as scattered dwellings), and discharge into the soil. Additional diffuse sources of nitrogen are from soil and plant fixation, and from atmospheric deposition. An additional diffuse source of phosphorus is represented by emissions from non-agricultural land (background emissions). Point sources include industrial and domestic emissions collected in sewerage systems and discharged directly in the stream network or in coastal areas.

The model assesses annual loads of nutrients (t/y) considering the upstream-downstream accumulation of sources, less retention in land of diffuse emissions, and retentions in rivers and lakes. Land retention is an inverse function of total annual precipitation, and thus changes annually. Conversely, river retention is a function of reach length, whereas lake retention is a function of lake depth and hydraulic residence time. Retention in land and rivers is regulated by two parameters that are calibrated against loads estimated at monitoring stations. From nutrient loads, the mean concentration of nutrient in rivers is calculated dividing loads by the mean annual discharge in the reach.

The full description of the model equations can be found in Grizzetti et al. (2021); the code of the model is published as open source in Udias et al. (2022).

Figure 2. Extent of the study area, showing basins draining into European marine regions.

2.2.2 Model inputs (1990-2018)

Modelling nutrient fluxes required foremost assembling data on annual nutrient inputs for the period of interest (1990-2018) and locating them in space. Temporal and spatial data sources are summarized in Table 1, whereas details for nutrient emission sources are described in Annex 1.

With the exception of precipitation and mean annual flow discharge, input time-series did not cover the full simulation period. Values for uncovered years were obtained by interpolation between available years, or extrapolation, generally assuming values equal to the first (extrapolation to the past) or to the last (extrapolation to the future) available reported data. As well, the spatial resolution of original data sources never coincided with CCM2 catchment resolution. Thus, downscaling and zonal statistics were used to derive CCM2 catchment data except for point data, which were attributed at spatial coordinates.

Table 1. Data sources and methods used to build GREEN model inputs in 1990-2018

Input	**Original dataset**	**Granularity of original data**		**Source reference**
		Time	Space	
Land cover classes	CORINE CLC	2000, 2006, 2012, 2018	100m pixels	CLC, 2021
	ESA CCI-LC	1992-2018	300m pixels	ESA, 2017
Mineral, manure fertilization, plant biofixation	CAPRI	1990-2014	NUTS2 for EU-28, NO, AL, BA, RS, XK, MA, MK, TR	Barreiro-Hurle et al., 2021
	FAOSTAT	1990-2018	Country (all other countries)	FAOSTAT, 2018
Nitrogen Atmospheric deposition	EMEP	2000-2018	0.1 degree	Simpson et al., 2012
Domestic emissions (scattered dwelling and point sources)	Population shares per treatment type	1970-2015	Country	EUROSTAT, 2021
	Population density: GHS-POP	1990, 2000, 2015	1 km^2 pixels	Schiavina et al., 2021
	FAO nutrient content in diet	1990-2018	Country	Malagò and Bouraoui, 2021
	P content in detergents	1990-2018	Country	
	UWWTD database	2016	Point coordinates	EEA, 2020
Industrial emissions to water (TN, TP; t/y)	EPRTR V18	2001, 2004, 2007-2017	Point coordinates	EEA, 2021a
	INDv3	2007-2019		EEA, 2021b
Annual precipitation (mm)	EMO-5	1990-2018	5x5 km^2 pixels	Thiemig et al., 2021 ; Gelati et al., 2020; De Roo et al., 2021
Mean annual flow	LISFLOOD			
Monitoring data	WISE Waterbase (EEA)	1990-2016	Point coordinates	EEA, 2019

2.2.3 Calibration of GREEN per marine region

The model GREEN needs two main parameters, alpha_P, which regulate land retention (as a function of annual rainfall), and alpha_L, which regulates river retention (as a function of reach length). A third GREEN parameter, sd_coeff, which regulates nutrient land retention of uncollected domestic emissions, is not sensitive and was kept constant (at 0.66667 for TN and 0.71429 for TP as in Grizzetti et al., 2021).

Model parameters were calibrated against nutrient loads assessed at monitoring stations of the European WISE Waterbase (EEA, 2019). The database reports the mean annual concentration per year, however it does not report associated water discharges. Thus, annual loads were obtained by multiplying the reported mean annual concentration times the mean annual discharge estimated with LISFLOOD model for the CCM2 catchment to which the stations were allocated to. Loads were assumed to be measured at the catchment outlet (exiting node). Not all Waterbase monitoring station data were used: if more than one station fell in the same catchment, only the most downstream station was kept. Also, stations placed on secondary channels or far from the main reach of the catchment were excluded. In total, 36269 data entries for TN and 55757 for TP were used.

To account for differences in climatic conditions and bioregions of Europe, and to obtain best possible estimations of loads to the seas, calibration was conducted per marine region (Table 2). In some cases, adjacent marine regions for which few monitoring station data were available, were merged. Monitored data entries available per year and region are reported in Annex 2 (Tables A2.1 and A2.2). The two parameters alpha_P and alpha_L were sampled with a Latin hypercube scheme within the possible range. For each marine region, 2000 simulations were performed. The best parameter sets were chosen on the basis of model performance measured with several goodness-of-fit indices, visual inspection of modelled versus observed loads, and analysis of parameter sensitivity. Udias et al. (2022) describe the methodological steps more in detail. As an example, Figure 3 shows the scatter plots of modelled versus observed TN loads estimated for ABI region. In Annex 2 calibration results for all marine regions are illustrated.

Table 2. Marine regions used for GREEN calibration. The region acronyms are used throughout the report.

Marine region	Acronym	Land extent (km^2)	CCM2 stream network length (km)
Bay of Biscay and the Iberian Coast	ABI	660,444	230,827
Celtic Seas	ACS	196,484	55,944
Greater North Sea, incl. the Kattegat and the English Channel	ANS	954,476	287,424
Baltic Sea	BAL	1,653,172	473,695
Black sea and sea of Marmara	BLK	1,121,650	388,489
Barents – Norwegian - White Seas combined region	BNM	582,277	181,552
Adriatic Sea	MAD	238,003	127,898
Aegean-Levantine Sea	MAL	354,114	126,942
Ionian Sea and the Central Mediterranean Sea	MIC	90,881	41,533
Western Mediterranean Sea	MWE	427,096	198,758

The final parameter sets for nitrogen (Table 3) and phosphorus (Table 4) largely confirm parameter values from the previous European-scale modelling efforts (Grizzetti et al., 2021). However, the regional approach allowed reaching better performance of GREEN simulations, especially for TP. Most notably, simulations performed consistently through the simulation period (e.g. Figure 3), confirming the robustness of the conceptual model approach for the scope of the analysis. The only marine region where

the model performed poorly was the Barents-Norwegian-White Seas combined region. In this area, nutrient loads could not be simulated properly. It is possible that the rigid climate, and thawing and freezing processes were not captured within the range of parameters defined for the analysis. As well, nutrient sources are poorly defined in this region. In the light of the poor calibration performance, in this region GREEN was ran with the parameters identified for the Baltic Sea. Given the limitations of the model inputs and calibration, and considering that these marine regions are outside the scope of Marine Strategy Framework Directive, loads to the sea from there region are not reported herein further.

Table 3. GREEN nitrogen calibration per marine region: number of available data (#data), model parameters and Nash-Sutcliffe Efficiency (NSE).

Marine region	#data	Alpha_P	Alpha_L	NSE
Bay of Biscay and the Iberian Coast	5228	32.50318	0.00901	0.84
Celtic Seas	1092	44.90737	0.00516	0.57
Greater North Sea, incl. the Kattegat and the English Channel	8146	32.0677	0.00518	0.95
Baltic Sea	10286	34.93044	0.00636	0.81
Black sea and sea of Marmara	3067	33.89308	0.00614	0.93
Barents – Norwegian - White Seas combined region([1])	490	24.56134 ([1])	0.00600 ([1])	0.36
Aegean-Levantine Sea + Ionian Sea and the Central Mediterranean Sea combined region	266	21.50102	0.00962	0.85
Adriatic Sea	3945	29.31004	0.08043	0.95
Western Mediterranean Sea	3749	32.75537	0.00851	0.95

([1]) For the Barents – Norwegian - White Seas combined region (BNM), the model could not be acceptably calibrated. Thus, GREEN simulations for this region were done by applying the parameter set of the Baltic sea (BAL).

Table 4. GREEN phosphorus calibration per marine region: number of available data (#data), model parameters and Nash-Sutcliffe Efficiency (NSE).

Marine region	#data	Alpha_P	Alpha_L	NSE
Bay of Biscay and the Iberian Coast	8937	44.54884	0.007757	0.54
Celtic Seas	1437	70.18887	0.000929	0.66
Greater North Sea, incl. the Kattegat and the English Channel	13674	70.69250	0.001180	0.79
Baltic Sea	10906	55.37878	0.030265	0.85
Black sea and sea of Marmara	7830	61.23140	0.008533	0.81
Barents – Norwegian - White Seas combined region([1])	444	98.5759([1])	0.246808([1])	-0.24
Aegean-Levantine Sea + Ionian Sea and the Central Mediterranean Sea combined region	779	17.55150	0.009100	0.41
Adriatic Sea	4620	67.43650	0.044564	0.75
Western Mediterranean Sea	7493	66.05295	0.098997	0.66

([1]) For the Barents – Norwegian - White Seas combined region (BNM), the model could not be acceptably calibrated. Thus, GREEN simulations for this region were done by applying the parameter set of the Baltic sea (BAL).

Figure 3. Example of GREEN TN calibration results in the Bay of Biscay and Iberian coast (ABI) region. Above: comparison of regional calibration (Local = red dots) versus a European-wide calibration (Global = black dots). Below: year by year comparison of simulated (CatchLoad) versus observed loads (ObsLoad; all loads in t/y).

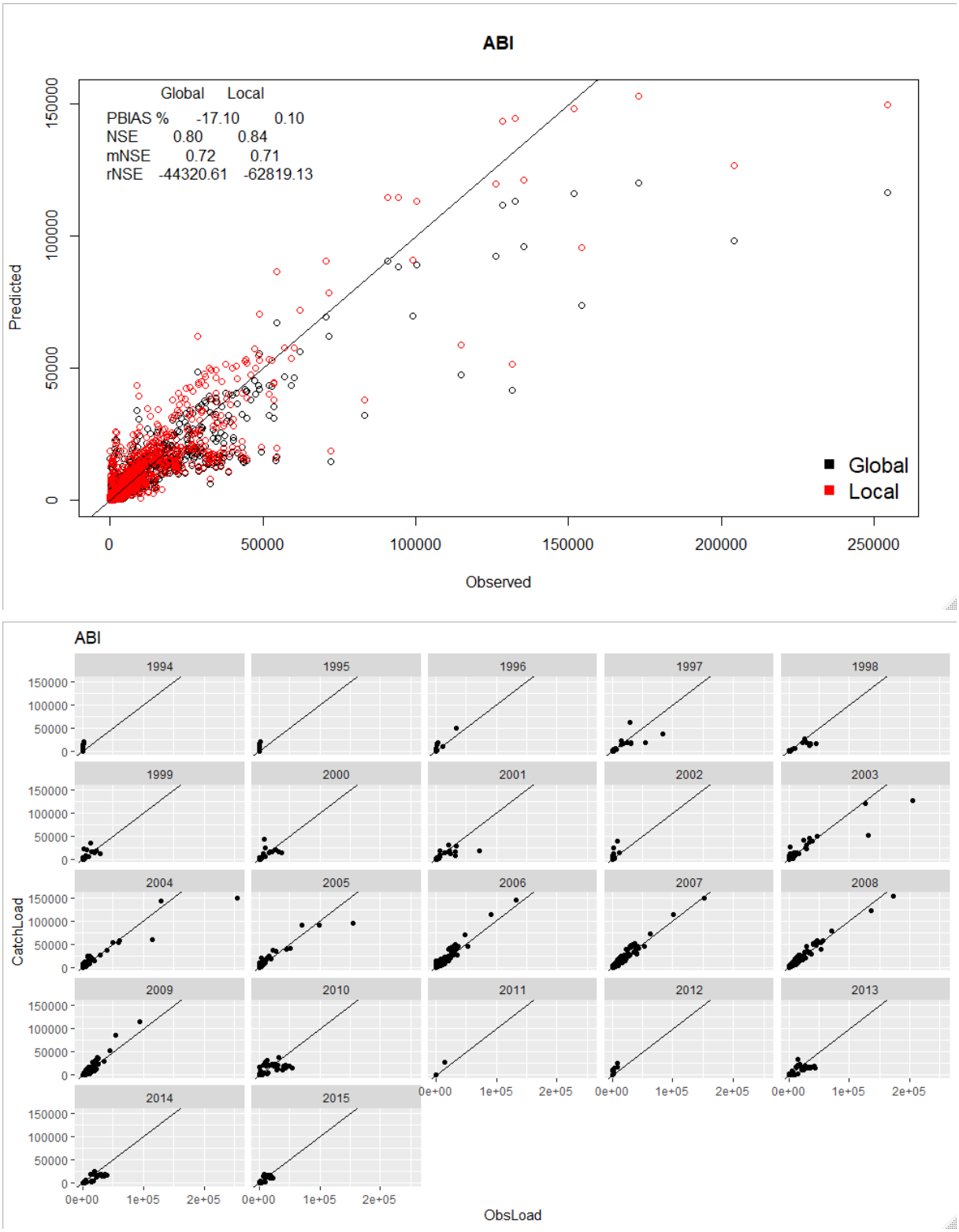

2.3 Modelling of water quantity and quality with SWAT model

The SWAT model is a physically based, spatially distributed model for simulating the impact of anthropogenic activities on water quality. In particular, it considers the impact of agricultural activities, point sources from wastewater treatment plants and industries and scattered dwellings. SWAT simulates daily concentrations of nitrogen (total nitrogen, nitrate, and ammonium), phosphorus (total phosphorus, ortho-phosphate), BOD, sediment as well as pesticides. It considers both surface waters (rivers and lakes) and groundwater bodies. The model has a flexible structure allowing to address different water resources and pollution problems and is well adapted to perform scenario analysis. Several measures have been simulated with SWAT in large European watersheds (A. Malagó et al., 2019; Malagó et al., 2017; Malagò and Bouraoui, 2019) including:

- Best fertilisation practices, manure management
- Crop rotation, cover crop, tillage, filter strip, alternative crops (climate adaptation), set-aside
- Irrigation optimisation for reducing nitrate leaching
- Selection of Nitrate Vulnerable Zones and associated action programmes

The SWAT version 2012.664 was setup to simulate water quantity and quality at monthly time steps to assess the effectiveness of several selected strategies for the mitigation of nutrient emissions to aquifers and rivers. The original SWAT structure was adapted to interact with R software (R Core Team, 2011) as explained in Figure 4.

In order to reduce the computational level of the model, the SWAT model domain was subdivided in 78 projects that represents the main hydrological basins (Malagò and Bouraoui, 2019). The domain covers the entire Europe, North Africa and Eastern Europe, including all the basins that drain into all European Seas (Figure 5).

Figure 4. The SWAT cross continental scale modelling interaction with R software.

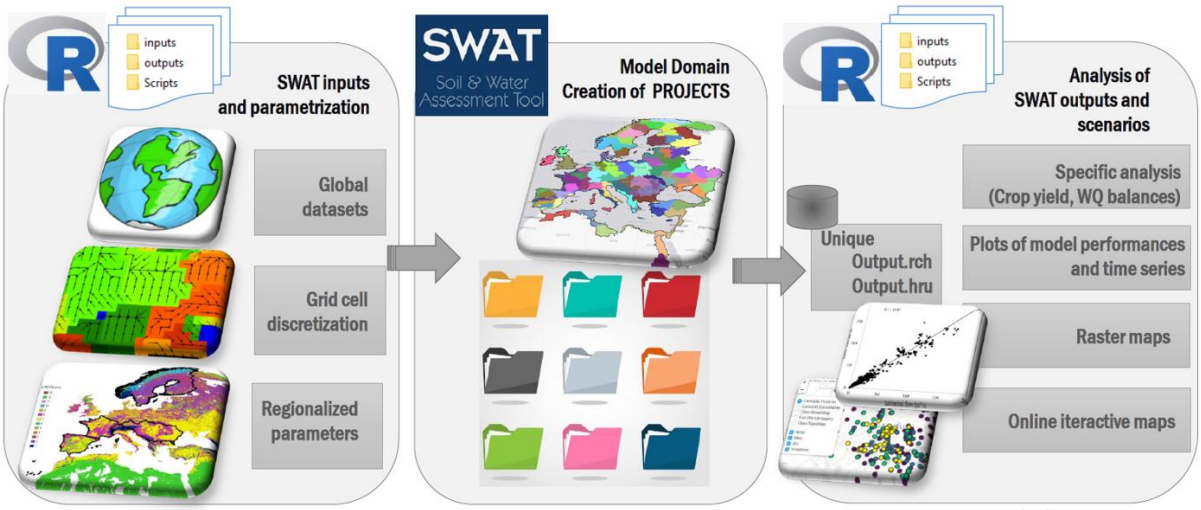

Figure 5. The 78 SWAT projects at cross continental scale.

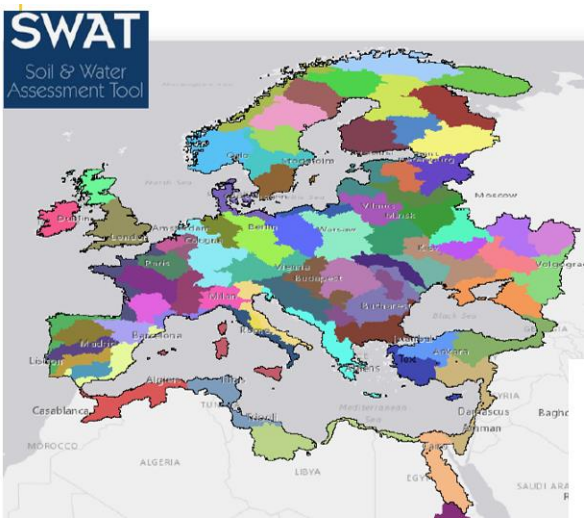

A watershed is divided into grid-cells, which are further subdivided into hydrologic response units (HRUs) that consist of unique combinations of soil, land use, and slope. The model structure comprises two phases: a land phase solved at HRU level, and a stream phase solved at reach level. In the land phase, the HRU water, sediment and nutrients cycles in soil, and losses are simulated and then aggregated at the grid cell level. The movement of water, sediments, and nutrients through the streams are simulated in the routing (stream) phase at daily time step. The results can be aggregated at river basins; WFD River Basin Districts; MSFD Marine Regions and Sub Regions, as well as at different temporal scale from daily to annual. SWAT requires several detailed input data related to topography, land use, soil, climate and land management, as explained in the following sub-sections (Figure 6).

Figure 6. The grid-cells input data in SWAT.

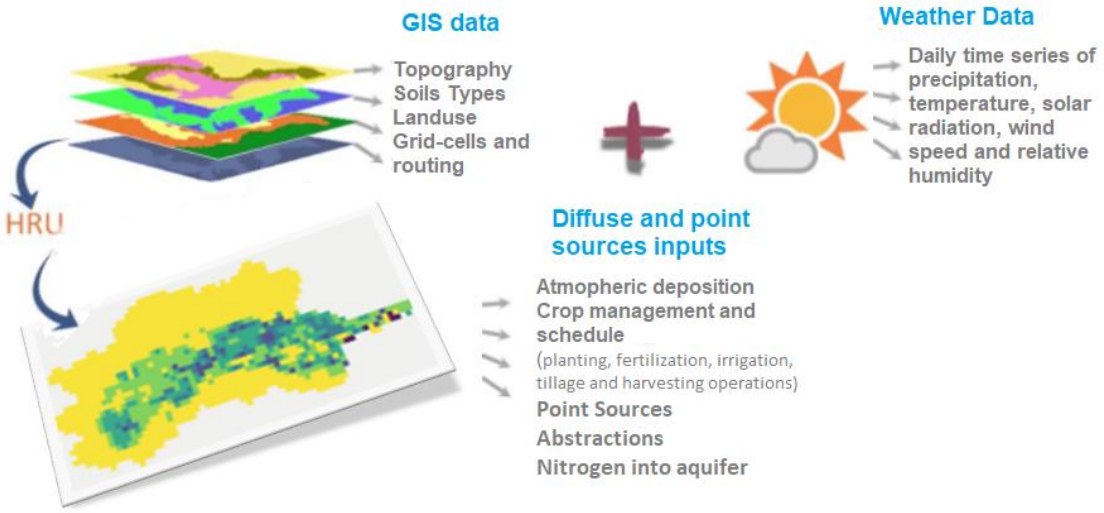

The model runs at the spatial resolution of a regular grid-cell (around 100 km^2) taking advantage of global spatial inputs (i.e. digital elevation model DEM, landuse and soils) that are readily available in gridded format. The choice of a regular grid was made to easily assimilate data readily available at global scale such as remote sensing information, population, etc. The major global inputs used are summarized in Annex 4.

2.3.1 Historical data

The model is setup to run for the period 1979 to 2019 including 10 years warming period using daily times series. Time series of anthropogenic pressures and weather data were reconstructed for the 1979-2019 period.

2.3.1.1 Land cover

The land use map was derived from 100 m x 100 m raster map built from the combination of the GLOBCOVER 2009 map (Arino et al., 2012) and Spatial Production Allocation Model (SPAM) (You et al., 2014) that provides crop-specific physical area, harvested area, and yields for 42 crops. Data are available for the year 2005 (average of 3 years centred on 2005) for four production systems: irrigated high inputs, rainfed high inputs, rainfed low inputs, and rainfed subsistence. This combination resulted in a raster of 219 landuse classes, including 9 classes of landcover fodder (FODG), grassland (GRAS), forest (FRST), shrub (SHRU), bare (BARE), urban area (URHD), water (WATR), sea (WSEA) and snow (SNOW) and the remaining are the SPAM crops (CROP). This raster was simplified grouping the crops only in irrigated and not irrigated crops based on the crops of the International Fertilizer Association IFA (IFASTAT, 2016), thus reducing the number of raster classes at maximum 35 for each grid-cell. The final crops considered in the model are: fiber crops (fiber), maize (maiz), other cereals (ocer), oil palm (oilp), oil crops (ooil), orts (orts), rice (rice), root tubers (roottuber), soybean (soyb), sugar crops (sugcrop), permanent crops (trof), vegetables (vege) and wheat (whea).

The landuse changes were calculated outside SWAT based on a global trend analysis performed by country (Bouraoui and Malagó, 2022). The trend analysis was performed for the period 1979-2019 using the Mann-Kendall trend test and the Sen Slope in R software. The harvest area for each crop was collected from FAOSTAT by country (FAOSTAT, 2021a) having grouped the crops using the IFA classification. The crops are taken from FAOSTAT rather than EUROSTAT because the model extent goes beyond Europe. The country-crop land use changes were then spatialized in SWAT by HRUs using a target method starting from the grid-cell where the crop object of the change is dominant. The crop area is thus increased or reduced changing proportionally the fodder grazing or grassland classes. The major changes in Europe's land cover for the past 40 years are shown below (Figure 7).

2.3.1.2 Meteorological data

Daily precipitation was obtained from the global gridded MSWEP dataset at 0.1-degree resolution (Beck et al., 2017). Daily data for the other atmospheric forcing variables (temperature, solar radiation, wind speed and relative humidity) were obtained from ERA-Interim (Dee et al., 2011) at 0.1-degree resolution. The whole dataset of climate data covers the period 01/01/1979–31/12/2019. To account for the increase in precipitation with elevation, that is typically observed in mountainous regions, four elevation/precipitation bands were implemented (Neitsch et al., 2011).

2.3.1.3 Diffuse nutrient inputs

The modelled crop management consists of planting, fertilization, irrigation, tillage and harvesting operations. The timing of management operations was implemented according to the heat units accumulated by crops (Arnold et al., 1998). The crop calendar was retrieved from the global dataset MIRCA2000 and kept the same in a preliminary run every year. This dataset provides the start and end of the cropping period for 26 irrigated and rainfed crops on global spatial units. The accumulated heat units (HU) for each crop were calculated using the average daily temperature, the duration of the growing season and the base temperature parameter provided by Malagó et al. (2019).

Each crop management was implemented in SWAT with a specific crop-management-package generated by R software. See the example of crop management implemented in SWAT in the following figure. The package is thus implemented differently every year from 1979 to 2019.

Figure 7. Major landcover changes implemented in SWAT.

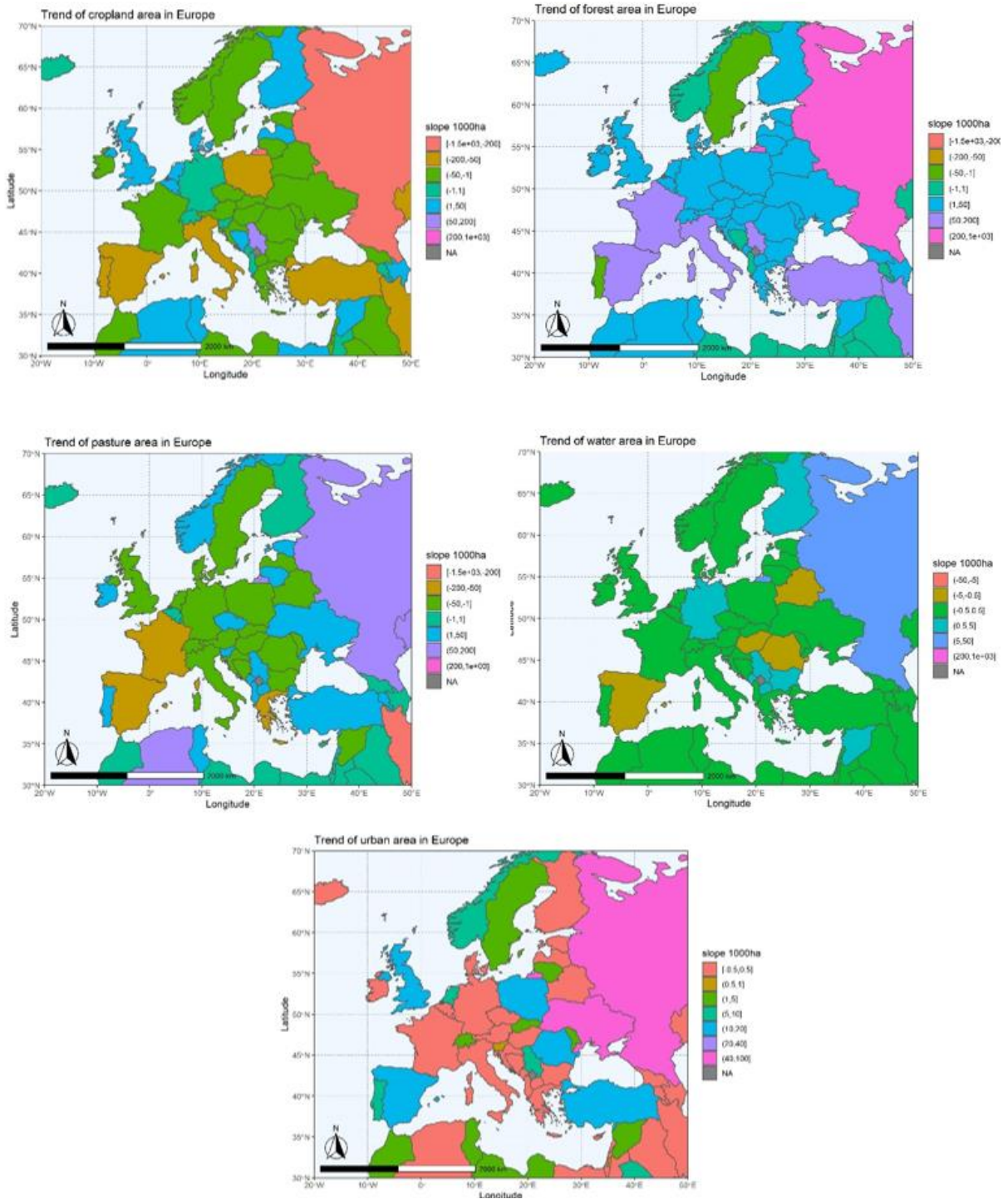

Figure 8. Example of Crop management package for maize for one year.

Scenario	Operation Code	Description	Month	Day	Application
Baseline	FERT MANN	Amount of N manure fertilizer application (0.99 ORGN)	10	14	112.2 kg/ha
	FERT MANP	Amount of P manure fertilizer application (0.99 ORGP)	10	14	24.7 kg/ha
	TILLAGE1	Disk Chisel (mulch Tiller) with depth of 150 mm and mixing efficiency of 0.55	10	15	
	TILLAGE2	Harrow 10 Bar Tine 36 Ft with depth of 25 mm and mixing efficiency of 0.2	10	24	
	PLANTING CORN	Beginning of plant growth	4	1	1787 HU
	FERT MINN	Amount of elemental N fertilizer applied to HRU	4	11	221.6 kg/ha
	FERT MINP	Amount of elemental P fertilizer applied to HRU	4	11	34.7 kg/ha
	IRRIGATION 1	Depth of irrigation water applied on HRU	4	22	12.6 mm
	IRRIGATION 2	Depth of irrigation water applied on HRU	5	7	12.6 mm
	IRRIGATION 3	Depth of irrigation water applied on HRU	5	22	12.6 mm
	IRRIGATION 4	Depth of irrigation water applied on HRU	6	6	12.6 mm
	IRRIGATION 5	Depth of irrigation water applied on HRU	6	21	12.6 mm
	IRRIGATION 6	Depth of irrigation water applied on HRU	7	6	12.6 mm
	IRRIGATION 7	Depth of irrigation water applied on HRU	7	21	12.6 mm
	IRRIGATION 8	Depth of irrigation water applied on HRU	8	5	12.6 mm
	IRRIGATION 9	Depth of irrigation water applied on HRU	8	11	12.6 mm
	IRRIGATION 10	Depth of irrigation water applied on HRU	8	17	12.6 mm
	HARVEST and KILL of CORN	Harvest and kill operation stops the plant growth in the HRU	9	1	

2.3.1.3.1 Irrigation 1979-2019 and irrigation sources

Following the method proposed by Puy et al. (2021) we predicted for each country the water withdrawals based on linear regression between the observed irrigation water withdrawals and the irrigated area of country retrieved from AQUASTAT (AQUASTAT database, 2021).

The effective water requirements by country were then calculated based on a percentage of water requirement retrieved from AQUASTAT. These annual values were then spatialized every 5 years, similar period to the landuse change, based on the difference between the annual potential evapotranspiration and precipitation and by crop based on the percentage provided by Siebert and Döll (2010).

The source of irrigation (surface and groundwater) were defined using the global map of irrigated areas (GMIA, 2021) that shows the percentage of the area equipped for irrigation that was actually used for irrigation and the percentages of the area equipped for irrigation that was irrigated with groundwater, surface water or non-conventional sources of water. In particular, we defined the source from groundwater if in the grid cell the total irrigated area from groundwater exceeds 40%, and from river if no lakes are present. In case of abstraction from lakes, we checked that the volume can cover the predicted abstraction.

2.3.1.3.2 Atmospheric deposition in the period 1979-2019

The atmospheric deposition was retrieved from the ISIMIP dataset (Lamarque et al., 2013b, 2013a; Tian et al., 2018). The historical monthly data for the period 1860-2016 were aggregated at annual scale (Figure 9). The long-term average annual values at 5 arc-minutes were used as input in atmospheric files of SWAT and also as input in the management file in order to simulate the annual variations.

Figure 9. Spatial distribution at 5 minutes of nitrogen deposition (Ndep, mg/l) for year 2015 from ISIMIP.

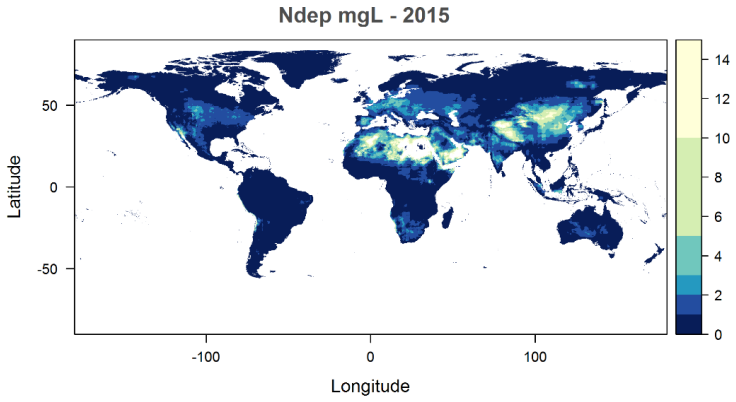

2.3.1.3.3 Mineral fertilizers in the period 1979-2019

The nitrogen (N) and phosphorus (P) mineral fertilizers application at 5 arc-minutes grid cells were estimated downscaling the total amount of mineral fertilizers by crop categories at country level for each year in the period 1979-2019. First, for each country the time series of N and P mineral fertilizers by crop, fodder and grassland were developed based on IFA values for year 2014. Then, a rescaling approach was applied to reconstruct the time series using the FAOSTAT datasets (FAOSTAT, 2021b). The example of nitrogen and phosphorus mineral fertilizer reconstructed time series for each crop in Italy is shown below (Figure 10).

Figure 10. Example of nitrogen and phosphorus mineral fertilizer reconstructed time series for each crop in Italy.

The crop-country time series were then spatialized in each grid cell and HRUs. In particular, the total mineral fertilizers were distributed by crop categories proportionally to the N and P used by the plant to reach the maturity every 5 years. The national mineral fertilizer applied on fodder and grassland was spatialized based on the area of fodder and grass in each cell.

2.3.1.3.4 Manure in the period 1979-2019

The amount of nitrogen and phosphorus from manure was computed for each cell multiplying the number of animal category (in heads) by the excretion coefficients per animal category (kg N or P/head year) as explained in Malagò and Bouraoui (2021). The procedure was updated using livestock from GeoNetwork rasters (GeoNetwork, 2007) at 0.05 decimal degrees resolution for year 2010. These rasters were used as the base for distributing 16 categories of livestock (FAOSTAT, 2021c) in each country for the period 1979-2019.

The excretion coefficients for the different years were calculated using the N excretion coefficient given in Bouwman et al. (1997) and the slaughtered weights (Yield/Carcass) from FAOSTAT (FAOSTAT, 2021d) following the procedure reported in Sheldrick et al. (2003). N excretion coefficients differ between

developed and developing country and stable and meadow type of production. The attribution of developed or developing country was adopted from Bouwman et al. (1997).

We considered for each country that the stable manure was applied only on crops, while the meadow type of manure was applied on FODG, GRAS, BARE and SHRU landcover classes proportionally to their areas. A similar procedure was applied to quantify the phosphorus manure considering that its excretion factor is a percentage of the nitrogen excretion factor.

The distribution of manure produced in stables and meadows for each category of livestock in each grid cell was calculated as follows: the manure produced in stable for each grid was distributed on cropland of the grid cell with a maximum limit of 50 kg/ha. The remaining part was distributed together with meadow type manure on FODG again with a limit of 50 kg/ha and the remaining part on GRAS, BARE and SHRU land cover class inside the same grid cell. The manure produced in meadow for each livestock class was distributed proportionally to the area between FODG, GRAS, BARE and SHRU landcover in each grid cell. In each cell with cropland, the manure was distributed proportionally to N and P uptakes calculated for year 2005 using MPASPAM dataset.

2.3.1.3.5 Nitrates into the aquifer

The initial values of nitrate concentrations in the shallow aquifer required to initialize the model were derived putting in relation the observed nitrate concentrations from the Nitrates Directive (EC, 1991) for the reporting period 2012-2015 with environmental variables including climatic, soil, hydrological, and management data using a stepwise regression approach as explained in Bouraoui and Malagó (2020).

2.3.1.4 Point sources inputs

Nutrient inputs from human settlements, i.e. wastewater treatment plants, industries, and phosphorus from detergents, were estimated considering urban and rural population, emission rates per person, the percentage of population connected to wastewater treatment plants system and the level of treatment.

The methodologies to define these nutrients specific emission (kg/person) at grid cell level consisted in determining the nutrient emission at country level and then to downscale the value using population density as a proxy.

2.3.1.4.1 Rural and urban population in the period 1979-2019

We distinguished between rural and urban population inside each grid cell using the GHSL datasets (Dijkstra and Poelman, 2014) at resolution of 1 km (Mollweide projection). The rural and urban population distribution of the GHSL dataset refer to years 1975, 1990, 2000 and 2015 and provides the following classes:

- Class30: urban centre
- Class23: dense urban cluster
- Class22: semi-dense urban cluster
- Class21: suburban or per-urban
- Class13: rural cluster
- Class12: low density rural
- Calss11: very low density rural
- Class10: water

The rasters were resampled at 5 arc-minutes, and for each grid-cell we grouped the classes 30, 23, 22, 21 for urban and the remaining for rural class of population. The urban and rural population of GHSL were then rescaled using the FAOSTAT statistics on the rural and urban population yearly counts for each country from 1979 to 2018 (FAOSTAT, 2021e). For the year 2019 we considered the same values of 2018.

2.3.1.4.2 Domestic N and P emissions in the period 1979-2019

Point source emissions are estimated according to the methodology described by Malagò and Bouraoui (2021). The procedure includes three steps: collection of national statistics of household connection to

sewers, connection to wastewater treatment plants and treatment level. A downscaling approach based on rural and urban population density is used to estimate at the grid level the pollutant load from domestic use of water. The N and P emission from human excretion are related to the human and vegetable protein intake taken from the FAO database (Herridge et al., 2008). Additional details are found in Malagò and Bouraoui (2021).

2.3.1.4.3 P emissions from detergents in the period 1979-2019

Because the information about the use of sodium triphosphate (STP) in detergents is very limited, we used selected countries around the world that have no ban or limitation on the use of STP in detergents including Albania, Bosnia and Herzegovina, Bulgaria, Croatia, Cyprus, Czech Republic, Estonia, Greece, Hungary, Latvia, Lithuania, the former Yugoslavia Republic of Macedonia, Malta, Republic of Moldavia, Poland, Portugal, Romania, Serbia, Slovakia, Spain, Ukraine and United Kingdom. We updated the estimation of 2005 provided in Malagò and Bouraoui (2021), with a new estimation for year 2010 where we used values from RPA (2006) and Schreiber et al. (2003) for European countries. The use of STP/detergent was related to the annual GDP. This relationship (Figure 11) was used when data was not available for a specific country-year. It is noteworthy that for countries with a known ban, the upper allowed limit by the ban was used.

Figure 11. The STP–detergents and GDP regression for year 2010.

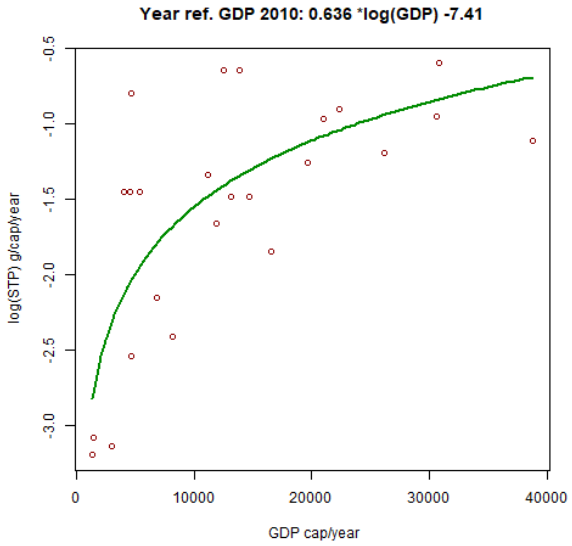

2.3.1.4.4 Nitrogen and phosphorus industrial emissions in the period 1979-2019

Due to the lack of available national data, the nitrogen and phosphorus industrial emissions were estimated as 15% of domestic emission as suggested by Morée et al. (2013). They were assumed also to follow the same spatial distribution.

2.3.1.4.5 Connected and unconnected population during the period 1970-2019

We reconstructed the rate of connected and unconnected population, as well the connected treated by treatment levels, scattered dwellings, treated not connected and not connected for both urban and rural population at country level for the period 1970-2019.

The procedure starts form the reconstruction of total connected treated population (CONNT) using a statistical approach based on relationship between the percentage of connected treated population (CONNT) and GDP (cap/year). Then all other categories (population connected for treatment level 1, level 2 and 3, scatter dwellings, treated not connected and not connected, for urban and rural population) were re-constructed filling the gaps using an interpolation method by years by countries starting in cascade from the population treated at different level to the unconnected population.

Two different sources of information were used:

- for European countries we used the EUROSTAT connection dataset that provides by countries-years (period 1970-2018) the total connected rate of population to wastewater treatment, also by treatment levels, and unconnected population (EUROSTAT, 2021). We completed this dataset adding also the EUROSTAT data for year 1990 from REFIT project (REFIT, 2019).
- for non-EU countries, we used the JMP dataset (JMP, 2019) that provides by countries for the period 2000-2017 the rate of connected population, septic tanks, open defecation, and unimproved systems by urban and rural population.

To find the best fit between the population connected treated (CONNT) and GDP (cap/year) we investigated several regression models, and the best model was selected for each country. Finally, for each country we obtained the predicted emission of urban and rural population according to the following categories: sewer connected, septic tanks, latrine or other systems. open defecation, and unimproved systems.

The country values by years were then spatialized at grid cell level using a rescaling approach. The rescaling procedure for connected urban and rural population consisted in the selection of the grid cell with the highest population in a moving window of 5 grid cells. The procedure was repeated until the target value of connection was reached. The unconnected population was then non-assigned population from the previous steps.

The nutrient emissions were thus used together with the predicted connection rates as explained in Malagò and Bouraoui (2021) for the calculation of N and P loads. Finally, the country years N and P loads were spatialized based on grid cell urban and rural connected and unconnected categories previously described. The final results are illustrated below for Hungary as example (Figure 12).

2.3.1.4.6 Water withdrawal by sectors in the period 1970-2019

The statistical annual values by country of water abstractions from different sources (agricultural, municipal/domestic and industrial sectors) are available from AQUASTAT. We used this dataset to find a relationship between the agricultural water withdrawals and GDP (WorldBank, 2017). The annual domestic and industrial water abstractions by country were then calculated as difference between the total abstraction and the predicted agricultural withdrawals, and proportionally we re-constructed the rate between domestic and industrial from the original data after applying a filling interpolation method. The final results of the whole procedure are illustrated below for Spain (Figure 13). These values were thus introduced in SWAT as abstractions from deep aquifers.

Figure 12. The point sources fact sheet for Hungary.

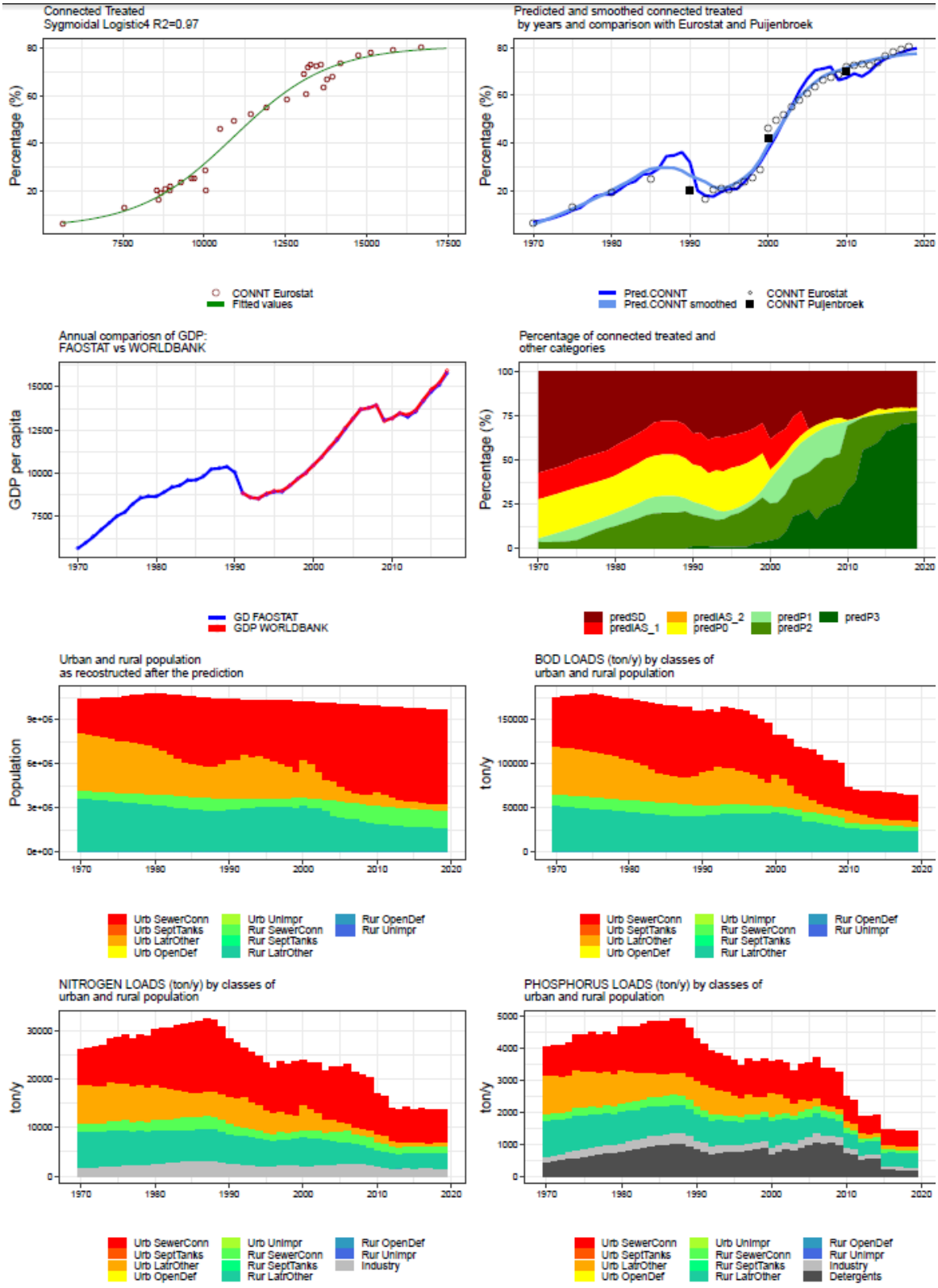

Figure 13. The water withdrawals by sectors for Spain.

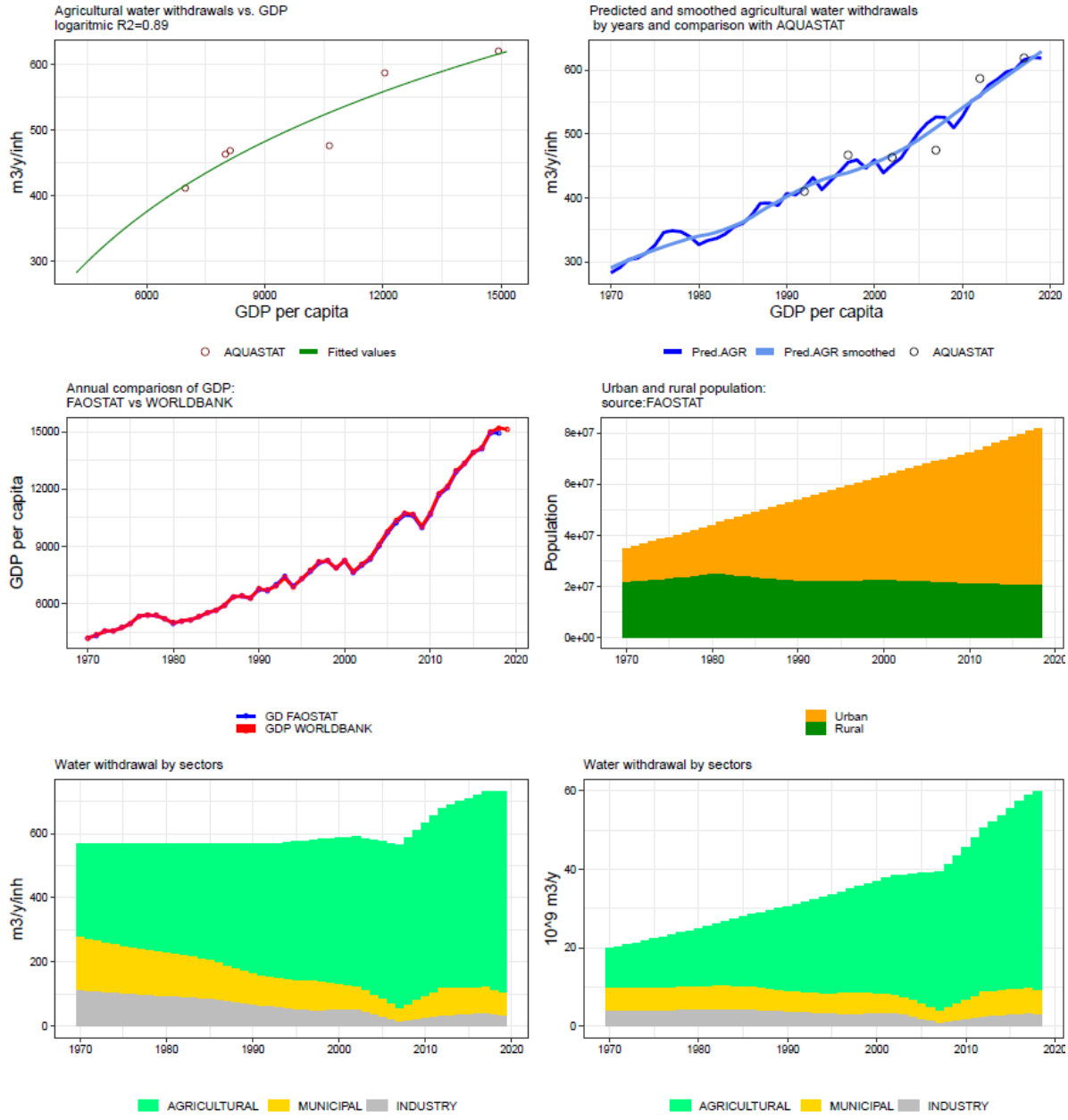

2.3.2 Model calibration and validation

An intensive effort was done to collect long time series of daily streamflow, nutrients, sediment. We collected and analysed more than 20 different datasets (global and local) (Malagó et al., 2022). In the modelling domain we collected around 2919 streamflow stations and 2630 water quality stations (Figure 14). An on-going effort is being done to calculate unbiased monthly nutrient concentration and loads that will be used in the calibration of SWAT.

The aggregated monthly streamflow and nutrient concentrations are being used in SWAT for calibration and validation using a cascade modelling approach starting from crop yield, then streamflow and finally nutrient concentrations (A. Malagó et al., 2019; Malagó et al., 2017, 2015).

Figure 14. Distribution of streamflow and water quality stations used in the calibration and validation of SWAT model.

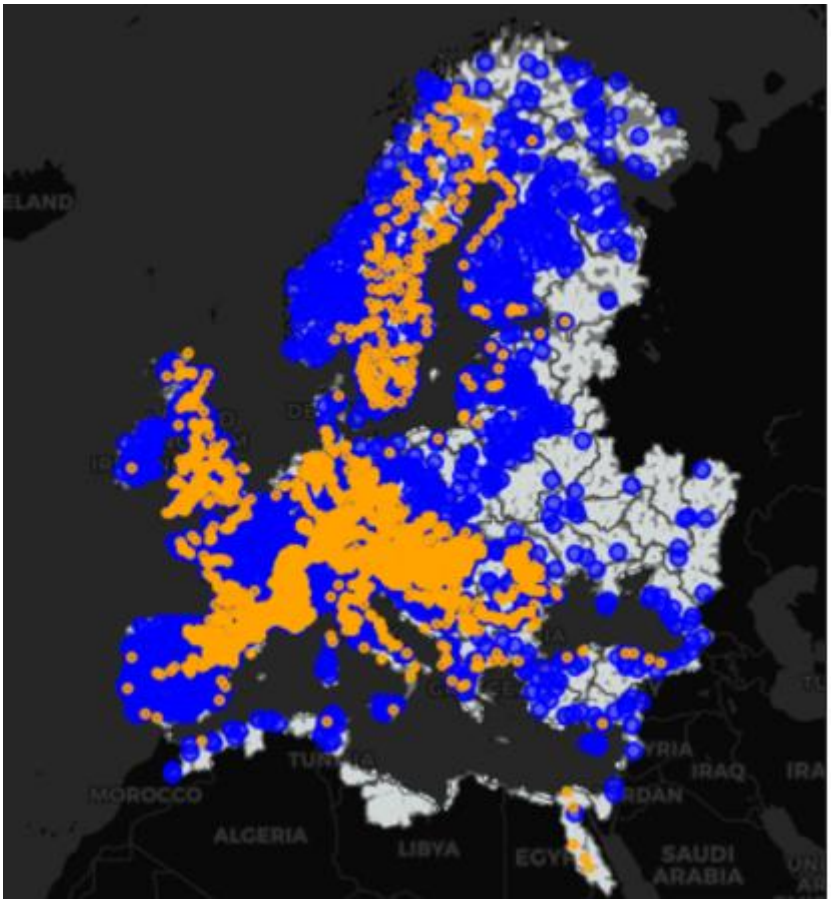

3 Historical data

This Section (Deliverable 2.2 part 1) describes the water quantity (Section 3.1) and quality data (Section 3.2) developed in the Blue2.2 project, delivered as input to the JRC marine team for the historical simulation and scenario analysis (see Macias et al. 2022), together with an analysis of water availability and nutrient pollution in Europe in the period 1990-2018.

3.1 Water quantity

A lack of water is a growing concern in many EU Member States, many of which until recently believed to have sufficient water. At present, there are approximately 52 million people or 11% of the population of the 27 states of the European Union plus the United Kingdom living in water scarce regions (Bisselink et al., 2020). This means that at least during part of the year, the demand for freshwater can scarcely be satisfied by the available freshwater. Of the aforementioned 52 million people, the majority live in Southern European countries including Spain (22 million; 50% of the national population), Italy (15 million; 26%), Greece (5.4 million; 49%) and Portugal (3.9 million; 41%). Furthermore, the entire population of Cyprus and Malta is considered to be living in conditions of water scarcity. During the summer, the exploitation of water in the Mediterranean area approaches 100%, meaning that all possible freshwater is being used, often including a substantial amount of fossil groundwater resources, causing groundwater depletion.

Water is being employed not only for drinking and sanitation, but also for agricultural irrigation, the cooling of electricity-production facilities, for industrial manufacturing (e.g. paper, textiles, soft drinks) and for the rearing of livestock. Furthermore, water is required to produce hydropower, while sufficient water needs to remain in rivers, lakes, and groundwater for ecological reasons. During episodes of low water availability, the demand for water may exceed the capacity to supply, which can lead to a series of conflicting situations.

We express the ratio between water consumption and water availability with the so-called Water Exploitation Index (WEI+). WEI+ illustrates the pressure on renewable freshwater resources due to water demand (see also section 2).

Water availability in a region is the local precipitation minus the evapotranspiration, but if appropriate added with river inflow coming from upstream countries. Best example here is Egypt, which has little annual runoff from local precipitation, but does have inflow water through the River Nile.

Net water consumption equals all water abstractions minus return flows. Water used for cooling power plants is partially returned back to the hydrological system, be it slightly warmer. Drinking water abstractions in the end largely flow back as treated wastewater.

WEI+ values > 0.20 are generally considered as an indication of water scarcity, while values equal or bigger than 0.40 indicate situations of severe water scarcity (EEA, 2015). In the case of WEI+ values larger than 0.4, the use of freshwater resources is likely unsustainable, with likely areas of groundwater depletion.

In Figure 15 we have estimated the Water Exploitation Index (WEI+) using the pan-European version of the integrated agro-hydrological LISFLOOD-EPIC model forced with observed weather data 1990-2018.

In present climate, southern regions of Europe already face water stress conditions, with the annual average WEI+ varying between 0.1-0.3 (Figure 15a) in the Mediterranean region. During up to 4 months per year the WEI+ value is higher than 0.2 in the most southern parts of Europe (Figure 15b). The highest average WEI+ values, up to 0.5, are found in Spain. These regions presently experience serious and severe water stress up to 6 months a year. During summer WEI+ can be close to 1.0, meaning that all possible water is being used, and often also a substantial amount of fossil groundwater.

Apart from the WEI+ based on water consumption vs. availability, we also use the WEI indicator based on abstraction vs. availability. WEI abstraction is always larger than WEI+ consumption. The difference between them is the accounting for the return flows of irrigation, cooling water, and waste water. Figure 16 shows the country average WEI+ (Figure 16a) and WEI abstraction (Figure 16b) values. The countries with the largest values are Cyprus, Spain, Greece, Italy, Malta and Portugal. However, several other countries have local hotspots of increased WEI+ values (Figure 15a).

Figure 15. (a) Estimated average Water Exploitation Index (WEI+) and (b) the number of days with a WEI+ exceeding 0.2 for present day climate (1990-2018) as simulated with the LISFLOOD-EPIC model.

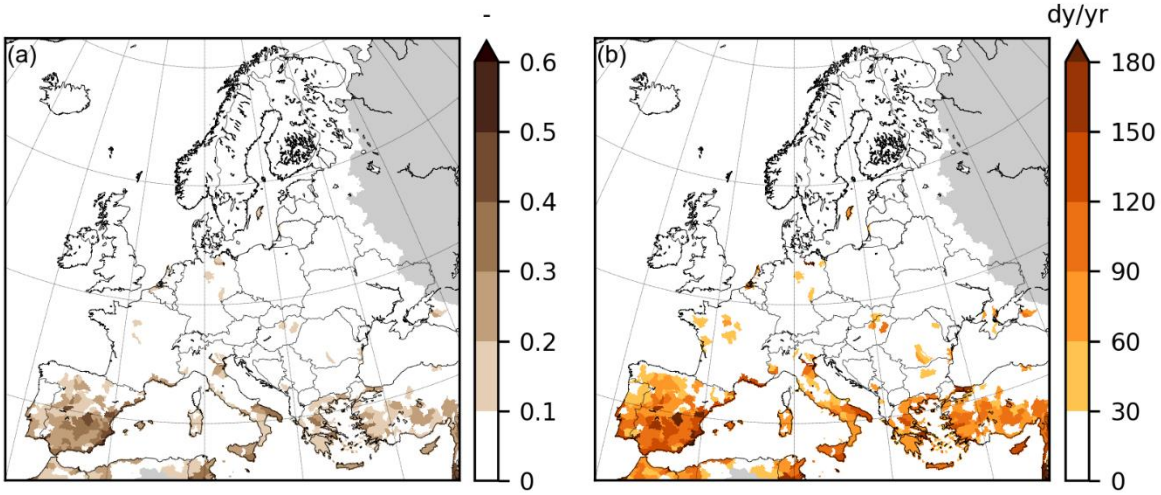

Figure 16. The Water Exploitation Index WEI averaged for European countries for 1990-2018 for (a) consumption WEI+ and (b) WEI abstraction.

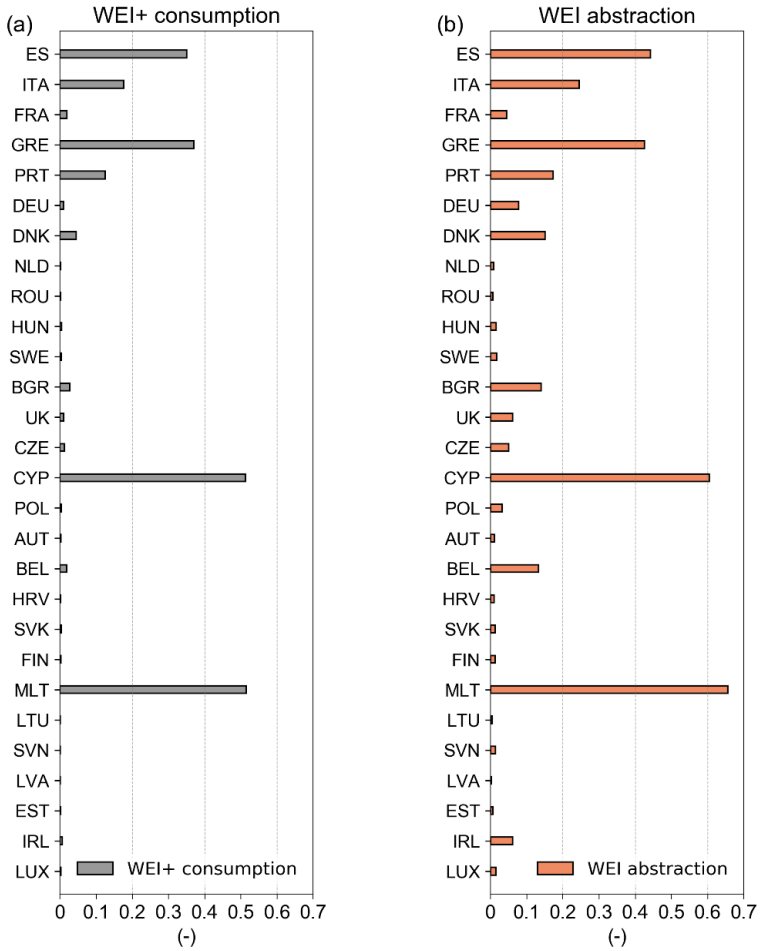

Figure 17. Groundwater depletion between 1990 and 2018, as estimated with the LISFLOOD-EPIC model.

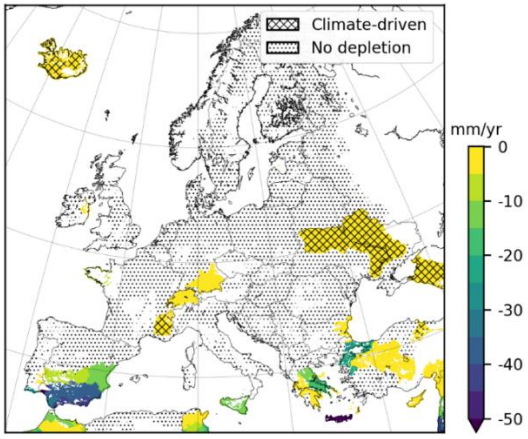

Source: Gelati et al. (2020)

Groundwater depletion is observed in the model if there is a difference in groundwater storage at the end of the model simulation in 2018, as compared to the start of the model simulation in 1990. Gelati et al. (2020) also evaluated the likely source of groundwater depletion. When we excluded irrigation - and separately also other water abstractions - from the model simulation, only a few areas were left with some groundwater depletion, which we assume to originate from climatic changes between 1990 and 2018. Figure 17 shows estimates of groundwater depletion for Europe, with some major groundwater depletion regions in southern Spain, Sicily, Greece, Turkey and Cyprus.

The WEI+ calculations show that in several parts of Europe, the annual renewable freshwater is used in an unsustainable way, and this is thus further confirmed by the estimated groundwater depletion (or by the estimated amount of groundwater depleted).

3.2 Water quality (nutrients)

3.2.1 GREEN nutrient sources (1990-2018)

Mean annual nutrient inputs per marine region at the beginning, middle and end of the historic study period are shown in Table 5 (annual means over five years, excluding the Barents-Norwegian-White Seas) (see also Vigiak et al., 2023). The largest share of nitrogen inputs is represented by mineral fertilizers, which accounts for about 43% of the nutrient sources, followed by organic fertilizers (manure, about 25%; Figure 18). The third source of nitrogen is atmospheric deposition, which accounts for about 17% of nitrogen inputs. Domestic emissions and industrial discharges contribute about 5% of nitrogen inputs.

Over the full extent (including the Barents-Norwegian-White Seas region, BNW), total nitrogen inputs were estimated of about 31.6 Tg/y in the early 1990s and 29.9 Tg/y currently (31.5 and 29.7 when excluding the BNW region; Table 5), with a reduction of about 6%, which occurred mainly in the first half of the historic period (Figure 18). From 1990 to 2018 domestic emissions reduced notably. Particularly, emissions from disconnected population reduced by 65%, partly due to an increase of connection to sewerage system thus shifting emissions from diffuse to point sources. Overall domestic and industrial emissions were reduced from 1.7 Tg/y in 1990-1994 to current 1.3 Tg/y (-22%). Atmospheric deposition went from about 6.2 Tg/y in the early 2000s to current 5.0 Tg/y (-19%). Conversely, mineral and organic fertilization levels in current times are close to those in the early 1990s. Mineral fertilization decreased in the first half of the period, going from 13.2 in 1990-1995 to 12.5 in 2002-2006 (-5.6%), but then increased again to current 13.3 Tg/y (+1% over the whole period). Organic fertilizer sources decreased by about 5% in the first half of the period, but increased again thereafter, so that current inputs (7.5 Tg/y) are close to levels of 1990-1994 (7.8 Tg/y).

There were notable regional differences in nitrogen input trends (Table 5). Figure 19 shows the historic input time-series for the marine regions with the largest drainage areas for each of the four main European seas (all marine regions are shown in Annex 3). In the Greater North Sea (ANS), nitrogen sources decreased by 13.7% from 1990 till 2018, registering the largest reduction in the Atlantic Ocean regions. The input reduction was constant throughout the period (Figure 19), especially for mineral fertilization (-15%), atmospheric deposition (-27%), and domestic and industrial emissions (-22%), whereas organic fertilization levels remained rather constant. Conversely, nitrogen sources changed only slightly in the Bay of Biscay & Iberian Coast (ABI, -2%), and lowered by about 8% in Celtic Seas (ACS, Table 5). Nitrogen inputs in the Baltic Sea (BAL) decreased by 6.5% in the first half of the period, but increased thereafter, up to a level close to the initial one (Figure 19). The application of mineral fertilizer increased throughout the period (27%), particularly from the 2000s. Application of organic fertilizers dropped initially by 18%, but then slightly recovered, so that this source decreased by 8% in the whole period. Atmospheric deposition decreased by 21%, and domestic and industrial emissions by 31%. Nitrogen sources in the Black Sea region (BLK, including the sea of Marmara) increased by 8% from the start to the end of the period. After a slight reduction in the first half (-5.1%), nitrogen sources increased sharply in the second half (+14%), especially due to an important increase in mineral fertilization (+39%) that was not compensated by reductions in organic fertilization (-10%), atmospheric deposition (-7%), and domestic and industrial emissions (-22%). In the Western Mediterranean Sea (MWE) nitrogen sources decreased by 13%, with improvements occurring especially in the new millennium. Application of mineral fertilizers decreased by 24%, atmospheric deposition by 20% and domestic and industrial emissions by 13%, whereas organic fertilization increased by 12%. The trends in other Mediterranean regions, however, differed (Table 5). In the Adriatic Sea (MAD) and Ionian Sea and Central Mediterranean Sea (MIC) nitrogen sources decreased by about 21%, due to important reductions in mineral fertilization, atmospheric deposition, and domestic/industrial emissions. Conversely nitrogen inputs slightly increased in the Aegean Levantine Mediterranean Sea (MAL, +2.5%), for increases in atmospheric deposition and organic fertilization. In the Mediterranean Sea as a whole, nitrogen sources decreased by 10%, driven by reductions in mineral fertilization (-21%), atmospheric deposition (-15%), and domestic/industrial emissions (-18%), whereas organic fertilization slightly increased (+5%).

Table 5. Annual nutrient inputs per marine region (mean over 1990-1994, 2002-2006, and 2014-2018).

Marine region(1)	Annual nitrogen inputs			Annual phosphorus inputs		
	1990-1994	2002-2006	2014-2018	1990-1994	2002-2006	2014-2018
	t/y			t/y		
ABI	4,015,967	3,982,672	3,952,779	816,925	722,716	630,255
ACS	2,266,825	2,069,843	2,079,761	407,830	339,601	346,417
ANS	9,181,687	8,582,234	7,925,348	1,495,163	1,232,822	1,078,225
BAL	4,661,535	4,346,410	4,648,033	813,857	640,013	667,067
BLK	5,723,390	5,433,140	6,189,786	1029,019	768,411	851,489
MAD	1,680,177	1,553,085	1,328,035	350,150	289,752	214,196
MAL	1,480,346	1,344,956	1,471,195	284,760	221,203	237,461
MIC	412,925	356,642	325,946	81,910	61,386	41,880
MWE	2,029,406	1,971,892	1,759,565	385,667	333,416	306,643
TOTAL	31,452,259	29,640,872	29,680,448	5,665,280	4,609,319	4,373,632

(1) Marine Regions: ABI=Bay of Biscay & Iberian Coast; ACS=Celtic Seas; ANS=Greater North Sea; BAL=Baltic Sea; BLK=Black Sea & Sea of Marmara; MAD=Adriatic Sea; MAL=Aegean Levantine Mediterranean Sea; MIC=Ionian Sea and Central Mediterranean Sea; MWE=Western Mediterranean Sea. TOTAL values refer to the study extent in Figure 2 except the Barents, Norwegian and White Seas.

Figure 18. Nitrogen inputs in Europe in 1990-2018. Values refer to full study extent in Figure 2. (Nitrogen sources: MinN=mineral fertilizer; ManN=manure; AtmN=atmospheric deposition; FixN=crop fixation; SoilN=soil fixation; SdN=scattered dwellings; PS=point sources).

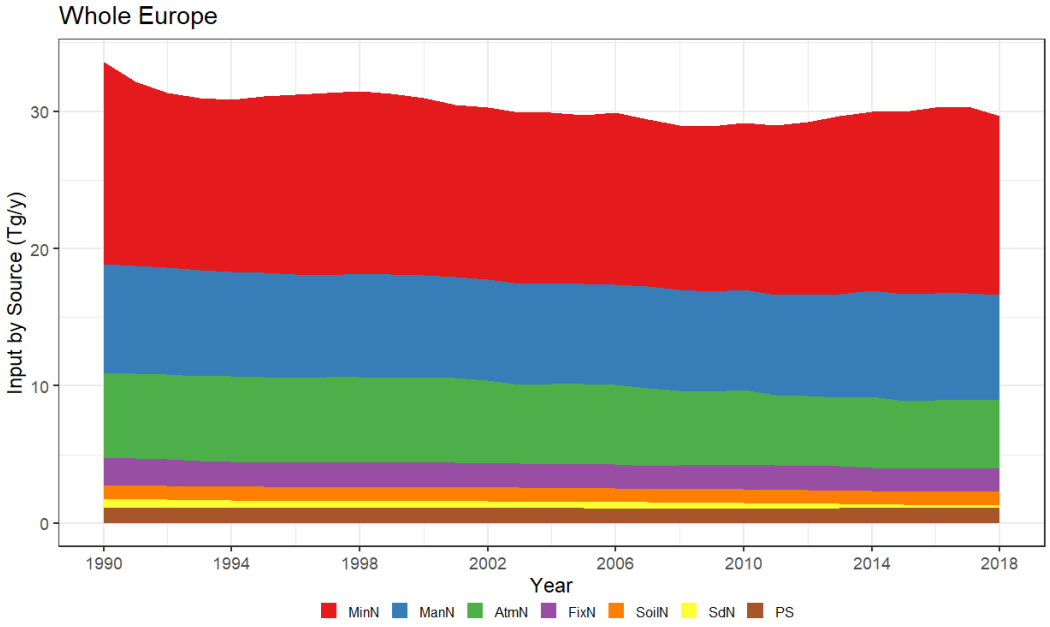

Figure 19. Nitrogen inputs in four marine regions: ANS=Greater North Sea; BAL=Baltic Sea; BLK=Black Sea & Sea of Marmara; MWE=Western Mediterranean Sea. (Nitrogen sources: MinN=mineral fertilizer; ManN=manure; AtmN=atmospheric deposition; FixN=crop fixation; SoilN=soil fixation; SdN=scattered dwellings; PS=point sources).

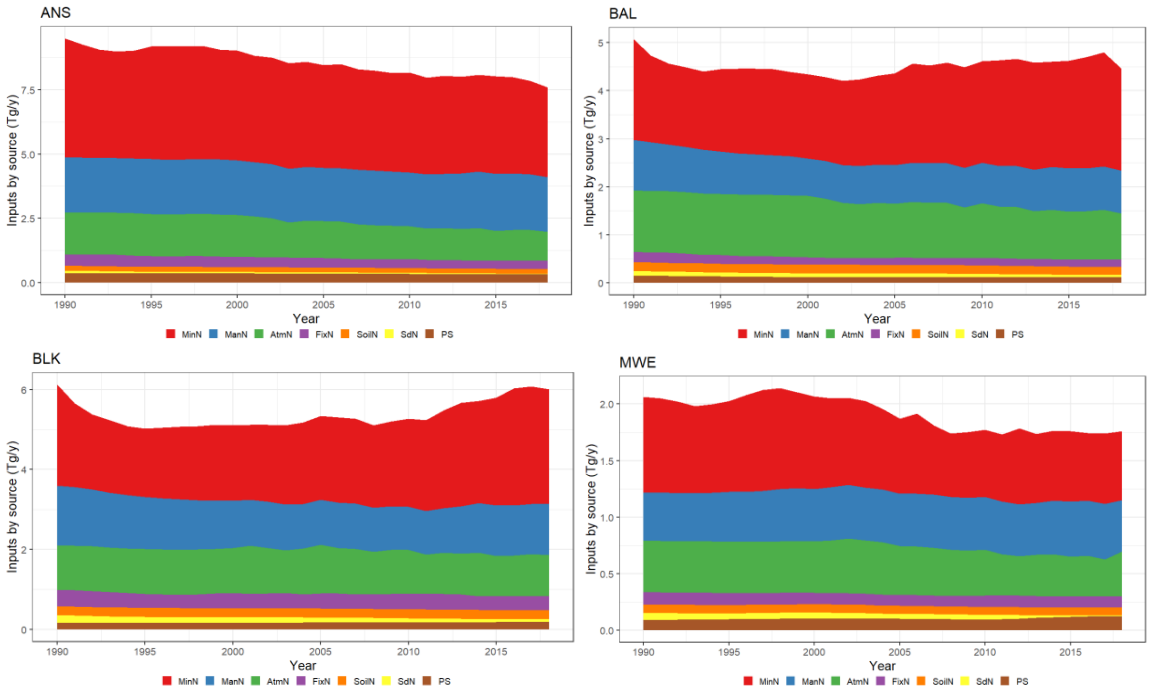

Figure 20. Phosphorus sources for the whole Europe in 1990-2018. Values refer to full study extent in Figure 2. (Phosphorus sources: MinP=mineral fertilizer; ManP=manure; BG=background losses; SdP=scattered dwellings; PS=point sources).

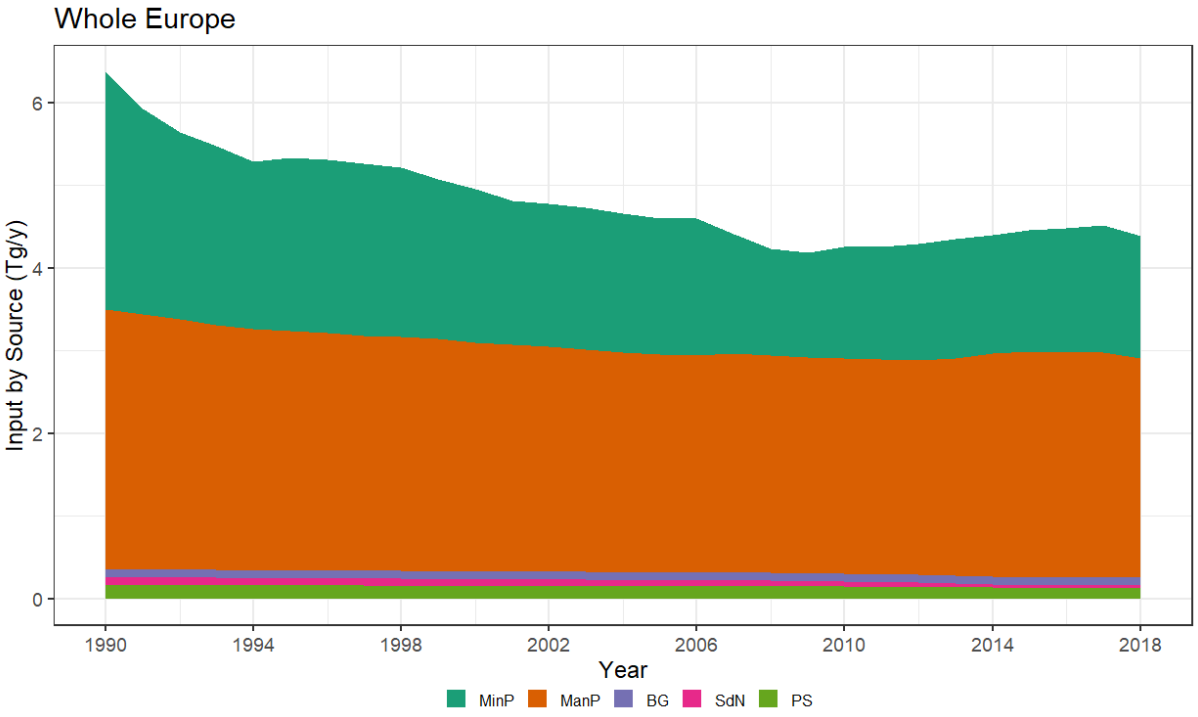

Figure 21. Phosphorus inputs in four marine regions: ANS=Greater North Sea; BAL=Baltic Sea; BLK=Black Sea & Sea of Marmara; MWE=Western Mediterranean Sea. (Phosphorus sources: MinP=mineral fertilizer; ManP=manure; BG=background losses; SdP=scattered dwellings; PS=point sources).

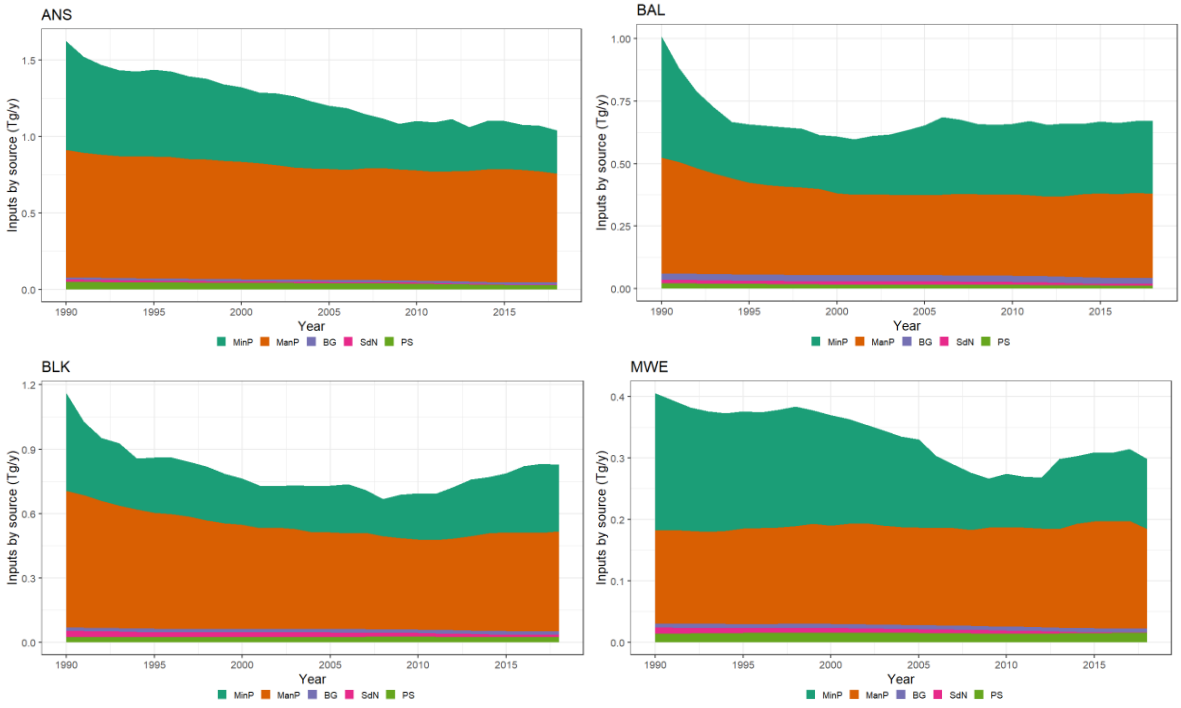

Total phosphorus sources decreased substantially in the period 1990-2010, from 6.4 to 4.4 when including the Barents-Norwegian-White (BNW) Sea (Figure 20) (5.7 Tg/y to 4.4 Tg/y, when excluding BNW region: Table 5), but inputs have remained more or less constant in the 2010s. Mineral fertilization and domestic/industrial emissions dropped by 37% from 1990-1994 to 2014-2018, and organic fertilization by 11%. Reductions in fertilization levels occurred mainly in the first half of the period, whereas that of domestic/industrial emissions was more important in the second half.

Also in the case of phosphorus, marine regions showed important differences (Figure 21; Table 5). In the Greater North Sea (ANS), mineral fertilization dropped from 1990 to 2018 by more than 50%; organic fertilization dropped by 9.8%, but this occurred before the 2000s. Domestic and industrial emissions dropped by 48%, accelerating in the second half of the period. Phosphorus inputs decreased importantly also in the other Atlantic Ocean regions, Bay of Biscay & Iberian Coast (ABI, -22%) and Celtic Seas (ACS, -15%). In the Baltic region (BAL), phosphorus inputs decreased by 18%, but once again these improvements occurred in the first half of the period (Table 5), whereas from the 2000s inputs increased slightly, due to variations in mineral and organic fertilization. Conversely, domestic/industrial emissions decreased throughout the period (-44%). Also in the Black Sea region (BLK) phosphorus inputs decreased (-17%), albeit an increase in inputs, especially as mineral fertilization, was observed from 2010. Conversely, organic fertilization dropped by 22%, and domestic/industrial emissions by 30%. In the Western Mediterranean Sea (MWE), phosphorus inputs reduced by 21%, due to a large decrease in mineral fertilization (-45%) and despite an increase of organic one (+13%). Domestic/industrial emissions dropped by 31% especially in the second half of the period. Phosphorus decreases were even more important in the Adriatic Sea (MAD, -39%), and in the Ionian Sea and Central Mediterranean Sea (MIC, -49%) regions, whereas in the Aegean Levantine Mediterranean Sea (MAL, -13% overall), phosphorus input reductions in the first half were followed by a gain in the second half. In the Mediterranean Sea, phosphorus inputs decreased by 22%, with larger gains obtained in the second part of the period.

3.2.2 GREEN nutrient loads to the seas (1990-2018)

Annual loads to sea estimated with GREEN varied from year to year, reflecting the model inbuilt dependency of land retention on annual precipitation. Loads to sea per marine region are reported as mean over 5 years at the beginning, middle and end of the study period in Table 6. (See also Vigiak et al., 2023).

The reductions in nutrient loads to the seas reflected the trends in nutrient sources. Nitrogen loads to the sea amounted to about 16% of nutrient inputs, and from about 5 Tg/y in 1990-1994 went down to 4.7 Tg/y in 2014-2018 (Figure 22, from 4.9 to 4.6 when excluding the Barents-Norwegian-White Seas combined region, Table 6). However, since diffuse emissions are attenuated by land retention, whereas point sources solely by retention in rivers and lakes, contributions of nutrient sources to loads at the outlet differ from the shares of source inputs. Mineral fertilization accounted for 25% of nitrogen loads to the sea in 1990-1994 and 28% in 2014-2018, organic fertilization went from 16% to 19%, nitrogen atmospheric deposition decreased from 24% in 1990-1994 to about 21% in 2014-2018, and domestic and industrial emissions contributed 29% in 1990-1994 down to about 26% in 2014-2018. Plant fixation accounted for about 4% of loads, and soil fixation for 2% (Figure 22).

Regional differences reflected source input trends (section 3.2.1), but also land and river retention (as calibrated in the model, section 2.2.3). In the Greater North Sea (ANS) nitrogen loads decreased by 17% in the study period, thanks to reduction in all nitrogen sources (Figure 23). Loads in Bay of Biscay & Iberian Coast (ABI) reduced to a much lesser extent (by 4.1%, Table 6). Conversely, loads in Celtic Seas (ACS) increased by 13%, with an increased contribution of fertilization inputs. In the Baltic Sea (BAL), nitrogen loads reduced by 13%, especially in the first period; contributions of domestic/industrial emissions decreased from 32% to 27%, whereas that of mineral fertilization increased from 16% to 24%. In the Black Sea (BLK) nitrogen loads to the sea increased by 10%, with a trend that accelerated in the second half of the period. The contribution of mineral fertilization to the load increased from 17% in 1990-1994 to 27% in 2014-2018, while that of domestic/industrial emissions decreased from 38% to 30%. Loads to the Western Mediterranean Sea (MWE) decreased by 13%, resulting from less contributions from mineral fertilization and atmospheric deposition (-3% each source) but with an increase of contribution from domestic and industrial emissions, from 34% in 1990-1994 to 37% to 2014-2018. Also in the Adriatic Sea (MAD) nitrogen loads to the sea reduced by 13% during the study period, improving especially in its second half. Reductions in Ionian Sea and Central Mediterranean Sea (MIC) were much less sizeable (-4%); mineral fertilization and domestic/industrial emission contributions lowered, but that of organic fertilization

increased. In the Aegean Levantine Mediterranean Sea (MAL) nitrogen loads to sea increased, probably linked to the shift of domestic emissions from diffuse (disconnected) to point sources. Overall, loads to the Mediterranean Sea reduced by only 3%.

Table 6. Annual nutrient loads to sea per marine region (mean over 1990-1994, 2002-2006, and 2014-2018).

Marine region(1)	Annual nitrogen inputs			Annual phosphorus inputs		
	1990-1994	2002-2006	2014-2018	1990-1994	2002-2006	2014-2018
	t/y			t/y		
ABI	606,120	578,176	581,174	71,066	60,486	51,113
ACS	281,740	273,092	318,237	23,166	21,388	21,792
ANS	1,515,375	1,402,917	1,252,124	79,262	65,123	47,608
BAL	604,731	513,260	520,983	45,507	36,832	32,590
BLK	743,883	767,347	819,739	62,878	57,442	52,395
MAD	352,068	359,474	306,711	19,993	20,931	16,995
MAL	323,450	345,129	384,790	74,469	68,041	74,807
MIC	109,306	116,602	105,311	22,650	21,875	15,926
MWE	396,166	382,177	345,707	26,464	24,289	20,558
TOTAL	4,932,839	4,738,174	4,634,775	425,455	376,406	333,784

(1) Marine Regions: ABI=Bay of Biscay & Iberian Coast; ACS=Celtic Seas; ANS=Greater North Sea; BAL=Baltic Sea; BLK=Black Sea & Sea of Marmara; MAD=Adriatic Sea; MAL=Aegean Levantine Mediterranean Sea; MIC=Ionian Sea and Central Mediterranean Sea; MWE=Western Mediterranean Sea. TOTAL values refer to the study extent in Figure 2 except the Barents, Norwegian and White Seas.

Phosphorus loads to sea decreased from 435 kt/y in 1990-1994 to 343 kt/y in 2014-2018 (-21%, Figure 24; from 425 to 334 when excluding the Barents-Norwegian-White Sea region, Table 6), i.e. about 8% of phosphorus inputs. Mineral fertilization contributed 20% of these loads in 1990-1994 and 16% in 2014-2018. Concurrently, contribution from organic fertilization increased from 24 to 32%. Domestic and industrial emissions accounted for 47% of the loads in 1990-1994, and 40% in 2014-2018 (Figure 24).

Improvements were registered in all marine regions, even though at different pace. The most important reduction of phosphorus loads to sea (-40%) occurred in the Greater North Sea (ANS), thanks to a large decrease in domestic/industrial emissions, which contributed 70% of loads in 1990-1994, down to 64% in 2014-2018 (Figure 25). Organic fertilization contribution instead increased from 15 to 20%. In the other Atlantic Ocean regions, phosphorus loads to the sea reduced importantly in the Bay of Biscay & Iberian Coast (ABI, -28%), and to a lesser extent in Celtic Seas (ACS, -6%, Table 6). In the Baltic Sea (BAL), phosphorus loads decreased by 28%; important gains resulted from reducing domestic/industrial emissions, whose contribution decreased from 55 to 44% (Figure 25). Phosphorus loads to sea decreased also in the Black Sea (BLK, -17%); improvements were linked to reduction in domestic and industrial emissions occurring especially in the second half of the study period. Loads to the Western Mediterranean Sea (MWE) reduced by 22%, especially in the second half of the study period linked to a reduction in mineral fertilization. Diffuse domestic emissions reduced from 22 to 4%, but point sources increased, so that currently point sources contribute 65% of loads to the sea. Phosphorus loads to the sea decreased by 15% in the Adriatic Sea (MAD), and by 30% in Ionian Sea and Central Mediterranean Sea (MIC), due to large reductions in mineral fertilization contribution. In the Aegean Levantine Mediterranean Sea

(MAL), loads decreased in the first half but then increased again in the second half, reaching in 2014-2018 levels close to those in 1990-1994 (Table 6). In these three regions, the contribution of organic fertilization increased during the study period. Overall, phosphorus loads to the Mediterranean Sea decreased by 10% from 1990-1994 to 2014-2018; the contribution of mineral fertilization decreased from 31 to 23%, whereas that of organic fertilization increased from 32 to 40%. Diffuse domestic emissions decreased from 12 to 4%, shifting towards point source discharges, whose contribution increased from 18 to 26%.

Figure 22. Nitrogen loads to the seas for the whole Europe in 1990-2018. Values refer to full study extent in Figure 2. (Nitrogen sources: MinN=mineral fertilizer; ManN=manure; AtmN=atmospheric deposition; FixN=crop fixation; SoilN=soil fixation; SdN=scattered dwellings; PS=point sources).

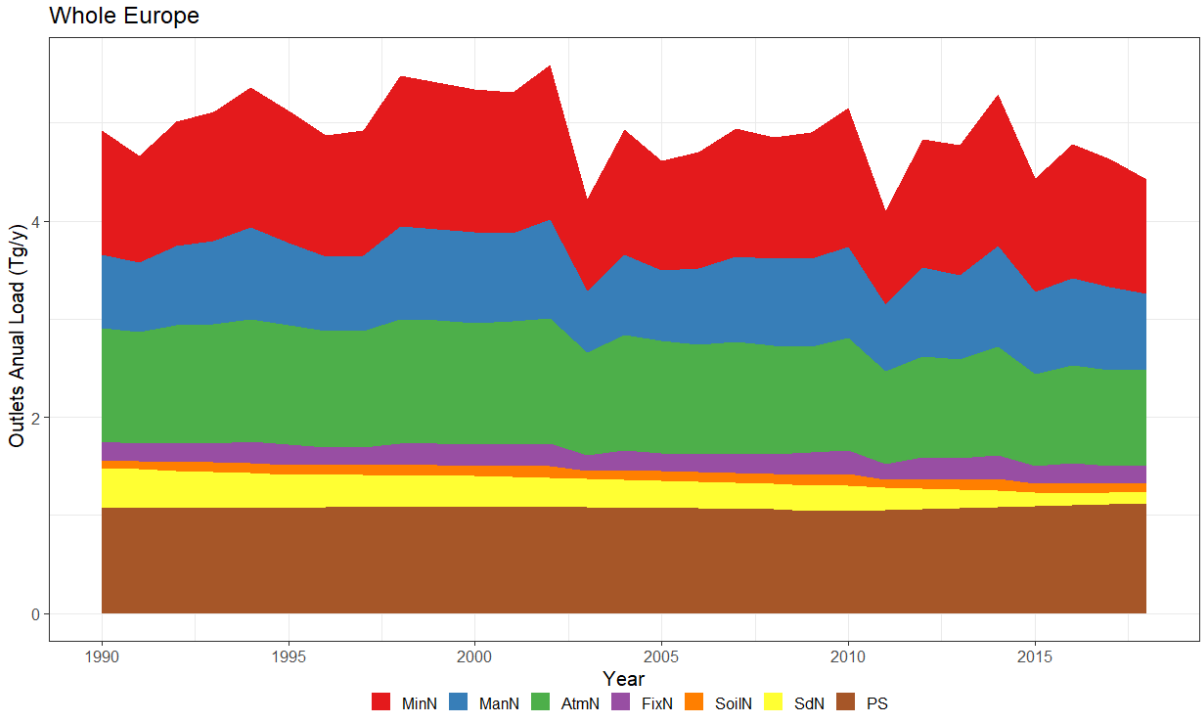

Figure 23. Nitrogen loads to the seas in four marine regions: ANS=Greater North Sea; BAL=Baltic Sea; BLK=Black Sea & Sea of Marmara; MWE=Western Mediterranean Sea. (Nitrogen sources: MinN=mineral fertilizer; ManN=manure; AtmN=atmospheric deposition; FixN=crop fixation; SoilN=soil fixation; SdN=scattered dwellings; PS=point sources).

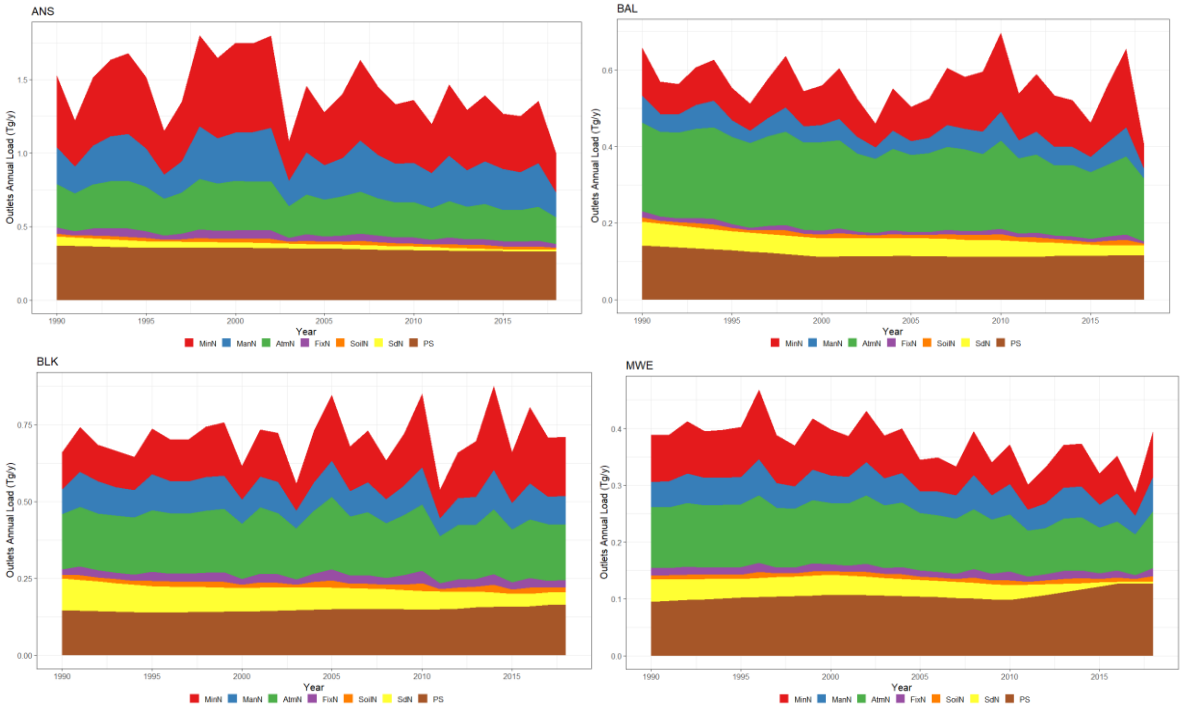

Figure 24. Phosphorus load to the seas for the whole Europe in 1990-2018. Values refer to full study extent in Figure 2. (Phosphorus sources: MinP=mineral fertilizer; ManP=manure; BG=background losses; SdP=scattered dwellings; PS=point sources).

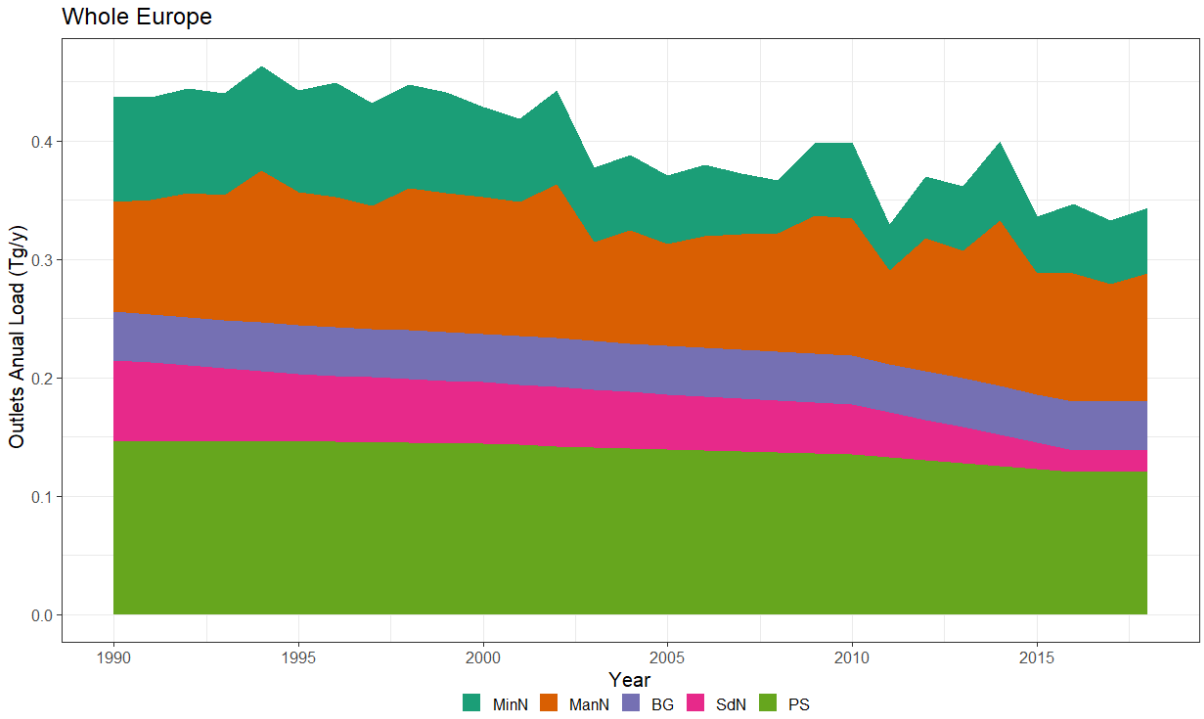

Figure 25. Phosphorus loads to the seas in four marine regions: ANS=Greater North Sea; BAL=Baltic Sea; BLK=Black Sea & Sea of Marmara; MWE=Western Mediterranean Sea. (Phosphorus sources: MinP=mineral fertilizer; ManP=manure; BG=background losses; SdP=scattered dwellings; PS=point sources).

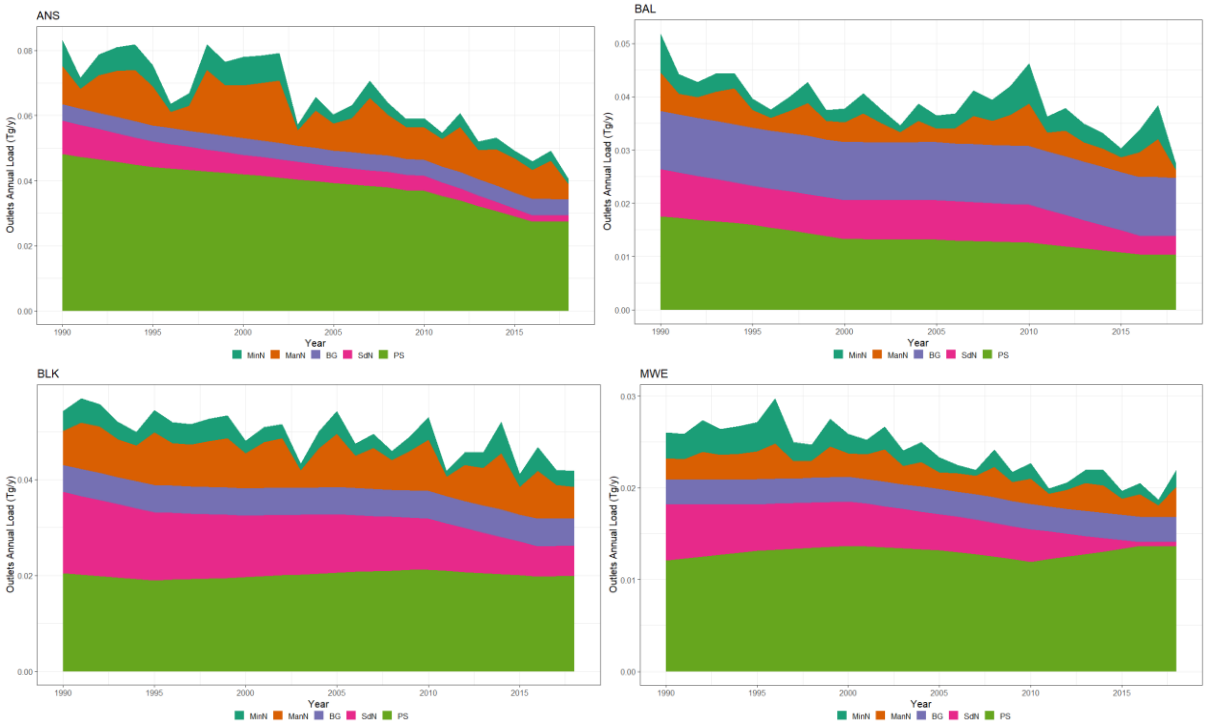

3.2.3 N:P ratio in marine regions (1990-2018)

The historic analysis showed that nutrient loads to the sea have decreased from 1990 to 2018, however phosphorus loads were reduced more than those of nitrogen. As a consequence, the ratio of N:P load ratios to marine regions changed (Figure 26). In all marine regions except the Adriatic Sea (MAD), where it remained constant at about 18, in 1990-2018 the N:P ratio increased by 0.7 in Mediterranean Sea, by 2.7 in Baltic seas, and by 4 in the Atlantic Ocean and the Black Sea. In the Greater North Sea (ANS), the already high N:P ratio in 1990-2004 (19) further increased throughout the historic period, up to 26 in 2014-2018. In the Ionian Sea and Central Mediterranean Sea (MIC) and Aegean Levantine Mediterranean Sea (MAL), the ratio N:P is generally low, but increased from about 4.5 in 1990-1994 to 6 in 2014-2018.

Nutrient imbalances affect the potential for eutrophication (e.g. Garnier et al., 2021) thus changes in N:P ratio are likely to bear consequences on the receiving marine regions. Marine modelling will help analysing the marine consequences of these imbalances more in depth.

Figure 26. Nitrogen:phosphorus load ratios in marine regions. Marine Regions: ABI=Bay of Biscay & Iberian Coast; ACS=Celtic Seas; ANS=Greater North Sea; BAL=Baltic Sea; BLK=Black Sea & Sea of Marmara; MAD=Adriatic Sea; MAL=Aegean Levantine Mediterranean Sea; MIC=Ionian Sea and Central Mediterranean Sea; MWE=Western Mediterranean Sea.

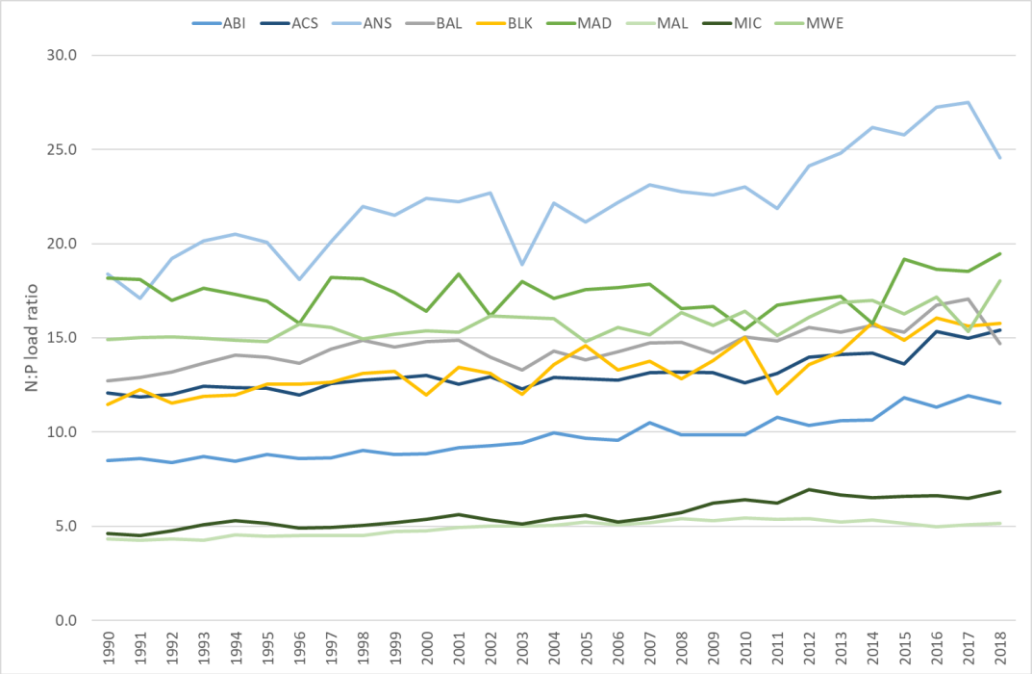

3.2.4 Nutrient concentrations in the surface waters (1990-2018)

Lowering of nutrient inputs from land helped reducing nutrient pollution in rivers and lakes. Figure 27 shows the shares of stream network length (in km of CCM2 reaches) whose mean annual nutrient concentration could be considered low (<2 mg N/L or < 0.1 mg P/L), medium, or high (=> 5 mg N/L or 0.5 mg P/L). To reduce the influence of hydrological cycle (rainfall and streamflow), the 5-yr mean annual concentrations at the beginning and end of the study period are compared. From 1990 to 2018, the share of reaches in low nitrogen concentration raised by 8% whereas reaches with high concentration lowered by 7% (from 21% at the beginning to 14% at the end of the study period).

In all regions improvements could be noted (Table 7, Figures 28 and 29). The highest reduction of reach length in high concentration class occurred in the Greater North Sea region (ANS, -18%), but important improvements also occurred in Aegean Levantine Mediterranean Sea (MAL) and Ionian Sea and Central Mediterranean Sea (MIC). Concurrently, the share in low N concentration class increased by more than

10% in Bay of Biscay & Iberian Coast (ABI), Aegean Levantine Mediterranean Sea (MAL), Ionian Sea and Central Mediterranean Sea (MIC) and Western Mediterranean Sea (MWE), thus generally in the Mediterranean Sea region. The share of reach length in low P class increased by 15% in Europe, whereas the share of reach length in high P class decreased from 15% to 9%, with the most important reductions in high P class shares occurring in Bay of Biscay & Iberian Coast, Aegean Levantine Mediterranean Sea, and Ionian Sea and Central Mediterranean Sea.

Figure 27. Shares of nutrient classes in low, medium and high concentrations in 1990-1994 and 2014-2018. Values refer to the study extent in Figure 2 except the Barents, Norwegian and White Seas.

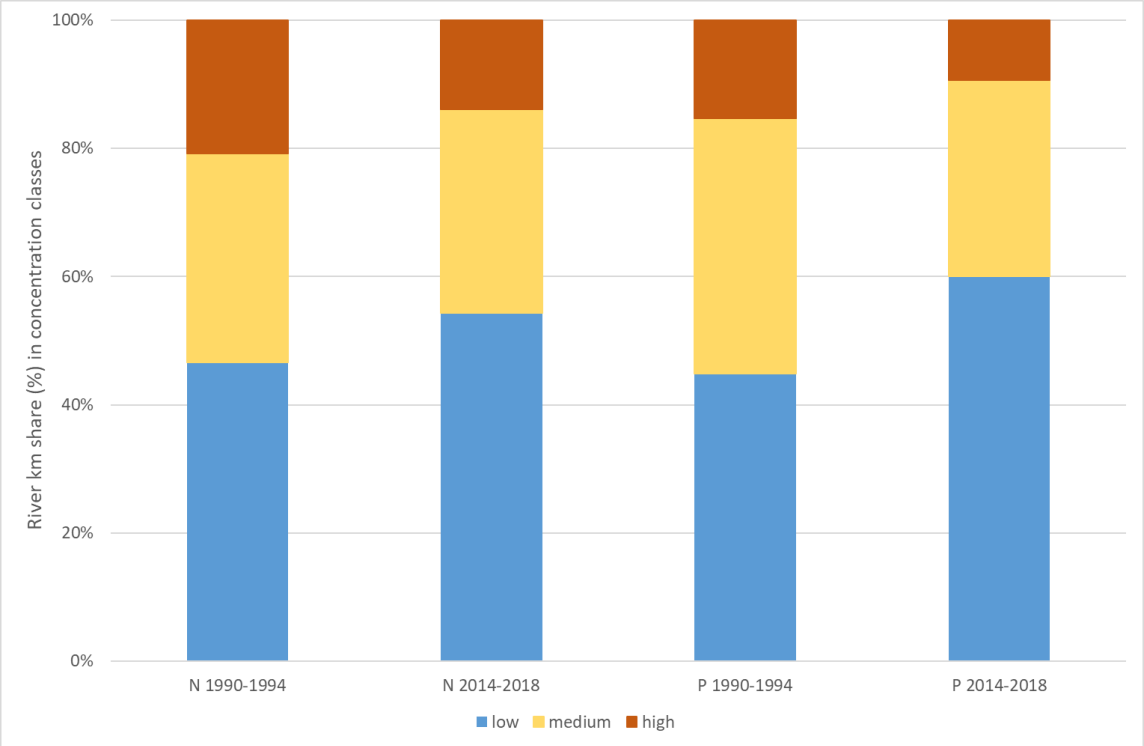

Table 7. Shares of stream network length with high (>=5 mg N/L or >= 0.5 mg P/L) mean annual concentration per marine region area.

Marine region([1])	Share of network in high nitrogen		Share of network in high phosphorus class	
	1990-1994	2014-2018	1990-1994	2014-2018
ABI	28%	19%	27%	14%
ACS	7%	4%	7%	3%
ANS	37%	19%	9%	3%
BAL	7%	5%	4%	2%
BLK	15%	10%	10%	4%
MAD	14%	11%	6%	4%
MAL	47%	35%	68%	52%
MIC	32%	23%	57%	37%
MWE	21%	20%	14%	13%
TOTAL	21%	14%	15%	9%

([1]) Marine Regions: ABI=Bay of Biscay & Iberian Coast; ACS=Celtic Seas; ANS=Greater North Sea; BAL=Baltic Sea; BLK=Black Sea & Sea of Marmara; MAD=Adriatic Sea; MAL=Aegean Levantine Mediterranean Sea; MIC=Ionian Sea and Central Mediterranean Sea; MWE=Western Mediterranean Sea. TOTAL values refer to the study extent in Figure 2 except the Barents, Norwegian and White Seas.

Figure 28. Mean annual nitrogen concentration in surface waters. Above: 1990-1994, below 2014-2018.

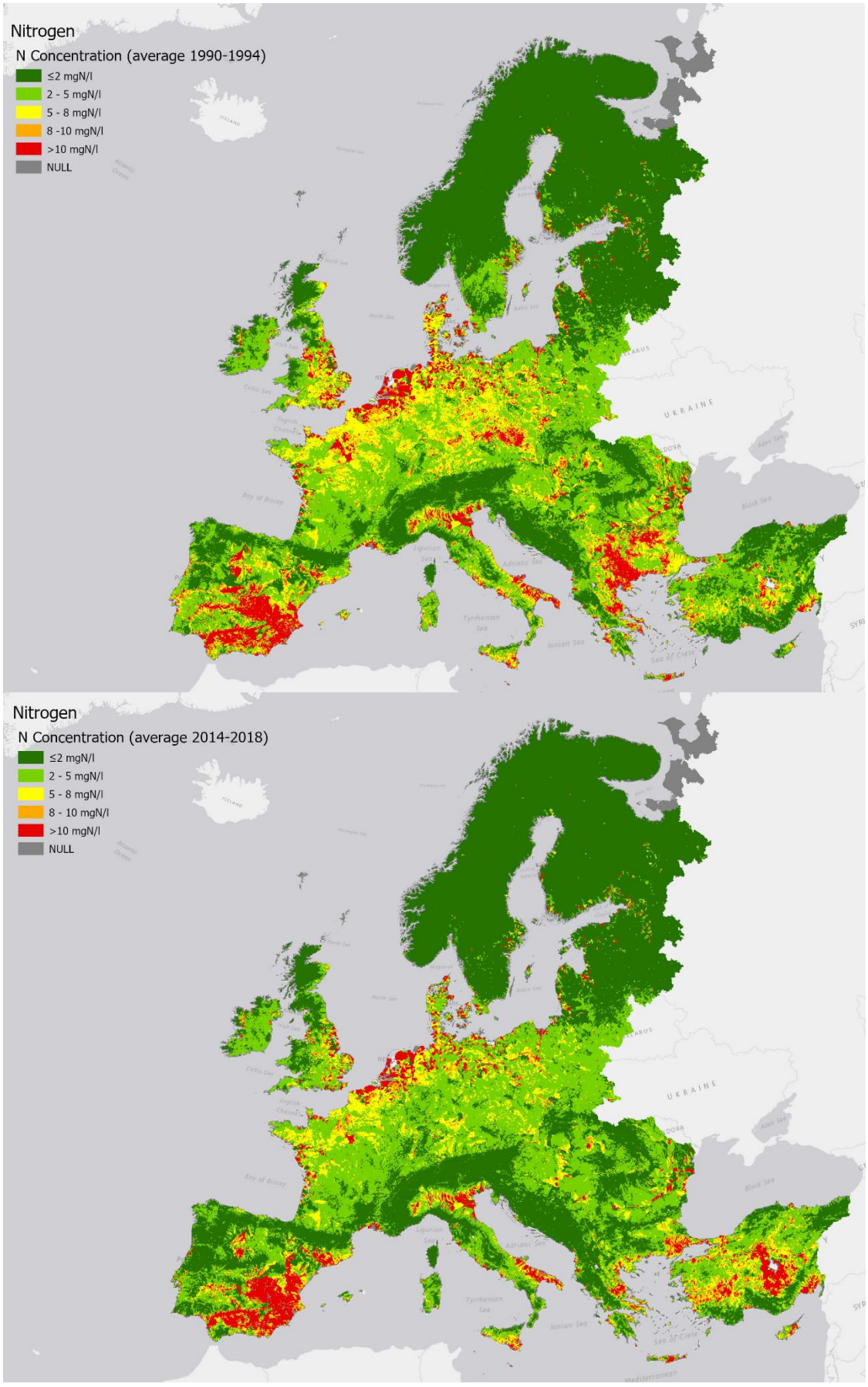

Figure 29. Mean annual phosphorus concentration in surface waters. Above: 1990-1994, below 2014-2018.

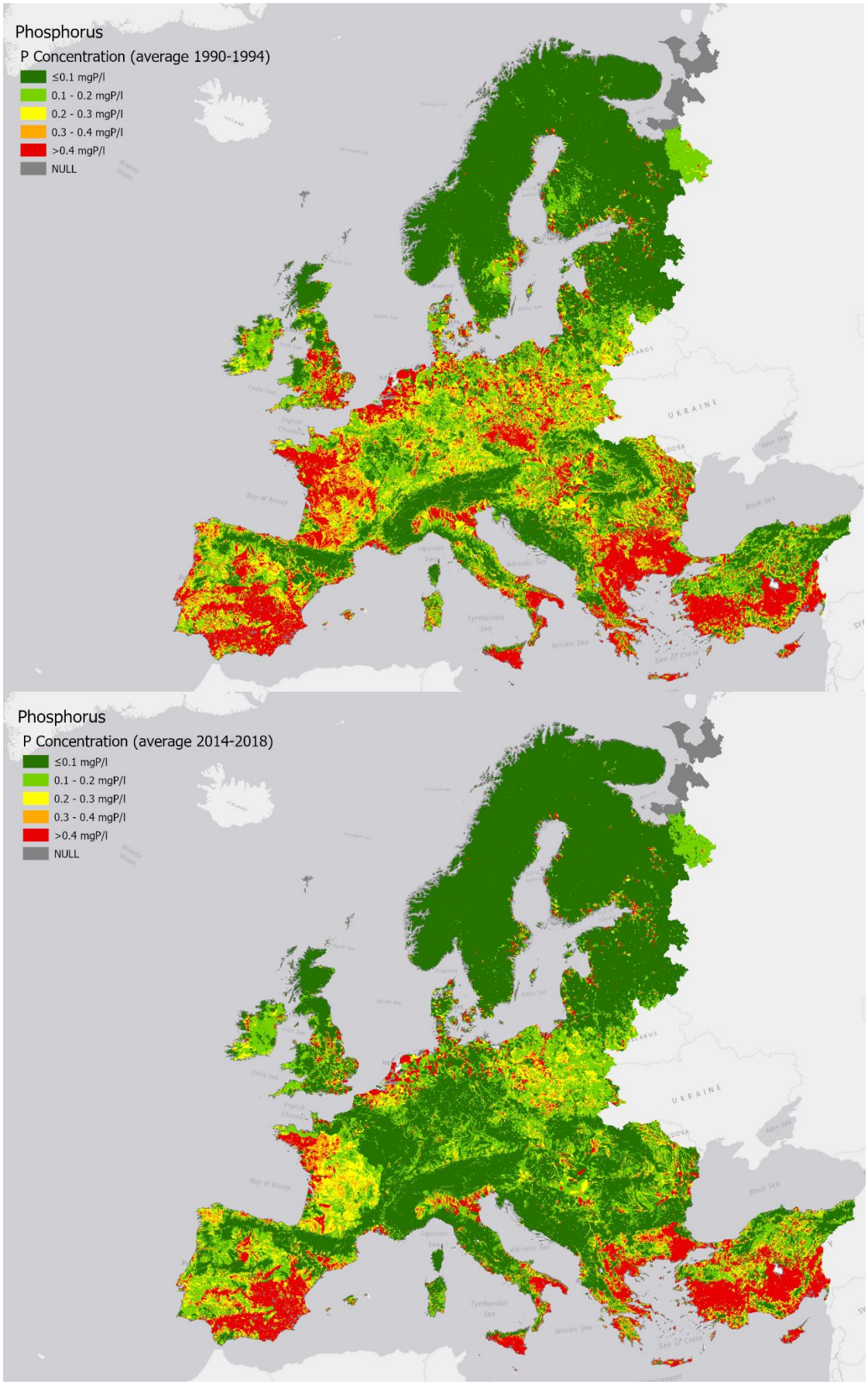

4 Scenarios of measures

This Section (Deliverable 2.2 part 2) describes the scenarios of measures to reduce water scarcity (Section 4.1) and nutrient pollution (Section 4.2) in European freshwater that were developed in the project Blue2.2 and used in marine modelling for the scenario analysis (Macias et al. 2022).

4.1 Water quantity

With the balance of water demand and water availability changing toward increased water scarcity in various parts of Europe, measures reducing net water consumption need to be implemented. Compared with the previous phase of the BLUE2 project we have additional data available for the water saving measures (Table 8). The data from Benitez Sanz et al. (2018) who assessed the WFD Programs of Measures submitted by the EU Member States and extracted investment data is complemented with waste water reuse and desalination data from Pistocchi et al. (2017).

Table 8. Water saving measures evaluated in the BLUE2 and BLUE2.2 project.

	Irrigation efficiency		**Waste water reuse**		**Energy water usage**		**Urban water savings**		**Desalination**	
	BAU	HAS	BAU	HAS	BAU	HAS	BAU	HAS	BAU	HAS
BLUE2	√	√	Only Spain	-	√	√	√	√	-	-
BLUE2.2	√	√	Only Spain	√	√	√	√	√	-	√

In BLUE2.2 we evaluate 5 different measures that may reduce water abstraction and net water consumption (abstraction minus return flows):

- Increasing irrigation efficiency in agriculture
- Increasing urban water efficiency by reducing leakage
- Re-using treated urban waste water for irrigated agriculture
- Water use efficiency in the energy sector by cooling water requirements
- Use of desalination of sea water for public water use

We describe the measures below and will explain which scenarios are identified as a baseline scenario (REF), a Business As Usual (BAU) scenario, and a High Ambition Scenario (HAS). In the next chapter we will then evaluate the impact of these measures on water resources in Europe. The results in this report are partially published in De Roo et al. (2021).

4.1.1 Irrigation Efficiency

As part of the European Member States (MS) River Basin Management Plans and Regional Investment Plans, countries are planning to invest in their irrigation areas to make them more water efficient, often changing the irrigation method from surface and sprinkling toward drip irrigation. The reported investments in irrigation efficiency as planned by MS and collected by Benitez Sanz et al. (2018) were used in the LISFLOOD-EPIC model (Gelati et al., 2020), where we can distinguish between the type of irrigation applied: surface including rice paddies, sprinkling and drip. Within LISFLOOD-EPIC we account in every single model pixel of 5x5 km for the percentage of forests, urban area, open water, crops (32 crops including paddy rice), and other land uses. For each crop in each pixel we can indicate rainfed and irrigated areas and, within the latter, the extent to which each irrigation method is applied.

In Figure 30a the actual irrigated areas for the 27EU+UK countries are given. Countries reported to have the largest absolute area of irrigation are Spain, Italy, France and Greece, followed by Portugal, Germany and Denmark. Benitez Sanz et al. (2018) collected the reported investments in irrigated area up to 2030. The investments are then translated into percentage efficiency gains in irrigation systems for the BAU (Figure 30b) and HAS (Figure 30c). Most MS plan only marginal new investments in irrigation efficiency up to 2030 in the BAU scenario resulting in a marginal shift from sprinkler to drip irrigation. For the HAS scenario, additional investments show a more stringent shift towards drip irrigation compared to the reference scenario.

Figure 30. Current (Eurostat, 2017), planned and additional investments in the BAU and HAS scenario (a) and the change in irrigation systems compared to the reference for the BAU (b) and HAS (c) scenarios.

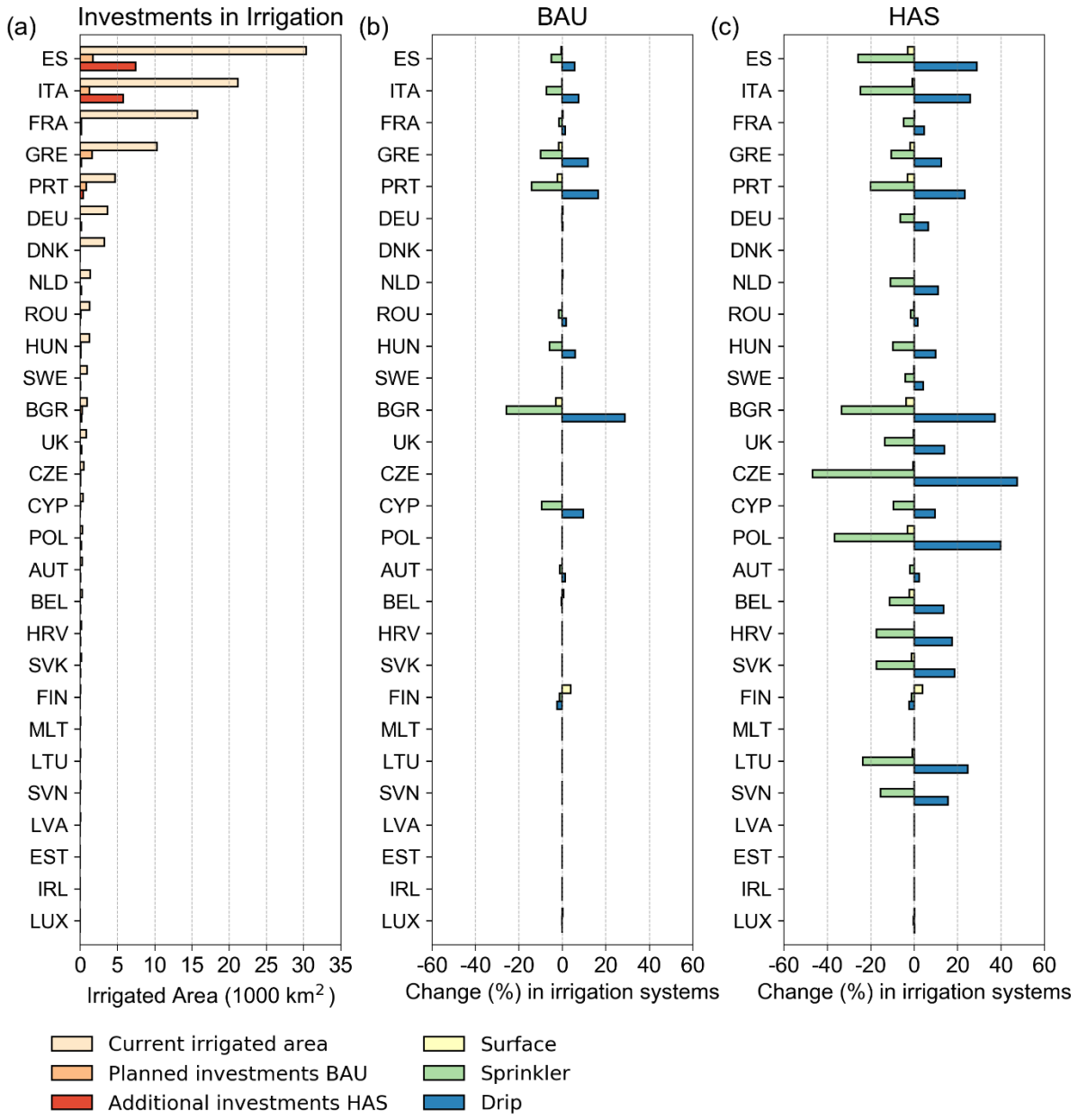

4.1.2 Urban Water Use Efficiency: Leakage Reduction

The second measure to potentially reduce water scarcity issues that is considered in this study is a reduction of leakage of the public water supply network. In Figure 31a the leakage fraction averaged at a country scale are presented. In the reference scenario, losses from urban water networks in Europe range from around 5% in Germany and The Netherlands up to 40–50% in Malta and Ireland (Benitez Sanz et al., 2018). Water scarce countries such as Spain (29% leakage), Italy (38%), Greece (21%) and Cyprus (24%) all lost considerable amounts of water in the public supply network. Benitez Sanz et al. (2018) used the public investments plans by the European countries envisaged between 2016 and 2027 to estimate the efficiency improvements that could be reached in the urban water supply (BAU). In most cases, the changes in the BAU scenario for water losses are only marginal as compared to the reference situation: less than 1% change in the total water losses.

For the HAS we assumed here that urban water efficiency would be raised in all MS to 5% losses – the actual loss percentage in the Netherlands. The requirement investment of this water loss reduction is calculated in Benitez Sanz et al. (2018). Changes to reach the HAS scenario are substantial, and also require substantial investments.

Figure 31. Average leakage fraction in the urban water supply (a) and (b) waste water reuse scenarios in function of the cost per m3 per MS.

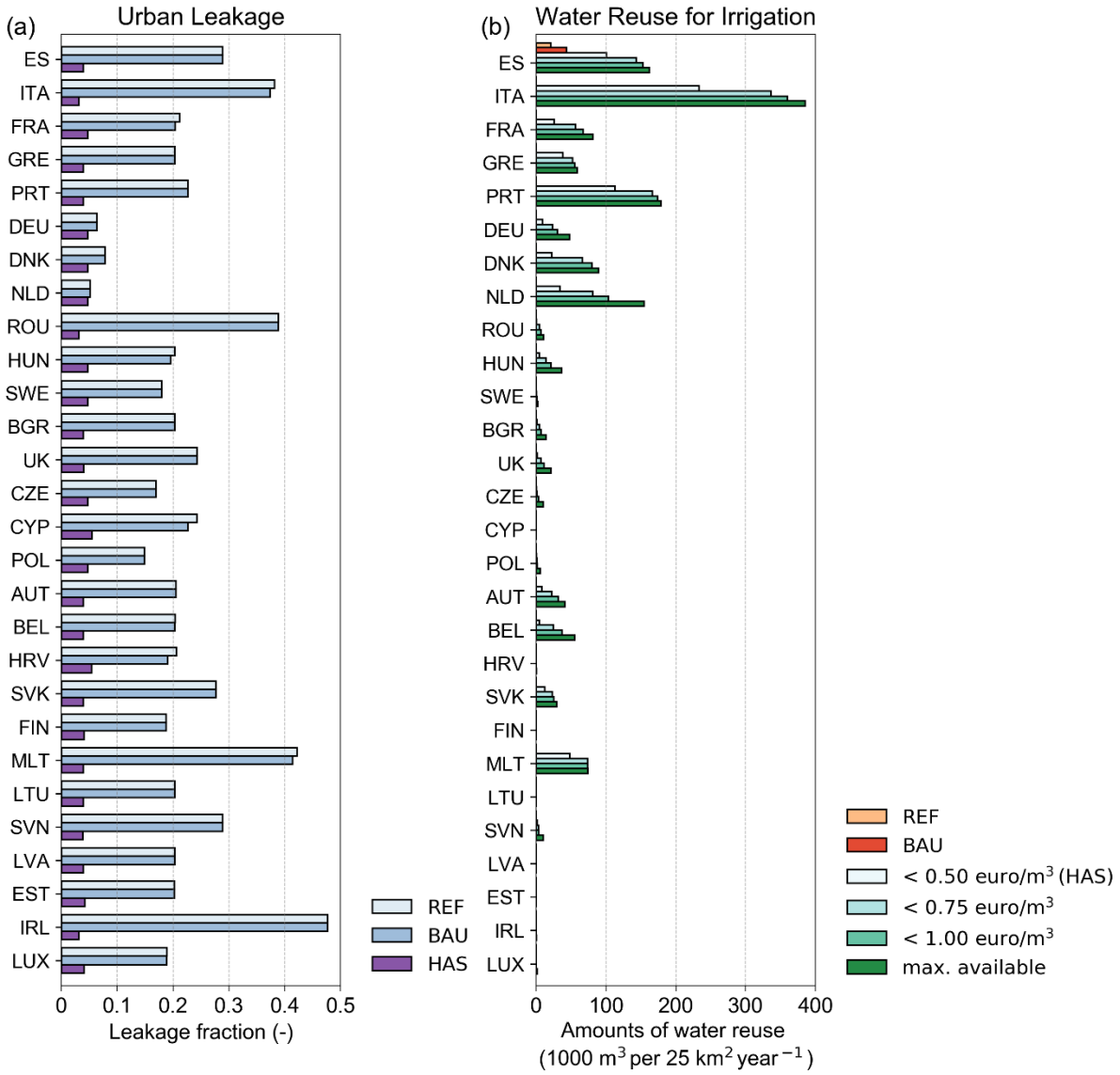

4.1.3 Water reuse

The third type of measure we considered in this work is water reuse. Reuse of treated wastewater for agricultural irrigation is a possible measure to reduce water stress. In a European scale hydro-economic analysis, Pistocchi et al. (2017) quantified the volumes of treated domestic wastewater that could be reused in agriculture at a cost below given thresholds. The costs were appraised including the additional treatment of wastewater effluents in order to meet European quality standards, as well as the cost of transport and storage of water. The volume of wastewater that may be reused economically depends for a large part on the distance between a wastewater treatment plant and the irrigated areas, and varies significantly across Europe. Pistocchi et al. (2017) estimated the volumes of treated wastewater available for irrigation in all European regions at levelled costs—including Capital expenditure (CAPEX) and Operational Expenditure (OPEX)— below 0.25, 0.50, 0.75, and 1 euro/m3. The scenario with costs not exceeding a threshold of 0.25 euro/m3 yields in very little water reuse, and has been omitted here. In Figure 31b the amounts of water reuse at a cost per m3 are presented at a country scale. Water reuse for irrigation can be an important water saving measure in Italy, Portugal and Spain. For the BAU scenario we used the planned wastewater reuse for irrigation until 2027 reported by Benitez Sanz et al. (2018), which covers only Spain (Figure 31b). For the HAS scenario we selected the amount of waste water reuse with costs not exceeding a threshold of 0.50 euro/m3, which is still a rather conservative scenario.

4.1.4 Cooling water in the energy sector

Another change in water consumption can be achieved by changes in the energy sector. In the energy sector, water is used for cooling (Magagna et al., 2019). Water is used throughout the energy industry, and the water system needs energy for collecting, pumping, treating and desalinising water. Increasing water and energy needs, or changes in water availability due to climate change could have significant effects on the energy system.

Water use in the energy industry depends on:

- The energy demands by society
- The energy mix, i.e. the part of energy generated by thermal power stations that need cooling
- The cooling type of the power station and the water use efficiency

The water requirements for the energy sector are based on the Global Energy Climate Outlook (GECO) projections up to 2050 (Kitous et al., 2016). The GECO scenarios were modelled using a common set of socio-economic assumptions (population, economic growth) and energy resources. In Figure 32a we present the projected future water requirements for the energy sector. The REF, BAU and HAS scenario are corresponding with the years 2015, 2030 and 2050 respectively from the reference scenario of the GECO. The HAS scenario needs less water requirements for cooling compared to the BAU and REF scenarios due to the projected increase of renewable energy sources over time.

Figure 32. Energy efficiency scenarios in the cooling water requirement (a) and (b) desalination scenarios at estimated cost of supplying desalinated water expressed as the fraction of served population per relevant MS.

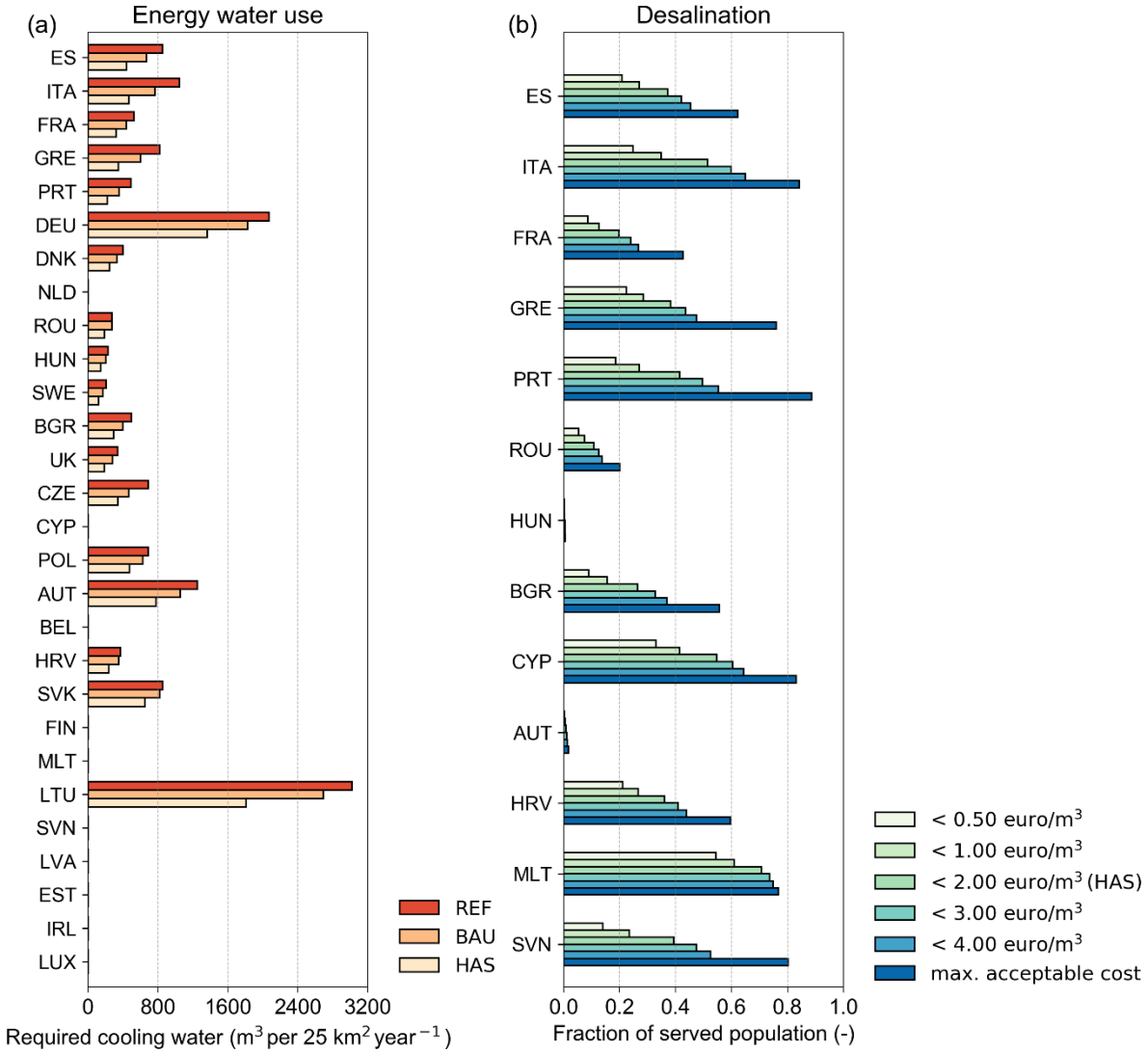

4.1.5 Desalination

A net reduction of consumptive water use is provided by desalination. Although largely regarded as a "brute force"—last resort solution—until recent times, desalination is increasingly affordable and may be turned into a sustainable solution with appropriate planning (Pistocchi et al., 2020). Pistocchi et al. (2018) estimated the cost of supplying desalinated water, taking into account the costs of developing and maintaining the infrastructure, and of pumping desalinated water inland from coastal areas. While desalinated water is in principle unlimited, its supply is constrained by the acceptable costs. We estimated the population potentially served by desalination in all European regions at levelized costs, presented in Figure 32b. For the BAU scenario, desalination is not considered and for the HAS desalination scenario a levelized cost not exceeding the 2 euro/m^3 is used. From here, a volume of wastewater potentially available for reuse is determined by the supply per capita and the percentage of the supply that ends up in the wastewater treatment plant. In this exercise, we estimate the supply per capita at 200 l/person/day, and the percentage ending in wastewater at 80%.

4.2 Water quality (nutrients)

For the construction of the scenarios of measures, we quantified possible reduction of nitrogen and phosphorus input from the major sources of point and diffuse nutrient pollution in the river basins, namely domestic waste water discharges, agriculture, and atmospheric deposition (for nitrogen), corresponding to nutrient reduction measures under different EU policies. We developed the spatial input data and run the GREEN model for several scenarios (Table 9):

- Reduction of nutrient discharges from domestic wastewaters. Five scenarios (PS1, PS2, PS3, PS4 and PS5) were prepared, supporting the Impact Assessment of the revision of the UWWT Directive. They include the full compliance with the measures established in the UWWTD (PS1), and a combination of additional measures for extending the efficiency of the level of treatment and the extent of the Sensitive Areas (where more stringent treatments are necessary) (The scenarios were developed in the ongoing Impact Assessment for the UWWTD revision, JRC Unit D2. They are presented in Pistocchi et al. (under review), see also Table 10).
- Reduction of nutrient emissions from agricultural sources. Two scenarios of nutrient reduction in the agricultural sector developed by the CAPRI model were considered. In specific the current CAP (business as usual scenario, capriBAU) and the implementation of the new CAP legislative proposal plus measures to achieve the Green Deal targets also using New Generation EU Funds (capriHAS) (Barreiro-Hurle et al. 2021). The work was developed in collaboration with the JRC Unit D4-D5.
- Reduction of nitrogen input from atmospheric deposition (ATM). A scenario of atmospheric nitrogen deposition reduction was developed by the EMEP model considering the measures adopted by the Commission to reduce atmospheric emissions by 2030 in the Fit for 55 package (the work was developed in collaboration with the JRC Unit C5 in the context of the project 'Knowledge for INMAP', Pisoni et al. under review).
- Reduction of different nutrient sources concurrently. A combined scenario (INMAX) was developed considering the highest nutrient reduction in the different sources simultaneously. The scenario represents the simultaneous implementation of measures in different sectors. It is a combination of the previous sectoral scenarios PS5, capriHAS and ATM.

Under future climate, two scenarios combining water quantity and nutrient reduction measures were constructed:

1. a Business As Usual scenario (BAU), which includes the BAU water quantity measures (see Section 4.1) and full implementation of the current UWWT Directive (scenario PS1) and old CAP policy (capriBAU);
2. a High Ambition Scenario (HAS), which encompasses the most ambitious water quantity (see Section 4.1) and nutrient reduction measures (scenario INMAX=PS5+ATM+capriHAS).

The scenarios of nutrient reduction offer an estimation of the impacts of sectoral measures (PS1, PS2, PS3, PS4, PS5, ATM, capriBAU, capriHAS) and their cumulative effects (INMAX), considering that water quantity and climate remain unchanged. On the other end, the scenarios of water quantity and quality (BAU, HAS) provide insight on the possible evolution of freshwater quality under the business as usual and the implementation of more ambitious EU environmental policies or strategies, some of which already in place (taking into account that water availability will also affect nutrient loads to the sea). In the Blue2.2 project, the latter scenarios have been run by the marine models to assess the improvements of sea ecosystem that could be achieved in view of the objectives of the MSFD (Macias et al. 2022).

Table 9. Scenarios of measures for nutrient reduction assessed by the model GREEN.

Scenario	Climate and period of simulation	Measures			
		Water quantity([1])	Point Sources	Agricultural	Atmospheric emissions
PS1	Historical climate (1990-2018)	Historical	UWWTD full compliance	Historical	Historical
PS2	Historical climate (1990-2018)	Historical	Extend Sensitive Areas	Historical	Historical
PS3	Historical climate (1990-2018)	Historical	Increase efficiency	Historical	Historical
PS4	Historical climate 1990-2018	Historical	Extend Sensitive Areas + Increase efficiency (PS2+PS3)	Historical	Historical
PS5	Historical climate (1990-2018)	Historical	Extend Sensitive Areas + Increase efficiency + lower Population Equivalent limit (PS4+lower PE)	Historical	Historical
ATM	Historical climate (1990-2018)	Historical	Historical	Historical	Air emissions reduction by 2030 in the EU Fit For 55 package
capriBAU	Historical climate (1990-2018)	Historical	Historical	CAP 2013-2020 (business as usual scenario) Baseline 2030	Historical
capriHAS	Historical climate (1990-2018)	Historical	Historical	Combined effects of F2F and BDS strategies targets with the new CAP and the Next Generation EU (NGEU)	Historical
INMAX	Historical climate (1990-2018)	Historical	As scenario PS5	As scenario capriHAS	As scenario ATM
REF	Future climate (2005-2030)	Historical (2018)	Historical (2016)	Historical (2018)	Historical (2018)
BAU	Future climate (2005-2030)	BAU	As scenario PS1	As scenario capriBAU	Historical (2018)
HAS	Future climate (2005-2030)	HAS	As scenario PS5	As scenario capriHAS	As scenario ATM

([1]) Water quantity estimated with LISFLOOD.

Table 10. Description of the UWWT Directive Impact Assessment scenarios.

Scenario	Scenario description	Area	Efficiency	Population Equivalents (PE)	Blue2.2 scenario analysis
PS0	Current situation (around 2016)	Sensitive Areas (SA)	According to level of treatment reported by country	As reported by country	historical
PS1	Full compliance	Current SA	80% N; 90% P	10000	Business As Usual
PS2	Extend SA	ALL country	80% N; 90% P	10000	
PS3	Increase efficiency	Current SA	90% N; 95% P	10000	
PS4	Extend SA + Increase efficiency (PS2+PS3)	ALL country	90% N; 95% P	10000	
PS5	Extend SA + Increase efficiency + lower PE limit (PS4+lower PE)	ALL country	90% N; 95% P	2000	High Ambition Scenario

Source: Pistocchi et al. (under review).

4.2.1 Reduction of nutrient input in EU27 countries

The scenarios of measures developed in the study (Table 9) foresee a decrease of N input in EU27 compared to current values up to 45% for domestic wastewaters (PS5), 65% for atmospheric deposition (ATM), and 39% for mineral and manure fertiliser application (capriHAS). Concerning P, the reduction in EU27 is up to 52% for domestic wastewater (PS5) and almost 10% for mineral and manure fertiliser application (capriHAS) (Table 11). Nutrient reduction in the scenarios INMAX, BAU and HAS are a combination of the measures foreseen in the scenarios PS1, PS5, ATM, capriBAU, and capriHAS (for the combination see Table 9). Reduction of N and P input per EU27 countries in the different scenarios are shown in Figures 33, 34 and 35.

Table 11. Nutrient inputs in EU27 from domestic wastewater, atmospheric deposition (for N) and agricultural fertilizers (mineral and manure) in the current situation (average 2014-2018), and relative changes under the scenarios of measures analyzed (presented in Table 9). The scenario INMAX is a combination of measures: PS5 + ATM + capriHAS. Values refer to full study extent in Figure 2.

	Current	**Scenarios**							
	Average 2014-2018	PS1	PS2	PS3	PS4	PS5	ATM	Capri BAU	Capri HAS
Nitrogen input	(ton N/y)	Change (%)							
Point sources and scattered dwellings	875963	-6	-16	-21	-39	-45			
Atmospheric deposition	3756063						-65		
Agricultural fertilisers (mineral and manure)	16242454							-15	-39
Phosphorus input	(ton P/y)	Change (%)							
Point sources and scattered dwellings	88336	-11	-28	-22	-44	-52			
Agricultural fertilisers (mineral and manure)	3164657							5	-10

Figure 33. Nitrogen (above) and phosphorus (below) input to surface water from domestic wastewaters (point sources plus scattered dwellings) per EU27 countries under current situation (Current, data of 2016) and five scenarios of reduction: full compliance UWWT Directive (PS1) and a combination of additional measures for extending the efficiency of the level of treatment and the extent of the Sensitive Areas (PS2-PS5).

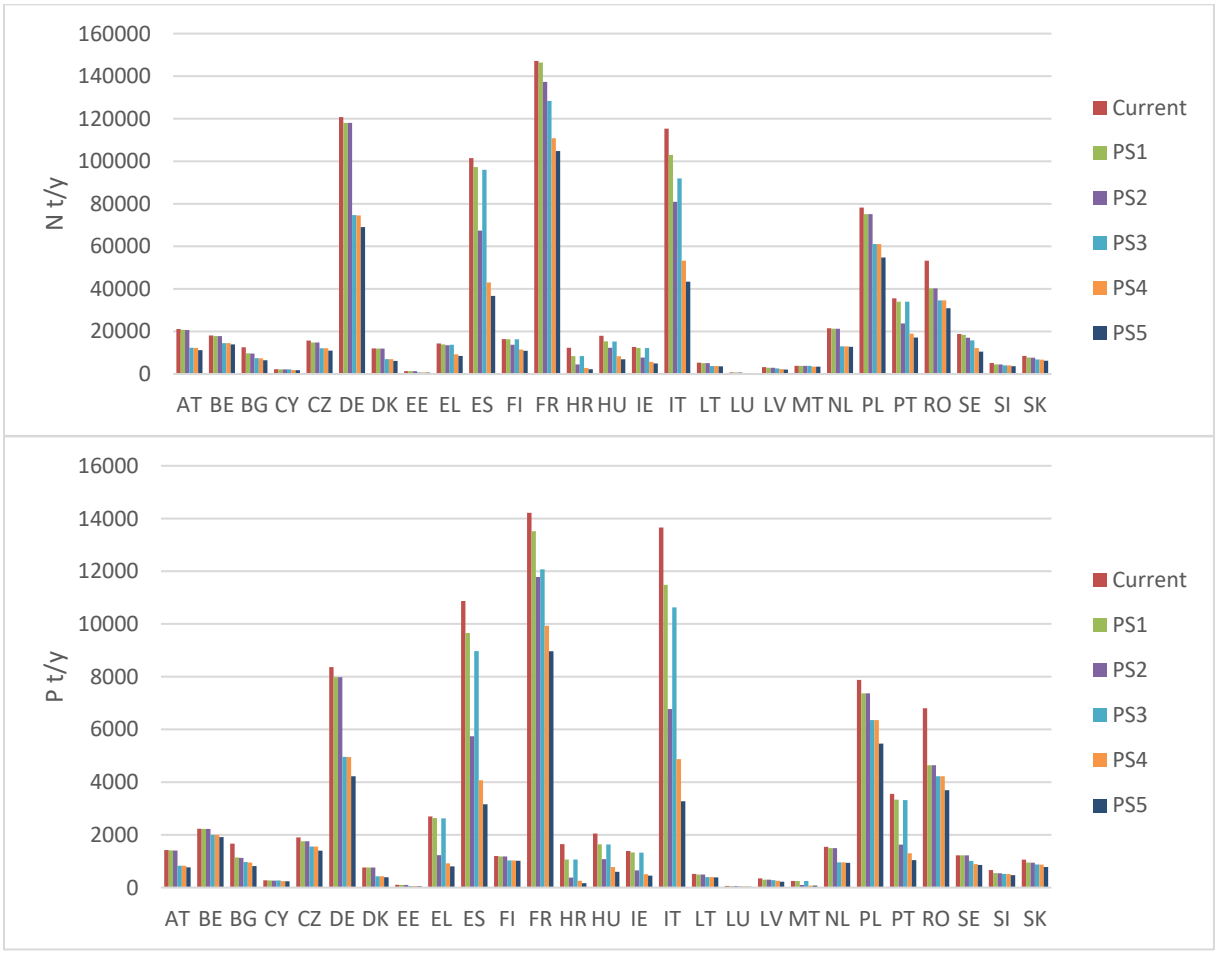

Figure 34. Nitrogen input to land from atmospheric deposition per EU27 countries under current situation (Current, average values 2014-2018) and the scenario Fit for 55 package (ATM).

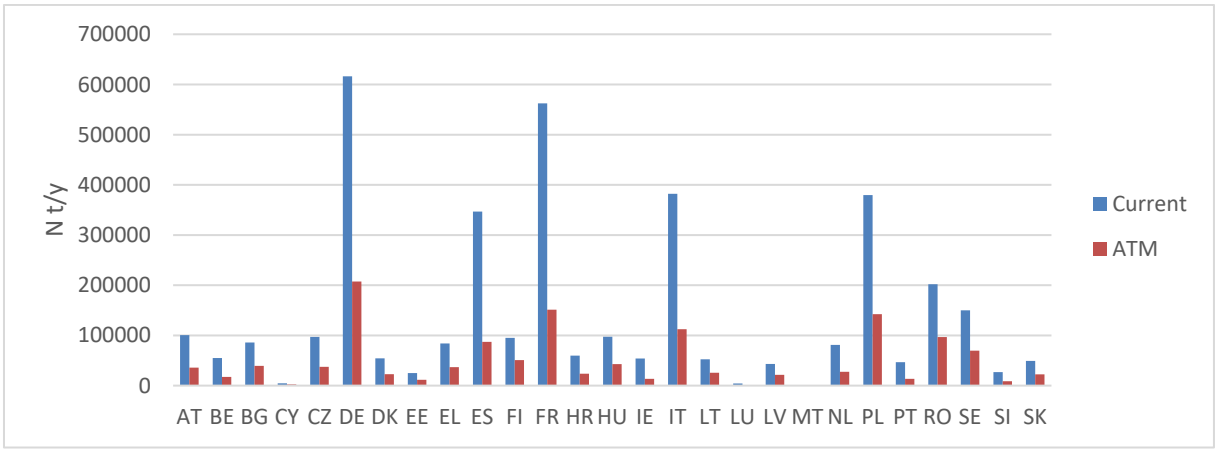

Figure 35. Nitrogen (above) and phosphorus (below) input to agricultural land from mineral and manure input from agriculture per EU27 countries under current situation (Current, average values 2014-2018) and two CAPRI scenarios of reduction: Business As Usual (capriBAU) and implementation of the new CAP legislative proposal plus measures to achieve the Green Deal targets also using New Generation EU Funds (capriHAS).

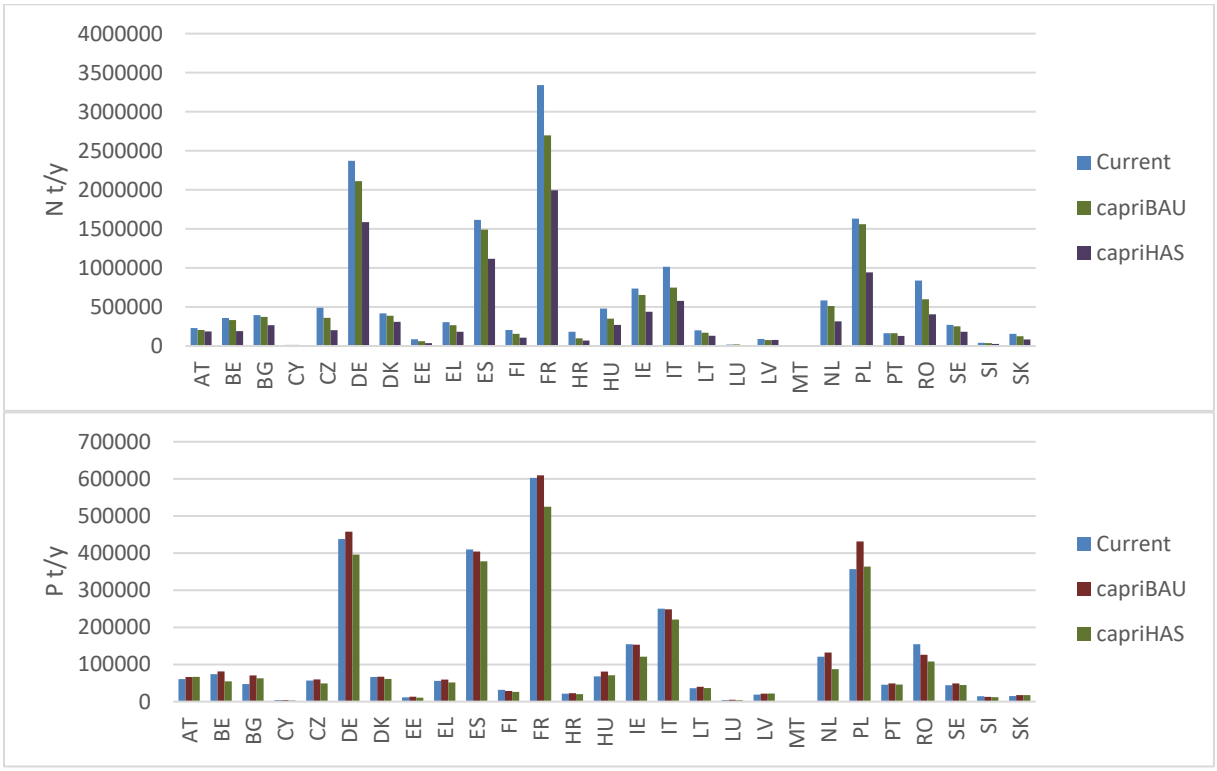

5 Scenarios analysis

This Section (Deliverable 2.3) describes the results of the scenarios analysis for European freshwater developed in the project Blue2.2. We present the effects of measures for fighting water scarcity and reducing nutrient pollution in freshwater considering the current climate condition (Section 5.1) and under future climate (Section 5.2). The latter were used in the project Blue2.2 as input for the marine modelling scenario analysis.

Hydrological simulations have been performed with the LISFLOOD-EPIC water resources model. Using the measures, the weather and climate data, the LUISA land use projections, as well as population projections for Europe. A set of scenarios for freshwater quantity analysis have been evaluated for:

- A reference situation (REF)
- A BAU scenario including the reported MS planned measures
- A HAS scenario for all individual measures

The scenarios are simulated with:

- Observed climate (1990-2018)
- EURO-CORDEX control climate (1981-2005) from the MPI-ESM-LR model downscaled with the COSMO-CLM model to evaluate the impact of climate change.
- The future climate (2005-2030) from the MPI-ESM-LR model downscaled with the COSMO-CLM model for the RCP4.5 emission scenario.

Nutrient loads to inland waters and European seas were estimated with the model GREEN for different scenarios. First, we analyzed the effects of measures for reducing nutrient pollution in water, considering the current climate condition and water management, looking at sectoral measures addressing domestic waste waters, atmospheric deposition and agricultural sources (scenarios PS1, PS2, PS3, PS4, PS5, ATM, capriBAU, capriHAS) and their cumulative effects (scenario INMAX). Then we assessed scenarios of measures tackling both water quantity and nutrient pollution, under future climate. In particular, we compared possible future water quality improvements following the application of the current EU policies (Business As Usual scenario, BAU) and in case of the implementation of more ambitious EU environmental policies and strategies (High Ambition Scenario, HAS).

5.1 Effects of measures of water quantity and quality under current climate

5.1.1 Water quantity

In total we have performed 24 simulations with all the individual measures and combined measures for the current climate and 13 simulations for the measures with future climate projection including 1 control climate simulations. Here we will present the impact of some of the water savings measures in the BAU and HAS scenario for the WEI abstraction and WEI+ (consumption) under current climate.

Figure 36 shows the effect of examined measures on the WEI abstraction. While the WEI and WEI+ are calculated on a sub-riverbasin basis, the results are averaged here per country to achieve a better insight for Europe. What can be deducted from the results is that irrigation efficiency improvements in the BAU scenario is the most effective measure. For the HAS scenario urban leakage reduction and desalination — in sea bordering countries — are the most effective measures. Water reuse is helpful in some countries to reduce the WEI abstraction, in particular Italy, Portugal, Spain and France.

Figure 36. Effects of water savings measures on WEI abstraction as estimated with the LISFLOOD-EPIC model.

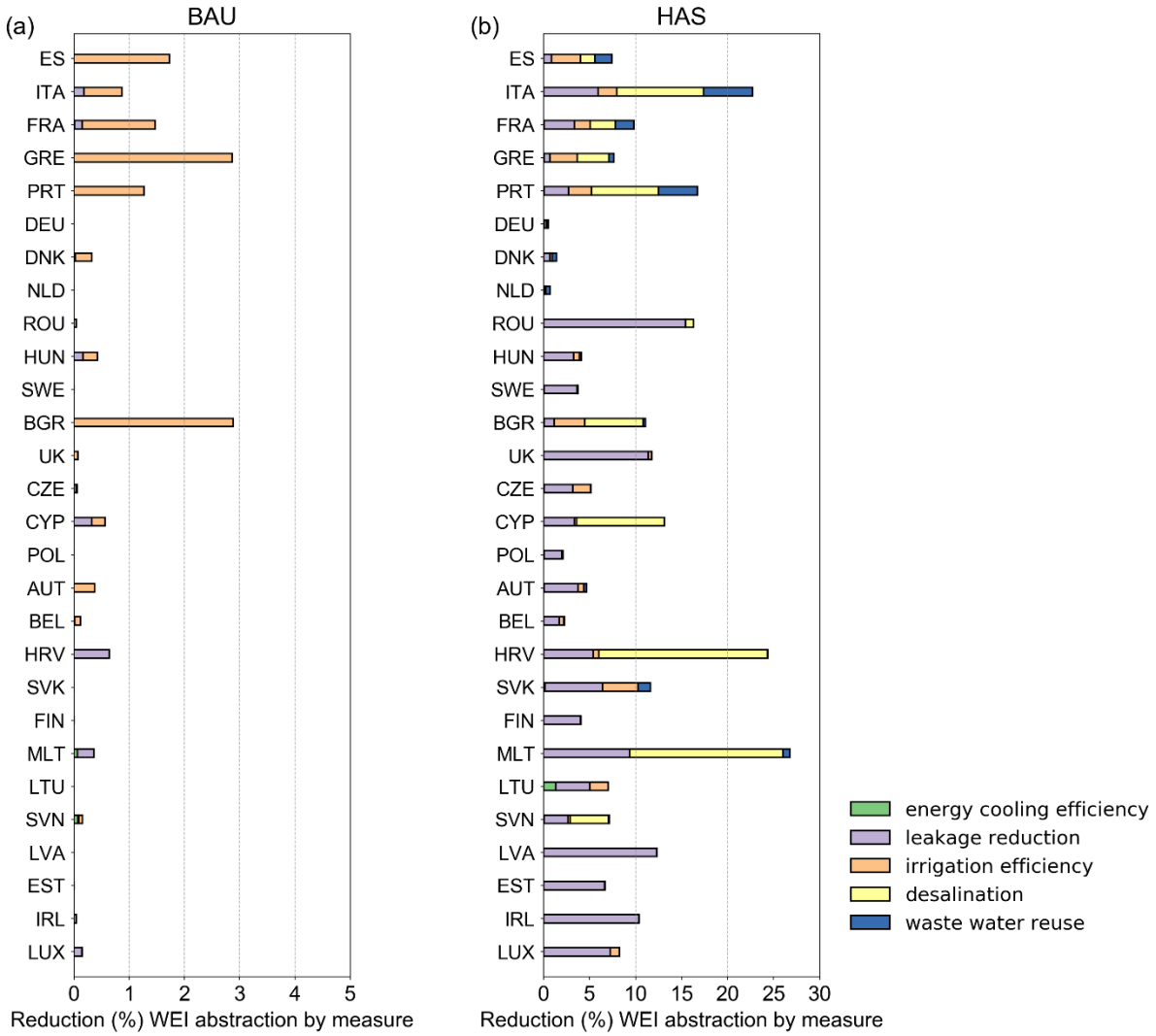

Evaluating the effect of the individual water saving measures for the BAU and HAS scenarios on net consumption, as visualized with the WEI+ indicator (Figure 37), we see that water reuse is not reducing net consumption. Water reuse is reducing new abstractions needed for irrigation, by double using the urban water later for irrigated agriculture. Leakage reduction also does not help to reduce net consumption, as the leakage is entering the subsurface hydrological system and eventually will be part of the soil and groundwater resources. Increasing irrigation efficiency is an effective measure. However, as the investments in irrigation for the MS are marginal in the BAU scenario, the reduction in the WEI+ indicator remains lower than 5% for the MS (Figure 37a), except for Bulgaria where investments in current irrigated land are relatively high. Increasing the investment in irrigation results in a further reduction of the WEI+ in the HAS scenario (Figure 37b). Desalination is also an effective measure which is only considered in the HAS scenario. Particularly in Malta, Bulgaria, Croatia and Slovakia the WEI+ could be reduced up to 20% applying these measures. In many other countries however, the effect of the measures on net water consumption and thus reduction of the WEI+ in the HAS scenario is in the order of 4% (Greece), 6% (Spain) to 8% (Italy, Portugal). It should be noted that these are country averages, and local effects may be larger.

Figure 37. Effects of water efficiency measures on WEI+ (consumption) as estimated with the LISFLOOD-EPIC model for the (a) BAU and (b) HAS. Note: water reuse does not influence WEI+ as it is used by irrigation.

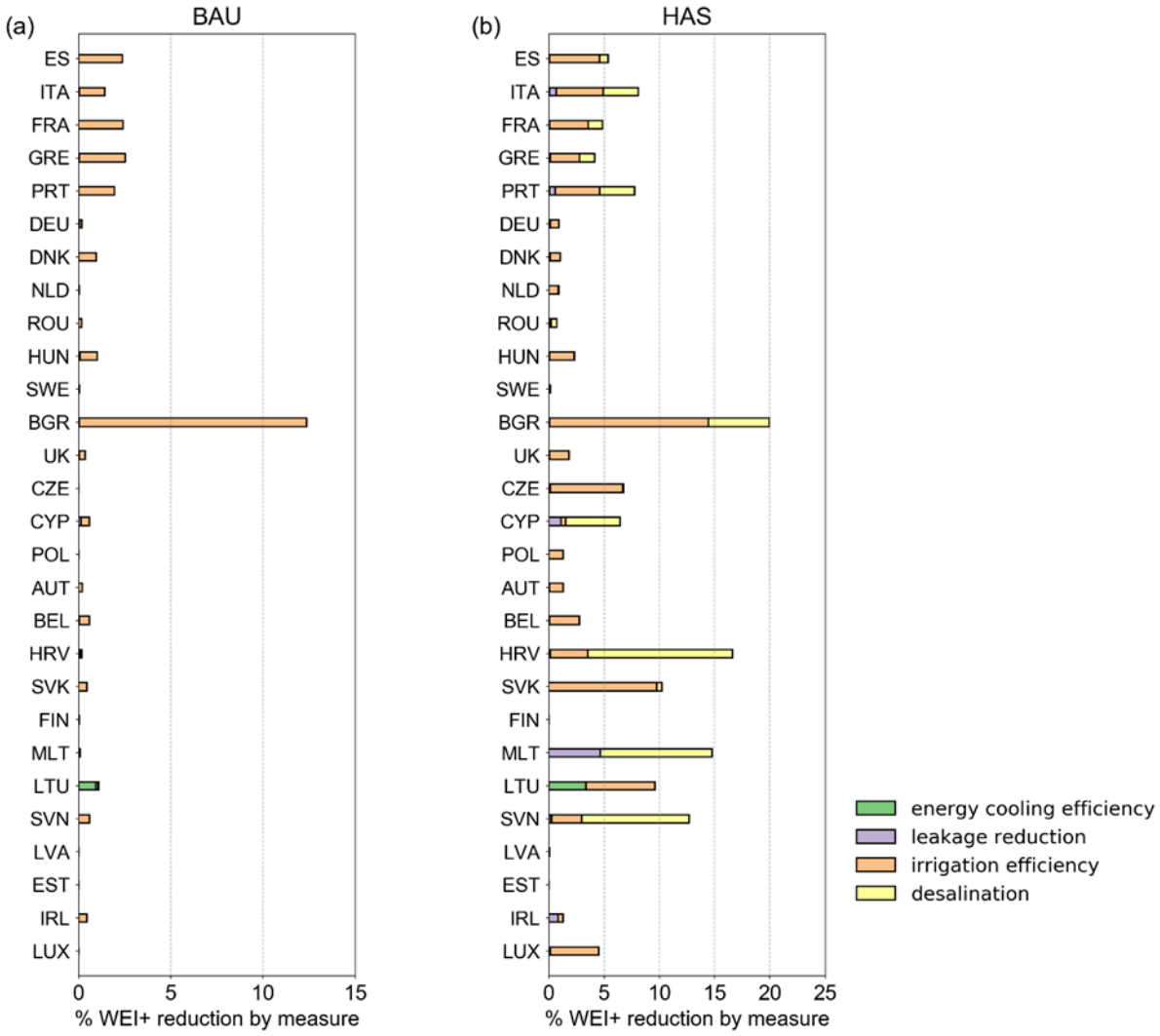

5.1.2 Water quality

5.1.2.1 Nutrient load to the European seas and sources contribution

Annual nitrogen (N) and phosphorus (P) load delivered to European seas under the different scenarios of measures were estimated by the model GREEN (Figure 38). Improvement of domestic wastewaters treatment (PS1-PS5) decreases the nutrient export to the European seas by 8% for N and 13% for P. Reduction of atmospheric nitrogen deposition (ATM) could lower the N export to the sea by 11%. Measures under the new CAP and to achieve BDS and F2F strategy targets (capriHAS) could lead to a decrease of N and P load to the seas of 13% and 3%, respectively. Adopting all the measures together could reduce the nutrients load to the European seas around 30% for N and 15% for P (Table 12).

Figure 38. Nitrogen (above) and phosphorus (below) annual riverine export from land to European seas (values refer to full study extent in Figure 2) under current condition of nutrient inputs (Current) and the scenarios of measures analysed in the study (Table 9): improvement of domestic wastewaters treatment (PS1, PS2, PS3, PS4 and PS5), reduction of atmospheric N deposition (ATM), and agricultural measures (capriBAU and capriHAS). Average annual values consider the climatology of 2014-2018. Colours represent the contribution of different sources to the total load. (For phosphorus the scenario ATM is the same as Current).

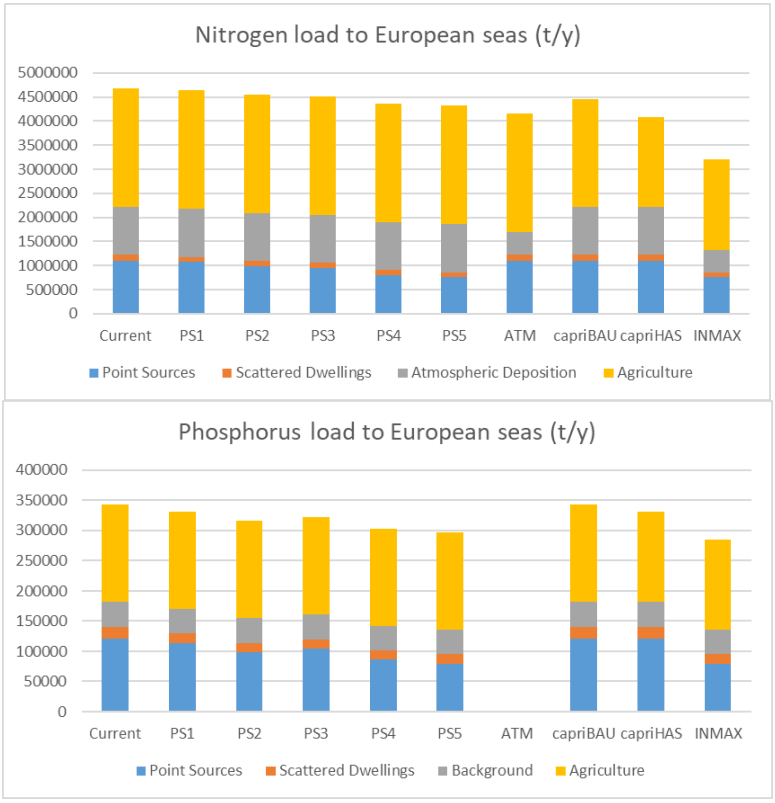

Table 12. Mean annual nutrient loads to the sea estimated under different nutrient management scenarios (presented in Table 9, current climate of 2014-2018). Values refer to full study extent in Figure 2.

	Total Load (tN/y)	Change compared to Current (%)	Total Load (tP/y)	Change compared to Current (%)
Current	4680444		342580	
PS1	4633125	-1	331094	-3
PS2	4549545	-3	316146	-8
PS3	4512770	-4	321859	-6
PS4	4362173	-7	303310	-11
PS5	4315438	-8	297023	-13
ATM	4155212	-11		
capriBAU	4461558	-5	343719	0
capriHAS	4089585	-13	330869	-3
INMAX	3199347	-32	285312	-17

The effect of measures varies in the different marine regions for the specific anthropogenic activities and the climatic and hydrological characteristics of the draining basins (Figures 39 and 40). According to the modelling analysis, measures to reduce pollution from domestic wastewater (scenario PS5) would be effective in the Bay of Biscay and Iberian Coast, Greater North Sea, Baltic Sea, Black Sea and Western Mediterranean Sea, both for N and P. Measures reducing agricultural inputs (scenario capriHAS) would benefit Greater North Sea, Baltic Sea, Black Sea for N. Cuts in N emissions would lower significantly N discharges to all marine regions (Figure 39).

Figure 39. Nitrogen riverine export from land to European seas per marine regions, under current condition (Current) and the scenarios of measures analysed INMAX. Colours represent the contribution of different sources to the total load. Marine Regions: ABI=Bay of Biscay and Iberian Coast; ACS=Celtic Seas; ANS=Greater North Sea; BAL=Baltic Sea; BLK=Black Sea; BLM=Black Sea – Sea of Marmara; MAD=Adriatic Sea; MAL=Aegean Levantine Mediterranean Sea; MIC=Ionian Sea and Central Mediterranean Sea; MWE=Western Mediterranean Sea.

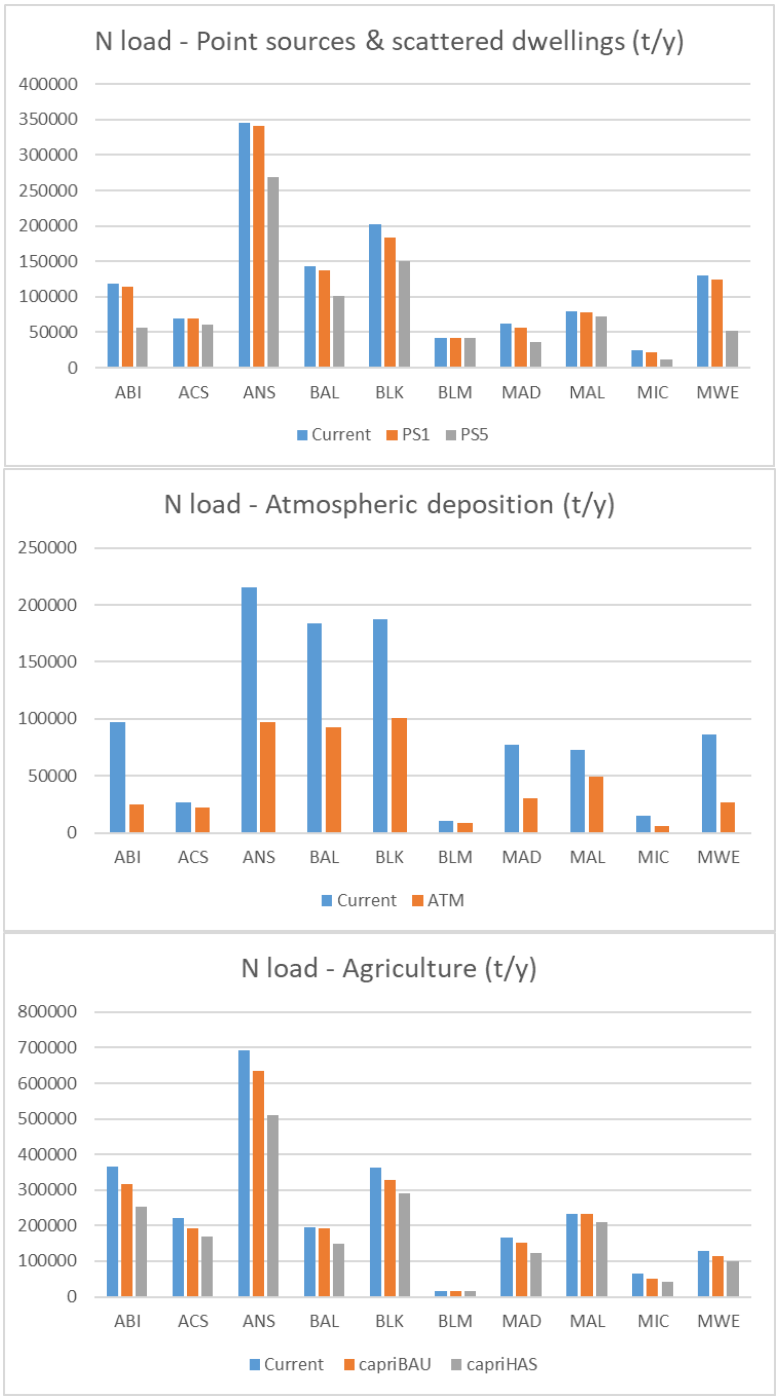

Figure 40. Phosphorus riverine export from land to European seas per marine regions, under current condition (Current) and the scenarios of measures analysed INMAX. Colours represent the contribution of different sources to the total load. Marine Regions: AB=Bay of Biscay and Iberian Coast; ACS=Celtic Seas; ANS=Greater North Sea; BAL=Baltic Sea; BLK=Black Sea; BLM=Black Sea – Sea of Marmara; MAD=Adriatic Sea; MAL=Aegean Levantine Mediterranean Sea; MIC=Ionian Sea and Central Mediterranean Sea; MWE=Western Mediterranean Sea.

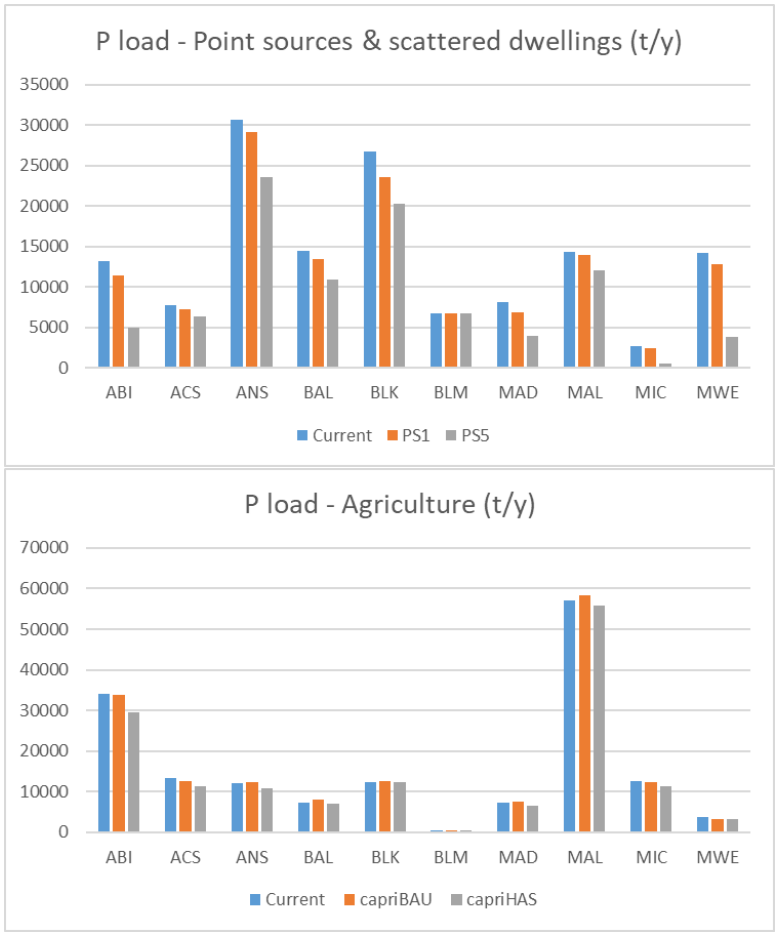

The measures tested in the scenarios produce different effects on nitrogen and phosphorus in surface water and can alter the N:P ratio in the riverine input to the sea, with potential impact on coastal and marine ecosystems. Overall, the N:P ratio is expected to decrease in case of measures addressing diffuse sources of pollution (scenarios ATM, capriBAU, capriHAS) and if all measures are applied together (scenario INMAX), but to increase if only point sources emission are tackled (scenarios PS1-PS5), as the latter are more effective on P than on N (Figure 41). The level of change of N:P ratio varies from region to region but following a similar pattern (Table 13).

Figure 41. N:P ratio in riverine load to European seas (ALL Regions) and per Marine Regions under current situation and different scenarios of measures to reduce nutrient pollution. Values refer to average 2014-2018 under current climate and water management. Colours indicate the different scenarios (Table 9). (Marine Regions: ABI=Bay of Biscay and Iberian Coast; ACS=Celtic Seas; ANS=Greater North Sea; BAL=Baltic Sea; BLK=Black Sea; BLM=Black Sea – Sea of Marmara; MAD=Adriatic Sea; MAL=Aegean Levantine Mediterranean Sea; MIC=Ionian Sea and Central Mediterranean Sea; MWE=Western Mediterranean Sea. ALL values refer to the study extent in Figure 2 except the Barents, Norwegian and White Seas.

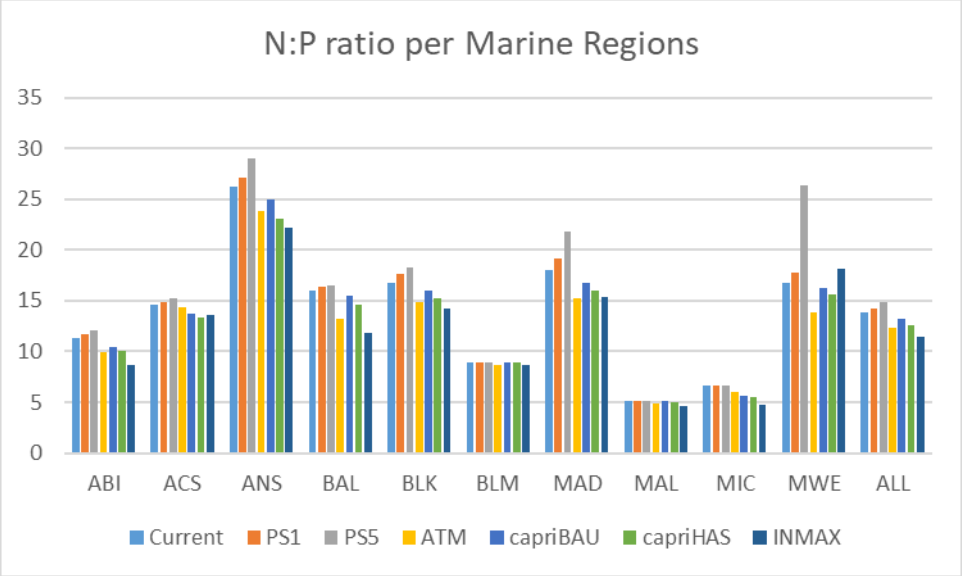

Table 13. N:P ratio in the riverine load to the sea per Marine Region under current condition (Current, average annual values 2014-2018) and relative changes under different scenarios of measures (PS1, PS5, ATM, capriBAU, capriHAS, INMAX).

	N:P ratio	**Change (of the scenario with respect to Current) (%)**					
Marine Region(1)	Current	PS1	PS5	ATM	capriBAU	capriHAS	INMAX
ABI	11	3	7	-12	-8	-12	-24
ACS	15	2	4	-1	-6	-9	-6
ANS	26	3	10	-9	-5	-12	-15
BAL	16	2	3	-17	-3	-9	-26
BLK	17	5	9	-12	-5	-9	-16
BLM	9	1	1	-3	0	0	-2
MAD	18	6	21	-15	-7	-11	-15
MAL	5	0	1	-6	-2	-4	-10
MIC	7	0	1	-8	-14	-17	-28
MWE	17	6	57	-17	-3	-7	8
ALL regions	14	3	7	-11	-5	-10	-18

(1) Marine Regions: ABI=Bay of Biscay & Iberian Coast; ACS=Celtic Seas; ANS=Greater North Sea; BAL=Baltic Sea; BLK=Black Sea & Sea of Marmara; MAD=Adriatic Sea; MAL=Aegean Levantine Mediterranean Sea; MIC=Ionian Sea and Central Mediterranean Sea; MWE=Western Mediterranean Sea. TOTAL values refer to the study extent in Figure 2 except the Barents, Norwegian and White Seas.

5.1.2.2 Nutrient concentration in freshwater

The measures tested in the scenarios are expected to reduce nutrient concentration in inland surface water. To quantify possible improvements, the share of stream network length falling in classes of nutrient concentration was evaluated for the current condition (average 2014-2018) and the different scenarios. Three classes of nutrient concentration were considered: low concentration: concentration <2 mgN/L for N and <0.1 mgP/L; high concentration >=5 mgN/L for N and >=0.5 mgP/L for P; medium concentration for values in between (Figure 42 and Table 14). The scenario INMAX foresees a significant increase of the river network with low N concentration (from 54% to 71%), and also a decrease of river network with high concentration (from 14% to 8%) (Table 14). The improvements are less prominent for P concentration. These shares provide insight on the effects of the measures but depend on the values adopted for the classes of water quality.

Figure 42. Shares of stream network length with nutrient concentration in classes of low (<2 mg N/L or < 0.1 mg P/L), medium and high concentration (>=5 mg N/L or >= 0.5 mg P/L) in the different scenarios. Values refer to the study extent in Figure 2 except the Barents, Norwegian and White Seas.

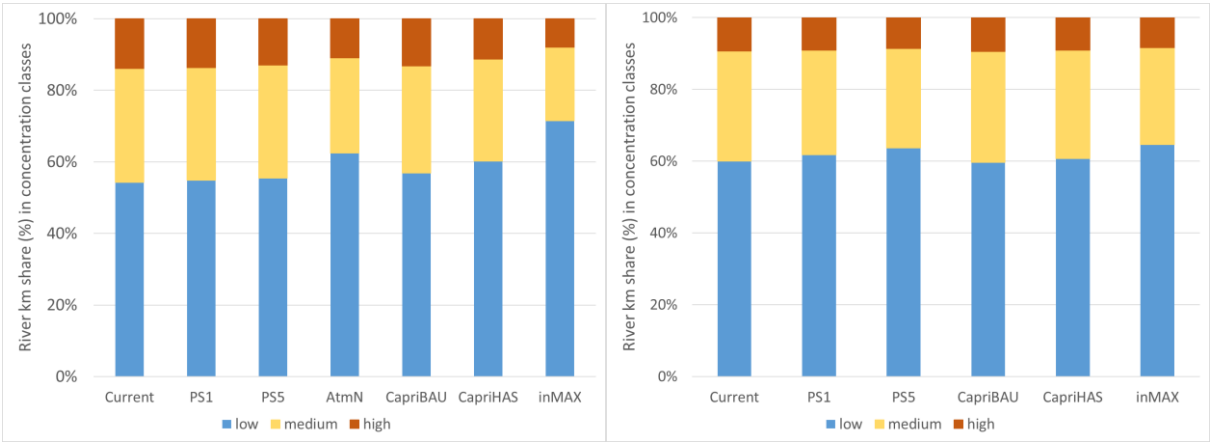

Table 14. Shares of stream network length with low (<2 mg N/L or < 0.1 mg P/L), medium, and high (>=5 mg N/L or >= 0.5 mg P/L) mean annual concentration for Europe in different scenarios. Values refer to the study extent in Figure 2 except the Barents, Norwegian and White Seas.

Scenarios	**Nitrogen concentration in surface waters class share (%)**			**Phosphorus concentration in surface waters class share (%)**		
	low	medium	high	low	medium	high
Current	54	32	14	60	31	9
PS1	55	31	14	62	29	9
PS5	56	31	13	64	28	9
AtmN	62	27	11	(1)	(1)	(1)
CapriBAU	57	30	13	60	31	9
CapriHAS	60	29	11	61	30	9
INMAX	71	21	8	65	27	8

(1) as Current for P concentration.

5.2 Effects of measures of water quantity and quality under future climate (2030)

5.2.1 Water quantity

In this section we take climate change projections into account, which can give us an idea if the projected change in WEI abstraction and WEI+ can be compensated by the water savings measures in the BAU and HAS scenarios. As the climatology from the simulated climate projections is different compared to the observed meteorology, it can be expected that the impact of the measures differs compared to the impact of the measures simulated with the observed weather (Figure 43). Although there are some differences between the two simulations, the general picture between the countries remains similar. Irrigation efficiency improvements in BAU scenario are the most effective measure. This effect is hardly noticeable (Figure 43a) as the effect of climate change to increase the WEI abstraction are manifold compared with the water savings measures in the BAU scenario. In the HAS scenario (Figure 43b) urban leakage reduction and desalination are the most effective measures and might have a positive effect in decreasing the WEI abstraction in most of the MS adjacent to the sea. Desalination increases the water availability while an improvement in urban leakage reduces the abstraction of water from ground – or surface water. Note that the combined effect of the measures is in general lower compared to the effect of the summed individual measures due to some cross over effects.

Figure 43. Individual and combined effects of water savings measures on WEI abstraction as estimated with the LISFLOOD model forced with a EURO-CORDEX climate scenario for the (a) BAU and (b) HAS scenario.

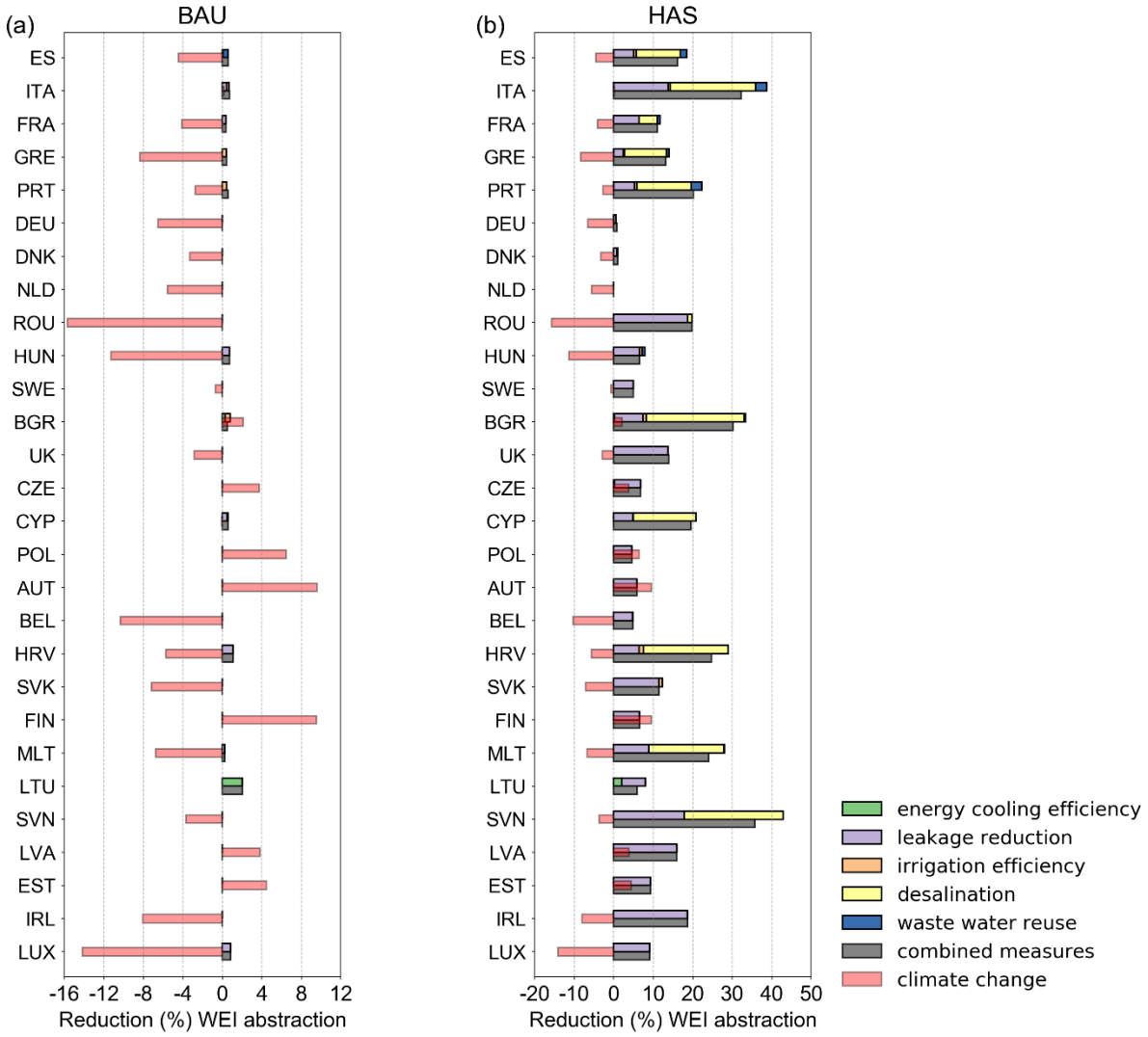

Figure 44. Individual and combined effects of water savings measures on WEI+ consumption as estimated with the LISFLOOD model forced with a EURO-CORDEX climate scenario for the (a) BAU and (b) HAS scenario.

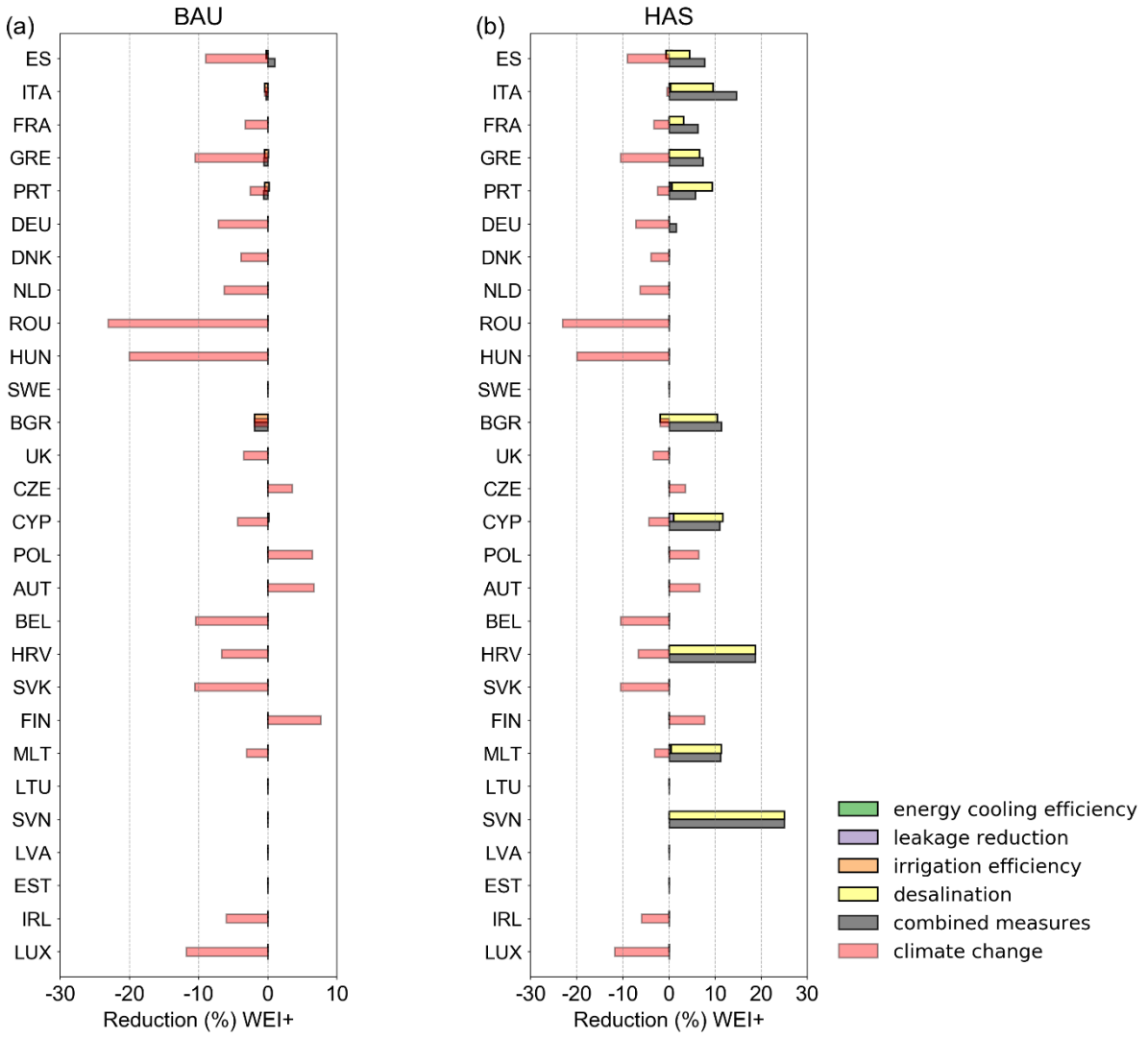

Although increasing irrigation efficiency is an effective measure to reduce the net consumption in the simulations with observed meteorology (Figure 43), we see a minimal effect of this measure in the simulation for the projected future climate (Figure 44). Note that for the simulations with the climate projections we use the LISFLOOD model without the EPIC module as some future input needed for EPIC is not ready to use yet. Irrigation is then estimated based on the required amount of transpiration by vegetation. If this amount of water is not available from soil moisture above wilting point level, the missing amount is designed as the irrigation water demand, which is strongly dependent on the climatology. However, even if we add the WEI+ reduction from irrigation efficiency from the simulation with the observed meteorology (Figure 43) to the combined measures in Figure 44, the measures are not efficient enough to compensate for the climate signal for most countries in the BAU scenario, particularly Cyprus, Greece, Hungary, Spain, Croatia, Malta and Romania. For the HAS scenario, the measures, especially desalination, could be sufficient to compensate for climate change in some MS.

5.2.2 Water quality

5.2.2.1 Nutrient load to the European seas and sources contribution

Ambitious measures to reduce nutrient pollution in water represented in the HAS scenario could lower the annual riverine load to European seas by 28% for N and 17% for P (annual average for the climate 2026-2030), compared to the measures in the business as usual scenario (BAU) (Figure 45, Table 15 for N, Table 16 for P).

The effect of the measures varies in the different marine regions. With regard to N, large reduction in loads to the sea could be achieved by ambitious measures addressing domestic wastewater and atmospheric emissions in the Bay of Biscay and Iberian Coast, Western Mediterranean Sea and Black Sea regions, while reduction of nutrient inputs in agriculture will also play a role in Greater North Sea and Baltic Sea regions (Figure 46 and Table 15). Concerning P, measures for enhancing domestic wastewater treatment could lead to significant improvements, especially in the Mediterranean marine regions and in the Bay of Biscay and Iberian Coast (Figure 47 and Table 16).

Table 15. Total nitrogen loads to sea foreseen under the REF, BAU and HAS scenarios per marine region (annual average of 5-year period 2026-2030).

Marine Regions([1])	**Tot Load REF**	**Tot Load BAU**	**Tot Load HAS**	**Change (%) (HAS-REF)*100/REF**				**Change (%) (HAS-BAU)*100/BAU**			
	(tN/y)	(tN/y)	(tN/y)	Total load	Point sources & scattered	Atmospheric deposition	Agriculture	Total load	Point sources & scattered	Atmospheric deposition	Agriculture
ABI	606760	556884	348605	-43	-52	-76	-30	-37	-50	-76	-21
ACS	309696	278596	240860	-22	-12	-15	-26	-14	-11	-15	-14
ANS	1259738	1225832	906985	-28	-22	-53	-23	-26	-21	-53	-20
BAL	482182	484158	325863	-32	-28	-47	-20	-33	-27	-47	-23
BLK	604724	562109	428263	-29	-25	-46	-21	-24	-18	-46	-11
BLM	59759	59759	57077	-4	0	-27	0	-4	0	-27	0
MAD	277329	262941	172357	-38	-41	-62	-24	-34	-37	-62	-18
MAL	288982	288012	249972	-13	-10	-33	-7	-13	-8	-33	-7
MIC	80456	69339	44184	-45	-55	-61	-35	-36	-50	-61	-18
MWE	332626	311743	163721	-51	-60	-71	-24	-47	-58	-71	-12
ALL regions	4302251	4099373	2937885	-32	-30	-53	-24	-28	-27	-53	-17

([1]) Marine Regions: ABI=Bay of Biscay & Iberian Coast; ACS=Celtic Seas; ANS=Greater North Sea; BAL=Baltic Sea; BLK=Black Sea & Sea of Marmara; MAD=Adriatic Sea; MAL=Aegean Levantine Mediterranean Sea; MIC=Ionian Sea and Central Mediterranean Sea; MWE=Western Mediterranean Sea. TOTAL values refer to the study extent in Figure 2 except the Barents, Norwegian and White Seas

Figure 45. Nitrogen (left) and phosphorus (right) load to the European seas estimated by the model GREEN for the REF, BAU and HAS scenarios under future climate (annual average of 5-year period 2026-2030). Colours represent the contribution of different sources to the total load. Values refer to the study extent in Figure 2 except the Barents, Norwegian and White Seas.

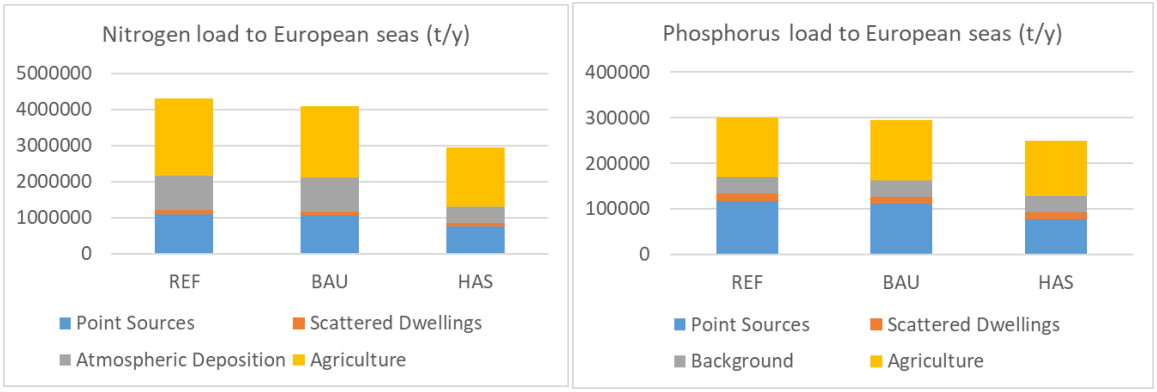

Figure 46. Nitrogen load to the sea for different Marine Regions estimated by the model GREEN for the BAU and HAS scenarios under future climate (annual average of 5-year period 2026-2030). Colours represent the contribution of different nutrient sources to the total load.

Table 16. Total phosphorus loads to sea foreseen under the REF, BAU and HAS scenarios per marine region (annual average of 5-year period 2026-2030).

Marine Regions(1)	Tot Load REF	Tot Load BAU	Tot Load HAS	Change (%) (HAS-REF)*100/REF				Change (%) (HAS-BAU)*100/BAU			
	(tP/y)	(tP/y)	(tP/y)	Total load	Point sources & scattered	Background	Agriculture	Total load	Point sources & scattered	Background	Agriculture
ABI	51441	50898	40037	-22	-60	0	-11	-21	-56	0	-13
ACS	20467	19935	17660	-14	-13	0	-15	-11	-13	0	-11
ANS	47249	47552	40373	-15	-20	0	-8	-15	-19	0	-12
BAL	30725	30824	27539	-10	-22	0	-3	-11	-19	0	-12
BLK	39476	36937	33793	-14	-22	0	2	-9	-14	0	2
BLM	7170	7170	7170	0	0	0	0	0	0	0	0
MAD	14853	14325	10813	-27	-49	0	-3	-25	-42	0	-11
MAL	57006	57475	54232	-5	-15	0	-2	-6	-13	0	-3
MIC	11940	11983	9300	-22	-79	0	-5	-22	-76	0	-9
MWE	19325	18023	9058	-53	-73	0	-1	-50	-70	0	-1
ALL regions	299652	295122	249974	-17	-31	0	-6	-15	-27	0	-8

(1) Marine Regions: ABI=Bay of Biscay & Iberian Coast; ACS=Celtic Seas; ANS=Greater North Sea; BAL=Baltic Sea; BLK=Black Sea & Sea of Marmara; MAD=Adriatic Sea; MAL=Aegean Levantine Mediterranean Sea; MIC=Ionian Sea and Central Mediterranean Sea; MWE=Western Mediterranean Sea. TOTAL values refer to the study extent in Figure 2 except the Barents, Norwegian and White Seas

Figure 47. Phosphorus load to the sea for different Marine Regions estimated by the model GREEN for the BAU and HAS scenarios under future climate (annual average of 5-year period 2026-2030). Colours represent the contribution of different nutrient sources to the total load.

Overall the N:P ratio in nutrient load discharged to the European seas is expected to decrease in the HAS scenario compared to the BAU (-15%) (future climate average 2026-2030) (Figure 48 and Table 17). The reduction would be more prominent in the Baltic Sea (-25%) and in the Bay of Biscay and Iberian Coast (-20%). The Western Mediterranean Sea would be the only region with a slightly increase of the N:P ratio (4%). These changes are the results of the measures in the HAS scenario that would produce a relative higher reduction of riverine loads for N than for P compared to the BAU scenario.

Figure 48. N:P ratio in riverine load to European seas and per Marine Regions under different scenarios of measures (REF, BAU and HAS) to reduce nutrient pollution. Values refer to annual average of 5-year period 2026-2030 under future climate and including measures for water management. (Marine regions: ABI=Bay of Biscay and Iberian Coast; ACS=Celtic Seas; ANS=Greater North Sea; BAL=Baltic Sea; BLK=Black Sea; BLM=Black Sea – Sea of Marmara; MAD=Adriatic Sea; MAL=Aegean Levantine Mediterranean Sea; MIC=Ionian Sea and Central Mediterranean Sea; MWE=Western Mediterranean Sea; ALL values refer to the study extent in Figure 2 except the Barents, Norwegian and White Seas).

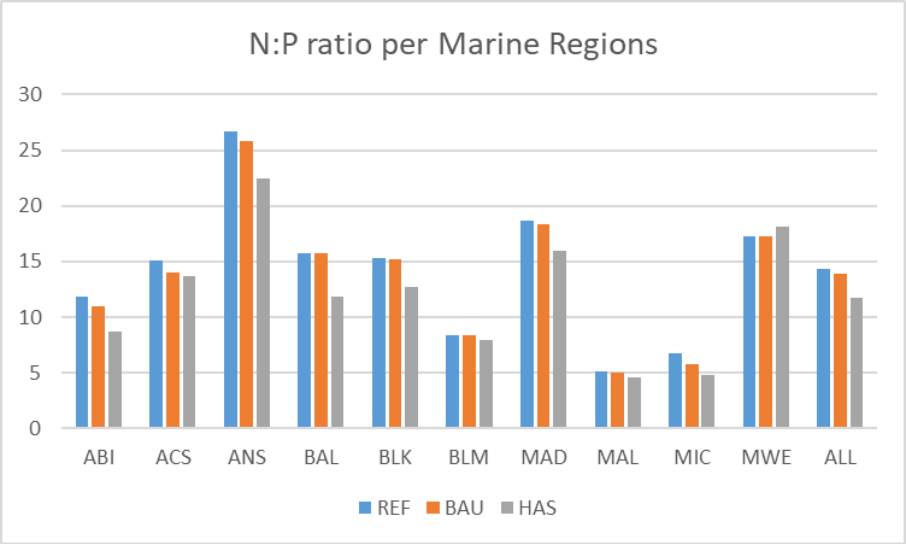

Table 17. N:P ratio and change in the riverine load the sea per Marine Regions under the REF, BAU and HAS scenarios (average annual values 2026-2030).

Marine Regions(1)	N:P ratio	N:P ratio	N:P ratio	Change (%)	Change (%)
	REF	BAU	HAS	(HAS-REF)*100/REF	(HAS-BAU)*100/BAU
ABI	12	11	9	-26	-20
ACS	15	14	14	-10	-2
ANS	27	26	22	-16	-13
BAL	16	16	12	-25	-25
BLK	15	15	13	-17	-17
BLM	8	8	8	-4	-4
MAD	19	18	16	-15	-13
MAL	5	5	5	-9	-8
MIC	7	6	5	-29	-18
MWE	17	17	18	5	4
ALL regions	14	14	12	-18	-15

(1) Marine Regions: ABI=Bay of Biscay & Iberian Coast; ACS=Celtic Seas; ANS=Greater North Sea; BAL=Baltic Sea; BLK=Black Sea & Sea of Marmara; MAD=Adriatic Sea; MAL=Aegean Levantine Mediterranean Sea; MIC=Ionian Sea and Central Mediterranean Sea; MWE=Western Mediterranean Sea. TOTAL values refer to the study extent in Figure 2 except the Barents, Norwegian and White Seas

5.2.2.2 Nutrient concentration in freshwater

The improvements on nutrient concentration in surface water that could be achieved in the HAS scenario compared to the BAU scenario are more prominent for N than for P. They amount to an additional 17% of stream network with low N concentration (below 2 mgN/L) and a further 3% of stream network with low P concentration (below 0.1 mgP/L) (average for the period 2026-2030, future climate) (Figure 49 and Table 18).

Figure 49. Shares of stream network length with nutrient concentration in classes of low (<2 mg N/L or < 0.1 mg P/L), medium and high concentration (>=5 mg N/L or >= 0.5 mg P/L) in the REF, BAU and HAS scenarios (average of 5-year period 2026-2030). Values refer to the study extent in Figure 2 except the Barents, Norwegian and White Seas.

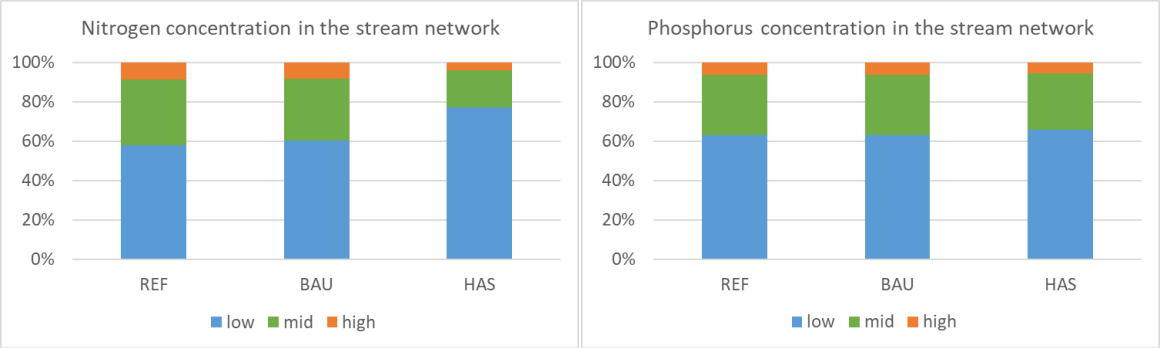

Table 18. Shares of stream network length with low (<2 mg N/L or < 0.1 mg P/L), medium, and high (>=5 mg N/L or >= 0.5 mg P/L) mean annual concentration for Europe (including all marine regions except Barents, Norwegian and White Seas) in REF, BAU and HAS scenarios (average of 5-year period 2026-2030). Values refer to the study extent in Figure 2 except the Barents, Norwegian and White Seas.

Scenarios	**Nitrogen concentration in surface waters class share (%)**			**Phosphorus concentration in surface waters class share (%)**		
Future climate	low	medium	high	low	medium	high
REF	58	33	9	63	31	6
BAU	60	31	8	63	31	6
HAS	77	19	4	66	29	5

6 Conclusions

In the project Blue2.2 (Deliverables 2.1, 2.2 and 2.3) we performed an analysis of European freshwater quantity and quality, assessing their evolution over the last decades (1990-2018) and the effects of measures (scenario analysis) to address water scarcity and nutrient pollution (under current climate condition and possible future climate in 2030). We considered the improvement that could be achieved under the current EU legislation (Business As Usual, BAU scenario) and possible more ambitious measures (High Ambition Scenario, HAS). Different modelling tools were developed and applied for estimating water availability and nutrient load in inland waters and discharged to the seas. The modelling simulations for the period 1990-2018 and for the scenarios have been used as input in the JRC marine models to estimate the effects of measures on the marine environment (JRC freshwater-marine modelling framework, Macias et al. 2022).

Water quantity

With the aim to reduce the already existing pressures on Europe's freshwater resources, EU Member States are planning and implementing various water saving measures, as described in the Programs of Measures under the Water Framework Directive (WFD). The set of measures are evaluated for the BAU and HAS scenarios. These measures consist of increasing irrigation efficiency, treated wastewater reuse for irrigation to reduce new abstractions, urban water efficiency measures, energy cooling efficiencies and desalination.

All these changes interact, and the resulting water resources and locations with pressures are evaluated. Various water saving measures are evaluated and compared with the current situation using LISFLOOD-EPIC. Furthermore, these measures are evaluated under current and future climate and land use, using a EURO-CORDEX projection and the LUISA land use projection until 2050.

Changes in irrigation efficiency and desalination prove to be an important measure to reduce water quantity pressures presented with the WEI+ and WEI abstraction water scarcity indicator. Irrigation efficiency reduces the water abstraction from groundwater- or surface water- and desalination increases the water availability, particularly for the Mediterranean countries. Other measures, such as water reuse and urban water efficiency improvements do have a positive effect for the WEI abstraction, but not for the WEI+. The difference between the cooling scenarios (switch to renewable) seem to be too minimal to have an effect on the water resources. As the return flow is very high compared to the abstraction (minimum losses), this measure is more important for ecosystem services (water temperature) than for water quantity.

Although the water savings measures have a positive effect on the water resources, planned investments in the BAU scenario are not sufficient to compensate for the projected reduction in water availability. The potential measures in the HAS scenario might improve water scarcity in already water scarce countries around the Mediterranean, but that might only happen when desalination is considered, which is however not much implemented yet. Depending on how fast the global temperature will rise, there might still be time to increase current level of investments or implement one or more additional cycles of investments of increasing irrigation efficiency and other effective water efficiency measures to keep up with the decreasing water availability caused by global warming.

Water quality

Several sectors and sources contribute to nutrient pollution in European freshwater and to high nutrient load to coastal water. Measures to reduce nutrient pollution analysed in the study include: improvements in domestic wastewater treatments (under consideration in the revision of UWWT Directive), reduction of nitrogen emissions into air following the EU Fit For 55 package, measures foreseen in the CAP and targets of the Farm to Fork and Biodiversity Strategies.

The results of the study indicate that:

- Measures tackling different sectors and sources (domestic wastewater, air emissions, agriculture) are necessary to achieve significant reduction in nutrient loads in freshwater and coastal waters.
- The impact of the measures is specific to the region, its climatic and hydrological characteristics and anthropogenic inputs.

— Measures will change N:P ratio in the aquatic ecosystems, with impact on the biodiversity and condition of the aquatic ecosystem, thus they need to be targeted to the receiving freshwater and marine environment.

— Ambitious measures (HAS scenario) could lower the annual riverine load to European seas by around 30% for N and 15% for P compared to the measures in the business as usual scenario (BAU).

Modelling assessments have uncertainties and remain theoretical. Concerning modelling nutrient pollution in waters, a main source of uncertainty is the capacity to take into account the legacy of nitrogen and phosphorus in soils and groundwater, and to estimate the delay in time between the application of measures and the detection of improvements in water quality. In addition, the ambitious measures imply drastic changes in several sectors, including agriculture with major social and economic impacts on farmers. Even though the ambitious scenario is realistic, implementing it requires a high political will.

References

AQUASTAT database [WWW Document], 2021. URL http://www.fao.org/nr/water/aquastat/data/query/index.html (accessed 3.29.19).

Arino, O., Perez, R.J.J., Kalogirou, V., Bontemps, S., Defourny, P., and Van Bogaert, E., *Global Land Cover Map for 2009 (GlobCover 2009)*. Eur. Sp. Agency Univ. Cathol. Louvain (UCL), PANGAEA, 2012, https//doi.org/10.1594/PANGAEA.787668.

Arnold, J.G., Srinivasan, R., Muttiah, R.S., and Williams, J.R., Large area hydrologic modeling and assessment part 1: model development. *J. Am. Water Resour. Assoc*. 34, 1998, 73–89. https://doi.org/10.1111/j.1752-1688.1998.tb05961.x

Baranzelli, C., et al., *The reference scenario in the LUISA platform – Updated configuration 2014 towards a common baseline scenario for EC impact assessment procedures*, EUR 27019 EN, Publications office of the European Union, Luxembourg, 2014.

Barreiro-Hurle, J., Bogonos, M., Himics, M., Hristov, J., Pérez-Domiguez, I., Sahoo, A., Salputra, G., Weiss, F., Baldoni, E., Elleby, C. *Modelling environmental and climate ambition in the agricultural sector with the CAPRI model. Exploring the potential effects of selected Farm to Fork and Biodiversity strategies targets in the framework of the 2030 Climate targets and the post 2020 Common Agricultural Policy*, EUR 30317 EN, Publications Office of the European Union, Luxembourg, 2021, ISBN 978-92-76-20889-1, doi:10.2760/98160, JRC121368.

Batista e Silva, F., Gallego, J., and C. Lavalle, A high-resolution population grid map for Europe, *J. Maps*, 9, 2013, 16-28, 10.1080/17445647.2013.764830.

Beck, H.E., Vergopolan, N., Pan, M., Levizzani, V., Van Dijk, A.I.J.M., Weedon, G.P., Brocca, L., Pappenberger, F., Huffman, G.J., and Wood, E.F., Global-scale evaluation of 22 precipitation datasets using gauge observations and hydrological modeling. *Hydrol. Earth Syst. Sci* 21, 2017, 6201–6217. https://doi.org/10.5194/hess-21-6201-2017

Benitez Sanz, C., Wolters, H., Martí B., and B. Mora, *EU Water and Marine Measures Data base. Deliverable to Task B2 of the BLUE2 project "Study on EU integrated policy assessment for the freshwater and marine environment, on the economic benefits of EU water policy and on the costs of its non-implementation*, Report to DG ENV—BLUE2 study; INTECSA-INARSA S.A., Madrid, Spain, 2018.

Bernhard, J., Reynaud, A., de Roo, A., Karssenberg, D., and S.D. Jong, Household water use in Europe at regional scale: analysis of trends and quantification of main drivers, 2020a, *in preparation*.

Bernhard, J., Reynaud, A., de Roo, A., Karssenberg, D., and S.D. Jong, Mapping industrial water use and water productivity levels in Europe at high sectoral and spatial detail, 2020b, *in preparation*.

Bisselink, B., de Roo, A., Bernhard, J., and E. Gelati, Future projections of water scarcity in the Danube river basin due to land use, water demand and climate change, *J. Environ. Geogr.*, 2018a, 11, 25–36, https://doi.org/10.2478/jengeo-2018-0010

Bisselink, B., Bernhard, J., Gelati, E., Adamovic, M., Guenther, S., Mentaschi, L., and A. de Roo, *Impact of a changing climate, land use, and water usage on Europe's water resources*, EUR 29130 EN, Publications Office of the European Union, Luxembourg, 2018b, https://doi.org/10.2760/847068.

Bisselink, B., Bernhard, J., Gelati, E., Adamovic, M., Guenther, S., Mentaschi, L., et al., *Climate change and Europe's water resources*, EUR 29951 EN. Luxembourg: Publications Office of the European Union, 2020.

Bouraoui, F., and Malagó, A., Global Time Series of Nitrogen and Phosphorus Mineral Fertilizers in the period 1979-2019, 2022, in preparation.

Bouraoui, F., and Malagó, A., *Groundwater quality and vulnerability Assessment tools to prevent and control groundwater pollution by nitrates* [WWW Document], 2020, URL https://water.jrc.ec.europa.eu/groundwater.html (accessed 2.8.22).

Bouwman, A.F., Lee, D.S., Asman, W.A.H., Dentener, F.J., Van Der Hoek, K.W., and Olivier, J.G.J., A global high-resolution emission inventory for ammonia. *Global Biogeochem. Cycles* 11, 1997, 561–587. https://doi.org/10.1029/97GB02266

Burek, P., van der Knijff, J., and A. de Roo, *LISFLOOD Distributed Water Balance and Flood Simulation Model – Revised User Manual*, Joint Research Centre, European Commission, Ispra (VA), Italy, 2013, https://doi.org/10.2788/24719.

Chen, M., and Graedel, T.E., A half-century of global phosphorus flows, stocks, production, consumption, recycling, and environmental impacts. *Glob. Environ. Chang.* 36, 2016, 139–152. https://doi.org/10.1016/j.gloenvcha.2015.12.005

CLC, 2021. *CORINE Land Cover maps*, 2021, Available at https://land.copernicus.eu/pan-european/corine-land-cover (access March 2021)

Dee, D.P., Uppala, S.M., Simmons, A.J., Berrisford, P., Poli, P., Kobayashi, S., Andrae, U., Balmaseda, M.A., Balsamo, G., Bauer, P., Bechtold, P., Beljaars, A.C.M., van de Berg, L., Bidlot, J., Bormann, N., Delsol, C., Dragani, R., Fuentes, M., Geer, A.J., Haimberger, L., Healy, S.B., Hersbach, H., Hólm, E. V., Isaksen, L., Kållberg, P., Köhler, M., Matricardi, M., McNally, A.P., Monge-Sanz, B.M., Morcrette, J.-J., Park, B.-K., Peubey, C., de Rosnay, P., Tavolato, C., Thépaut, J.-N., and Vitart, F., The ERA-Interim reanalysis: configuration and performance of the data assimilation system. *Q. J. R. Meteorol. Soc.* 137, 2011, 553–597. https://doi.org/10.1002/qj.828

de Roo, A. P. J., Wesseling, C. G., and W. P. A Van Deursen, Physically based river basin modelling within a GIS: the LISFLOOD model, *Hydrol. Process.*, 14, 2020, 1981–1992.

de Roo, A., Trichakis, I., Bisselink, B., Gelati, E., Pistocchi, A., and Gawlik, B., The Water-Energy-Food-Ecosystem Nexus in the Mediterranean: Current Issues and Future Challenges. *Front. Clim.* 3, 2021, 782553, doi: 10.3389/fclim.2021.782553

Dijkstra, L., and Poelman, H., A harmonised definition of cities and rural areas: the new degree of urbanisation Working Papers, 2014.

EC, *European Council Directive of 12 December 1991 concerning the protection of waters against pollution caused by nitrates from agricultural sources (91/676/EEC)*, 1991.

EEA, *The European environment – State and outlook 2005*, 2005

EEA, https://www.eea.europa.eu/data-and-maps/explore-interactive maps/water-exploitation-index-for-river-2, 2015

EEA, *Waterbase - UWWTD: Urban Waste Water Treatment Directive – reported data*, 2020, https://www.eea.europa.eu/data-and-maps/data/waterbase-uwwtd-urban-waste-water-treatment-directive-6, 2020, (download October 2020)

EEA, *E-PRTR* V18, https://www.eea.europa.eu/data-and-maps/data/member-states-reporting-art-7-under-the-european-pollutant-release-and-transfer-register-e-prtr-regulation-23, European Environment Agency, 2021a, (download 21/01/2021)

EEA, *Industrial Reporting under the Industrial Emissions Directive 2010/75/EU and European Pollutant Release and Transfer Register Regulation (EC) No 166/2006*, European Environment Agency, 2021b (download 21/04/2021).

ESA, *Land Cover CCI Product User Guide Version 2*. Tech. Rep., 2017, Available at: maps.elie.ucl.ac.be/CCI/viewer/download/ESACCI-LC-Ph2-PUGv2_2.0.pdf (access March 2021)

ETC/ICM, *Use of freshwater resources in Europe 2002-2012*. Supplementary document to the European Environment Agency's core set indicator 018. ETC/ICM Technical Report 1/2016, Magdeburg: European Topic Centre on inland, coastal and marine waters, 2016, 62 pp.

EUROSTAT, *Design capacity, in terms of biochemical oxygen demand (BOD), of urban wastewater treatment plants with advanced treatment - 1 000 kg O2/day1 (ten00028)*, 2018, http://ec.europa.eu/eurostat/tgm/table.do?tab=table&init=1&plugin=1&language=en&pcode=ten00028 (download 13/07/2018 for years 2003-2014; currently the dataset cannot be found on the database).

EUROSTAT, *Population connected to wastewater treatment plants* (env_ww_con), 2021a, https://ec.europa.eu/eurostat/databrowser/product/page/ENV_WW_CON (download 27.01.2021)

EUROSTAT, *Population change - Demographic balance and crude rates at national level* (DEMO_GIND), 2021b,

https://ec.europa.eu/eurostat/databrowser/view/DEMO_GIND__custom_571312/default/table?lang=en (download 15/02/2021)

Faergemann, H., *Update on water scarcity and droughts indicator development*, May 2012, presented at the Water Director's Meeting, 4–5 June, 2012, Denmark.

FAO/IIASA/ISRIC/ISSCAS/JRC, *Harmonized World Soil Database (version 1.2)*. FAO, Rome, Italy IIASA, Laxenburg, Austria, 2012.

FAOSTAT, http://www.fao.org/faostat/en/#data (data access in May 2018), 2018.

FAOSTAT, *Land use indicators* [WWW Document]. URL http://www.fao.org/faostat/en/#data/EL (accessed 2.5.20), 2021a.

FAOSTAT, *Fertilizers by Nutrient* [WWW Document]. URL http://www.fao.org/faostat/en/#data/RFN (accessed 2.5.20), 2021b.

FAOSTAT, *Live Animals* [WWW Document]. URL http://www.fao.org/faostat/en/#data/QA (accessed 2.5.20), 2021c.

FAOSTAT, *Livestock Primary* [WWW Document]. URL http://www.fao.org/faostat/en/#data/QL (accessed 2.5.20), 2021d.

FAOSTAT, *Annual population* [WWW Document]. URL http://www.fao.org/faostat/en/#data/OA (accessed 2.5.20), 2021e.

Garnier, J., Billen, G., Lassaletta, L., Vigiak, O., Nikolaidis, N.P., and Grizzetti, B., Hydromorphology of coastal zone and structure of watershed agro-food system are main determinants of coastal eutrophication, *Environ. Res. Lett.* 16, 2021, 023005.

GDP, FAOSTAT [WWW Document]. URL https://www.fao.org/faostat/en/#data/CS (accessed 2.8.22), 2021.

Gelati, E., Zuzanna, Z., Andrej, C., Simona, B., Bernard, B., Marko, A., et al., Assessing groundwater irrigation sustainability in the Euro-Mediterranean region with an integrated agro-hydrologic model. *Adv. Sci. Res.* 17, 2020, 227–253, doi: 10.5194/asr-17-227-2020

GeoNetwork, *GeoNetwork opensource portal to spatial data and information*, 2007

GMIA, *Global Map of Irrigation Areas (GMIA)* | Land & Water | Food and Agriculture Organization of the United Nations | Land & Water | Food and Agriculture Organization of the United Nations [WWW Document]. URL https://www.fao.org/land-water/land/land-governance/land-resources-planning-toolbox/category/details/en/c/1029519/ (accessed 2.22.22), 2021.

Grizzetti, B., Bouraoui, F., and Aloe, A., Changes of nitrogen and phosphorus loads to European seas. *Global Change Biology* 18, 2012, 769–782, doi: 10.1111/j.1365-2486.2011.02576.x

Grizzetti, B., Pistocchi, A., Liquete, C., Udias, A., Bouraoui, F., Van De Bund, W. Human pressures and ecological status of European rivers. 2017. *Scientific Reports.* 7:205. https://doi.org/10.1038/s41598-017-00324-3.

Grizzetti, B., Vigiak, O., Udias, A., Aloe, A., Zanni, M., Bouraoui, F., Pistocchi, A., Dorati, C., Friedland, R., De Roo, A., Benitez Sanz, C., Leip, A., and M. Bielza., How EU policies could reduce nutrient pollution in European inland and coastal waters, *Global Environmental Change* 69, 2021, 102281, doi: 10.1016/j.gloenvcha.2021.102281

Hengl, T., de Jesus, J.M., MacMillan, R.A., Batjes, N.H., Heuvelink, G.B.M., et al., SoilGrids1km — Global Soil Information Based on Automated Mapping, *PLoS ONE* 9(8): e105992, 2014, doi:10.1371/journal.pone.0105992.

Herridge, D.F., Peoples, M.B., and Boddey, R.M., Global inputs of biological nitrogen fixation in agricultural systems. *Plant Soil*, 2008, https://doi.org/10.1007/s11104-008-9668-3

IFASTAT, *Fertilizer Use by Crop* [WWW Document]. URL https://www.ifastat.org/faq (accessed 2.5.20), 2016

Jacob, D., et al., EURO-CORDEX: new high-resolution climate change projections for European impact research, *Reg. Environ. Change*, 14, 2014, 563–578, doi: 10.1007/s10113-013-0499-2.

Jacobs-Crisioni, C., Diogo, V., Perpiña Castillo, C., Baranzelli, C., Batista e Silva, F., Rosina, K., Kavalov, B., and C. Lavalle, *The LUISA Territorial Reference Scenario 2017: A technical description*, Publications Office of the European Union, Luxembourg, 2017, doi:10.2760/902121, JRC10816.

JMP, *Joint Monitoring Programme for Water Supply, Sanitation and Hygiene*. Estimates on the use of water, sanitation and hygiene by country (2000-2017) [WWW Document], 2019. URL https://washdata.org/ (accessed 2.23.22)

Joint Research Centre, *Zero pollution outlook 2022*, Publications Office of the European Union, Luxembourg, 2022, doi:10.2760/39491, JRC129655.

Jönsson, H., and Vinnerås, B., Adapting the nutrient content of urine and faeces in different countries using FAO and Swedish data. *Proceedings of Ecosan–Closing the loop,* 2003.

Kitous, A., Keramidas, K., Vandyck, T., and B. Saveyn, *GECO 2016. Global Energy and Climate Outlook, Road from Paris*, EUR 27952 EN, 2016. Doi: 10.2791/662470.

Kundu, S., Vassanda Coumar, M., Rajendiran, S., Ajay, and Subba Rao, A., Phosphates from detergents and eutrophication of surface water ecosystem in India. *Curr. Sci.* 108, 2015, 1320–1325. https://doi.org/10.18520/cs/v108/i7/1320-1325

Lamarque, J.F., Dentener, F., McConnell, J., Ro, C.U., Shaw, M., Vet, R., Bergmann, D., Cameron-Smith, P., Dalsoren, S., Doherty, R., Faluvegi, G., Ghan, S.J., Josse, B., Lee, Y.H., Mackenzie, I.A., Plummer, D., Shindell, D.T., Skeie, R.B., Stevenson, D.S., Strode, S., Zeng, G., Curran, M., Dahl-Jensen, D., Das, S., Fritzsche, D., and Nolan, M., Multi-model mean nitrogen and sulfur deposition from the atmospheric chemistry and climate model intercomparison project (ACCMIP): Evaluation of historical and projected future changes. *Atmos. Chem. Phys.* 13, 2013a, 7997–8018. https://doi.org/10.5194/acp-13-7997-2013

Lamarque, J.F., Shindell, D.T., Josse, B., Young, P.J., Cionni, I., Eyring, V., Bergmann, D., Cameron-Smith, P., Collins, W.J., Doherty, R., Dalsoren, S., Faluvegi, G., Folberth, G., Ghan, S.J., Horowitz, L.W., Lee, Y.H., MacKenzie, I.A., Nagashima, T., Naik, V., Plummer, D., Righi, M., Rumbold, S.T., Schulz, M., Skeie, R.B., Stevenson, D.S., Strode, S., Sudo, K., Szopa, S., Voulgarakis, A., and Zeng, G., The atmospheric chemistry and climate model intercomparison Project (ACCMIP): Overview and description of models, simulations and climate diagnostics. Geosci. *Model Dev. 6*, 2013b, 179–206. https://doi.org/10.5194/gmd-6-179-2013

LP DAAC, *Global 30 Arc-Second Elevation Data Set GTOPO30*. Land Process Distributed Active Archive Center. 2004, Available online: https://www.usgs.gov (accessed on 10/10/2016).

Lavalle C., Baranzelli, C., Batista e Silva, F., Mubareka, S., Rocha Gomes, C., Koomen, E., and M. Hilferink, A high resolution land use/cover modelling framework for Europe. In: *ICCSA 2011*, Part I, LNCS 6782, 2011, 60–75.

Lehner, B., Verdin, K., and A. Jarvis, New global hydrography derived from spaceborne elevation data, *Eos*, Transactions, AGU, 89(10), 2008, 93-94.

Macias, D., Stips, A., Grizzetti, B., Aloe, A., Bisselink, B., de Meij, A., De Roo, A., Duteil, O., Garcia-Gorriz, E., González-Fernández, D., Hristov, J., Miladinova, S., Oliveira, N., Parn, O., Piroddi, C., Pisoni, E., Pistocchi, A., Polimene, L., Serpetti, N., Thoma, C., Udias, A., Vigiak, O., Weiss, F., Wilson, J., Zanni, M. *Water/marine Zero Pollution Outlook. A forward-looking, model-based analysis of water pollution in the EU.* Publications Office of the European Union, Luxembourg, 2022, doi:10.2760/681817 (online), JRC131197.

Magagna D., Hidalgo González I., Bidoglio G., Peteves S., Adamovic M., Bisselink B., De Felice M., De Roo A., Dorati C., Ganora D., Medarac H., Pistocchi A., Van De Bund W. and Vanham D. *Water – Energy Nexus in Europe*, Publications Office of the European Union, Luxembourg, 2019, doi: 10.2760/968197, JRC115853.

Malagò, A., and Bouraoui, F., Water quality modelling at continental scale using the SWAT model. *INTERNATIONAL SOIL AND WATER ASSESSMENT TOOL CONFERENCE* 2019 Vienna, Austria, 2019.

Malagó, A., and Bouraoui, F., Global anthropogenic and natural nutrient fluxes: from local to planetary assessments. *Environ. Res. Lett.* 16, 2021, 054074, https://doi.org/10.1088/1748-9326/abe95f

Malagó, A., Pagliero, L., Bouraoui, F., and Franchini, M., Comparing calibrated parameter sets of the SWAT model for the Scandinavian and Iberian peninsulas. *Hydrol. Sci. J.* 60, 2015, 949–967. https://doi.org/10.1080/02626667.2014.978332

Malagó, A., Bouraoui, F., Vigiak, O., Grizzetti, B., and Pastori, M., Modelling water and nutrient fluxes in the Danube River Basin with SWAT. *Sci. Total Environ*. 603–604, 2017, 196–218. https://doi.org/10.1016/J.SCITOTENV.2017.05.242

Malagó, A., Bouraoui, F., Grizzetti, B., and de Roo, A., Modelling nutrient fluxes into the Mediterranean Sea. *J. Hydrol. Reg. Stud*. 22, 2019a, 100592. https://doi.org/10.1016/J.EJRH.2019.01.004

Malagó, A., Bouraoui, F., Pastori, M., and Gelati, E., Modelling nitrate reduction strategies from diffuse sources in the Po River Basin. *Water* (Switzerland) 11. 2019b, https://doi.org/10.3390/w11051030

Malagó, A., Bouraoui, F., and Comero, S., *Global database of nutrients monitoring points*, 2022, in preparation.

Messager, M.L., Lehner, B., Grill, G., Nedeva, I., and Schmitt, O., Estimating the volume and age of water stored in global lakes using a geo-statistical approach. *Nat. Commun*. 7117, 2016, 1–11. https://doi.org/10.1038/ncomms13603

Morée, A.L., Beusen, A.H.W., Bouwman, A.F., and Willems, W.J., Exploring global nitrogen and phosphorus flows in urban wastes during the twentieth century. *Global Biogeochem. Cycles* 27, 2013, 836–846. https://doi.org/10.1002/gbc.20072

Mubareka, S., Maes, J., Lavalle, C., and de Roo, A., Estimation of water requirements by livestock in Europe, *Ecosyst. Serv.*, 4, 2013, 139–145.

Neitsch, S.L., Arnold, J.G., Kiniry, J.R., and Williams, J.R., *Soil and Water Assessment Tool Theoretical Documentation* Version 2009. Grassland, Soil Water Res. Lab. Agric. Res. Blackl. Res. Center, Texas. Agric. Exp. Station. Coll. Station. Texas, 2011.

Olivera, F., Lear, M.S., Famiglietti, J.S., and Asante, K., Extracting low-resolution river networks from high-resolution digital elevation models. *Water Resour. Res.* 38, 2002, 131–138. https://doi.org/10.1029/2001WR000726

Pisoni E., Thunis P., De Meij A., Wilson J., Bessagnet B., Crippa M., Guizzardi D., Belis C.A., Van Dingenen R. Modelling the benefits of EU policies through the integration of two different health impact methodologies (under review).

Pistocchi, A., Aloe, A., Dorati, C., Alcalde Sanz, L., Bouraoui, F., Gawlik, B., et al., *The potential of water reuse for agricultural irrigation in the EU: a hydro economic analysis*, EUR 28980 EN, Publications Office of The European Union, Luxembourg, 2017.

Pistocchi, A., Dorati, C., Huld, T., and M. Salas Herrero, *Hydro-economic assessment of the potential of PV-RO desalinated seawater supply in the Mediterranean region: Modelling concept and analysis of water transport costs*, EUR 28982 EN, Publications Office of the European Union, Luxembourg, 2018.

Pistocchi, A., Dorati, C., Grizzetti, B., Udias, A., Vigiak, O., Zanni, *Water quality in Europe: effects of the Urban Wastewater Treatment Directive. A retrospective and scenario analysis of Dir. 91/271/EEC*, EUR 30003 EN, Publications Office of the European Union, Luxembourg, 2019, doi:10.2760/303163, JRC115607.

Pistocchi, A., Bleninger, T., Breyer, C., Caldera, U., Dorati, C., Ganora, D., et al., Can seawater desalination be a win-win fix to our water cycle? *Water Res.*, 182:20, 2020, doi: 10.1016/j.watres.2020.115906

Pistocchi A., Grizzetti B., Nielsen P.H., Parravicini V., Steinmetz H., Thornberg D., Vigiak O. *An assessment of options to improve the removal of excess nutrients from European wastewater* (under review).

Puy, A., Borgonovo, E., Lo Piano, S., Levin, S.A., and Saltelli, A., Irrigated areas drive irrigation water withdrawals. *Nat. Commun*. 2021 12 1 12, 2021, 1–12. https://doi.org/10.1038/s41467-021-24508-8

R Core Team, https://www.r-project.org/ [WWW Document]. URL https://www.r-project.org/ (accessed 4.1.20), 2011

REFIT, *COMMISSION STAFF WORKING DOCUMENT EVALUATION of the Council Directive 91/271/EEC of 21 May 1991, concerning urban waste-water treatment* [WWW Document], 2019. URL https://ec.europa.eu/environment/water/water-urbanwaste/pdf/UWWTD Evaluation SWD 448-701 web.pdf (accessed 1.4.21).

RPA, *Non-surfactant Organic Ingredients and Zeolite-based Detergents* [WWW Document], 2006. URL https://ec.europa.eu/docsroom/documents/14124/attachments/1/translations/ (accessed 2.23.22).

Schiavina, M., Freire, S., MacManus, K., *GHS population grid multitemporal* (1975, 1990, 2000, 2015) R2019A. European Commission, Joint Research Centre (JRC), 2019, DOI: 10.2905/42E8BE89-54FF-464E-BE7B-BF9E64DA5218 PID: http://data.europa.eu/89h/0c6b9751-a71f-4062-830b-43c9f432370f (download 5/3/2020)

Schreiber, H., Constantinescu, L.T., Cvitanic, I., Drumea, D., Jabucar, D., Juran, S., Pataki, B., Snishko, S., Zessner, M., and Behrendt, H., Environmental Research of the Federal Ministry of the Environment, Nature Conservation and Nuclear Safety *Harmonised Inventory of Point and Diffuse Emissions of Nitrogen and Phosphorus for a Transboundary River Basin*, 2003.

Schvitz, G., Girardin, L., Rüegger, S., Weidmann, N.B., Cederman, L.E., and Gleditsch, K.S., *Mapping the International System, 1886-2019: The CShapes 2.0 Dataset*, https://doi.org/10.1177/00220027211013563 66, 2021, 144–161. https://doi.org/10.1177/00220027211013563

Sharpley, A. N. and Williams, J. R., *EPIC–Erosion/Productivity Impact Calculator*: *1. Model Documentation*, US Department of Agriculture Technical Bulletin, 1990.

Sheldrick, W., Keith Syers, J., and Lingard, J., Contribution of livestock excreta to nutrient balances. Nutr. Cycl. *Agroecosystems* 66, 2003, 119–131. https://doi.org/10.1023/A:1023944131188

Siebert, S., and, Döll, P., Quantifying blue and green virtual water contents in global crop production as well as potential production losses without irrigation. *J. Hydrol.* 384, 2010, 198–217. https://doi.org/10.1016/J.JHYDROL.2009.07.031

Simpson, D., Benedictow, A., Berge, H., Bergström, R., Emberson, L.D., Fagerli, H., Flechard, C.R., Hayman, G.D., Gauss, M., Jonson, J.E., Jenkin, M.E., Nyíri, A., Richter, C., Semeena, V.S., Tsyro, S., Tuovinen, J.-P., Valdebenito, Á., and Wind, P., The EMEP MSC-W chemical transport model – technical description, *Atmos. Chem. Phys.*, 12, 2012, 7825–7865, https://doi.org/10.5194/acp-12-7825-2012.

Thiemig, V., Gomes, G. N., Skøien, J. O., Ziese, M., Rauthe-Schöch, A., Rustemeier, E., Rehfeldt, K., Walawender, J. P., Kolbe, C., Pichon, D., Schweim, C., and Salamon, P., EMO-5: A high-resolution multi-variable gridded meteorological data set for Europe, *Earth Syst. Sci. Data Discuss.*, [preprint], https://doi.org/10.5194/essd-2021-339, in review, 2021.

Tian, H., Yang, J., Lu, C., Xu, R., Canadell, J.G., Jackson, R.B., Arneth, A., Chang, J., Chen, G., Ciais, P., Gerber, S., Ito, A., Huang, Y., Joos, F., Lienert, S., Messina, P., Olin, S., Pan, S., Peng, C., Saikawa, E., Thompson, R.L., Vuichard, N., Winiwarter, W., Zaehle, S., Zhang, B., Zhang, K., and Zhu, Q., The global N2O model intercomparison project. *Bull. Am. Meteorol. Soc.* 99, 2018, 1231–1251. https://doi.org/10.1175/BAMS-D-17-0212.1

Udias, A., Grizzetti, B., Vigiak, O., Gomez, J., Alfaro, C., and Aloe, A., *GREENeR: Geospatial Regression Equation for European Nutrient Losses (GREEN).*, 2022, https://cran.r-project.org/web/packages/GREENeR/index.html

Vandecasteele, I., Bianchi, A., Batista e Silva, F., Lavalle, C., and Batelaan, O., Mapping current and future European public water withdrawals and consumption, *Hydrol. Earth Syst. Sci.*, 18, 407- 416, 2014,doi:10.5194/hess-18-407-2014.

van der Knijff, J. M., Younis, J., and de Roo, A.P.J., LISFLOOD: a GIS-based distributed model for river basin scale water balance and flood simulation, *Int. J. Geogr. Inform. Sci.*, 24, 189–212, 2010, https://doi.org/10.1080/13658810802549154.

Vigiak, O. et al. *Estimation of domestic and industrial waste emissions to European waters in the 2010s*, Report EUR29451EN, Publications Office of the European Union, Luxembourg, 2018, doi: https://doi.org/10.2760/204793

Vigiak, O., Grizzetti, B., Zanni, M., Aloe, A., Dorati, C., Bouraoui, F., and Pistocchi, A. Domestic waste emissions to European waters in the 2010s. *Scientific Data* 7, 2020, 33, doi: 10.1038/s41597-020-0367-0

Vigiak O, Udías A, Grizzetti B, Zanni M, Aloe A, Weiss F, Hristov J, Bisselink B, de Roo A, Pistocchi A. Recent regional changes in nutrient fluxes of European surface waters. *Science of the Total Environment* 858, 160063, 2023.

Vogt, J., Soille, P., De Jager, A., Rimaviciute, E., Mehl, W., Foisneau, S., Bodis, K., Dusart, J., Paracchini, M., Haastrup, P., and Bamps, C., *A pan-European River and Catchment Database*. JRC Reference Report EUR 22920 EN, Luxembourg, 2007. http://publications.jrc.ec.europa.eu/repository/handle/JRC40291.

Vogt, J., Rimaviciute, E., and de Jager, A., *CCM2 River and Catchment Database for Europe Version 2.1* Release Notes, 2008. http://ccm.jrc.ec.europa.eu/documents/JVogt_etal_CCM21.pdf.

Williams, J. R, *The EPIC Model, in: Computer Models of Watershed Hydrology*, chap. 25, edited by Singh, V. P., Water Resources Publications, Highlands Ranch, CO, USA, 1995, 909–1000.

Williams, J. R., Jones, C. A., Kiniry, J. R., and Spanel, D.A., The EPIC Crop Growth Model, *T. ASAE*, 32, 0497–0511, 1989, https://doi.org/10.13031/2013.31032.

WorldBank, *Agricultural water withdrawals vs. GDP per capita*, [WWW Document], 2017. URL https://ourworldindata.org/grapher/agricultural-water-withdrawals-vs-gdp-per-capita (accessed 2.23.22).

Wu, H., Kimball, J.S., Li, H., Huang, M., Leung, L.R., and Adler, R.F., A new global river network database for macroscale hydrologic modeling, *Water Resour. Res.*, 48(9), 2012, doi:10.1029/2012WR012313.

You, L., Wood-Sichra, U., Fritz, S., Guo, Z., See, L., and Koo, J., *Spatial Production Allocation Model (SPAM)* 2005 v2.0 (accessed on 01/09/2016), 2014, Available from http://mapspam.info. https://doi.org/10.1016/J.JAG.2005.06.010

List of figures

List of tables

Annexes

Annex 1. GREEN model - Historical nutrient input data

Table A1.1 Overview of nutrient sources considered in the GREEN model.

Type	Source	Nitrogen	Phosphorus	Spatial allocation
Diffuse	Mineral fertiliser	√	√	Agricultural
	Manure fertiliser	√	√	Agricultural
	Crop fixation	√		Agricultural
	Soil fixation	√		Agricultural
	Atmospheric deposition	√		All catchment
	Background losses		√	All catchment
	Scattered dwellings	√	√	All catchment
Point	Urban waste water discharges + Industrial emissions	√	√	Point discharges

A1.1 Land cover

For constructing the time series of land cover, spatial data from the Corine Land Cover maps (grid at 100 m resolution) available for year 2000, 2006, 2012 and 2018 for Europe were used. These maps were combined with ESA CCI Land Cover time-series v2.0.7 (1992 - 2015) and v2.1.1 (2016 – 2018) (ESA, 2017) (global grid at 300 m resolution, yearly maps) for countries not covered by the CLC, namely Andorra, Belarus, Republic of Moldova, Russian Federation, and Ukraine (Table A1.2). Original land cover classes were grouped into 5 main classes that were used for the spatialisation of nutrients input in the modelling (Table A1.3).

Table A.1.2. Assumptions made for the construction of the land cover map timeseries.

Year	CLC Version	ESA Version
1990	1990	1992
1991	1990	1992
1992	1990	1992
1993	1990	1993
1994	1990	1994
1995	1990	1995
1996	2000	1996
1997	2000	1997
1998	2000	1998
1999	2000	1999
2000	2000	2000
2001	2000	2001
2002	2000	2002

2003	2000	2003
2004	2006	2004
2005	2006	2005
2006	2006	2006
2007	2006	2007
2008	2006	2008
2009	2006	2009
2010	2012	2010
2011	2012	2011
2012	2012	2012
2013	2012	2013
2014	2012	2014
2015	2012	2015
2016	2018	2016
2017	2018	2017
2018	2018	2018

Table A1.3. Reclassification of the CLC and ESA land cover classes for the modelling

GREEN land cover class	CLC land cover classes	ESA land cover classes
Agricultural area	12 Non-irrigated arable land 13 Permanently irrigated land 14 Rice fields 15 Vineyards 16 Fruit trees and berry plantations 17 Olive groves 18 Pastures 19 Annual crops associated with permanent crops 20 Complex cultivation patterns 21 Land principally occupied by agriculture, with significant areas of natural vegetation 22 Agro-forestry areas	10 Cropland, rainfed 11 Herbaceous cover 12 Tree or shrub cover 20 Cropland, irrigated or post-flooding 130 Grassland

Artificial area	1	Continuous urban fabric	190	Urban areas
	2	Discontinuous urban fabric		
	3	Industrial or commercial units		
	4	Road and rail networks and associated land		
	5	Port areas		
	6	Airports		
	7	Mineral extraction sites		
	8	Dump sites		
	9	Construction sites		
	10	Green urban areas		
	11	Sport and leisure facilities		

Forest	23 Broad-leaved forest 24 Coniferous forest 25 Mixed forest 26 Natural grasslands 27 Moors and heathland 28 Sclerophyllous vegetation 29 Transitional woodland-shrub 30 Beaches, dunes, sands 31 Bare rocks 32 Sparsely vegetated areas 33 Burnt areas 34 Glaciers and perpetual snow	30 Mosaic cropland (>50%) / natural vegetation (tree, shrub, herbaceous cover) (<50%) 40 Mosaic natural vegetation (tree, shrub, herbaceous cover) (>50%) / cropland (<50%) 50 Tree cover, broadleaved, evergreen, closed to open (>15%) 60 Tree cover, broadleaved, deciduous, closed to open (>15%) 61 Tree cover, broadleaved, deciduous, closed (>40%) 62 Tree cover, broadleaved, deciduous, open (15-40%) 70 Tree cover, needleleaved, evergreen, closed to open (>15%) 71 Tree cover, needleleaved, evergreen, closed (>40%) 72 Tree cover, needleleaved, evergreen, open (15-40%) 80 Tree cover, needleleaved, deciduous, closed to open (>15%) 81 Tree cover, needleleaved, deciduous, closed (>40%) 82 Tree cover, needleleaved, deciduous, open (15-40%) 90 Tree cover, mixed leaf type (broadleaved and needleleaved) 100 Mosaic tree and shrub (>50%) / herbaceous cover (<50%) 110 Mosaic herbaceous cover (>50%) / tree and shrub (<50%) 120 Shrubland 121 Shrubland evergreen 122 Shrubland deciduous 140 Lichens and mosses 150 Sparse vegetation (tree, shrub, herbaceous cover) (<15%) 151 Sparse tree (<15%) 152 Sparse shrub (<15%) 153 Sparse herbaceous cover (<15%) 200 Bare areas 201 Consolidated bare areas 202 Unconsolidated bare areas 220 Permanent snow and ice

Wetland	35	Inland marshes	160 Tree cover, flooded, fresh or brakish water
	36	Peat bogs	170 Tree cover, flooded, saline water
	37	Salt marshes	180 Shrub or herbaceous cover, flooded, fresh/saline/brakish water
	38	Salines	
	39	Intertidal flats	
Water	40	Water courses	210 Water bodies
	41	Water bodies	
	42	Coastal lagoons	
	43	Estuaries	
	44	Sea and ocean	

A1.2 Agriculture sources

Data on nitrogen and phosphorus mineral fertiliser and manure applied to soils were retrieved from CAPRI model (Barreiro Hurle et al. 2021) at the regional level (correspondent mainly to administrative Nuts2 regions) and from FAOSTAT data (accessed in October 2021) at the country level (Table A1.4). Before using the CAPRI data, the timeseries was corrected to fill in few missing data. The CAPRI timeseries covers the EU27 countries, United Kingdom, Norway and Balkans (i.e. Albania, Bosnia and Herzegovina, Montenegro, North Macedonia, Serbia, Kosovo). For Andorra, Liechtenstein and San Marino, and small mainly urban areas, we used CAPRI data from a neighbouring region (Table A1.5).

For Belarus, Switzerland, Republic of Moldova, Russian Federation, Turkey and Ukraine, for which data on fertilization and agricultural area were not available from CAPRI, we used the data on agricultural area from the ESA land cover (1990-2018) and the data on fertilizer from FAOSTAT (Table A1.3). In specific, we used: "Fertilisers by Nutrient, agricultural use, N and P2O5" to compute N and P mineral fertiliser; "Livestock Manure, Manure left on pasture (N content) + Manure applied to soils (N content), total all animals" to compute nitrogen manure. We estimated phosphorus manure from N:P ratio in CAPRI country data (weighted average for year 2014).

The CAPRI timeseries has annual data from 1990 to 2014, while FAOSTAT data cover the entire period 1990-2018. To complete the CAPRI timeseries for years 2015-2018, values of mineral fertiliser and manure of 2014 were multiplied by the percentage of annual change (compared to year 2014) of mineral fertiliser and (nitrogen) manure reported in FAOSTAT data.

Table A1.4. Agricultural data sources per country

Country Name	Country ISO2	Country CAPRI	EU 27	Land Cover Data	Fertiliser Data	Agricultural area
Albania	AL	AL	no	CLC	CAPRI data	CAPRI data
Andorra	AD	AD	no	ESA	CAPRI data assigned	ESA
Austria	AT	AT	yes	CLC	CAPRI data	CAPRI data
Bosnia and Herzegovina	BA	BA	no	CLC	CAPRI data	CAPRI data
Belgium	BE	BL*	yes	CLC	CAPRI data	CAPRI data

Bulgaria	BG	BG	yes	CLC	CAPRI data	CAPRI data
Belarus	BY	BY	no	ESA	FAOSTAT data	ESA
Switzerland	CH	CH	no	CLC	FAOSTAT data	ESA
Cyprus	CY	CY	yes	CLC	CAPRI data	CAPRI data
Czechia	CZ	CZ	yes	CLC	CAPRI data	CAPRI data
Germany	DE	DE	yes	CLC	CAPRI data	CAPRI data
Denmark	DK	DK	yes	CLC	CAPRI data	CAPRI data
Estonia	EE	EE	yes	CLC	CAPRI data	CAPRI data
Spain	ES	ES	yes	CLC	CAPRI data	CAPRI data
Finland	FI	FI	yes	CLC	CAPRI data	CAPRI data
France	FR	FR	yes	CLC	CAPRI data	CAPRI data
United Kingdom of Great Britain and Northern Ireland	GB	UK	no	CLC	CAPRI data	CAPRI data
Greece	GR	EL	yes	CLC	CAPRI data	CAPRI data
Croatia	HR	HR	yes	CLC	CAPRI data	CAPRI data
Hungary	HU	HU	yes	CLC	CAPRI data	CAPRI data
Ireland	IE	IR	yes	CLC	CAPRI data	CAPRI data
Italy	IT	IT	yes	CLC	CAPRI data	CAPRI data
Liechtenstein	LI	LI	no	CLC	CAPRI data assigned	CAPRI data assigned
Lithuania	LT	LT	yes	CLC	CAPRI data	CAPRI data
Luxembourg	LU	BL*	yes	CLC	CAPRI data	CAPRI data
Latvia	LV	LV	yes	CLC	CAPRI data	CAPRI data
Republic of Moldova	MD	MD	no	ESA	FAOSTAT data	ESA
Montenegro	ME	MO	no	CLC	CAPRI data	CAPRI data
North Macedonia	MK	MK	no	CLC	CAPRI data	CAPRI data
Malta	MT	MT	yes	CLC	CAPRI data	CAPRI data
Netherlands	NL	NL	yes	CLC	CAPRI data	CAPRI data
Norway	NO	NO	no	CLC	CAPRI data	CAPRI data
Poland	PL	PL	yes	CLC	CAPRI data	CAPRI data
Portugal	PT	PT	yes	CLC	CAPRI data	CAPRI data
Romania	RO	RO	yes	CLC	CAPRI data	CAPRI data

Serbia	RS	CS	no	CLC	CAPRI data	CAPRI data
Russian Federation	RU	RU	no	ESA	FAOSTAT data	ESA
Sweden	SE	SE	yes	CLC	CAPRI data	CAPRI data
Slovenia	SI	SI	yes	CLC	CAPRI data	CAPRI data
Slovakia	SK	SK	yes	CLC	CAPRI data	CAPRI data
San Marino	SM	SM	no	CLC	CAPRI data assigned	CAPRI data assigned
Turkey	TR	TR	no	CLC	FAOSTAT data	ESA
Ukraine	UA	UA	no	ESA	FAOSTAT data	ESA
Kosovo	XK	KO	no	CLC	CAPRI data	CAPRI data

Assumptions for gap filling:

NUTSII	neighbourNuts	countryCode	hasCorine
AD000000	ES510000	NULL	0
AT130000	AT120000	NULL	1
BL100000	BL240000	NULL	1
BY000000	NULL	NULL	0
CH000000	NULL	NULL	1
DE300000	DE400000	NULL	1
DE500000	DE930000	NULL	1
DE600000	DEF00000	NULL	1
LI000000	AT340000	NULL	1
MD000000	NULL	NULL	0
RU000000	NULL	NULL	0
SM000000	IT400000	NULL	1
TR000000	NULL	NULL	1
UA000000	NULL	NULL	0
UKI00000	UKJ00000	NULL	1

Nitrogen crop fixation were available from the CAPRI timeseries. For the six countries not covered by CAPRI we assigned the average BIOFIX value (kgN/ha agricultural area) of a neighbouring country with CAPRI timeseries (Table A1.5).

Table A1.5. Countries to which CAPRI data of nitrogen crop fixation was extended to.

country ESA	country CAPRI
Turkey	EL000000
Russia	FI000000
Switzerland	AT000000
Moldova	RO000000
Ukraina	PL000000

Belarus	PL000000

For nitrogen crop fixation of years from 2015 to 2018 we used the value of 2014 (last year of the CAPRI timeseries available).

Values from CAPRI timeseries were rescaled to the agricultural land class used in the modelling (derived from the CLC and ESA agricultural land cover class) to keep the total amount of agricultural input consistent with the agricultural area reported in the CAPRI timeseries. This was not necessary for the countries using exclusively FAOSTAT data, where the ESA agricultural land was used to distribute the total fertiliser input reported in FAOSTAT.

A1.3 Background sources

Background sources of nitrogen and phosphorus were considered in the modelling based on the literature. For nitrogen a soil fixation of 4 kgN/ha was added in the agricultural area. For phosphorus, background sources (originated from rock weathering and atmospheric deposition) of 0.15 kgP/ha (in all catchment area) were considered, as in the previous version of the model.

A1.4 Atmospheric deposition

Annual total nitrogen atmospheric deposition was computed using the annual data from the EMEP model (EMEP, 2020). In specific, we used 2000-2018 data from EMEP Status Report 2019. Values of year 2000 were used for years from 1990 to 1999 to complete the time series.

A1.5 Domestic emissions

The estimation of domestic emissions to water followed the methodology of Vigiak et al. (2018; 2020). For the period 1990-2010, domestic emissions in terms of Population Equivalent (PE) were assessed every 5 years from 1990 to 2010 based on the spatial distribution of population density and on national statistics of domestic waste treatment (population approach in Vigiak et al., 2018; 2020). For 2016, domestic emission was based on the 10th UWWTD database for the countries that reported in it (reported approach), and with the population approach for the remaining of the area covered as in Vigiak et al. (2020).

From PE, emissions of TN and TP were estimated based on national diet (FAO data on protein consumption) and P in detergents, and removal efficiencies per treatment level (as per Vigiak et al. 2020). Finally, CCM2 catchment domestic emissions of TN and TP estimated for 1990, 1995, 2000, 2005, 2010 and 2016 were then interpolated to all other years of the time-series. Estimations for 2016 were maintained also for 2017 and 2018.

A1.5.1 *National Statistics of population and treatment level*

The percentage population connected to sewer system and receiving waste treatment level were derived from national statistics (EUROSTAT, OECD, and JUMP WHO data).

The EUROSTAT (2021) 'Population connected to wastewater treatment plants' dataset (env_ww_con) report annual data (as percentage) from 1970 to 2018 on percentage of population as:

- TOTAL = Total connected to wastewater treatment;
- WWT_GE2 = Urban, independent and other wastewater treatment - at least secondary treatment;
- URB_CS = Urban wastewater collecting system;
- URB_OTH =Urban and other wastewater treatment plants – total;
- URB_OTH_T1 = Urban and other wastewater treatment plants - primary treatment;
- URB_OTH_T2 = Urban and other wastewater treatment plants - secondary treatment;

- URB_OTH_T3 = Urban and other wastewater treatment plants - tertiary treatment;
- URB_OTH_GE2 = Urban and other wastewater treatment plants - at least secondary treatment;
- URB_OTH_NSP = Urban and other wastewater treatment plants - treatment not specified;
- URB_OTH_NC = Resident population not connected to urban and other wastewater treatment plants;
- IND = Independent wastewater treatment – total;
- IND_T_GE2 = Independent wastewater treatment - at least secondary treatment;
- IND_TANK = Resident population whose wastewater is transported from independent storage tanks to wastewater treatment plants by means of trucks

The general rules defined in Vigiak et al. (2018) were adapted to new statistical items. Checks and adaptation were made country by country to ensure the interpretation of reported data was coherent, for examples some countries used URB_OTH_NC to report SD but in other cases they used to report the fraction of domestic waste collected but not treated (P0). The general rules were:

- Connected population:
    - conn = TOTAL
    - P0 = conn - (URB_OTH_T1+URB_OTH_T2+URB_OTH_T3) # often = URB_OTH_NC;
    - P1 = URB_OTH_T1 + URB_OTH_NSP
    - P2 = URB_OTH_T2
    - P3 = URB_OTH_T3
- Disconnected population:
    - IAS2 = IND_T_GE2 when available or 0
    - IAS1 = IND - IND_T_GE2; sometimes I had to use IND_TANK
    - SD = 100 – all else

When available, URB_OTH_GE2 was used to respect sum P2+P3. The annual sum of all items was corrected to 100. For 1990, when no EUROSTAT data was available, information on connections gathered through REFIT project was used (Pistocchi et al., 2019), which was aligned with information contained in EUROSTAT (2021).

Gaps between years were solved by interpolation. For extrapolation to the past, P3 and IAS2 were set to zero till the first available year. Only Norway had reported P3 higher than 0 In 1970. Most of the extrapolation rules affect the years 1970-1990; after 1990 usually more information was available. Exploratory analysis between treatment levels and GDP did not show strong relationships, and the trial was dropped. For extrapolation to most recent year (2018), the last available information of the time series was used.

National statistics for countries not reporting in EUROSTAT (i.e. AD AZ BY GE MD ME MK RU UA) were retrieved by merging information of 1990 and 2015 reported in Pistocchi et al. (2019) with data provided in van Puijenbroak et al., 2019 (doi: 10.1016/j.jenvman.2018.10.048) for 2000 and 2010. For these countries, lacking any information, IAS were set to 0. Data after last available information (usually 2015) were kept as the last data. Gaps were interpolated. Figure A1.1 shows the final percentage of population per country adopted in the study.

Figure A1.1. Country population fractions in time. LEGEND: continuous line: reported data, dashed line = interpolation/extrapolations

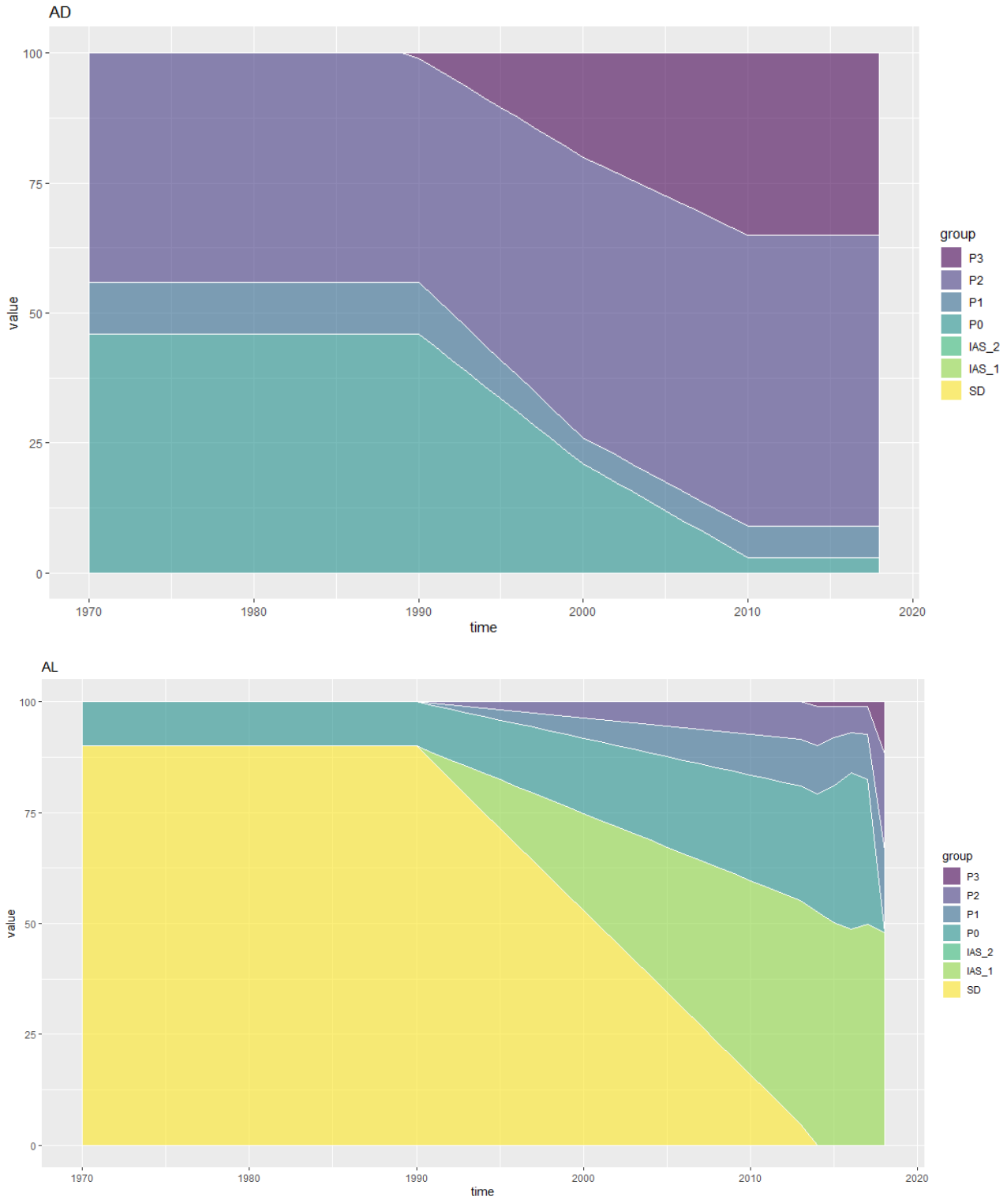

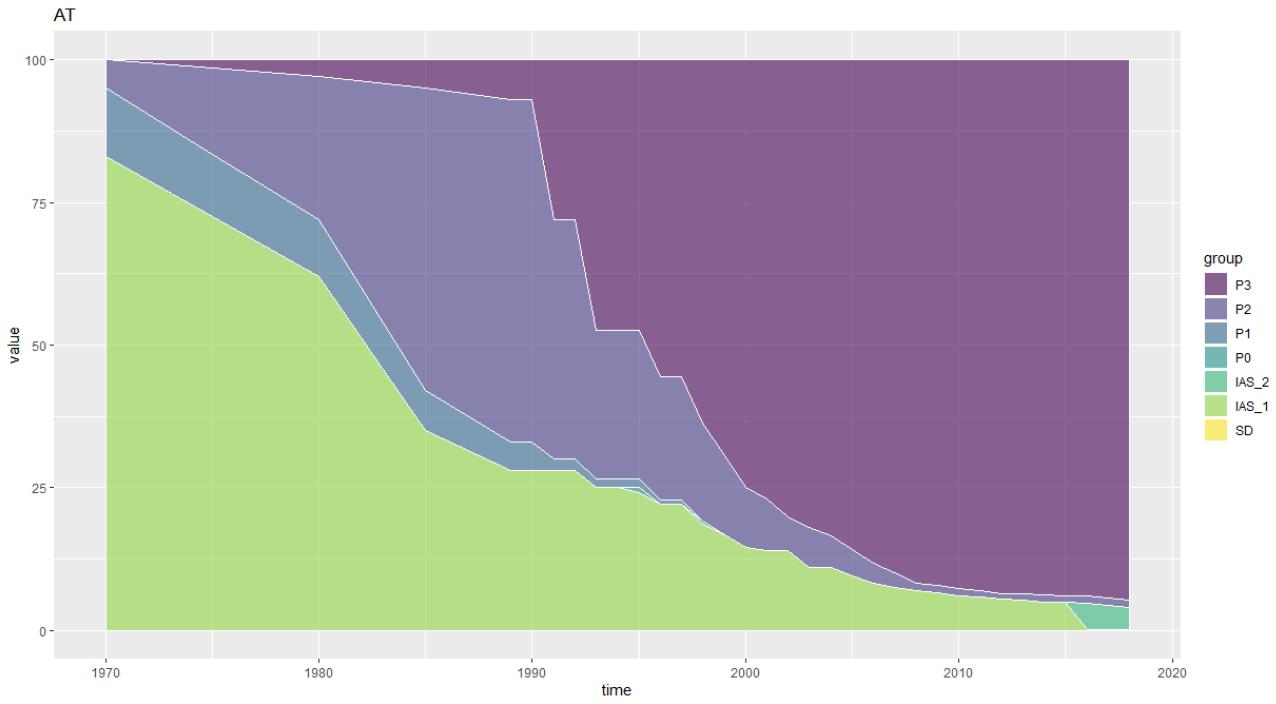
AT
100
75
50
25
0
value
1970
1980
1990
2000
2010
2020
time
group
P3
P2
P1
P0
IAS_2
IAS_1
SD

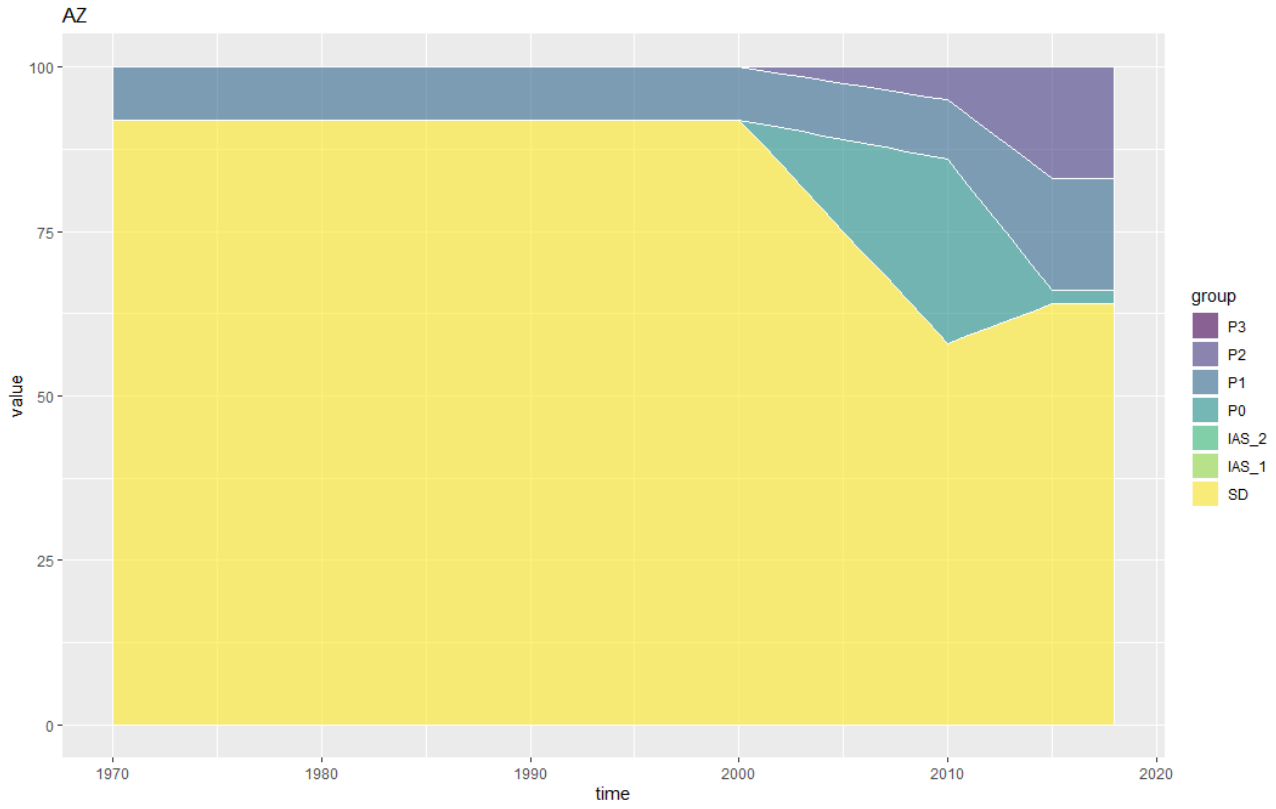
AZ
100
75
50
25
0
value
1970
1980
1990
2000
2010
2020
time
group
P3
P2
P1
P0
IAS_2
IAS_1
SD

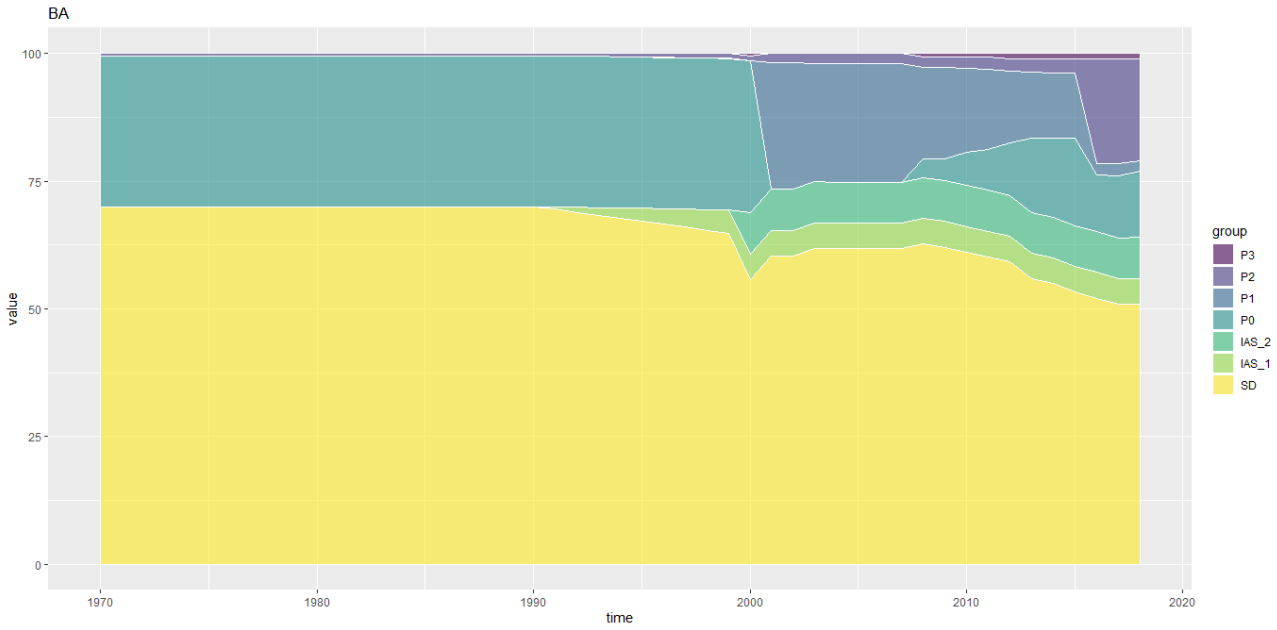
BA
100
75
50
25
0
value
1970
1980
1990
2000
2010
2020
time
group
P3
P2
P1
P0
IAS_2
IAS_1
SD

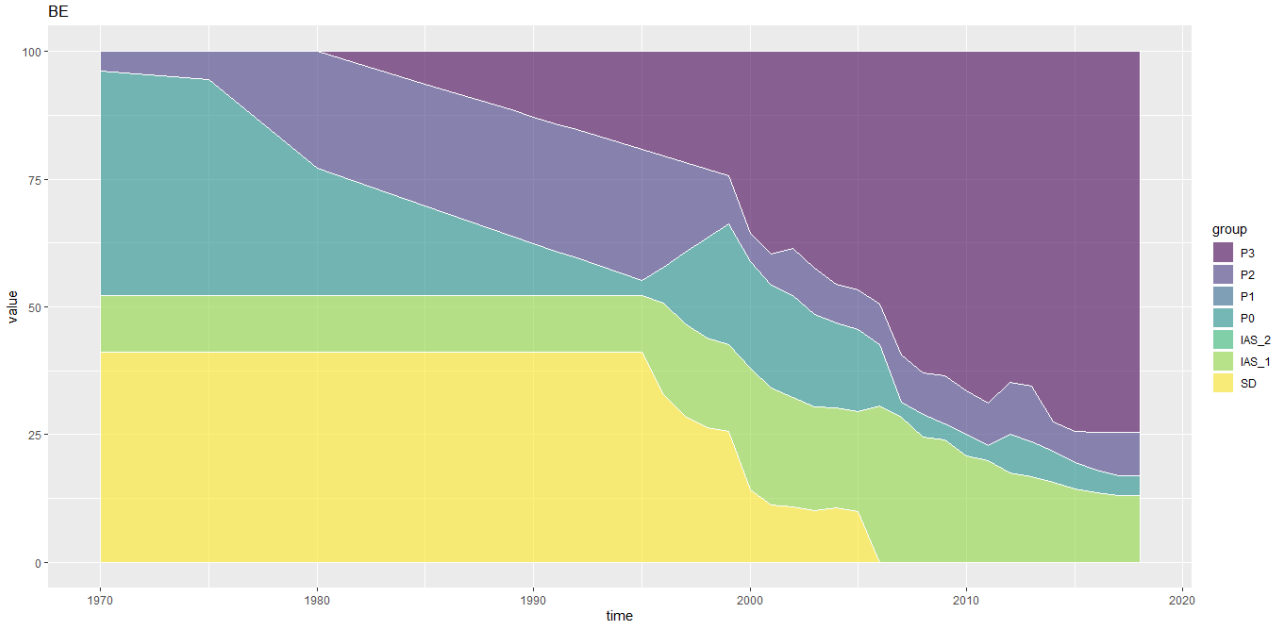
BE
100
75
50
25
0
value
1970
1980
1990
2000
2010
2020
time
group
P3
P2
P1
P0
IAS_2
IAS_1
SD

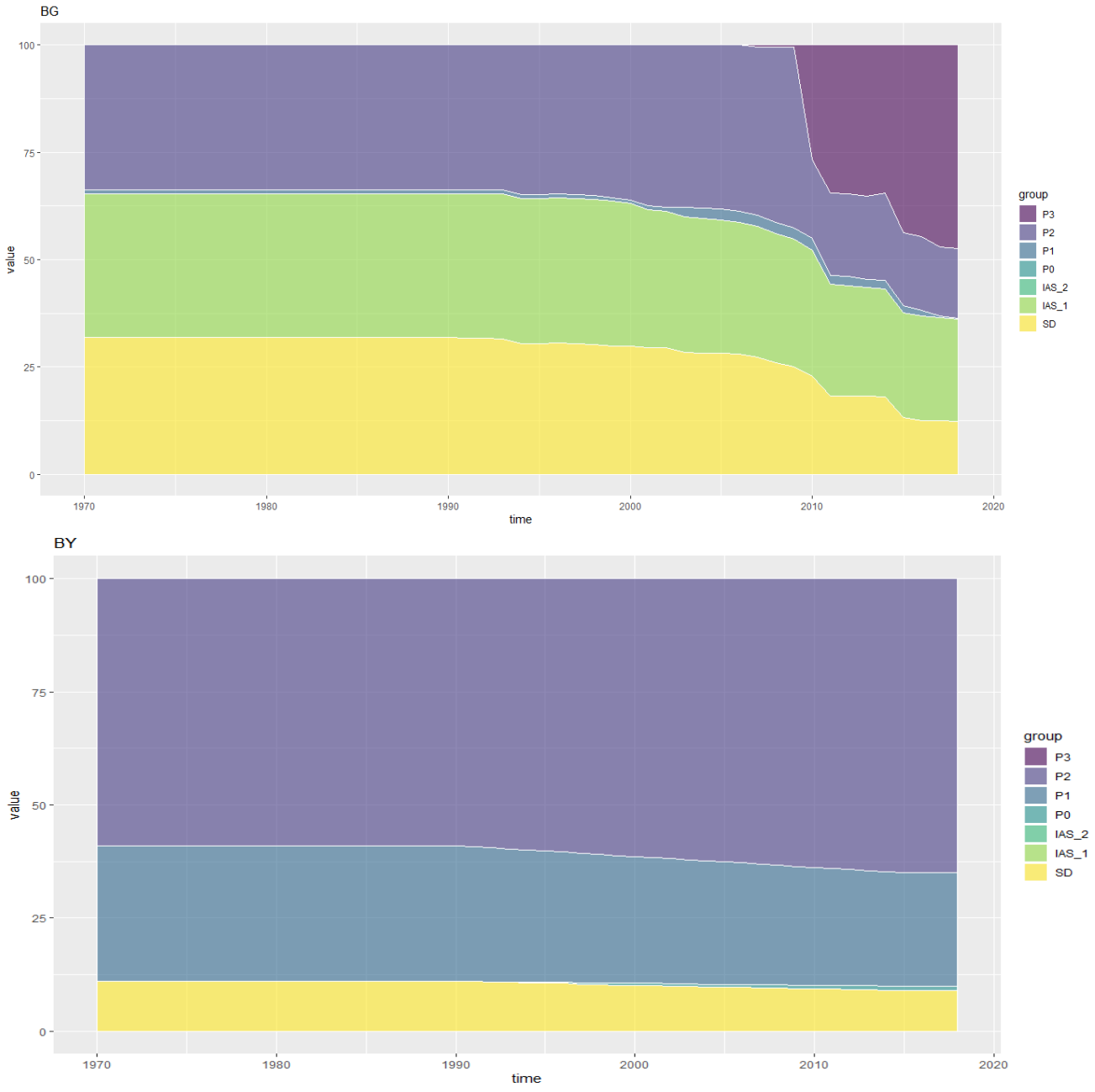
BG
100
75
50
25
0
value
1970
1980
1990
2000
2010
2020
time
group
P3
P2
P1
P0
IAS_2
IAS_1
SD
BY
100
75
50
25
0
value
1970
1980
1990
2000
2010
2020
time
group
P3
P2
P1
P0
IAS_2
IAS_1
SD

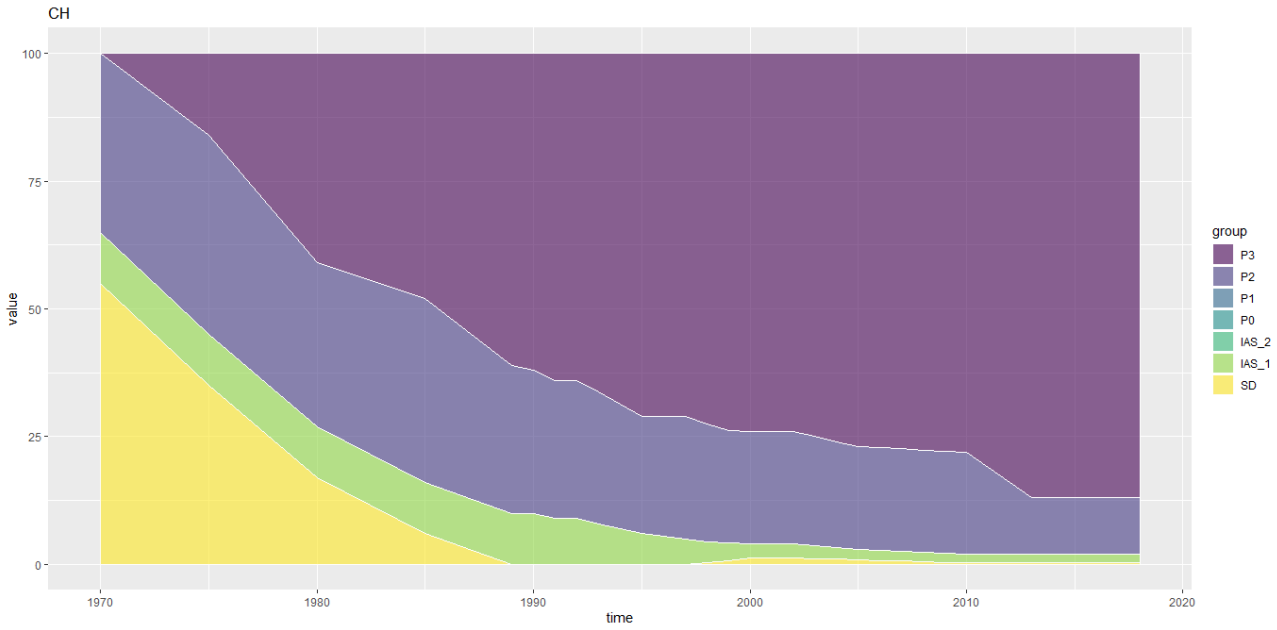
CH
100
75
50
25
0
value
1970
1980
1990
2000
2010
2020
time
group
P3
P2
P1
P0
IAS_2
IAS_1
SD

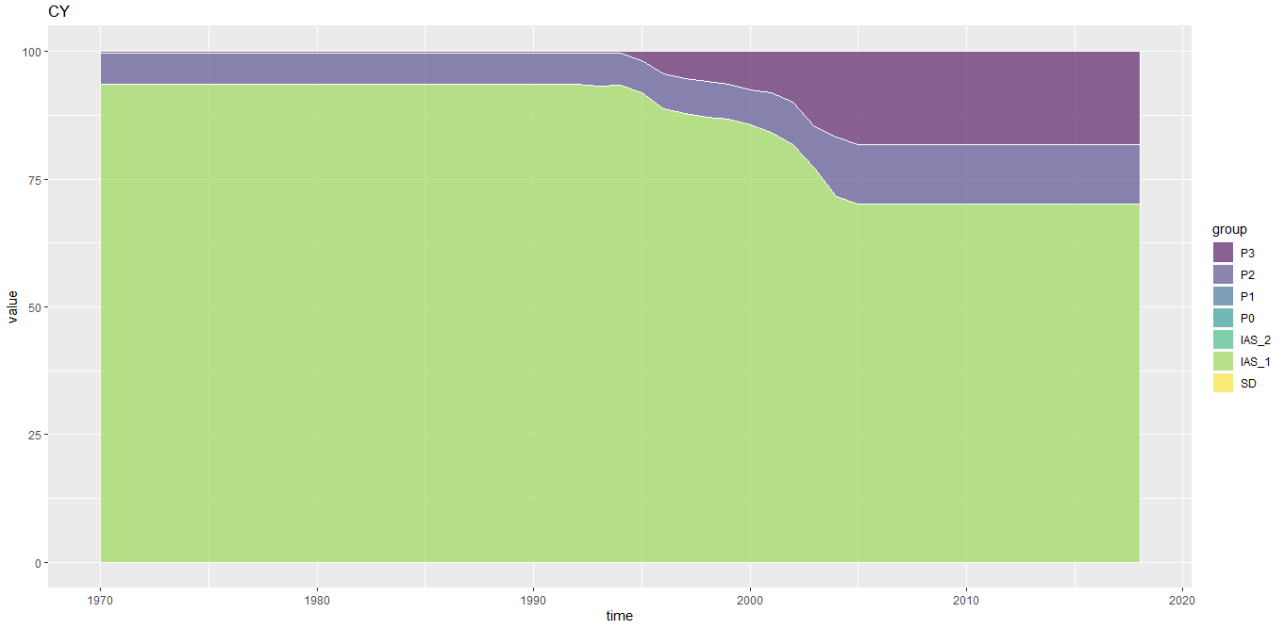
CY
100
75
50
25
0
value
1970
1980
1990
2000
2010
2020
time
group
P3
P2
P1
P0
IAS_2
IAS_1
SD

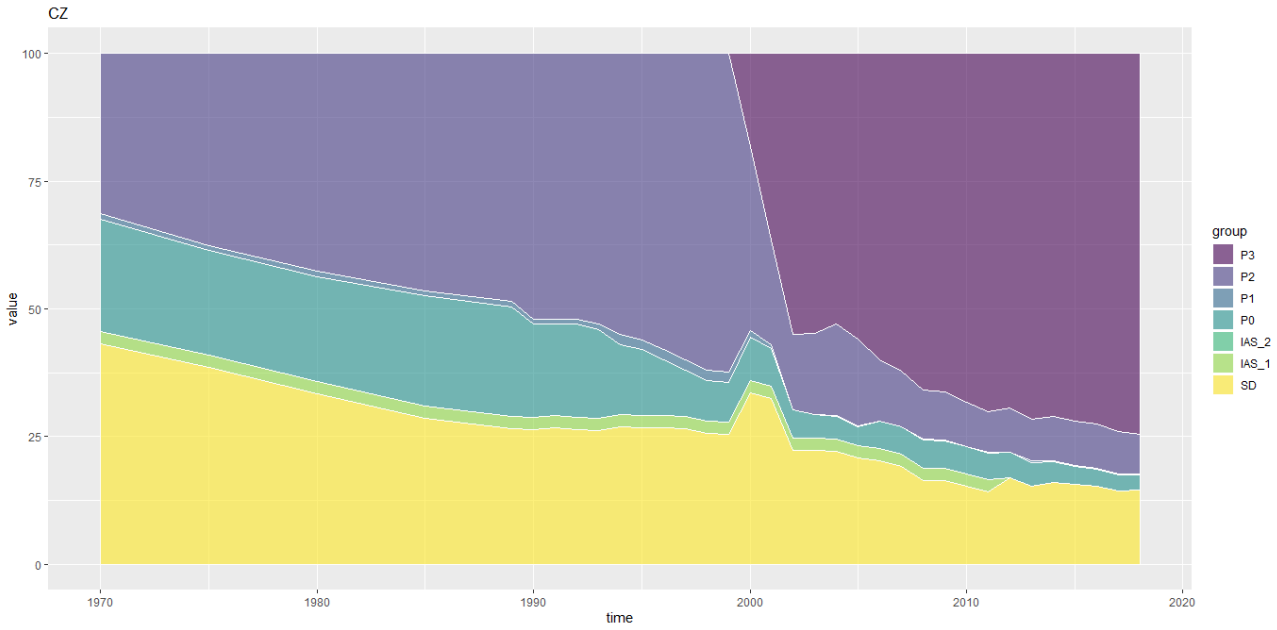
CZ
100
75
50
25
0
value
1970
1980
1990
2000
2010
2020
time
group
P3
P2
P1
P0
IAS_2
IAS_1
SD

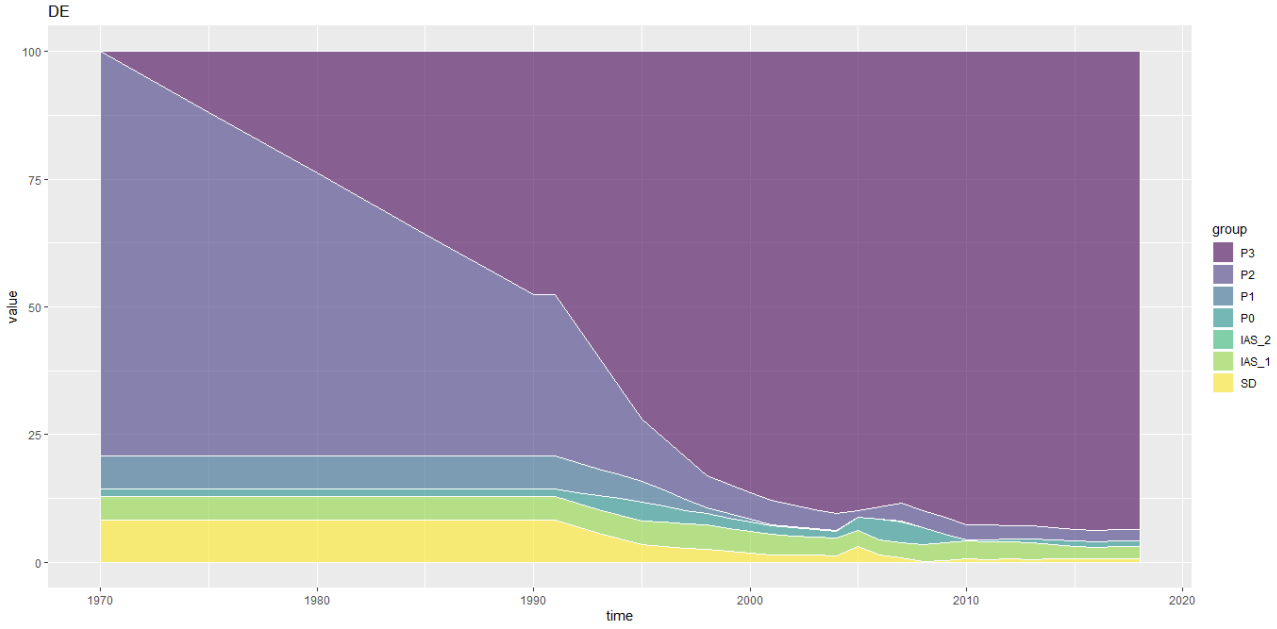
DE
100
75
50
25
0
value
1970
1980
1990
2000
2010
2020
time
group
P3
P2
P1
P0
IAS_2
IAS_1
SD

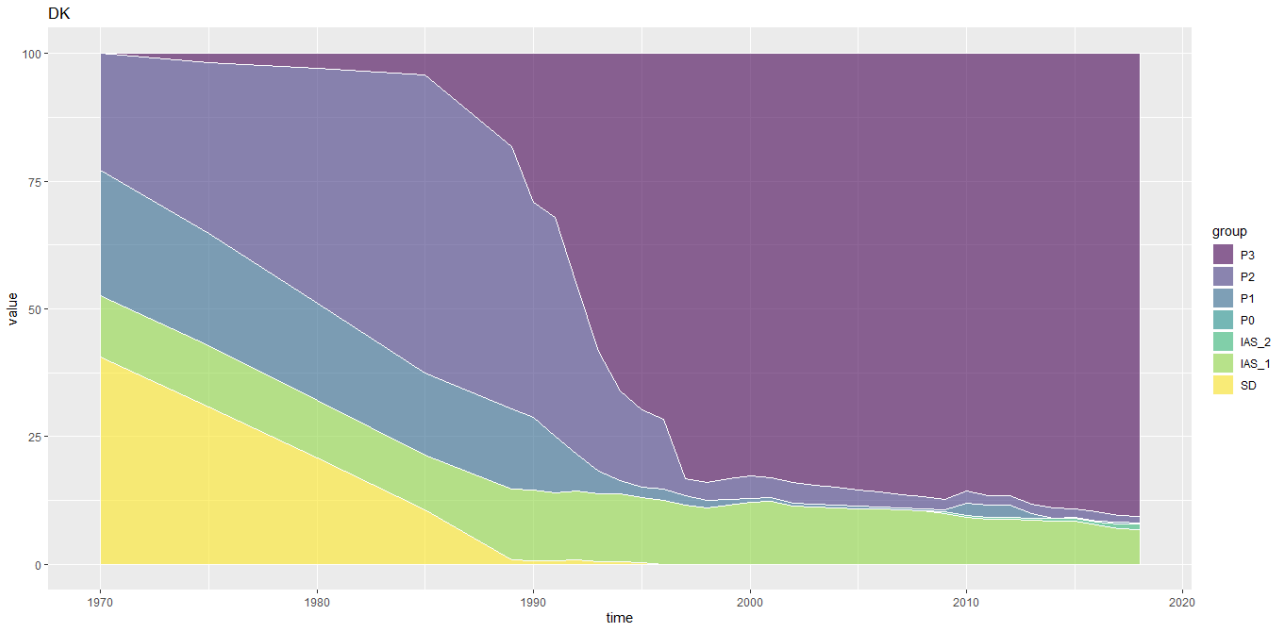
DK
100
75
50
25
0
value
1970
1980
1990
2000
2010
2020
time
group
P3
P2
P1
P0
IAS_2
IAS_1
SD

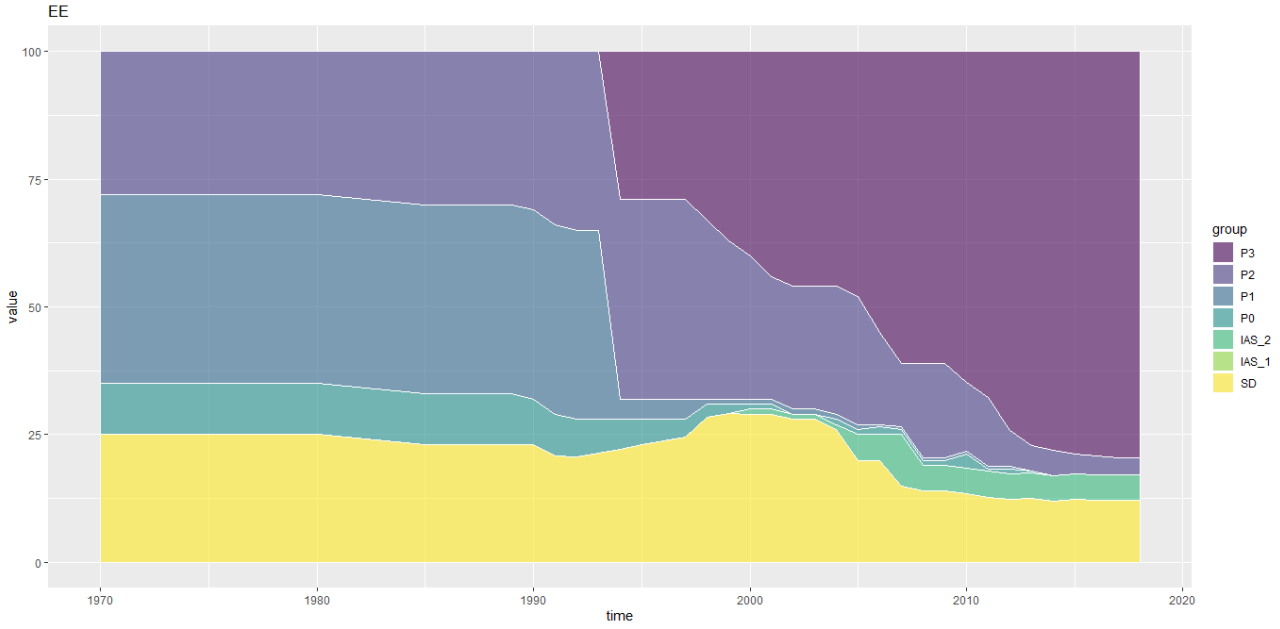
EE
100
75
50
25
0
value
1970
1980
1990
2000
2010
2020
time
group
P3
P2
P1
P0
IAS_2
IAS_1
SD

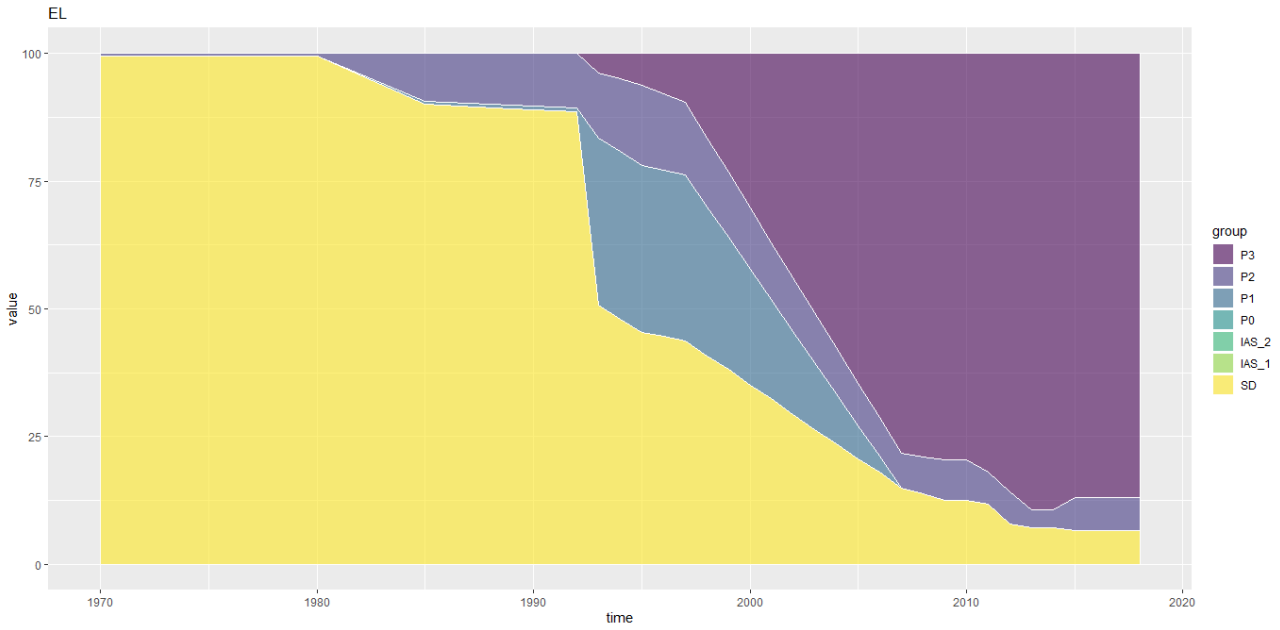
EL
100
75
50
25
0
value
1970
1980
1990
2000
2010
2020
time
group
P3
P2
P1
P0
IAS_2
IAS_1
SD

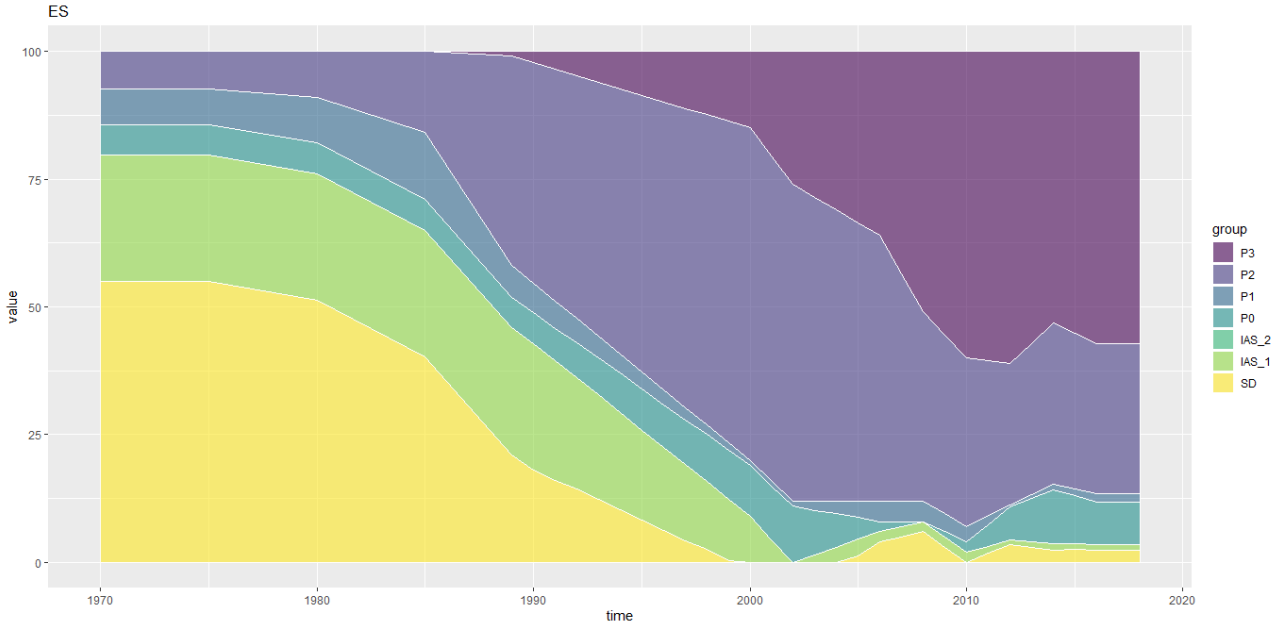
ES
100
75
50
25
0
value
1970
1980
1990
2000
2010
2020
time
group
P3
P2
P1
P0
IAS_2
IAS_1
SD

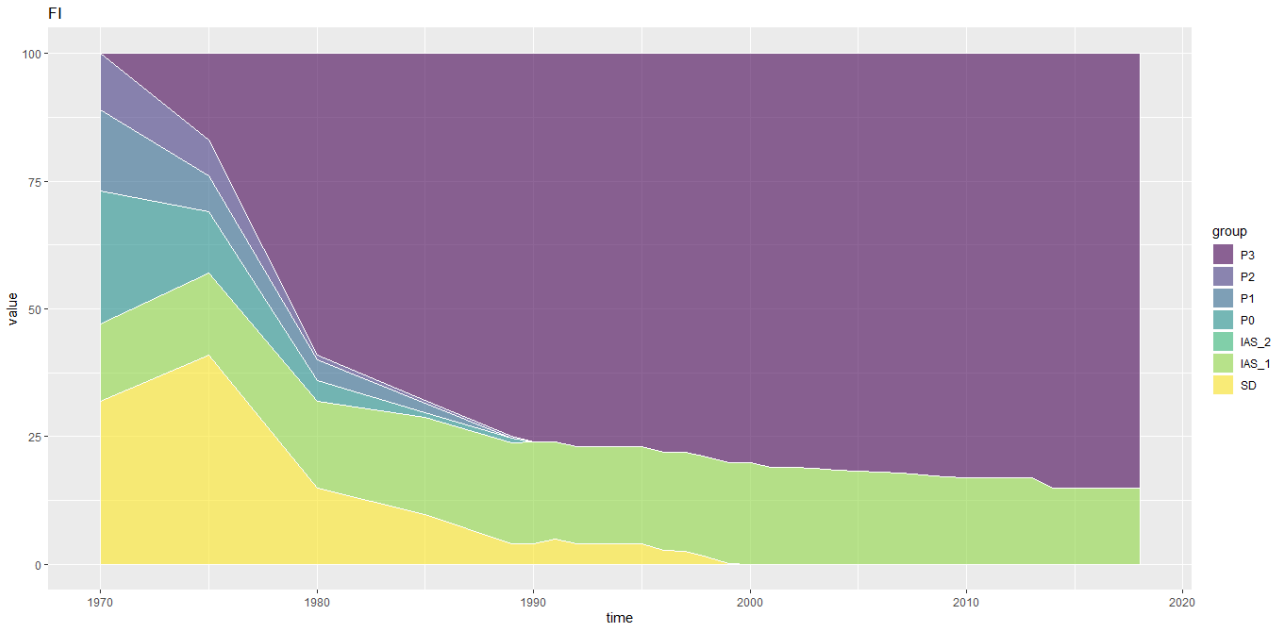
FI
100
75
50
25
0
value
1970
1980
1990
2000
2010
2020
time
group
P3
P2
P1
P0
IAS_2
IAS_1
SD

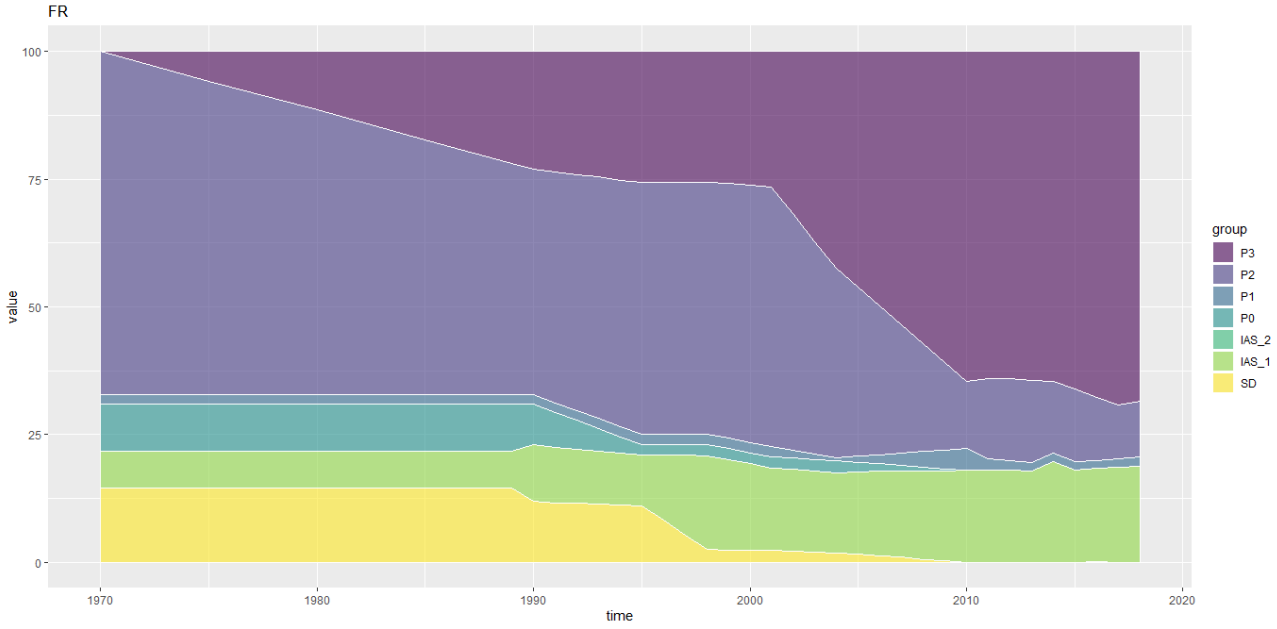
FR
100
75
50
25
0
value
1970
1980
1990
2000
2010
2020
time
group
P3
P2
P1
P0
IAS_2
IAS_1
SD

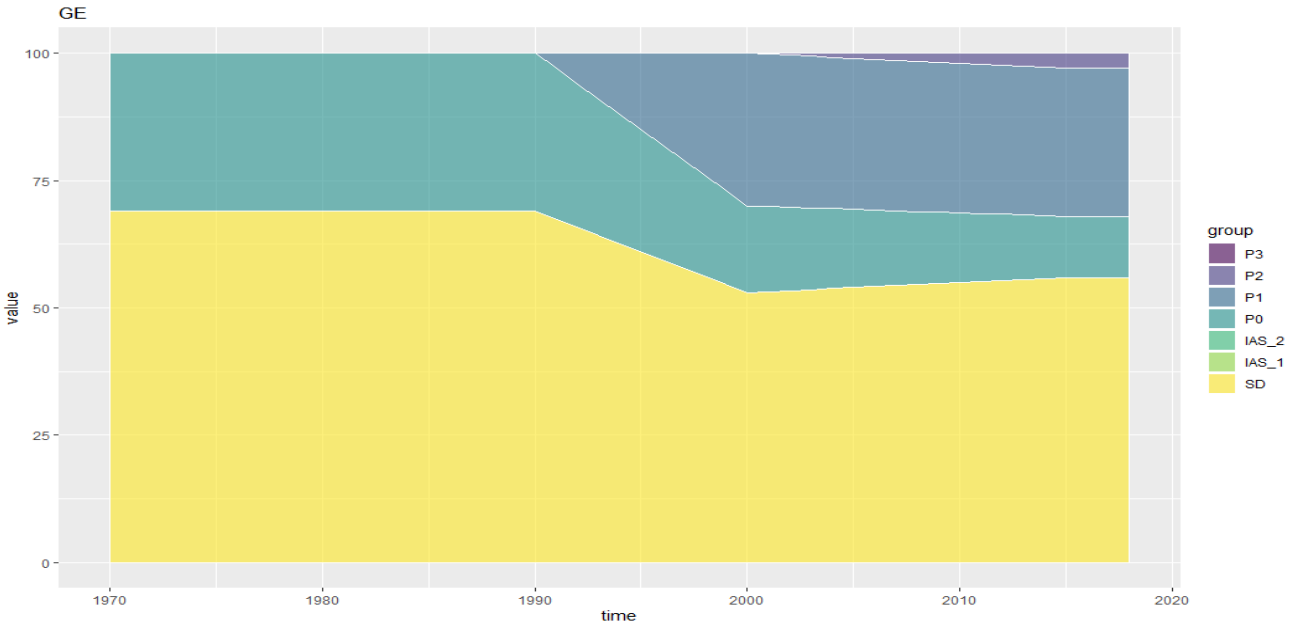
GE
100
75
50
25
0
value
1970
1980
1990
2000
2010
2020
time
group
P3
P2
P1
P0
IAS_2
IAS_1
SD

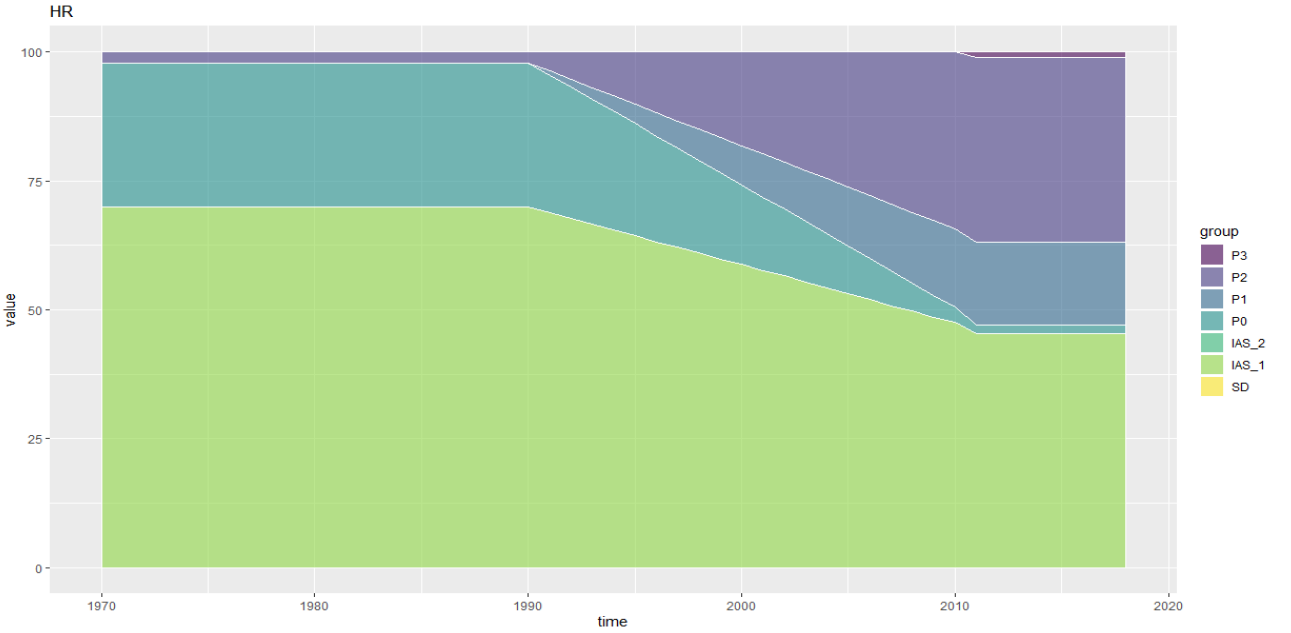
HR
100
75
50
25
0
value
1970
1980
1990
2000
2010
2020
time
group
P3
P2
P1
P0
IAS_2
IAS_1
SD

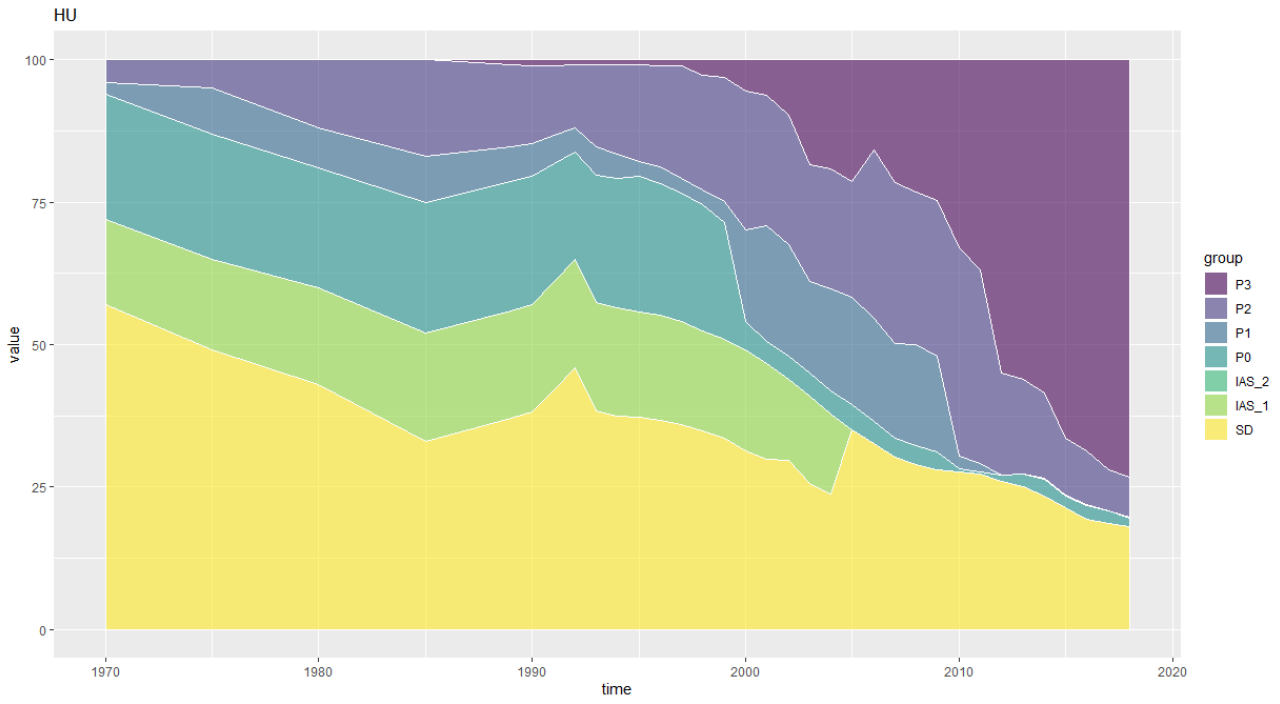
HU
100
75
50
25
0
value
1970
1980
1990
2000
2010
2020
time
group
P3
P2
P1
P0
IAS_2
IAS_1
SD

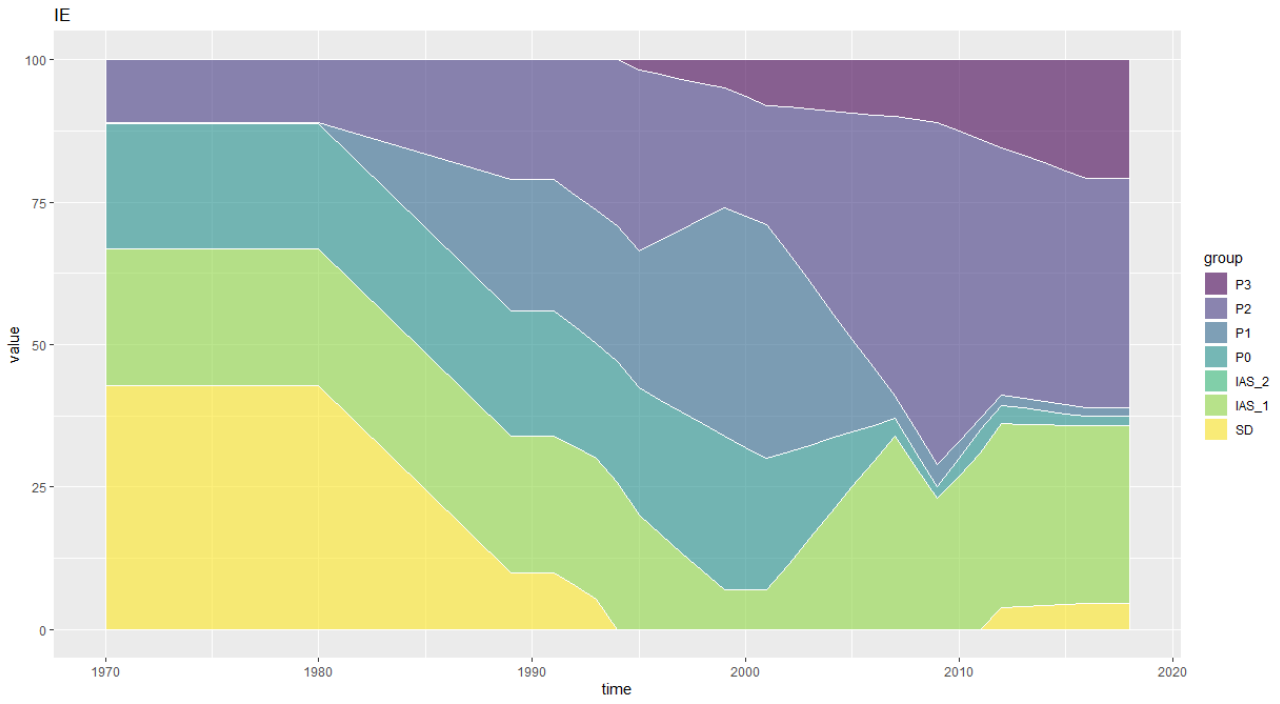
IE
100
75
50
25
0
value
1970
1980
1990
2000
2010
2020
time
group
P3
P2
P1
P0
IAS_2
IAS_1
SD

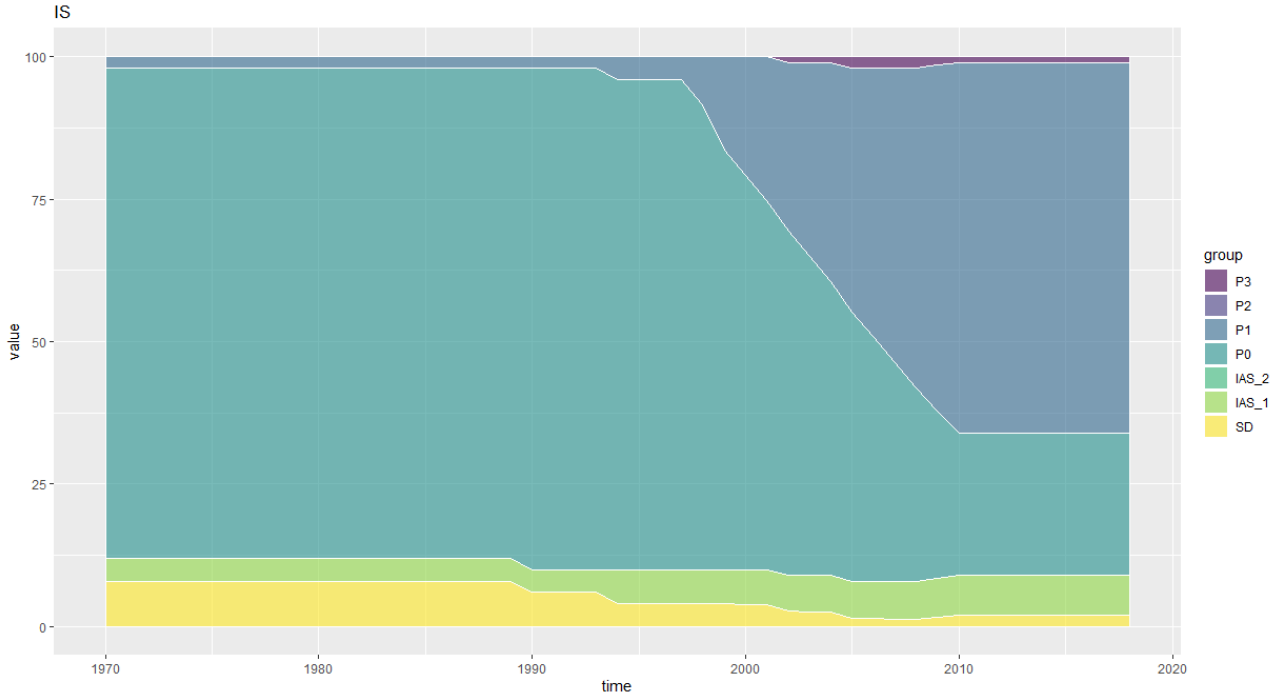
IS
100
75
50
25
0
value
1970
1980
1990
2000
2010
2020
time
group
P3
P2
P1
P0
IAS_2
IAS_1
SD

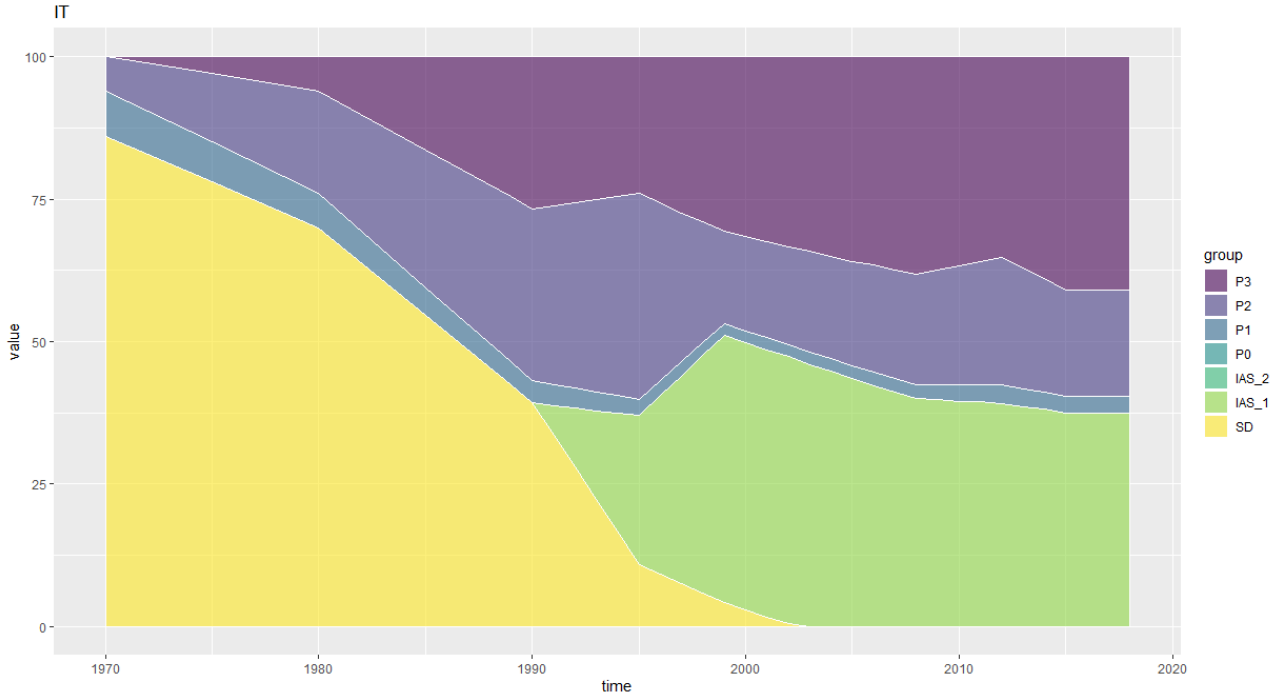
IT
100
75
50
25
0
value
1970
1980
1990
2000
2010
2020
time
group
P3
P2
P1
P0
IAS_2
IAS_1
SD

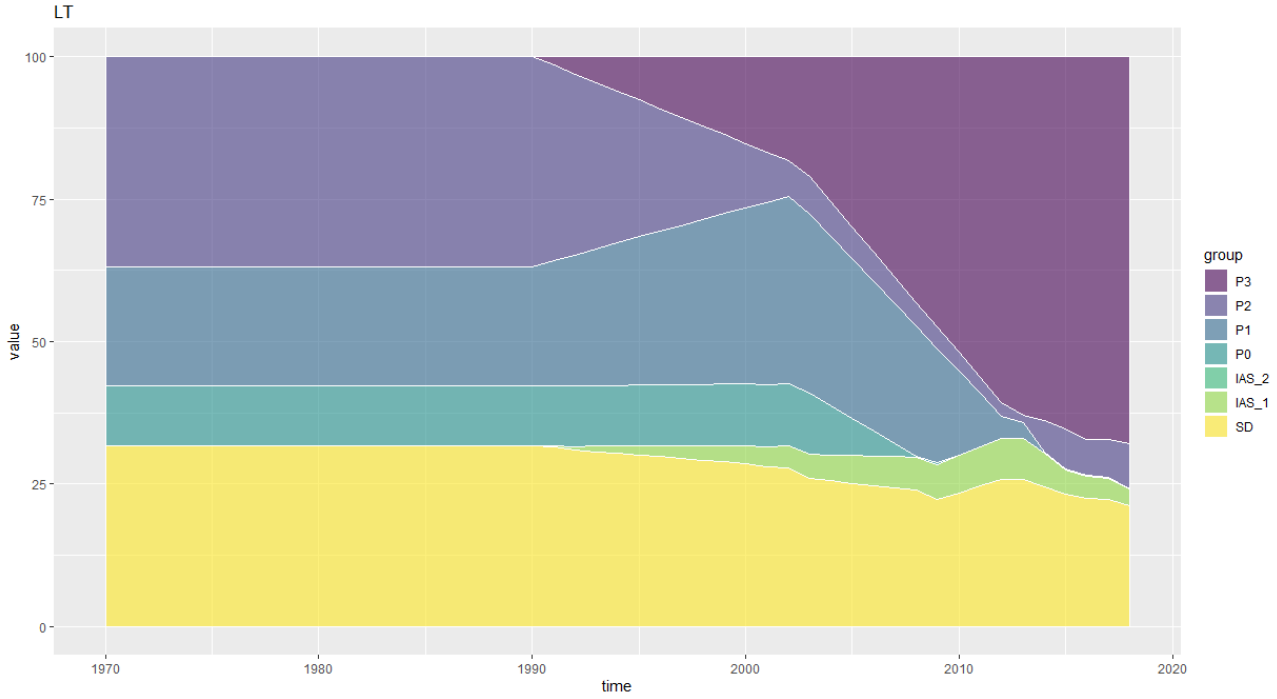
LT
100
75
50
25
0
value
1970
1980
1990
2000
2010
2020
time
group
P3
P2
P1
P0
IAS_2
IAS_1
SD

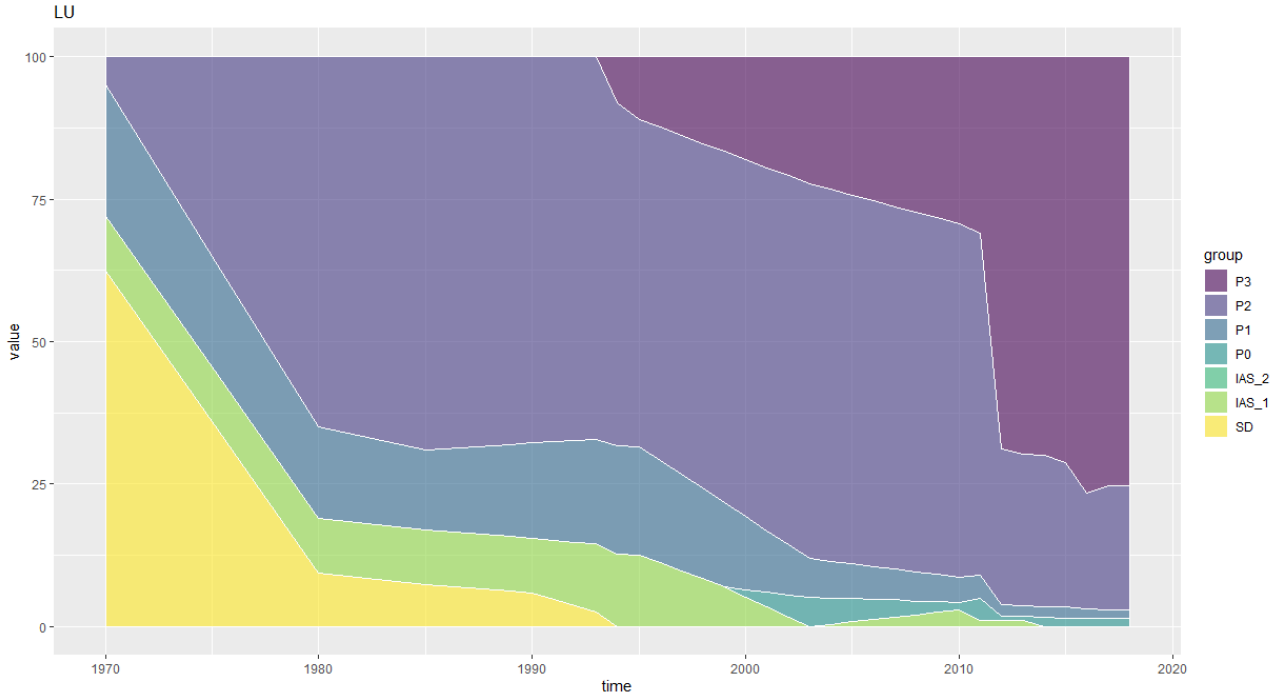
LU
100
75
50
25
0
value
1970
1980
1990
2000
2010
2020
time
group
P3
P2
P1
P0
IAS_2
IAS_1
SD

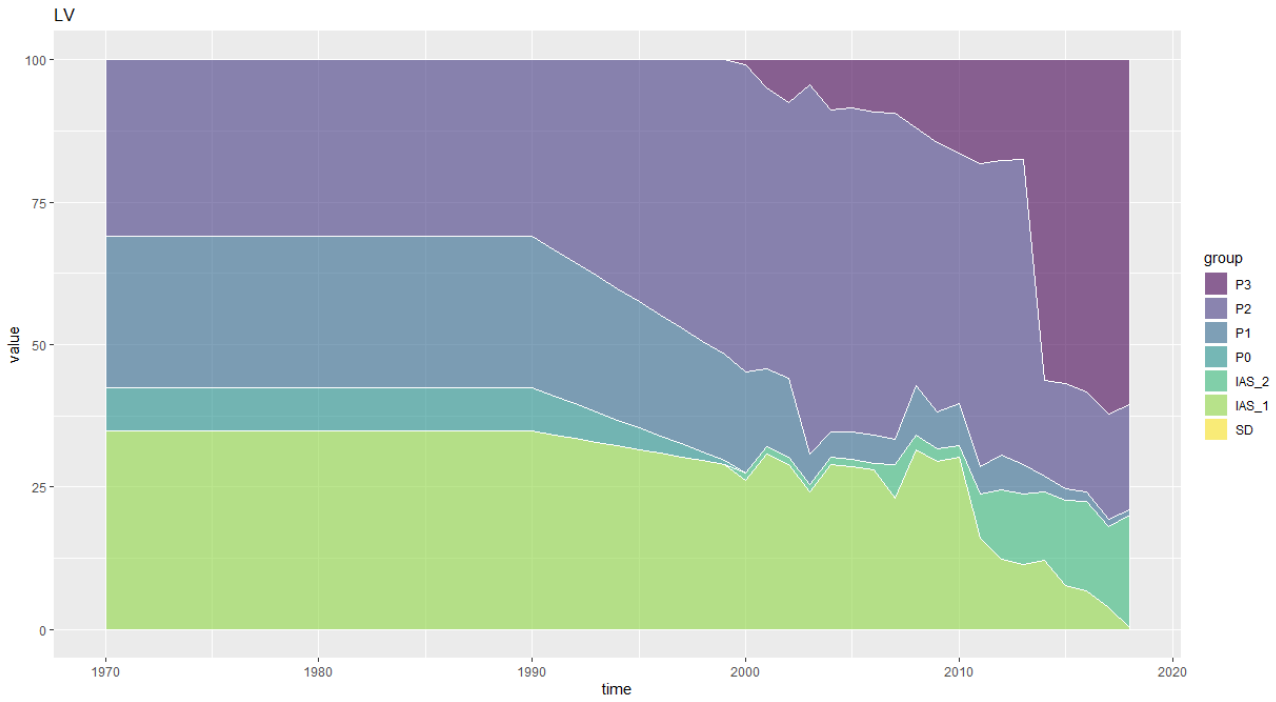
LV
100
75
50
25
0
value
1970
1980
1990
2000
2010
2020
time
group
P3
P2
P1
P0
IAS_2
IAS_1
SD

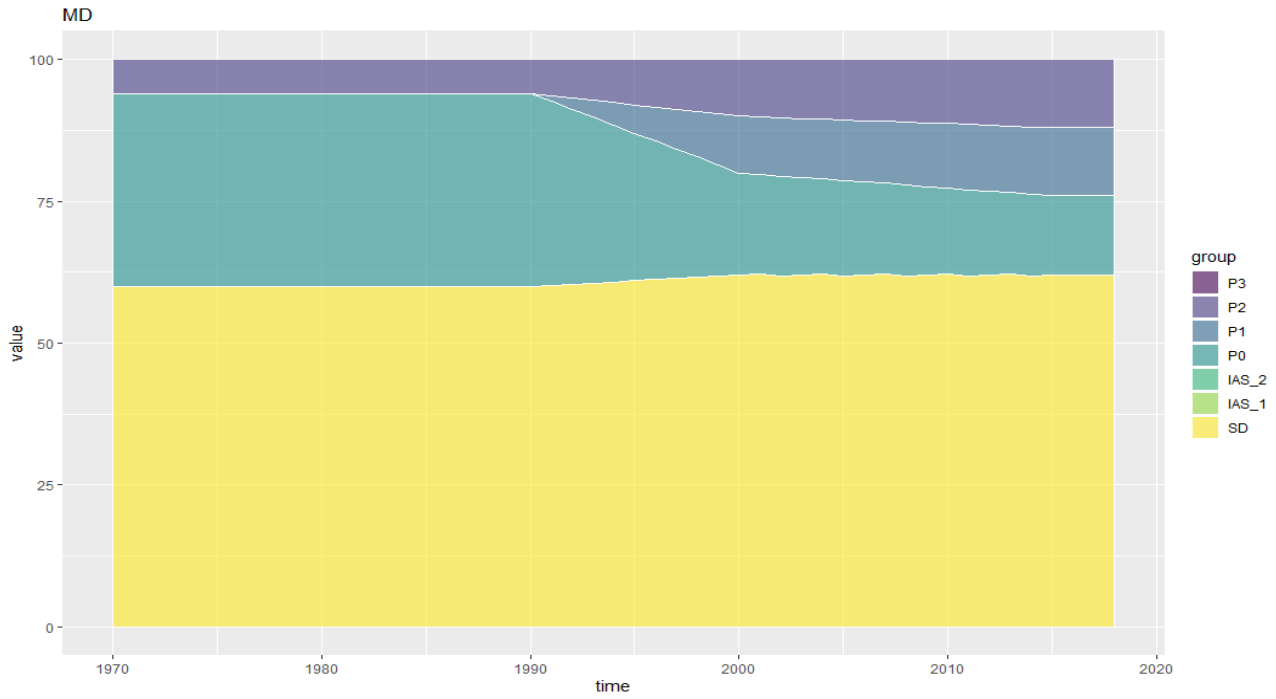
MD
100
75
50
25
0
value
1970
1980
1990
2000
2010
2020
time
group
P3
P2
P1
P0
IAS_2
IAS_1
SD

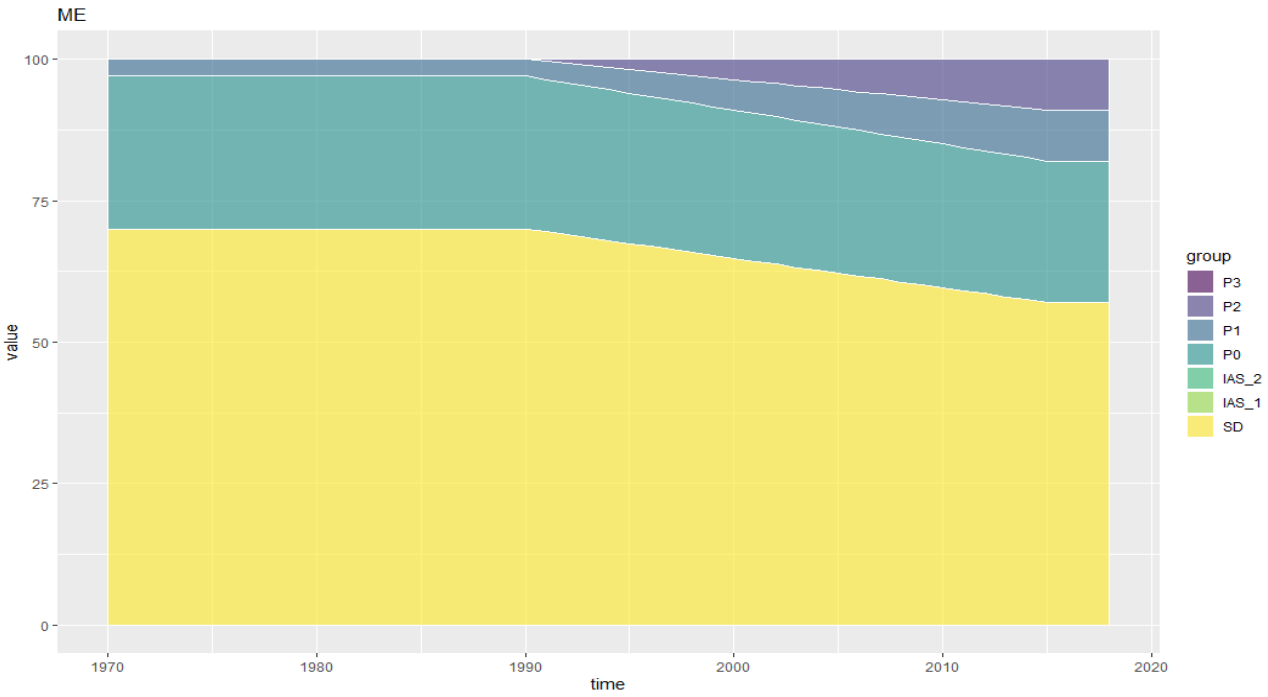
ME
100
75
50
25
0
value
1970
1980
1990
2000
2010
2020
time
group
P3
P2
P1
P0
IAS_2
IAS_1
SD

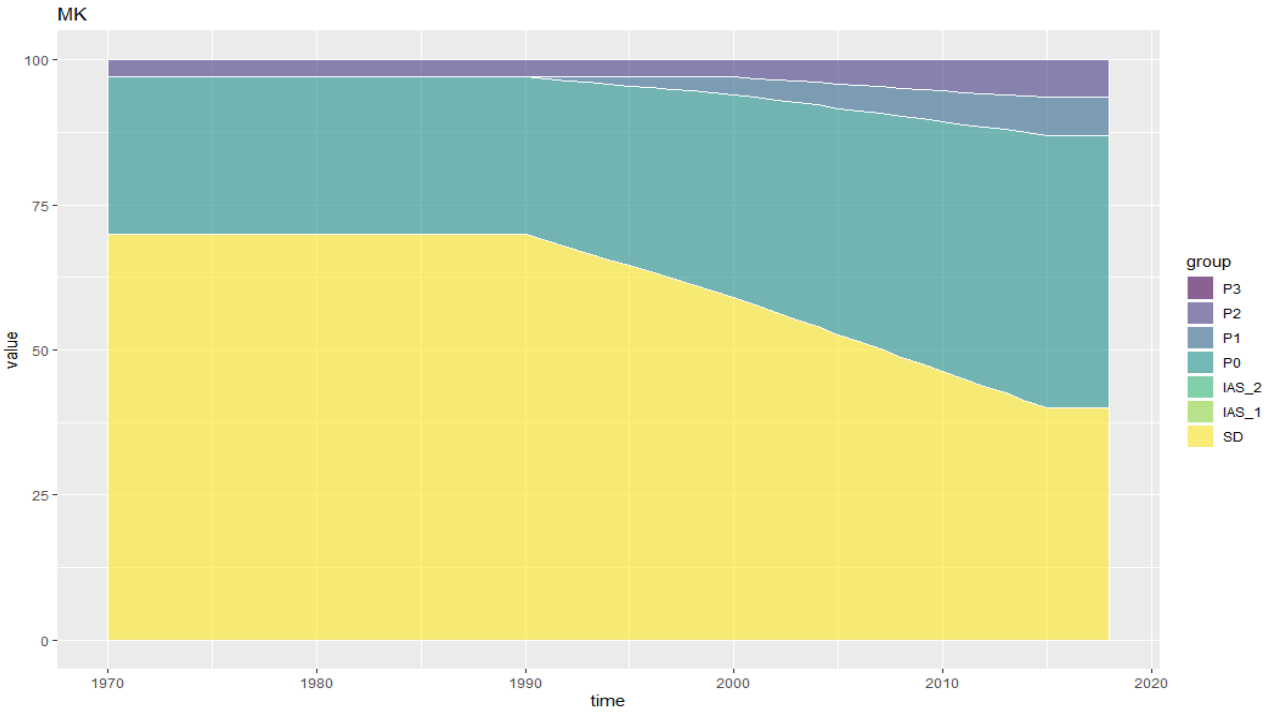
MK
100
75
50
25
0
value
1970
1980
1990
2000
2010
2020
time
group
P3
P2
P1
P0
IAS_2
IAS_1
SD

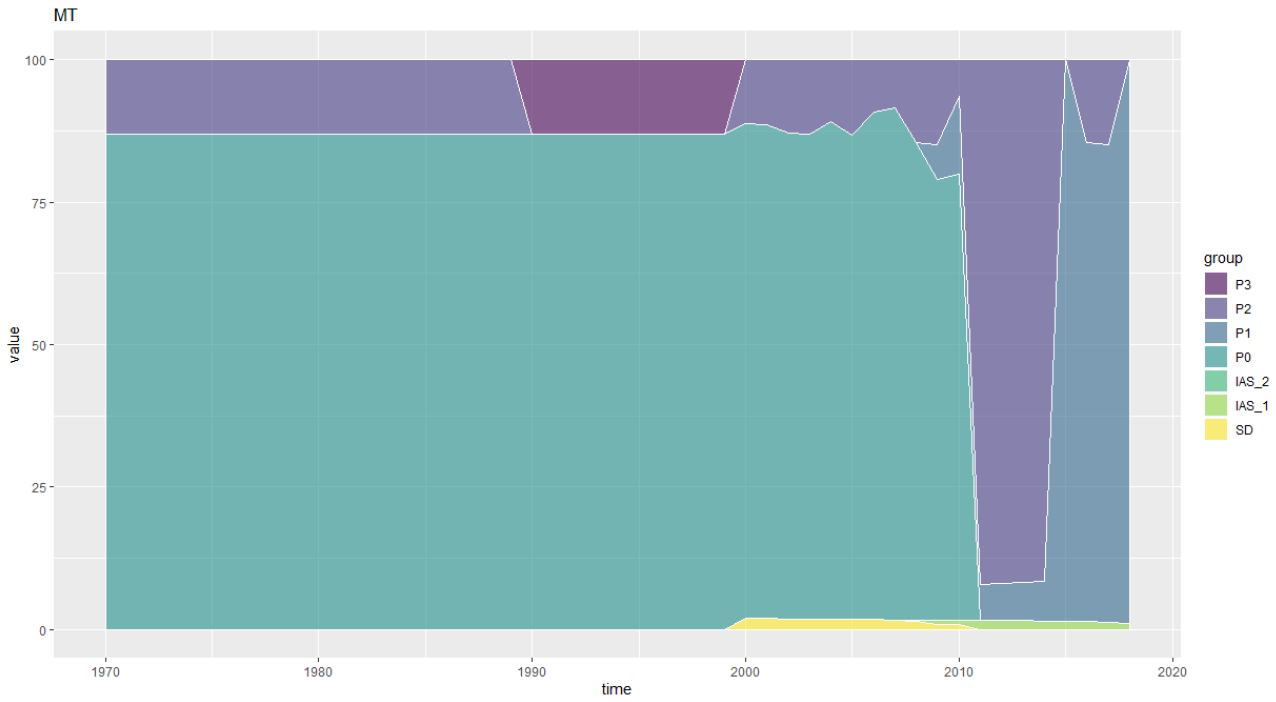
MT
100
75
50
25
0
value
1970
1980
1990
2000
2010
2020
time
group
P3
P2
P1
P0
IAS_2
IAS_1
SD

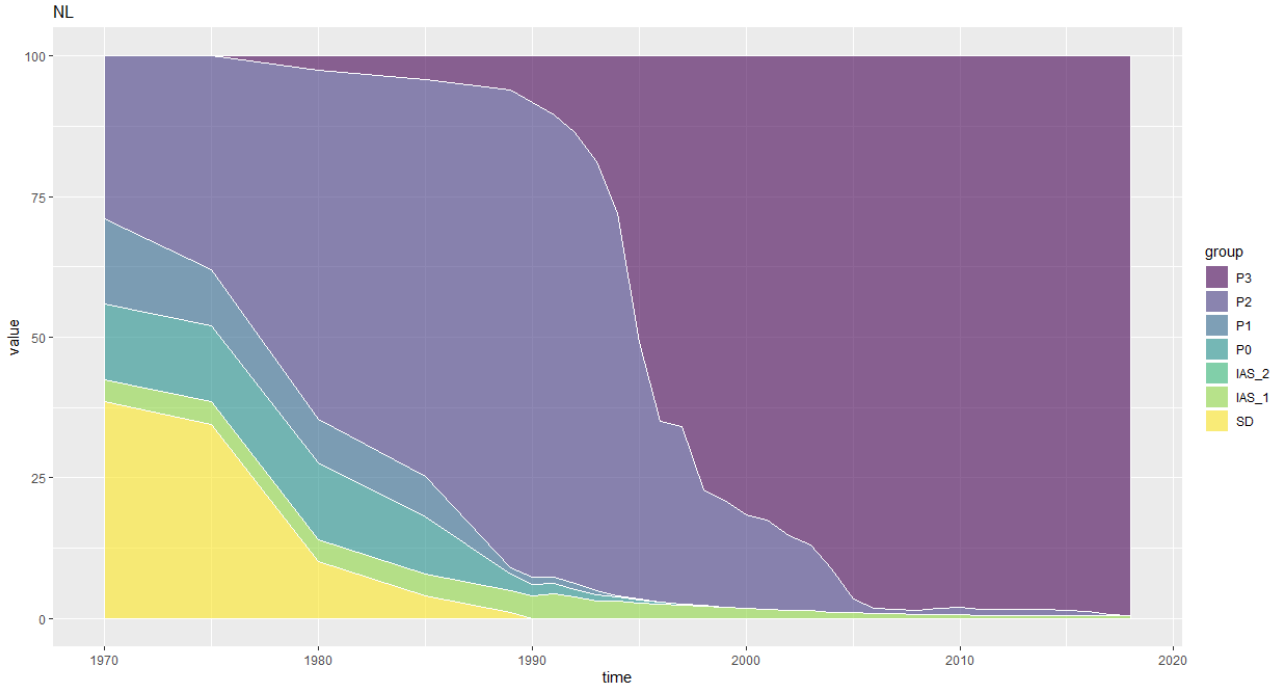
NL
100
75
50
25
0
value
1970
1980
1990
2000
2010
2020
time
group
P3
P2
P1
P0
IAS_2
IAS_1
SD

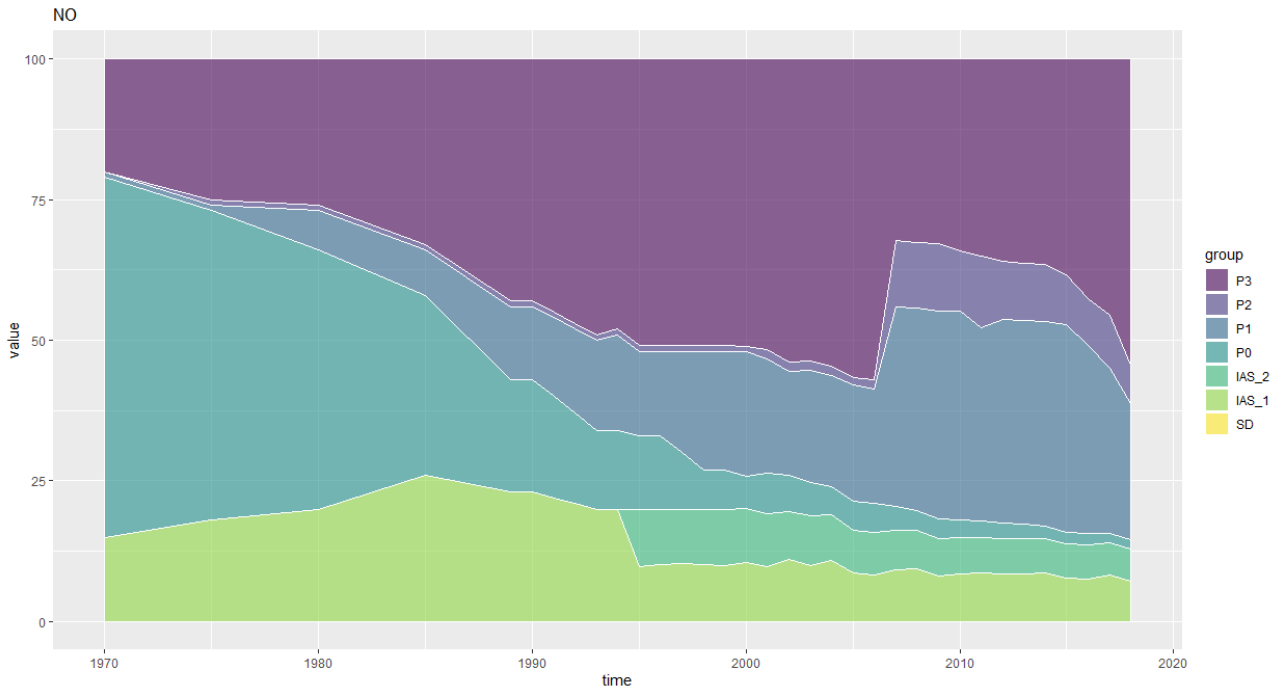
NO
100
75
50
25
0
value
1970
1980
1990
2000
2010
2020
time
group
P3
P2
P1
P0
IAS_2
IAS_1
SD

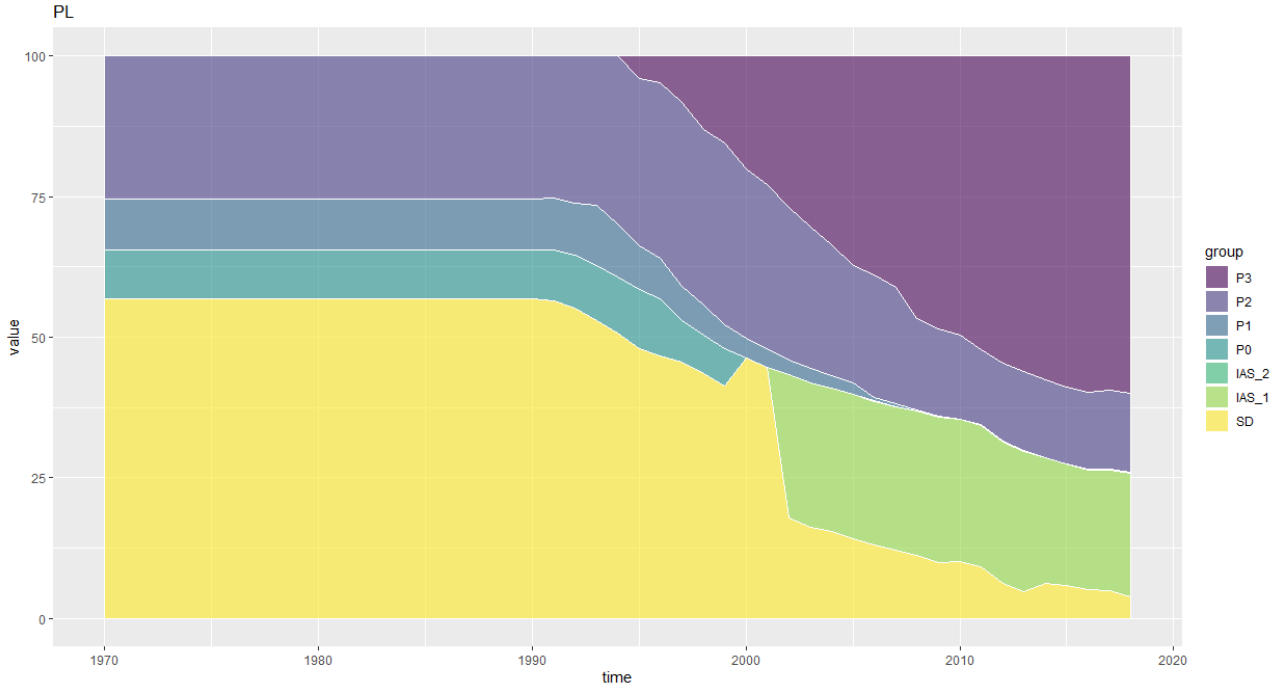
PL
100
75
50
25
0
value
1970
1980
1990
2000
2010
2020
time
group
P3
P2
P1
P0
IAS_2
IAS_1
SD

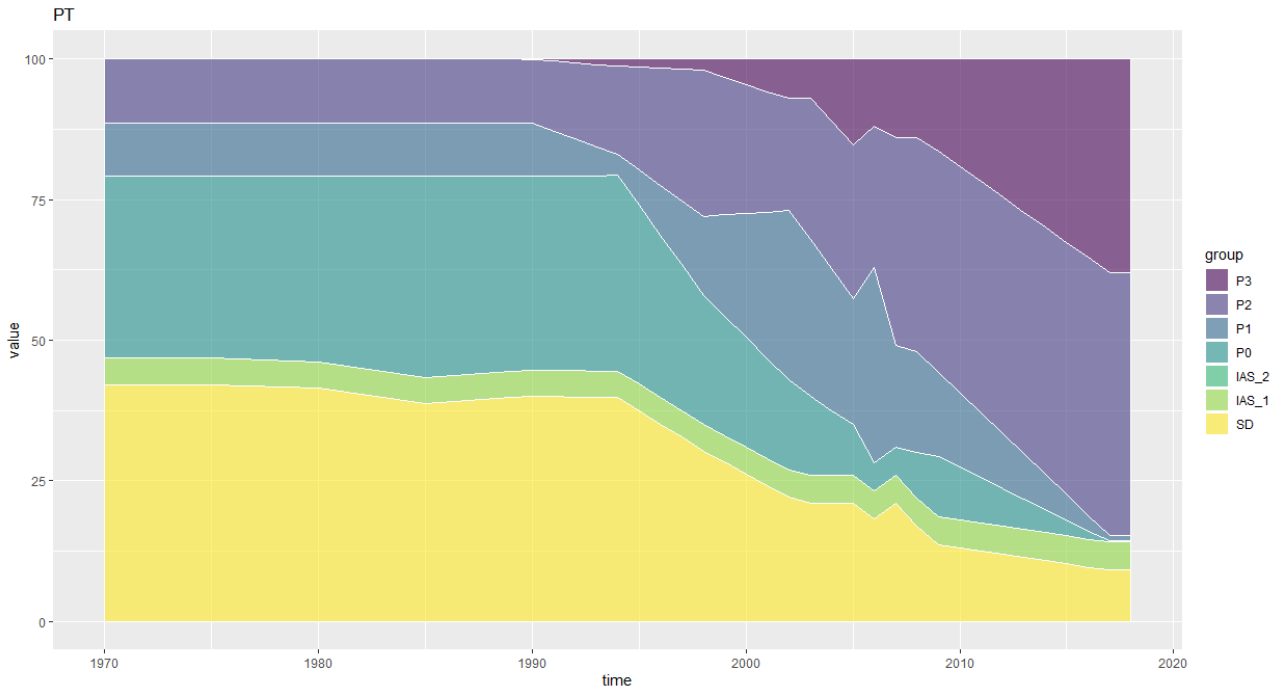
PT
100
75
50
25
0
value
1970
1980
1990
2000
2010
2020
time
group
P3
P2
P1
P0
IAS_2
IAS_1
SD

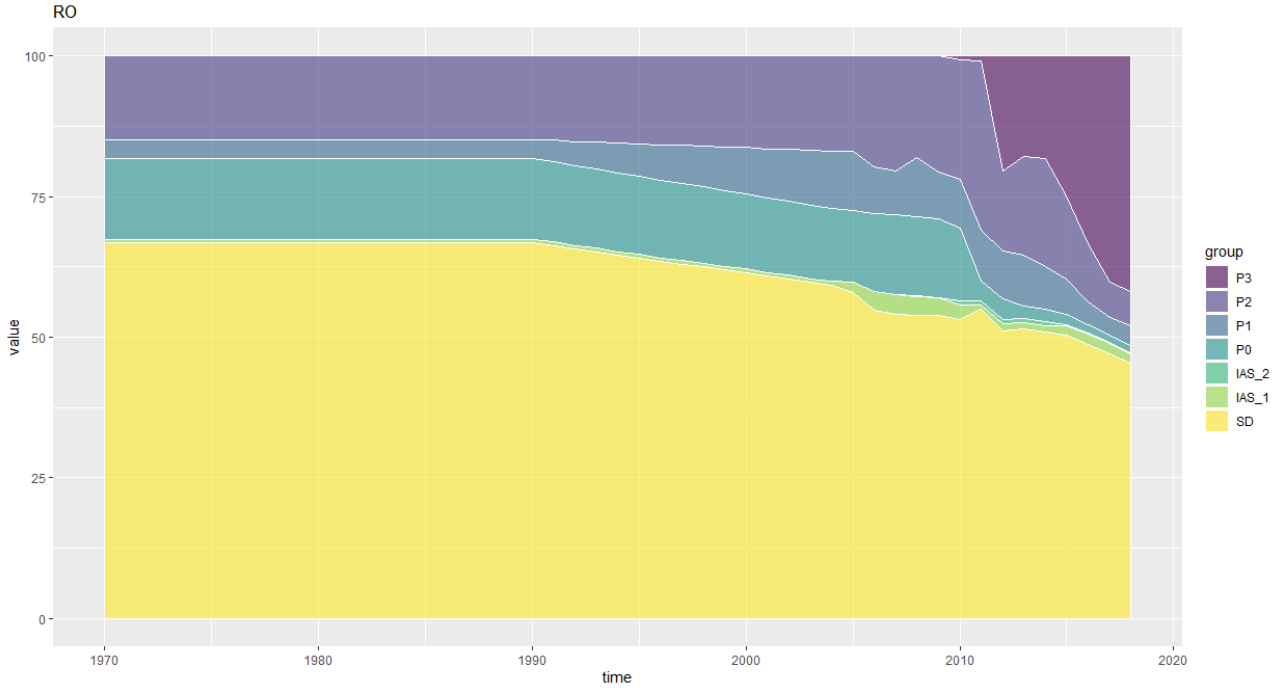
RO
100
75
50
25
0
value
1970
1980
1990
2000
2010
2020
time
group
P3
P2
P1
P0
IAS_2
IAS_1
SD

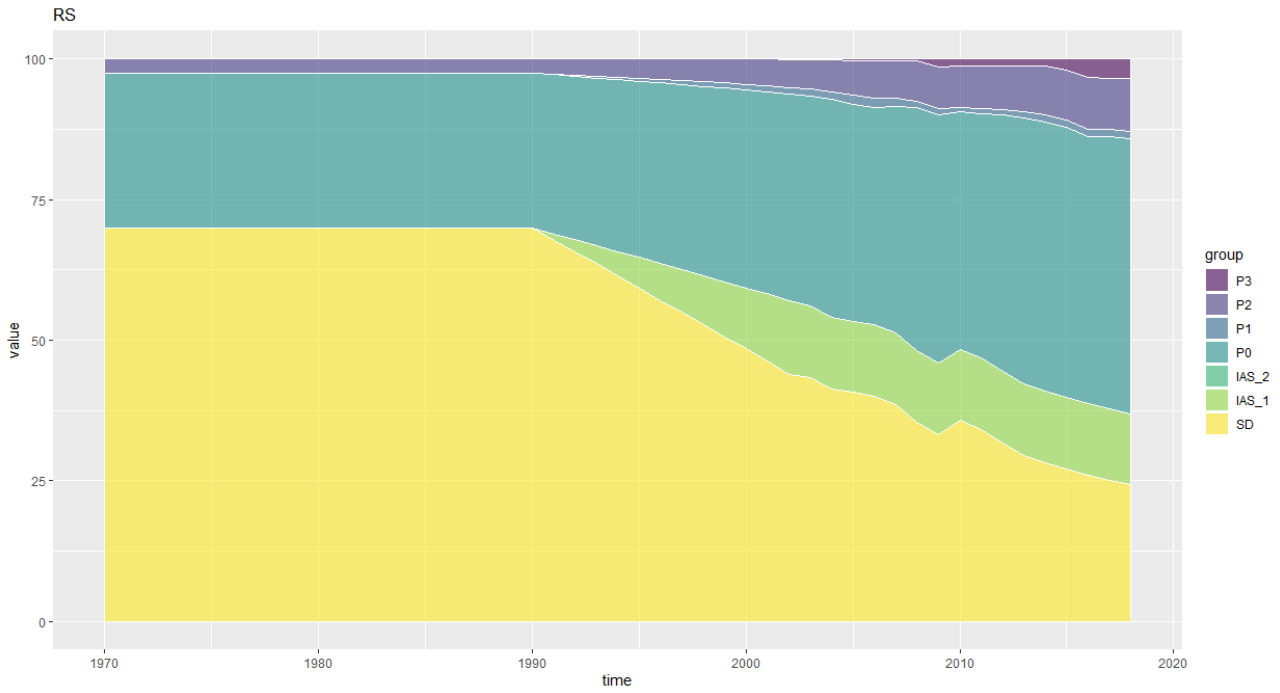
RS
100
75
50
25
0
value
1970
1980
1990
2000
2010
2020
time
group
P3
P2
P1
P0
IAS_2
IAS_1
SD

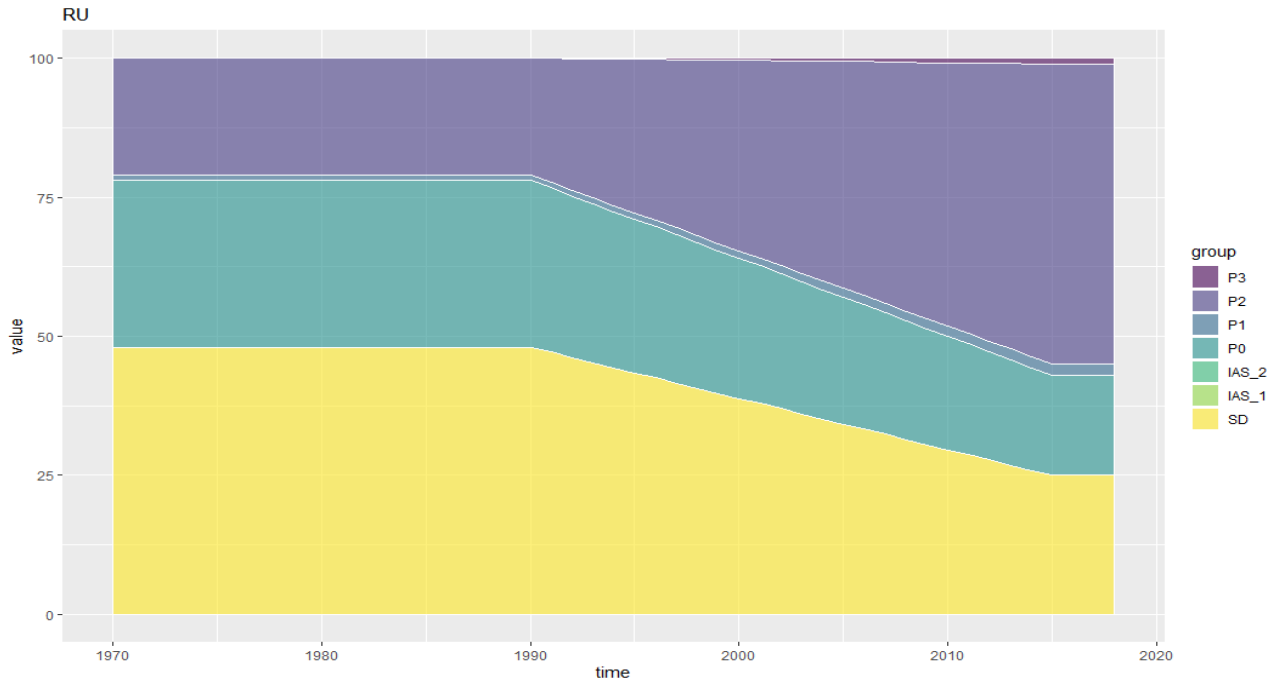
RU
100
75
50
25
0
value
1970
1980
1990
2000
2010
2020
time
group
P3
P2
P1
P0
IAS_2
IAS_1
SD

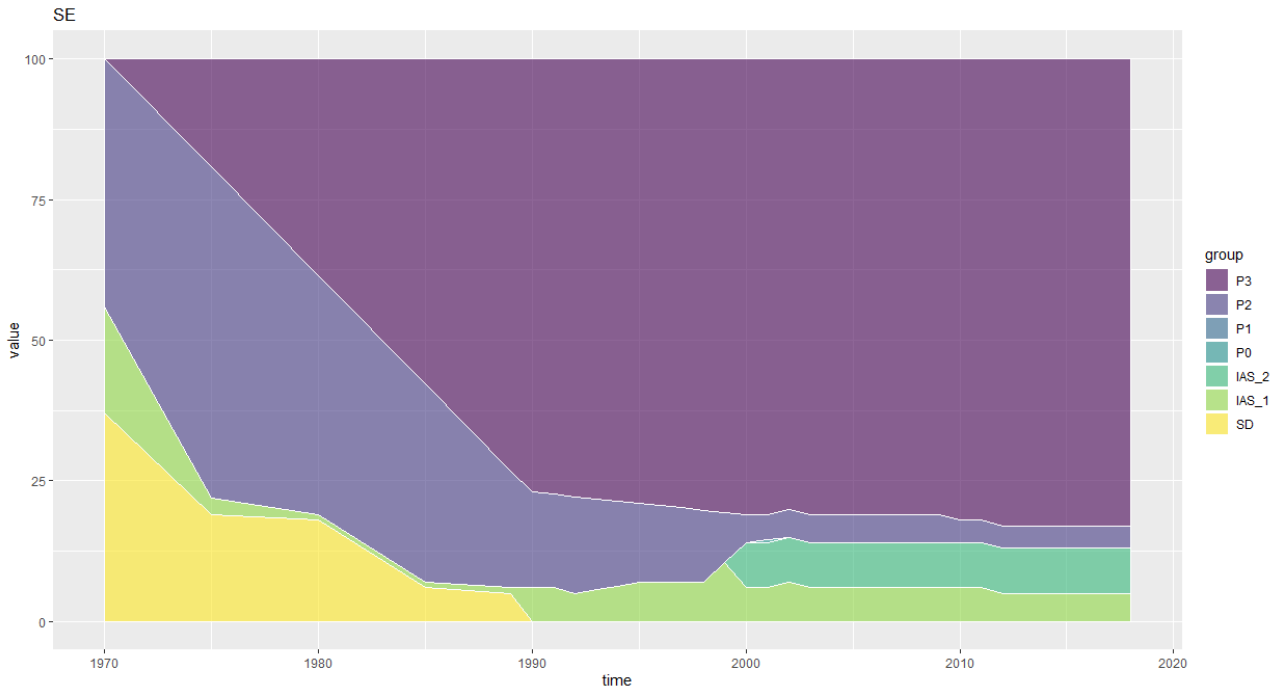
SE
100
75
50
25
0
value
1970
1980
1990
2000
2010
2020
time
group
P3
P2
P1
P0
IAS_2
IAS_1
SD

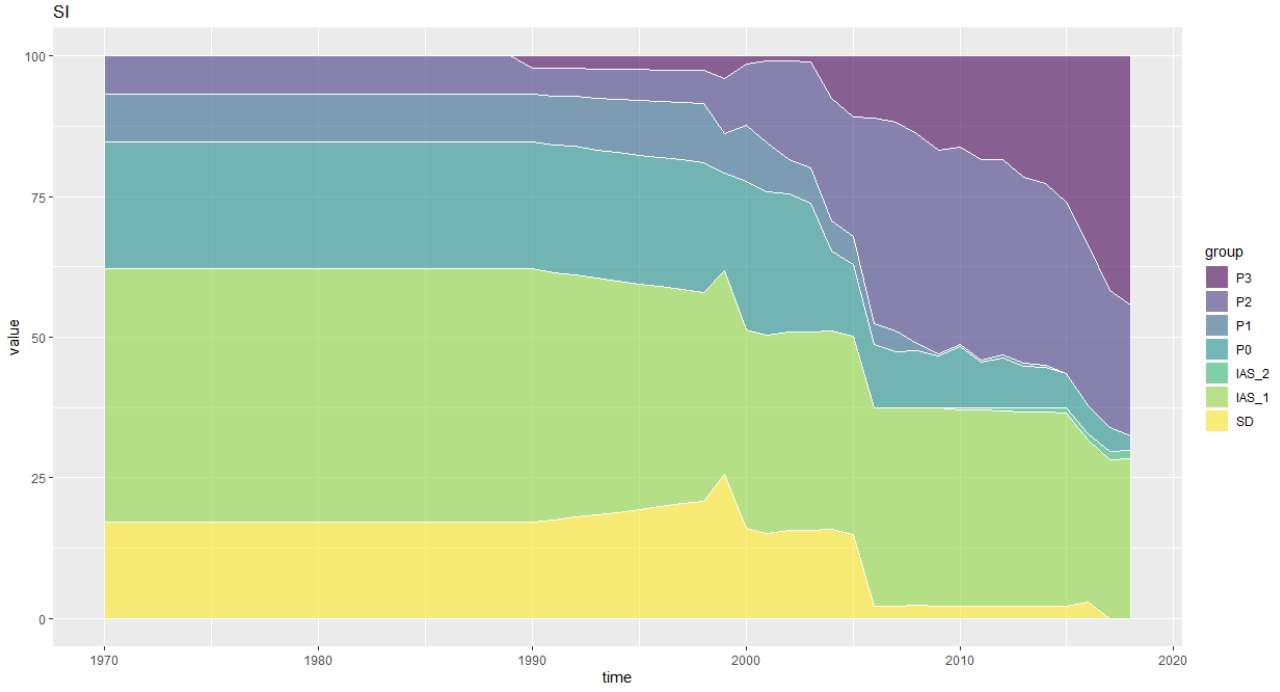
SI
100
75
50
25
0
value
1970
1980
1990
2000
2010
2020
time
group
P3
P2
P1
P0
IAS_2
IAS_1
SD

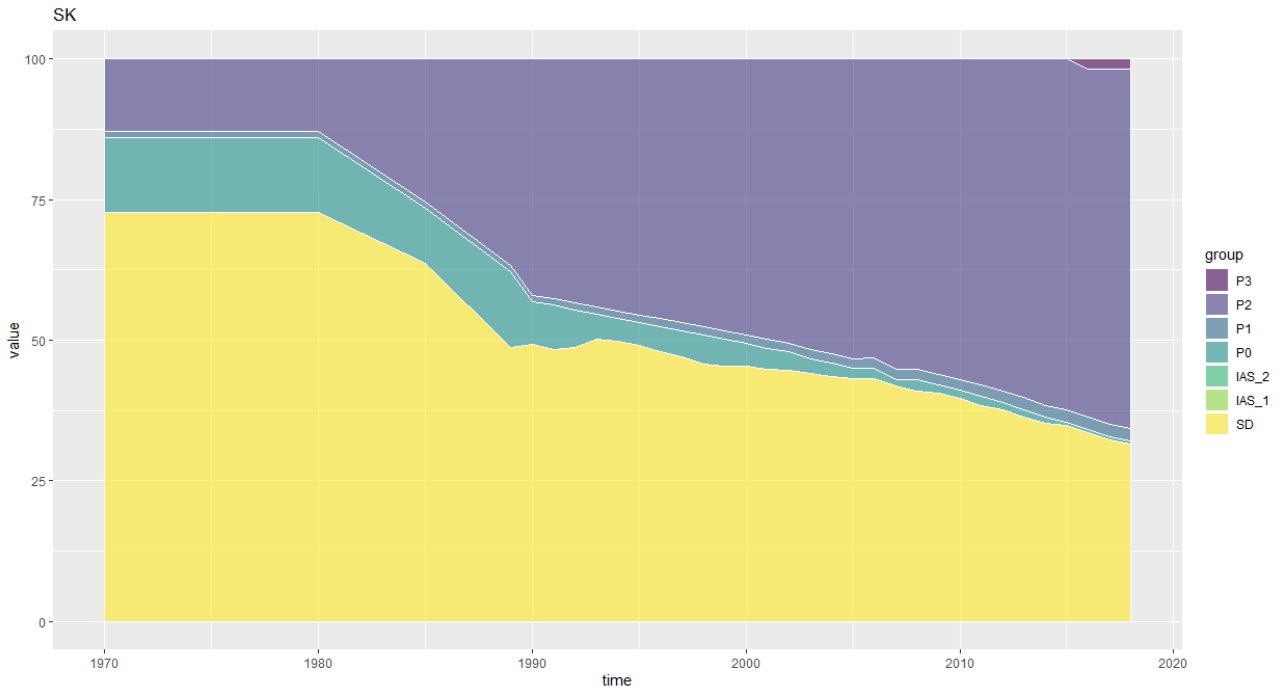
SK
100
75
50
25
0
value
1970
1980
1990
2000
2010
2020
time
group
P3
P2
P1
P0
IAS_2
IAS_1
SD

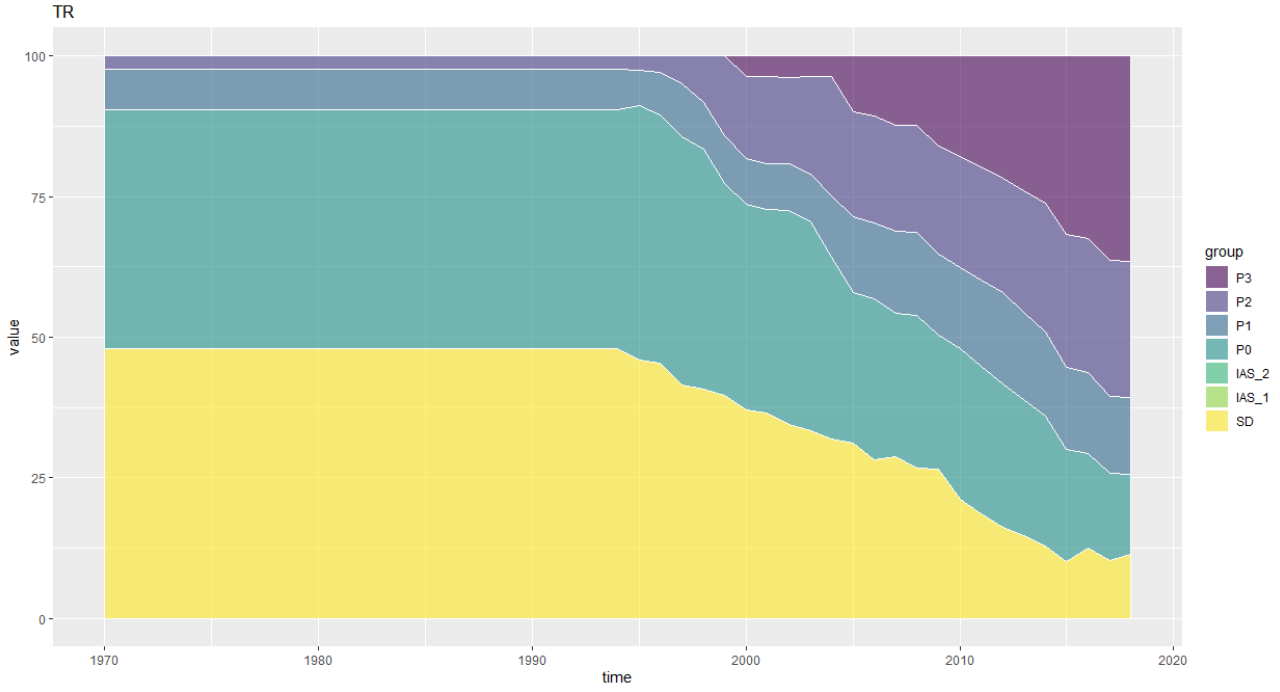
TR
100
75
50
25
0
value
1970
1980
1990
2000
2010
2020
time
group
P3
P2
P1
P0
IAS_2
IAS_1
SD

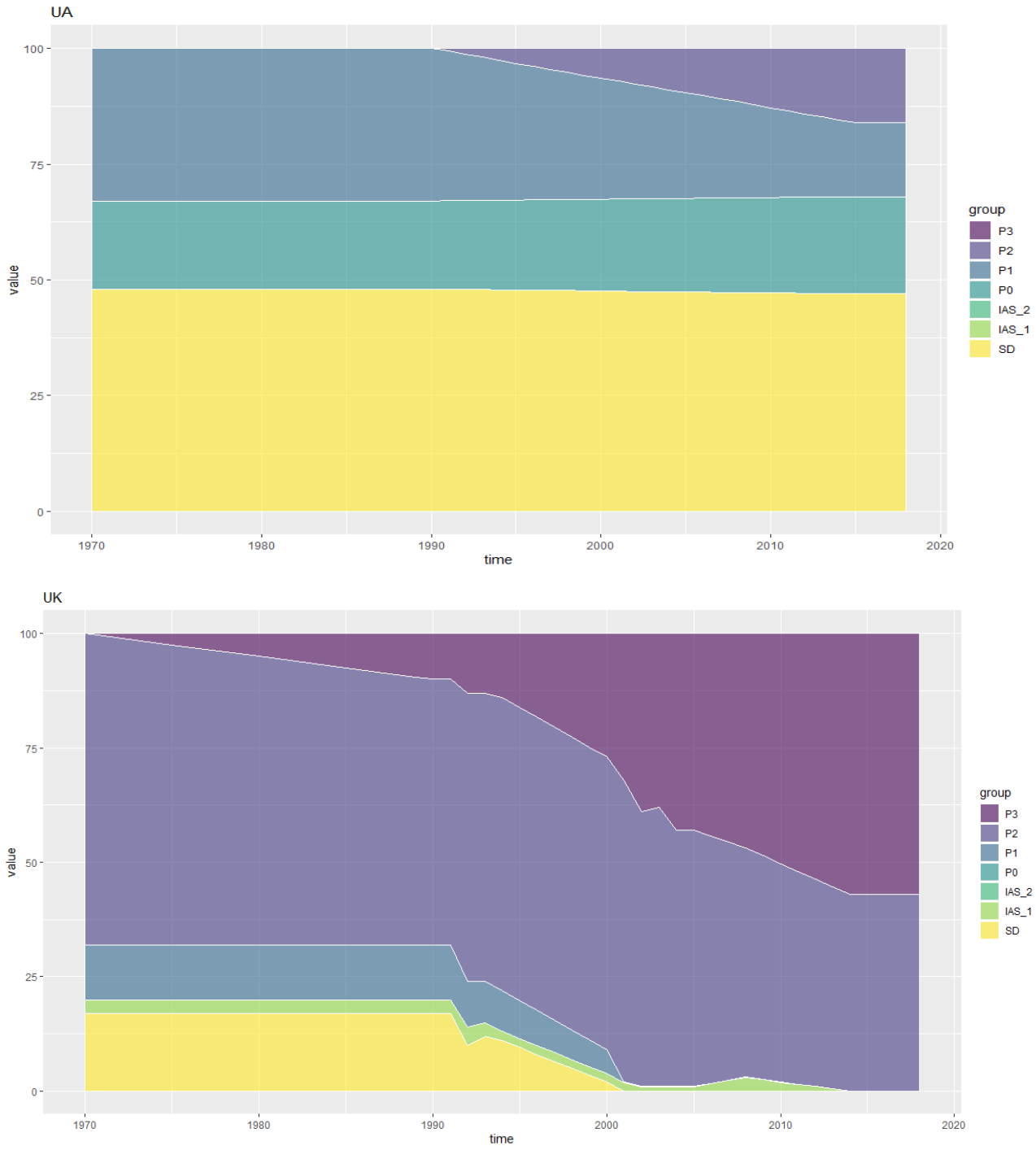

For years after 2010, domestic emissions were based on database of WWTPs reported by the EU's Member States compliant with the Urban Wastewater Treatment Directive (UWWTD) 91/271/EE, which are made available by the European Environment Agency (EEA, 2020). The derivation of domestic emissions from this database is detailed in Vigiak et al. (2018; 2020). Data was updated using the 10th UWWTD Implementation Report (EEA, 2020), which reports information for the year 2016. In particular, the reported information includes spatial location, capacity and treated load (as population equivalents, PE), level of treatment (primary, secondary, nitrogen and phosphorus removal). Note that the database reports emissions for agglomerations of at least 2000 PEs, so a quota of disconnected population was added by comparing national PE loads reported in the database with population reported in EUROSTAT. Vigiak et al., (2018, 2010) details the method, which was updated for year 2016.

A1.5.2 *Population density and spatialisation of domestic emissions*

The spatial attribution of population to each wastewater treatment was set according to population density, assuming that most densely populated areas would benefit of the best nationally available technology, and vice versa the least populated areas would not be connected to sewage systems. Population density was taken from Global Human Settlement Population density (GHS-POP; Schiavina et al., 2019) 1 km2 raster grid of 1990, 2000 and 2015. Population density in years 1995, 2005 and 2010 were obtained by interpolation. A check with total annual population as reported in EUROSTAT (2021b) showed that potential errors due to interpolation were generally less than +/- 2.5% of national population. The population was divided in terms of access to treatment type based on increasing density thresholds as belonging to: scattered dwellings (SD); collected but not treated (P0); treated in Independent Appropriate System at primary (IAS1) or at secondary level (IAS2); collected and treated at primary level (P1), secondary (P2) or with additional nutrient removal (P3, separated for nitrogen and or phosphorus). The mean density for each population segment per CCM2 catchment (CCM2, Vogt et al., 2007) was calculated and population derived as the mean times catchment area. Except for SD, population (inhabitants) were transformed into Population Equivalent by multiplying inhabitants per 1.23 to account for the share of commercial, tourism and industrial activities whose emissions are collected in sewage and wastewater treatment plants (Vigiak et al., 2020).

For 2016, the UWWTD data (EEA, 2020) provides coordinates of discharge points. These were attributed to the CCM2 catchment they feel in. For the years 2011-2015 the domestic emissions per catchment were interpolated between 2010 (population approach) and 2016 (reported approach), which results in a progressive concentration of domestic emissions towards the discharge points reported in the UWWTD database.

A1.5.3 *Determination of fractions of emission loads treated with N or P removal*

This information is used to separate P3 in P2Nrem and P3Nrem or P2Prem and P3Prem for calculation of emissions. We used EUROSTAT (2018) data on design of wastewater treatment plants, which report loads treated in tertiary WWTPs (P3), and the load treated in plants with N and P removal. The dataset had information for 2003-2014 in 22 countries, but with many gaps. Analysis of the data showed that (i) there was no trend on N and P removal fractions of tertiary loads did not change much within a country in the period reported (about a decade); (ii) no regional differences were noted; and (iii) there was no correlation between this fraction and the fraction of P3. Therefore, the following rules for filling gaps in the period 1990-2018 were applied:

- For countries that had reported in ten00028 dataset: any year before the first reported data was assumed as the first available data; any year after the last reported data was assumed as the last reported data; gaps were filled by simple interpolation
- For countries not included in the dataset ("AD" "AL" "BA" "BY" "EL" "FI" "GE" "GG" "IM" "IT" "JE" "LI" "MD" "ME" "MK" "MT" "NO" "PL" "PT" "RS" "RU" "SE" "SM" "TR" "UA" "XK"), the 0.20 trimmed mean of the filled dataset (including assumptions and interpolation) was used.

A1.5.4 *From PE to N and P emissions*

Emissions (TN, TP; t/y) were calculated from PE loads as:

PE * emission t/capita/year *(1-eff)

where PE = population equivalent per treatment type in the CCM2 catchment; emission /capita/year were calculated from global data on diet and P in detergents (Malagò and Bouraoui, 2021); eff = treatment level efficiency, set as in Vigiak et al. (2018; 2020).

Finally, domestic emissions in GREEN input time-series were grouped in:

- Scattered Dwellings (SdN, SdP): sum of emissions from SD, IAS_1 and IAS_2;
- Point Sources (part of PsN, PsP): sum of emissions from P0, P1, P2, P2NRem (or P2Prem) , P3NRem (or P3PRem)

Emissions were calculated for 1990, 1995, 2000, 2005, 2010 and 2016. In the remaining years, total emissions per HydroID catchment were interpolated; for 2017 and 2018, data was retained as in 2016.

A1.6 Industrial discharges

Annual emissions to waters of total nitrogen and total phosphorus to waters from large industries were retrieved from European databases merging two sources:

- The European Pollutant Release and Transfer Register Regulation (E-PRTR; EEA, 2021a). This database reports emissions for 2001, 2004, 2007-2017;
- The Industrial Reporting under the Industrial Emissions Directive 2010/75/EU (INDv3; EEA, 2021b). This dataset merge industrial emissions reported under two separate reporting obligations (and includes data from E-PRTR), and contains administrative and regulatory data beginning with reporting year 2017. It reports data for 2007 to 2019 by EU Member States, Iceland, Liechtenstein, Serbia, Switzerland and the United Kingdom. With reference to the version used in this study (download in Apr 2021), the dataset does not report information for Norway and Slovakia. Data is incomplete for reporting year 2018 for Germany, Italy, Latvia, Lithuania, Liechtenstein, Lithuania, and Portugal; and for reporting year 2019 for Germany, Italy, Latvia, Lithuania, Liechtenstein, Malta, Portugal, Slovenia and Switzerland. Thematic data on pollutant releases and transfers, waste transfers as well as data relating to large combustion plants is included as of reporting year 2017.

A comparison of data highlighted that not all E-PRTR data were contained in INDv3 database. Besides lack of data for Norway and Slovakia, old facilities reporting only in 2001 and 2004 and some facilities reporting in later years were not included. Both datasets appear to report some facilities with different names, i.e. in duplicates. An effort was made to remove duplicates; 631 cases of potential duplicates were identified based on proximity (some facilities had the same coordinates). These were checked one by one to identify true duplicates. In some cases, a doubt existed, e.g. when facilities that were close by and had the same activity reported emissions in different years. In this cases the choice was made to consider them as the same facility (preferring to underestimate industrial emissions rather than overestimating them).

To obtain time-series for 1990-2018 for each facility, the following rules were applied:

- Emissions to water were considered the sum of accidental + total quantity releases (t/y);
- any year before the first reported years were considered equal to the first emission data or nil if before the year of start of activity (when reported);
- any year after the last emission data = the last available data;
- gaps in between reporting years were filled by interpolation.

In general, emissions were added to the catchment in which the facility coordinates fell. Some industries fell outside CCM2 catchments, in some cases this could be due to an error in CCM2 delineation and discharges were allocated to the closest CCM2 catchment.

Industrial emissions that occurred directly in marine areas were excluded from GREEN Input time-series. These emissions comprised off-shore industries, or industries linked to aquaculture/fishery activities. They were provided as additional loads to the seas, to be added to marine areas at the coordinates provided in the industrial dataset.

References to Annex 1

Barreiro-Hurle, J., Bogonos, M., Himics, M., Hristov, J., Pérez-Domiguez, I., Sahoo, A., Salputra, G., Weiss, F., Baldoni, E., Elleby, C. Modelling environmental and climate ambition in the agricultural sector with the CAPRI model. Exploring the potential effects of selected Farm to Fork and Biodiversity strategies targets in the framework of the 2030 Climate targets and the post 2020 Common Agricultural Policy, EUR 30317 EN, Publications Office of the European Union, Luxembourg, 2021, ISBN 978-92-76-20889-1, doi:10.2760/98160, JRC121368.FAOSTAT (data access in May 2018) http://www.fao.org/faostat/en/#data

CLC, 2021. CORINE Land Cover maps. Available at https://land.copernicus.eu/pan-european/corine-land-cover (access March 2021)

EMEP, 2020. Data from The Norwegian Meteorological Institute (MET Norway)(data access in 2020) https://www.emep.int/mscw/mscw_moddata.html

ESA, 2017. Land Cover CCI Product User Guide Version 2. Tech. Rep. (2017). Available at: maps.elie.ucl.ac.be/CCI/viewer/download/ESACCI-LC-Ph2-PUGv2_2.0.pdf (access March 2021)

European Environment Agency (EEA), 2020. Waterbase - UWWTD: Urban Waste Water Treatment Directive – reported data https://www.eea.europa.eu/data-and-maps/data/waterbase-uwwtd-urban-waste-water-treatment-directive-6 (downloaded October 2020)

European Environment Agency (EEA), 2021a. E-PRTR V18;https://www.eea.europa.eu/data-and-maps/data/member-states-reporting-art-7-under-the-european-pollutant-release-and-transfer-register-e-prtr-regulation-23 (accessed 21/01/2021)

European Environment Agency (EEA), 2021b. Industrial Reporting under the Industrial Emissions Directive 2010/75/EU and European Pollutant Release and Transfer Register Regulation (EC) No 166/2006: Industrial Reporting under the Industrial Emissions Directive 2010/75/EU and European Pollutant Release and Transfer Register Regulation (EC) No 166/2006 — European Environment Agency (downloaded 21/04/2021).

EUROSTAT (2018). 'Design capacity, in terms of biochemical oxygen demand (BOD), of urban wastewater treatment plants with advanced treatment - 1 000 kg O2/day1 (ten00028). http://ec.europa.eu/eurostat/tgm/table.do?tab=table&init=1&plugin=1&language=en&pcode=ten00028 (downloaded 13/07/2018 for years 2003-2014; currently the dataset cannot be found on the database).

EUROSTAT (2021a). Population connected to wastewater treatment plants (env_ww_con)

https://ec.europa.eu/eurostat/databrowser/product/page/ENV_WW_CON (accessed 27.01.2021)

EUROSTAT (2021b). 'Population change - Demographic balance and crude rates at national level' (DEMO_GIND). https://ec.europa.eu/eurostat/databrowser/view/DEMO_GIND__custom_571312/default/table?lang=en (downloaded 15/02/2021)

Malagó, A., and Bouraoui, F. 2021. Global anthropogenic and natural nutrient fluxes: from local to planetary assessments. *Environ. Res. Lett.* 16 054074

Pistocchi, A., Dorati, C., Grizzetti, B., Udias, A., Vigiak, O., Zanni, M., 2019. Water quality in Europe: effects of the Urban Wastewater Treatment Directive. A retrospective and scenario analysis of Dir. 91/271/EEC, EUR 30003 EN, Publications Office of the European Union, Luxembourg, 2019, ISBN 978-92-76-11263-1, doi:10.2760/303163, JRC115607.

Schiavina, M., Freire, S., MacManus, K. (2019). GHS population grid multitemporal (1975, 1990, 2000, 2015) R2019A. European Commission, Joint Research Centre (JRC) DOI: 10.2905/42E8BE89-54FF-464E-BE7B-BF9E64DA5218 PID: http://data.europa.eu/89h/0c6b9751-a71f-4062-830b-43c9f432370f (download 5/3/2020)

Vigiak, O. et al. 2018. *Estimation of domestic and industrial waste emissions to European waters in the 2010s*. Report EUR 29451 EN, https://doi.org/10.2760/204793, https://publications.jrc.ec.europa.eu/repository/handle/JRC113729 (Publications Office of the European Union, 2018).

Vigiak, O., Grizzetti, B., Zanni, M., Aloe, A., Dorati, C., Bouraoui, F., and Pistocchi, A., 2020. Domestic waste emissions to European waters in the 2010s. *Sci. Data* 7, 33. https://doi.org/10.1038/s41597-020-0367-0.

Vogt, J., Soille, P., De Jager, A., Rimaviciute, E., Mehl, W., Foisneau, S., Bodis, K., Dusart, J., Paracchini, M., Haastrup, P., Bamps C. 2007. *A pan-European River and Catchment Database*. JRC Reference Report EUR 22920 EN. Luxembourg (Luxembourg): OPOCE. JRC40291 http://publications.jrc.ec.europa.eu/repository/handle/JRC40291.

Vogt, J., Rimaviciute, E., and de Jager, A. 2008. *CCM2 River and Catchment Database for Europe Version 2.1 Release Notes*. http://ccm.jrc.ec.europa.eu/documents/JVogt_etal_CCM21.pdf.

Annex 2. GREEN model - Calibration stations per marine region

Table A2.1. Observed TN load data entries per marine region used for calibration of GREEN model in 1990-2018. Marine Regions: ABI=Bay of Biscay & Iberian Coast; ACS=Celtic Seas; ANS=Greater North Sea; BAL=Baltic Sea; BLK=Black Sea & Sea of Marmara; MAD=Adriatic Sea; MAL=Aegean Levantine Mediterranean Sea; MIC=Ionian Sea and Central Mediterranean Sea; MWE=Western Mediterranean Sea

	Marine region													
	ABI	ACS	ANS	BAL	BAR	BLK	BLM	MAD	MAL	MIC	MWE	NOR	WHI	Total
1990		2	131	228	11	44						4	2	422
1991		2	130	225	11	46						4	2	420
1992		3	135	335	13	53						4	2	545
1993		4	151	395	13	54					2	4	2	625
1994	53	3	164	465	13	57					2	4	2	763
1995	37	3	199	467	13	53					2	5	2	781
1996	44	7	218	496	14	47					2	4	2	834
1997	88	6	214	504	14	50		1			2	4	2	885
1998	82	6	254	506	13	70		1			3	4	2	941
1999	82	11	252	516	14	68		1			4	4	e	954
2000	81	11	243	538	15	76		33			16	4	2	1019
2001	76	11	241	538	15	81		29			29	4	2	1026
2002	51	10	248	558	15	78		75		3	29	4	2	1073
2003	138	13	369	557	15	125		123		6	169	4	2	1521

2004	145	15	401	552	16	140		131		5	189	15	2	1611
2005	180	17	403	554	17	143		131		5	225	18	2	1695
2006	305	56	588	489	15	157		79		4	173	15	2	1883
2007	553	132	730	460	15	176		620	25	57	731	15	2	3516
2008	779	127	849	446	16	216		468	26	5	663	15	2	3612
2009	831	142	797	420	15	197		122	25		436	15	2	3002
2010	385	182	475	375	14	227		733		10	246	15	2	2664
2011	14	175	553	598	15	284		732	45		127	15	2	2560
2012	64	165	526	977	11	269		666	50		196	13	2	2939
2013	388		74	123		107					198			890
2014	442		75	111		113					162			903
2015	410		75	12		112					145			754
2016			72	12		111								195
2017			73	12		110								195
2018			53											53
Tot	5228	1092	8146	10286	275	3067	0	3945	171	95	3749	177	38	36269

Table A2.2. Observed TP load data entries per marine region used for calibration of GREEN model in 1990-2018. Marine Regions: ABI=Bay of Biscay & Iberian Coast; ACS=Celtic Seas; ANS=Greater North Sea; BAL=Baltic Sea; BLK=Black Sea & Sea of Marmara; MAD=Adriatic Sea; MAL=Aegean Levantine Mediterranean Sea; MIC=Ionian Sea and Central Mediterranean Sea; MWE=Western Mediterranean Sea

	Marine region													
	ABI	ACS	ANS	BAL	BAR	BLK	BLM	MAD	MAL	MIC	MWE	NOR	WHI	Total
1990	63	18	208	234	10	50					41	2	2	628
1991	66	19	257	231	10	58					53	2	2	698
1992	83	19	297	456	11	81					66	2	2	1017
1993	93	20	323	494	11	150					58	2	2	1153
1994	104	20	337	496	10	204					73	2	2	1248
1995	113	21	390	505	13	255					83	5	2	1387
1996	103	21	358	521	11	257					88	2	2	1363
1997	89	22	389	528	11	260		1	7		110	2	2	1421
1998	83	24	399	532	10	260		1	6		116	2	2	1435
1999	87	27	410	528	11	263		1	22		121	2	2	1474
2000	170	20	412	548	12	282		42	6	3	86	2	2	1585
2001	164	17	415	553	12	283		89			140	2	2	1677
2002	204	19	420	553	12	287		104	16	7	194	2	2	1820
2003	229	17	425	556	12	382		156	45	5	232	2	2	2063
2004	271	21	481	551	16	520		163	53	5	261	14	2	2358

2005	336	36	495	552	17	523		169	57	5	250	18	2	2460
2006	575	80	695	489	15	480		121	3	4	211	15	2	2690
2007	819	149	770	486	15	299		757	112	68	1049	15	2	4541
2008	1206	139	909	473	16	331		659	43	22	998	15	2	4813
2009	1096	149	958	472	15	359		65	58		775	15	2	3964
2010	1454	226	1008	390	14	365		684	64	10	1012	15	2	5244
2011	896	217	1110	611	15	373		712	75		920	15	2	4946
2012	938	212	1074	993	11	365		876	82	1	774	13	2	5341
2013			308	160		173								641
2014			312	144		174								630
2015			318	45		175		5						543
2016			303	42		175		5						525
2017			310	47		176		5						538
2018			668	131		246		5						1050
Tot	8937	1437	13674	10906	248	7467	0	4620	649	130	7493	158	38	55757

Figure A2.1. GREEN_TN calibration result in the Bay of Biscay/Iberian coast (ABI). Year by year comparison of simulated (CatchLoad) versus observed loads (ObsLoad; all loads in t/y).

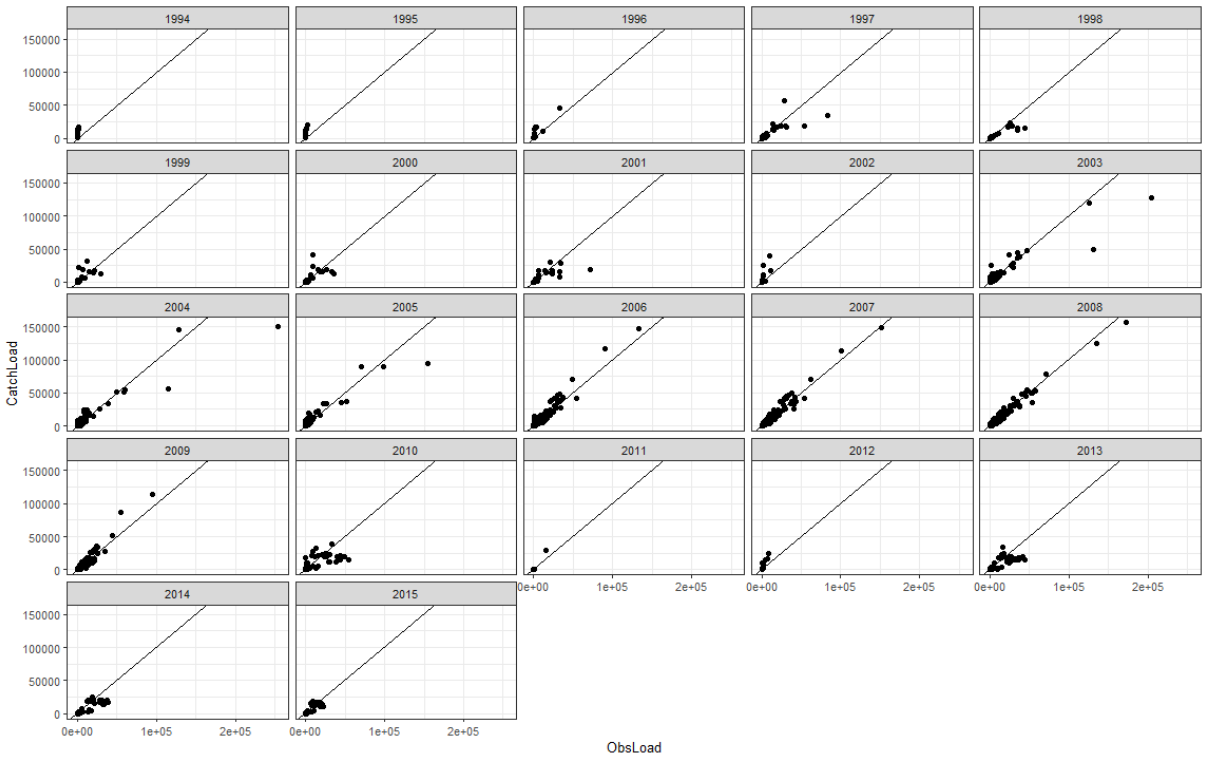

Figure A2.2. GREEN_TN calibration result in the Celtic Seas (ACS). Year by year comparison of simulated (CatchLoad) versus observed loads (ObsLoad; all loads in t/y).

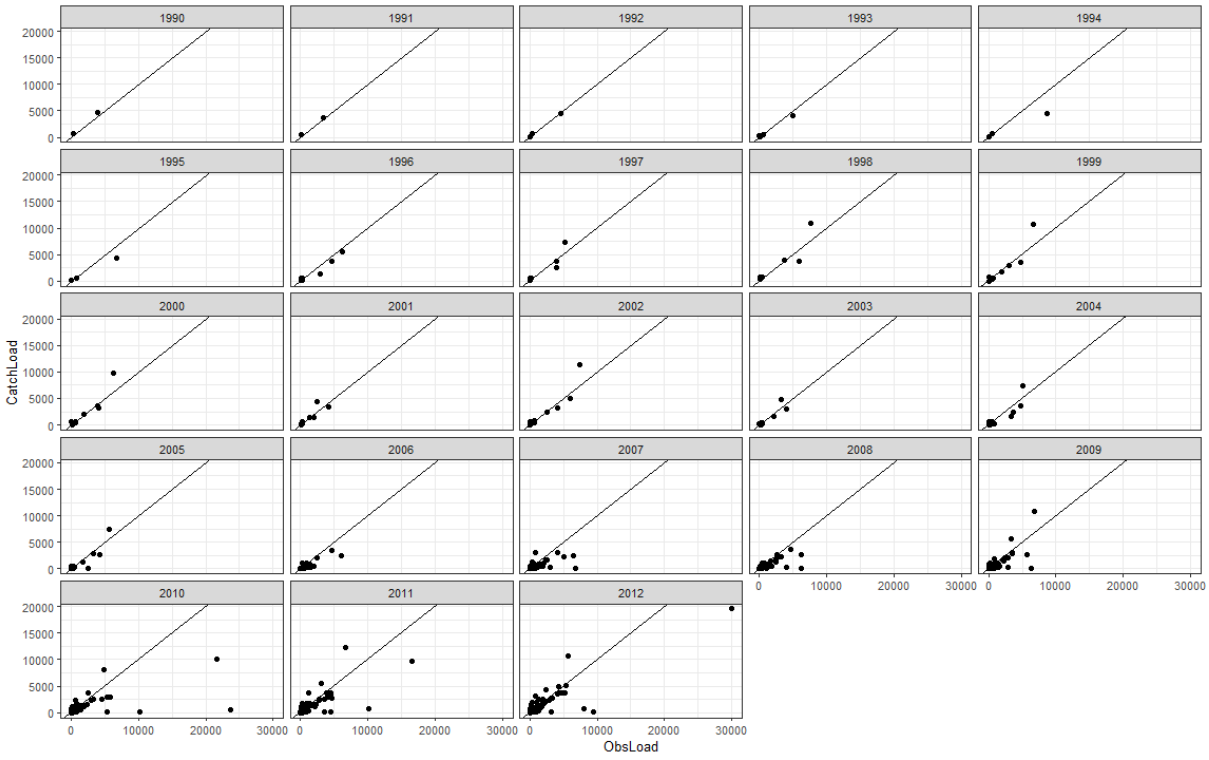

Figure A2.3. GREEN_TN calibration result in the Greater North Sea (ANS). Year by year comparison of simulated (CatchLoad) versus observed loads (ObsLoad; all loads in t/y).

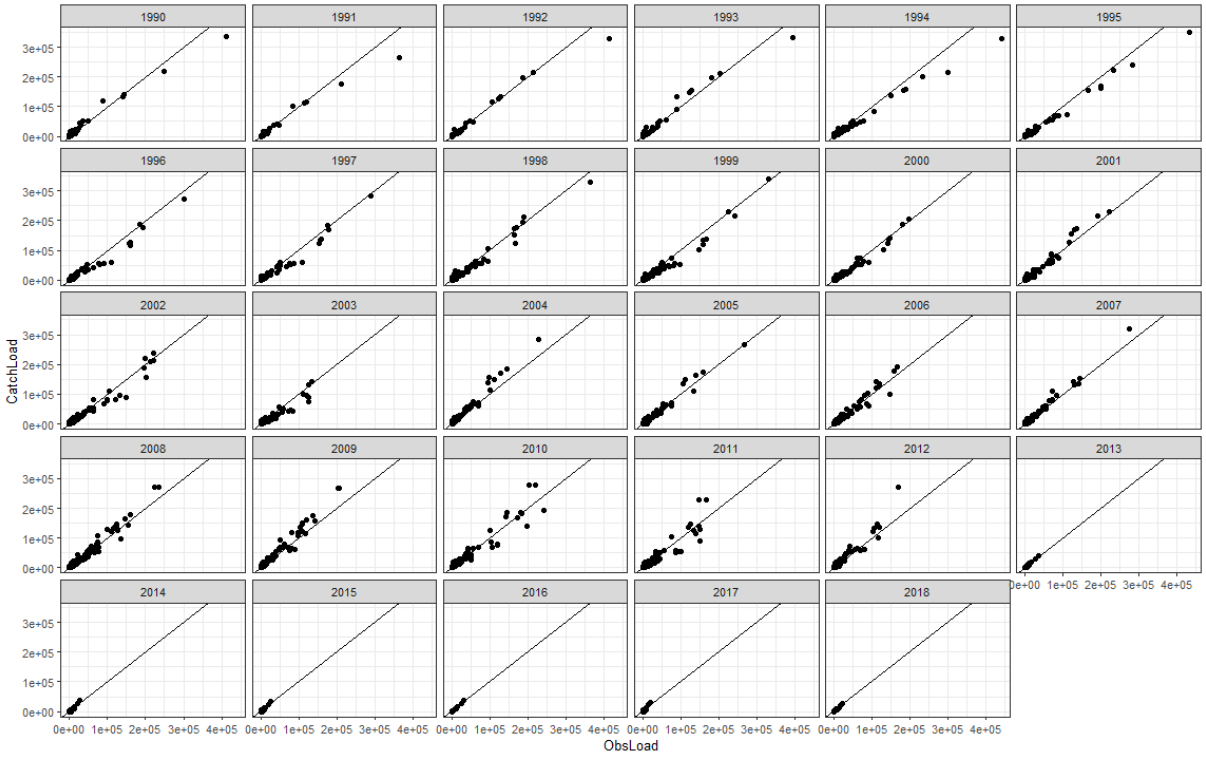

Figure A2.4. GREEN_TN calibration result in the Baltic Sea (BAL). Year by year comparison of simulated (CatchLoad) versus observed loads (ObsLoad; all loads in t/y).

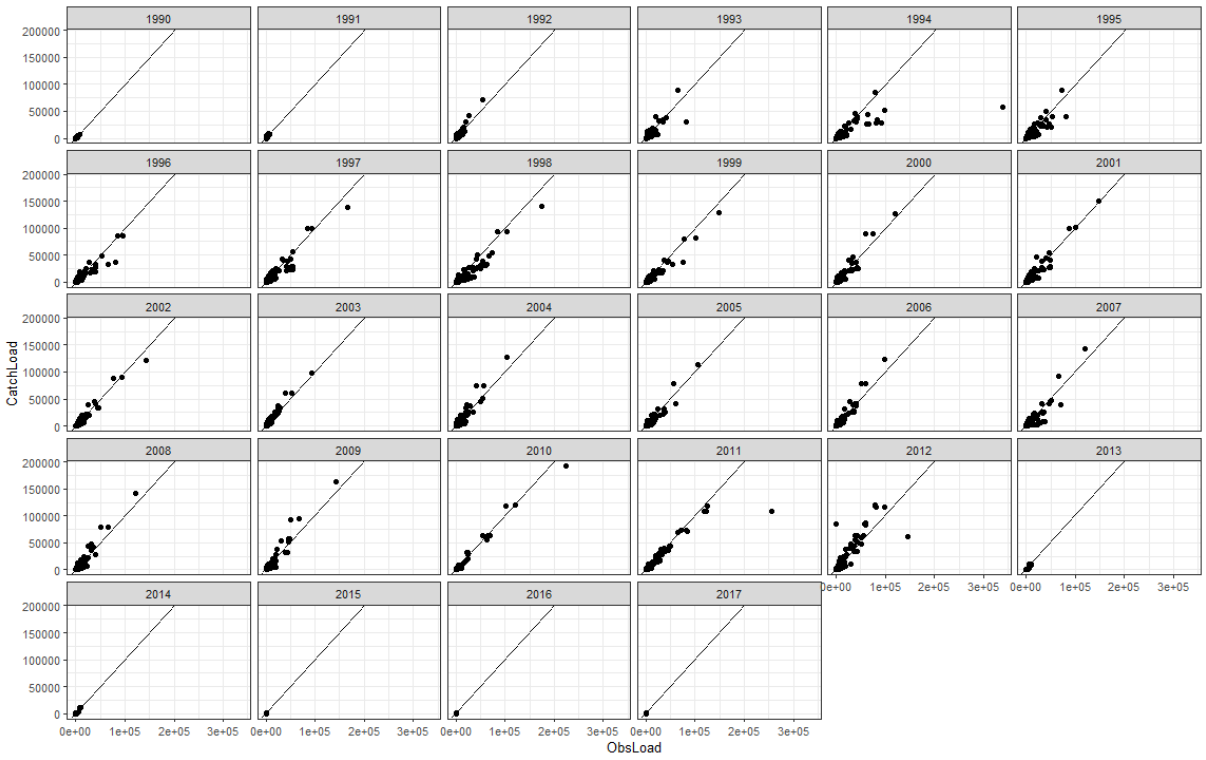

Figure A2.5. GREEN_TN calibration result in the combination of Black sea + Sea of Marmara (BLK). Year by year comparison of simulated (CatchLoad) versus observed loads (ObsLoad; all loads in t/y).

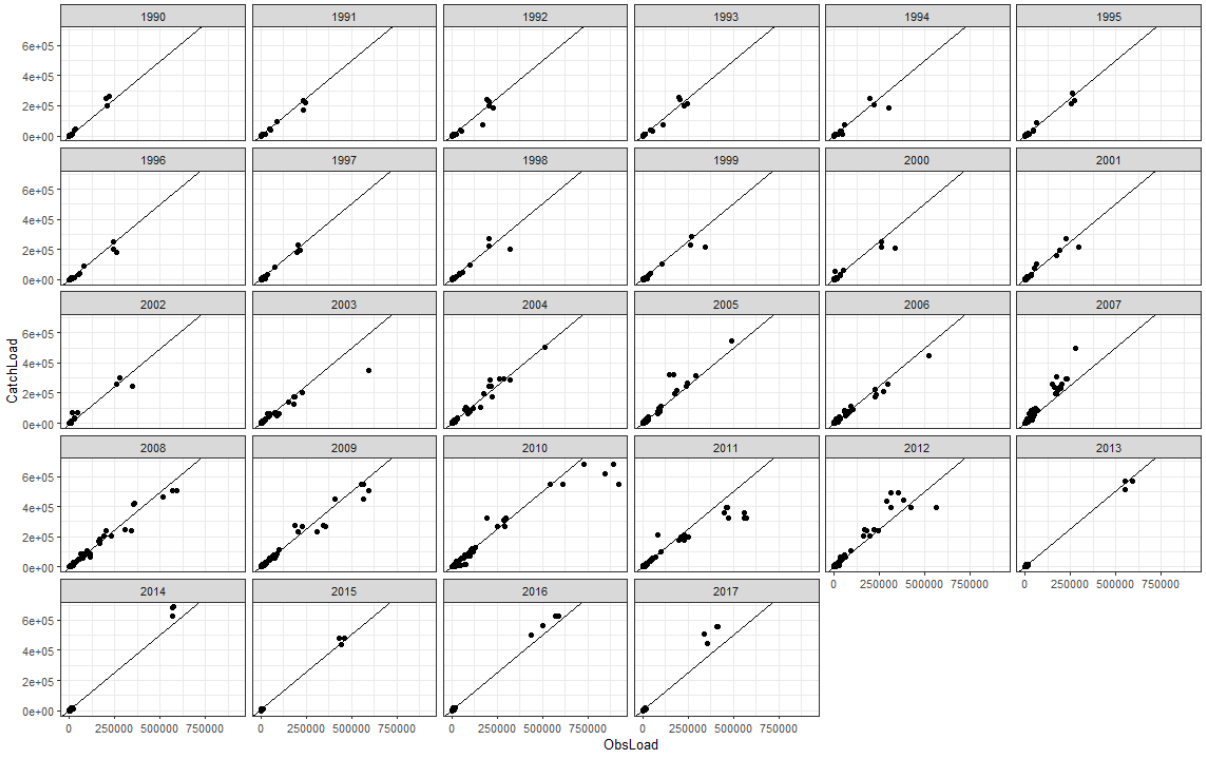

Figure A2.6. GREEN_TN calibration result in the Barents – Norwegian - White Seas combined region (BNM). Year by year comparison of simulated (CatchLoad) versus observed loads (ObsLoad; all loads in t/y).

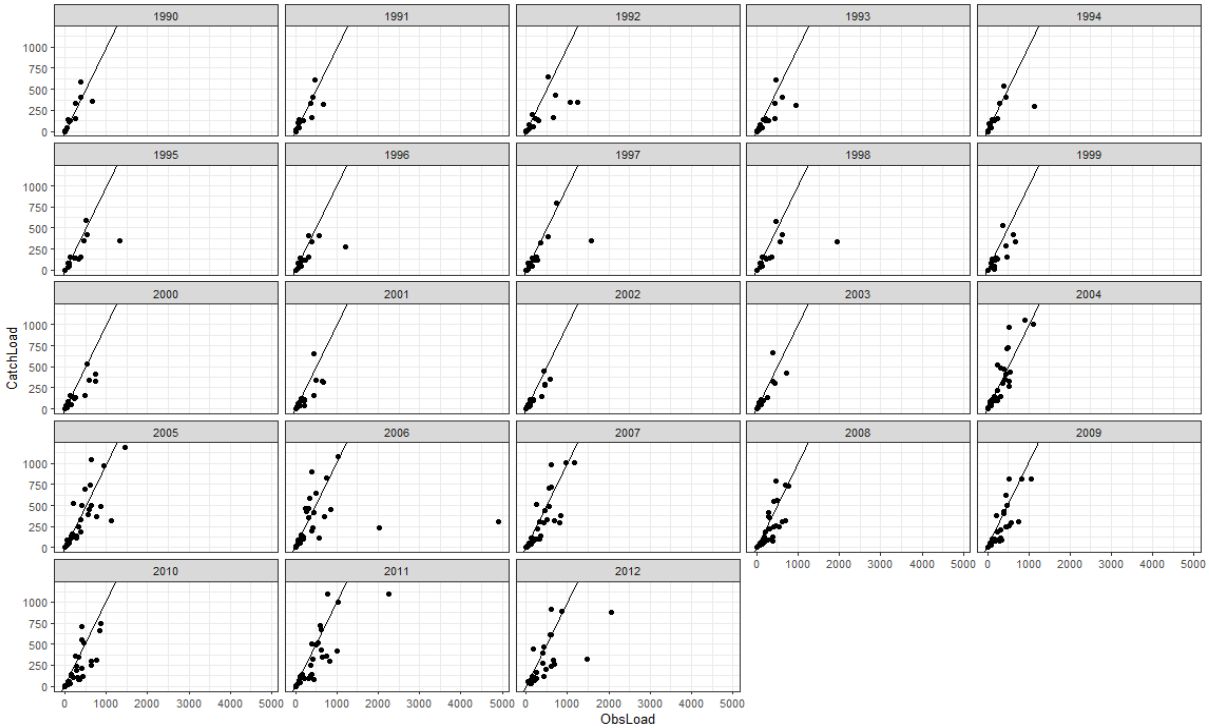

Figure A2.7. GREEN_TN calibration result in the Adriatic Sea (MAD). Year by year comparison of simulated (CatchLoad) versus observed loads (ObsLoad; all loads in t/y).

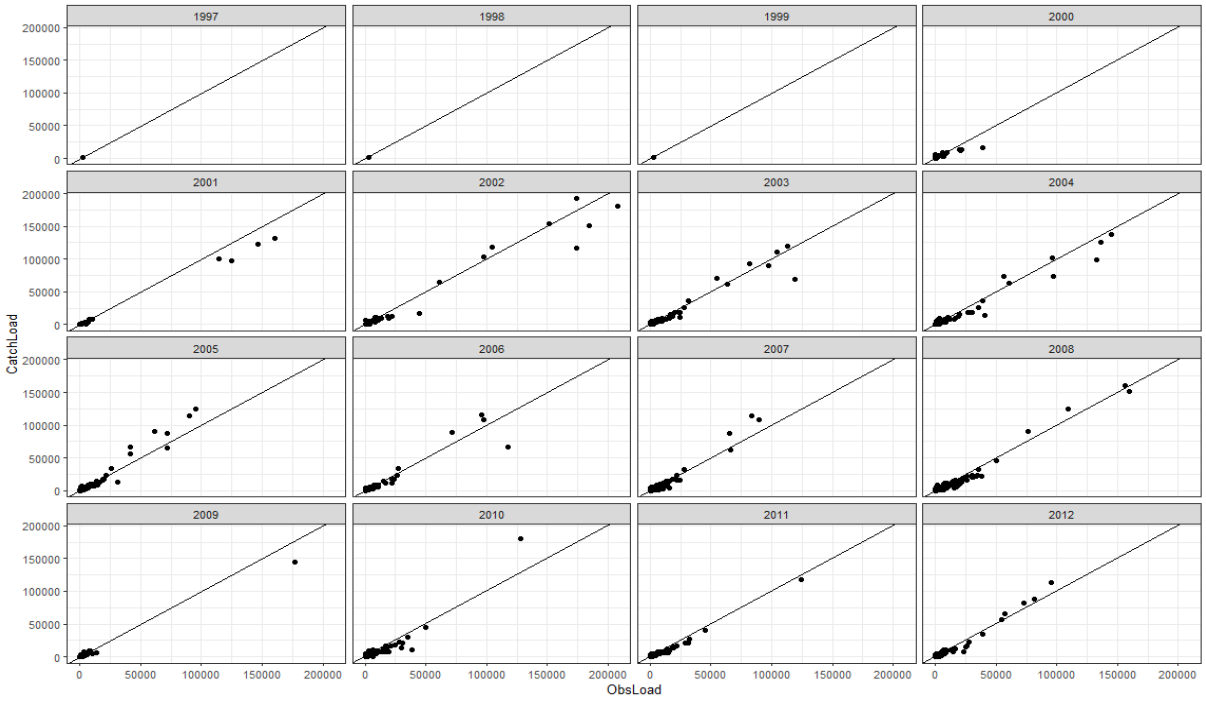

Figure A2.8. GREEN_TN calibration result in the Western Mediterranean Sea (MWE). Year by year comparison of simulated (CatchLoad) versus observed loads (ObsLoad; all loads in t/y).

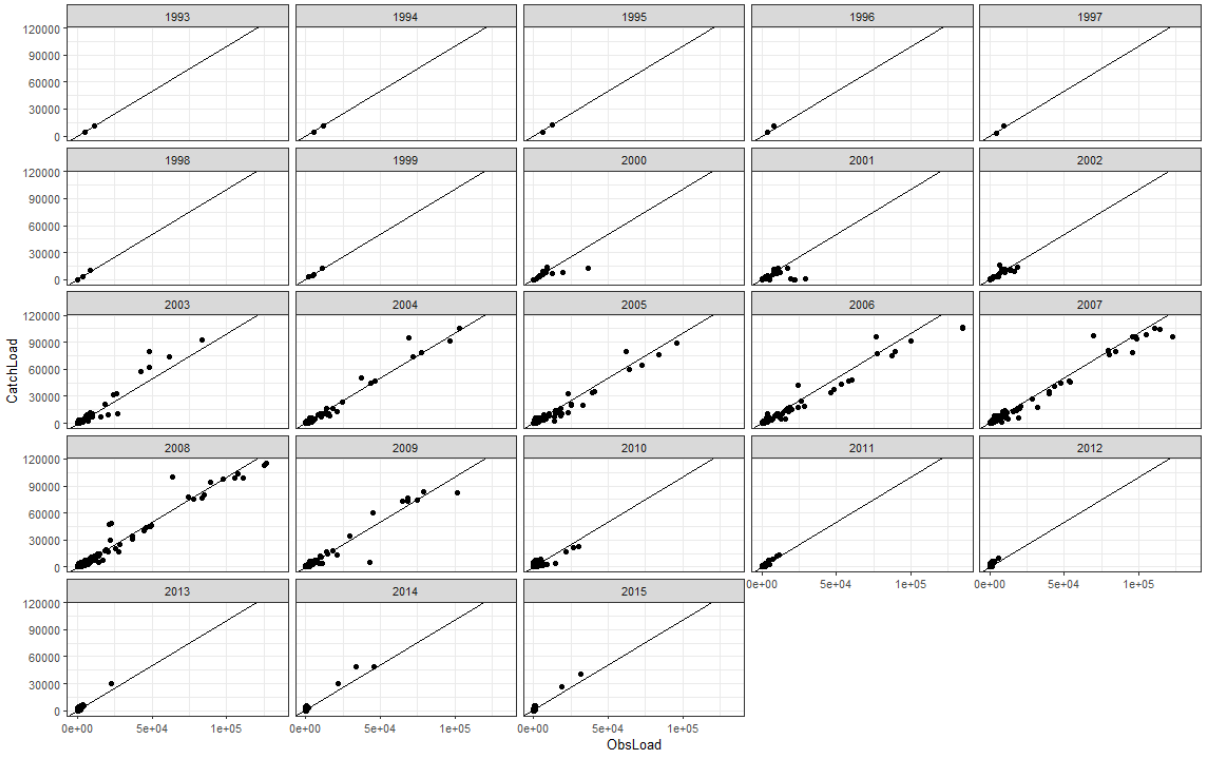

Figure A2.9. GREEN_TP calibration result in the Bay of Biscay/Iberian coast (ABI). Year by year comparison of simulated (CatchLoad) versus observed loads (ObsLoad; all loads in t/y).

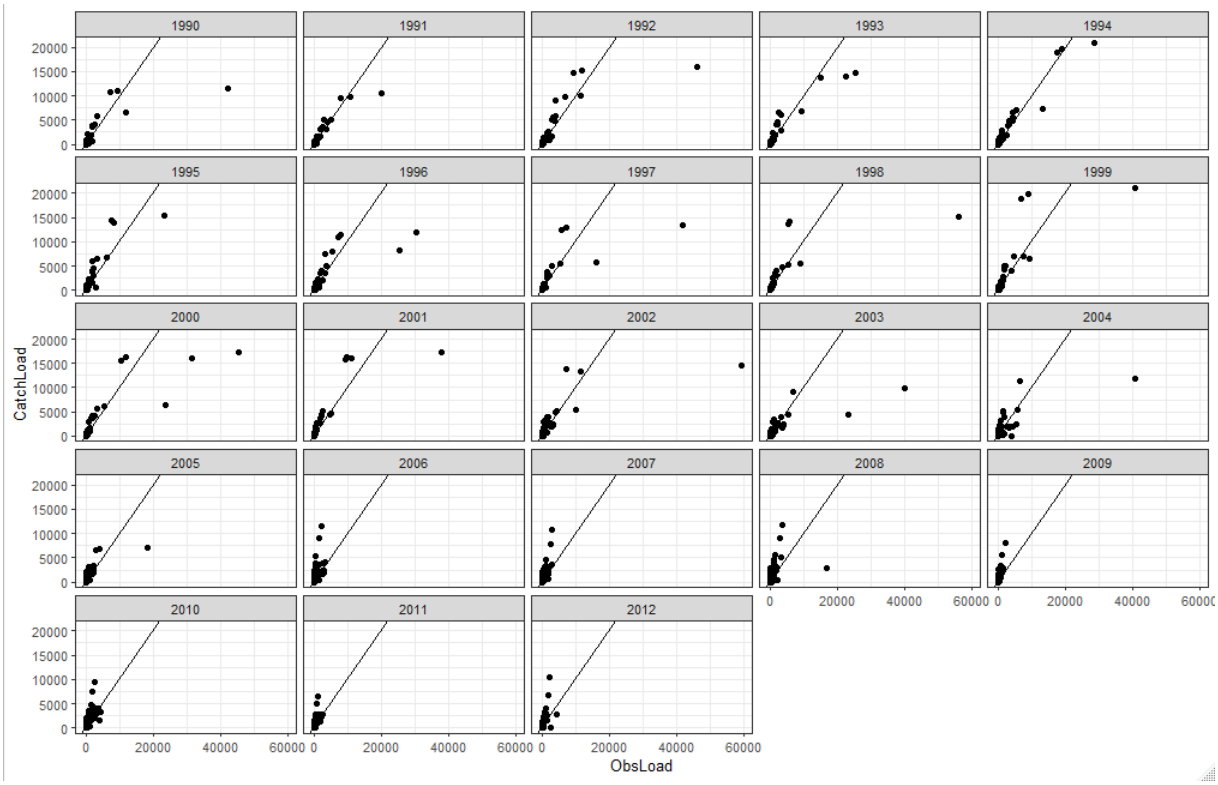

Figure A2.10. GREEN_TP calibration result in the Celtic Seas (ACS). Year by year comparison of simulated (CatchLoad) versus observed loads (ObsLoad; all loads in t/y).

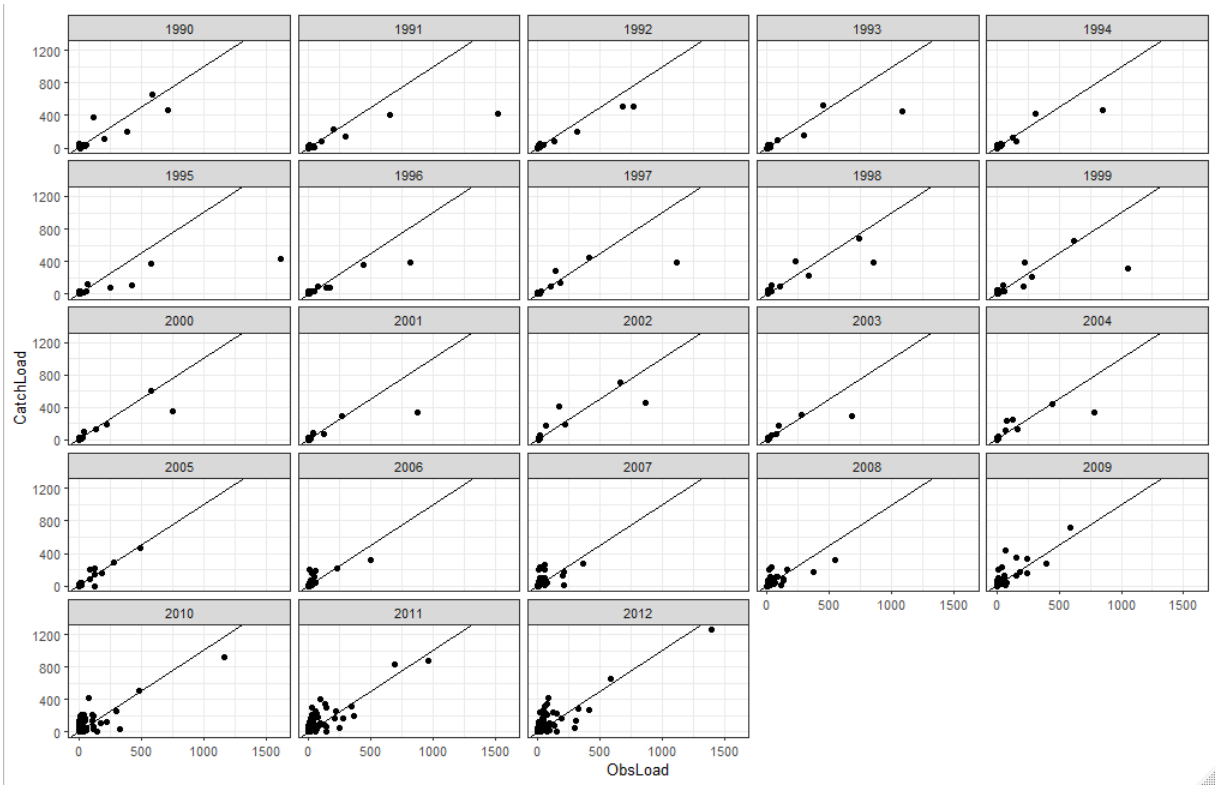

Figure A2.11. GREEN_TP calibration result in the Greater North Sea (ANS). Year by year comparison of simulated (CatchLoad) versus observed loads (ObsLoad; all loads in t/y).

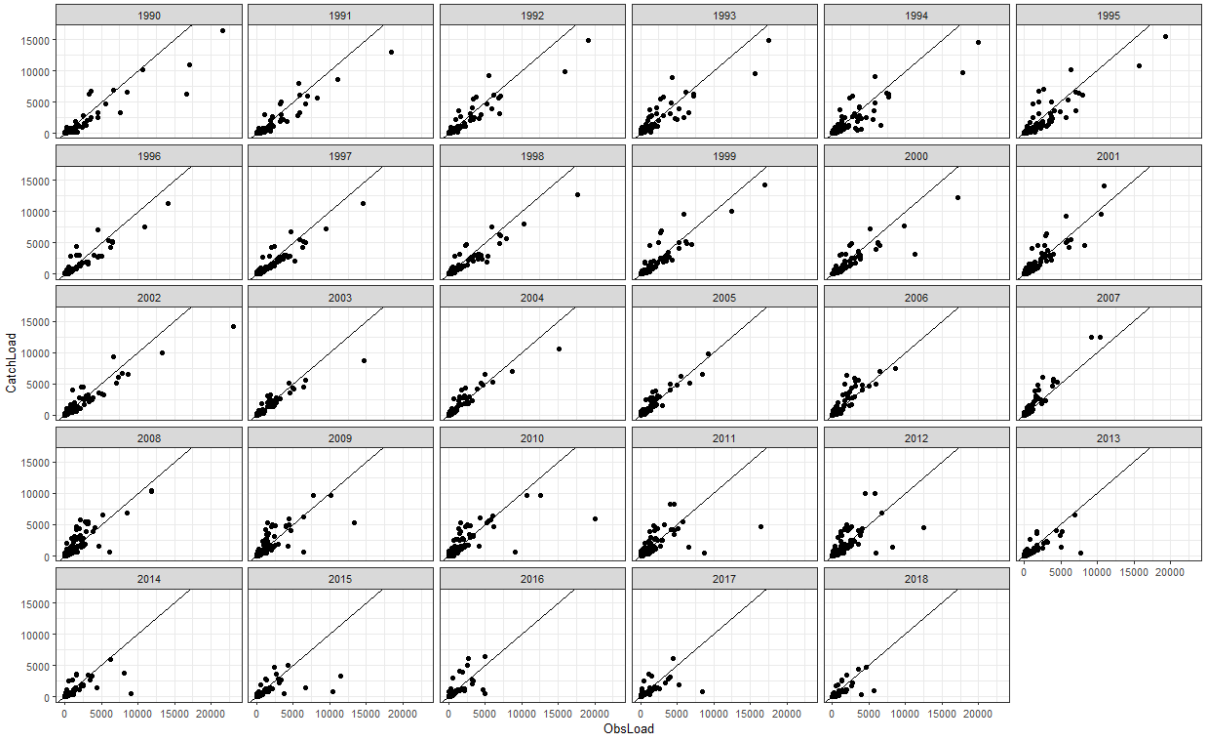

Figure A2.12. GREEN_TP calibration result in the Baltic Sea (BAL). Year by year comparison of simulated (CatchLoad) versus observed loads (ObsLoad; all loads in t/y).

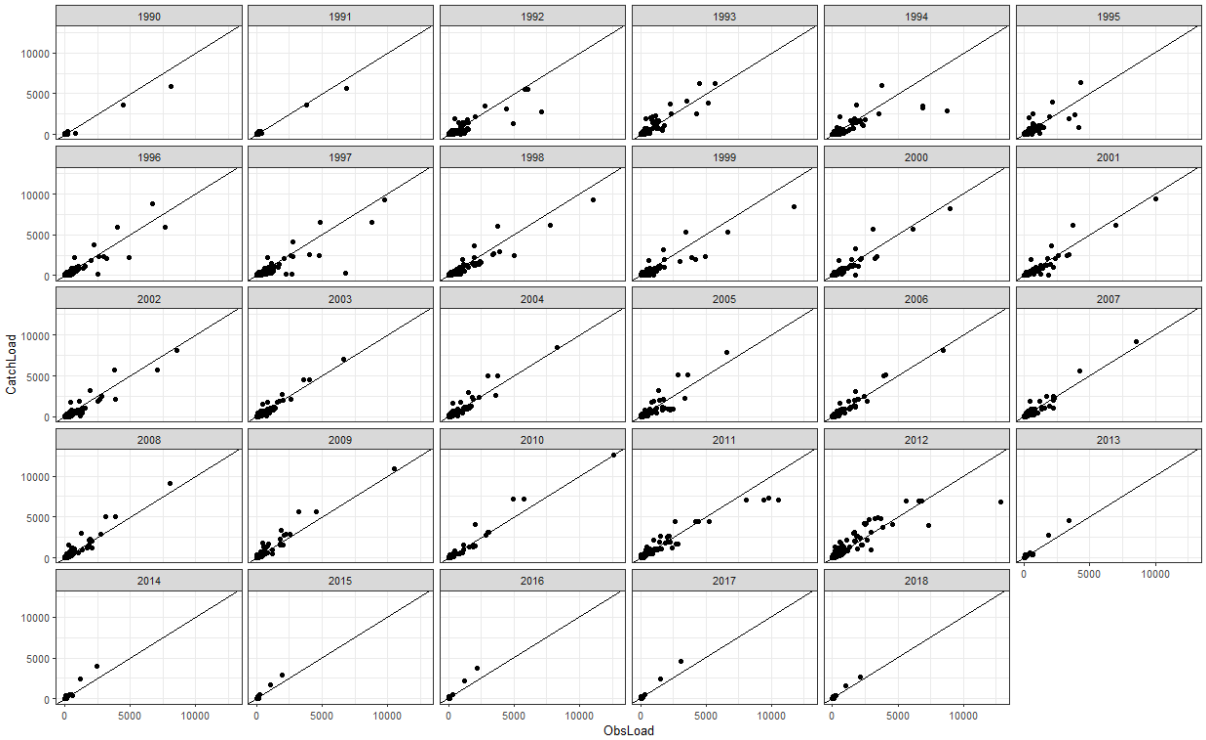

Figure A2.13. GREEN_TP calibration result in the combination of Black sea + Sea of Marmara (BLK). Year by year comparison of simulated (CatchLoad) versus observed loads (ObsLoad; all loads in t/y).

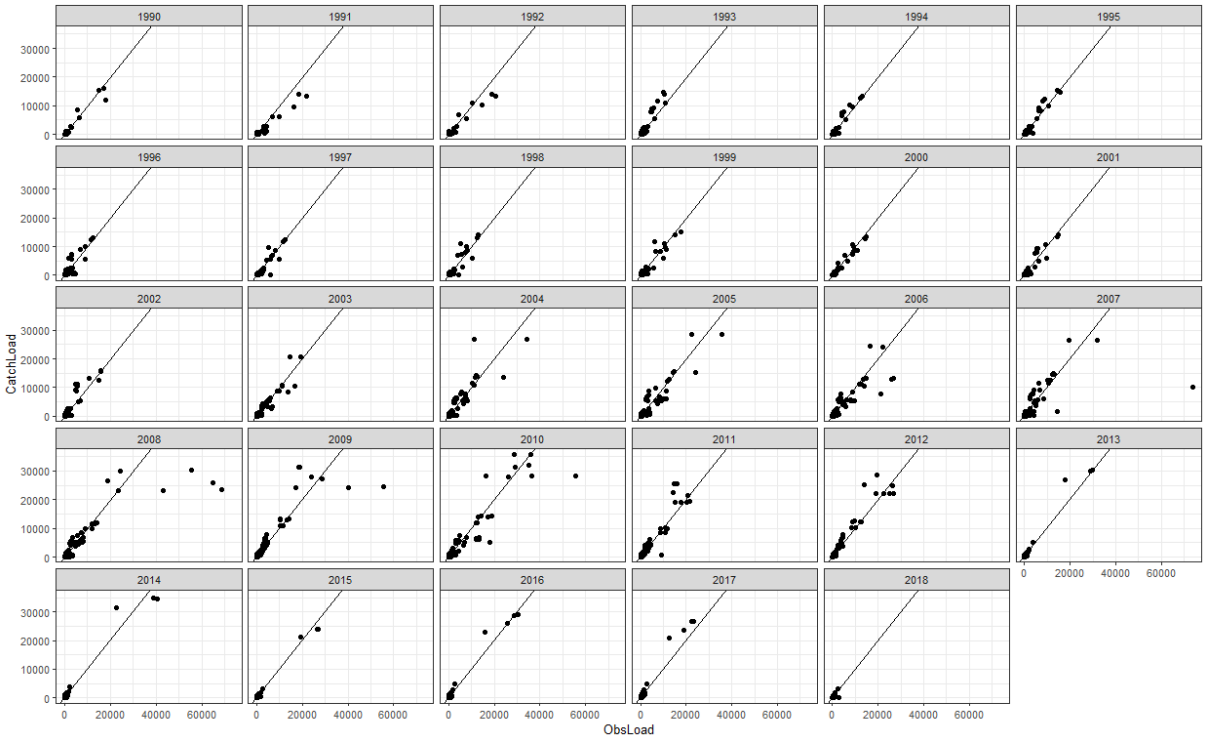

Figure A2.14. GREEN_TP calibration result in the Barents – Norwegian - White Seas combined region (BNM). Year by year comparison of simulated (CatchLoad) versus observed loads (ObsLoad; all loads in t/y).

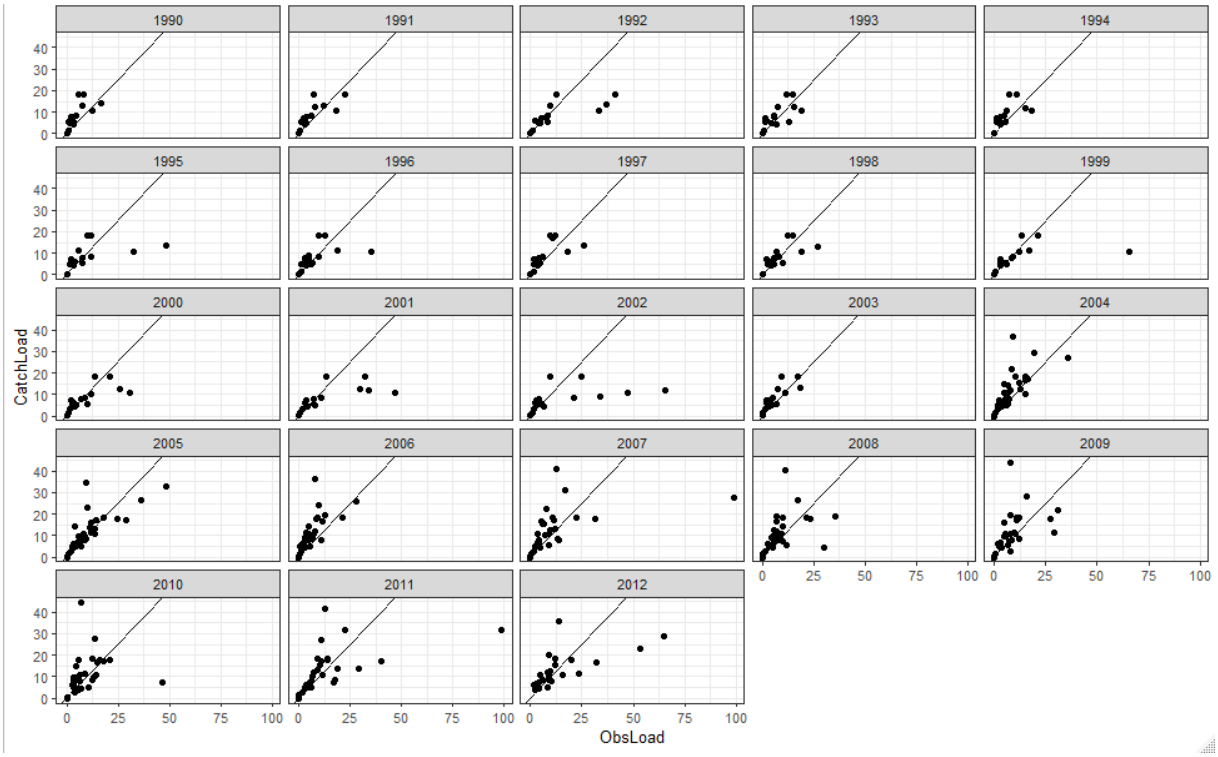

Figure A2.15. GREEN_TP calibration result in the Adriatic Sea (MAD). Year by year comparison of simulated (CatchLoad) versus observed loads (ObsLoad; all loads in t/y).

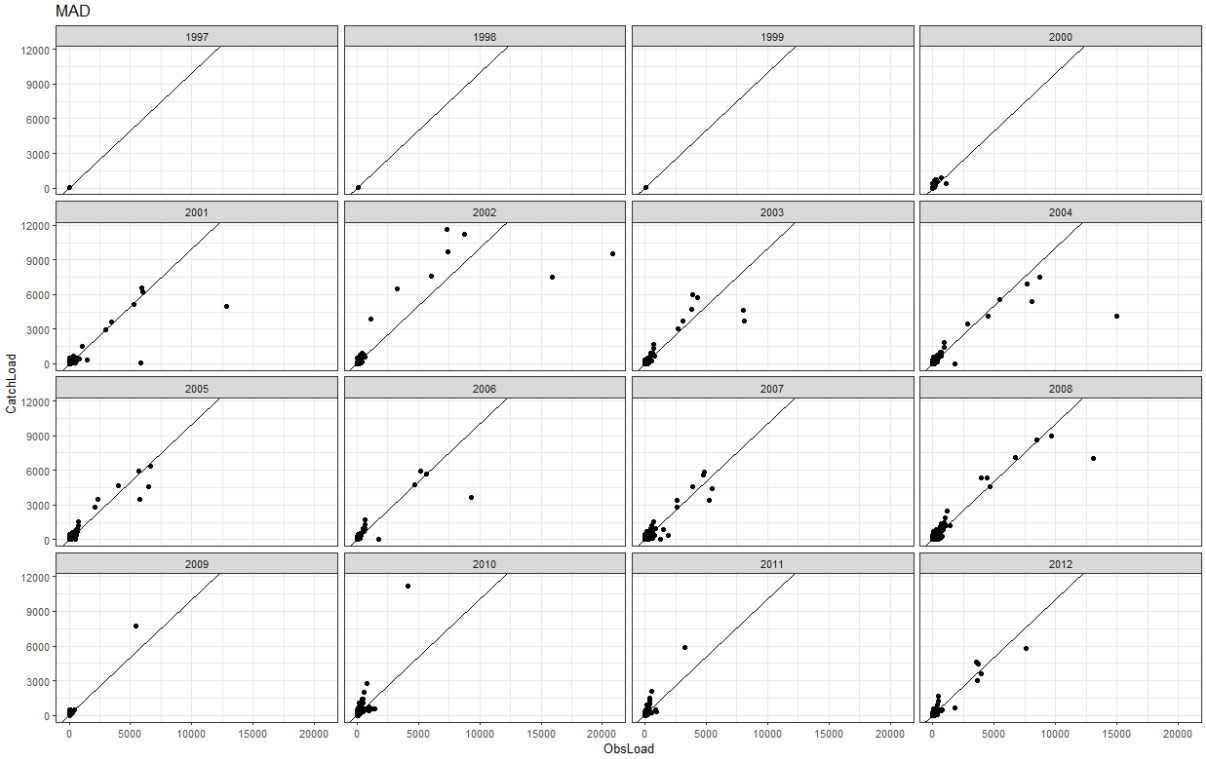

Figure A2.16. GREEN_TP calibration result in the Western Mediterranean Sea (MWE). Year by year comparison of simulated (CatchLoad) versus observed loads (ObsLoad; all loads in t/y).

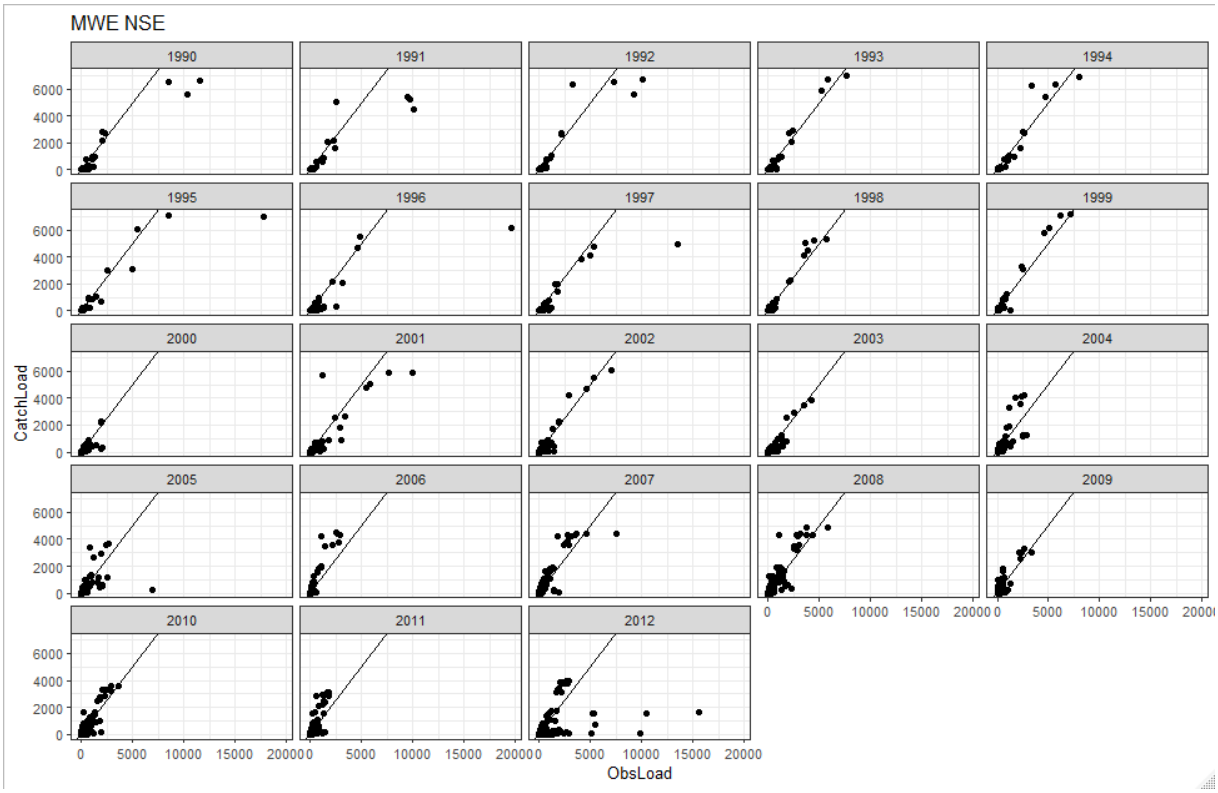

Annex 3. GREEN model – Inputs and outputs per marine region (1990–2018)

Figure A3.1 Nitrogen inputs to surface waters per marine region. Marine Regions: ABI=Bay of Biscay & Iberian Coast; ACS=Celtic Seas; ANS=Greater North Sea; BAL=Baltic Sea; BLK=Black Sea & Sea of Marmara; MAD=Adriatic Sea; MAL=Aegean Levantine Mediterranean Sea; MIC=Ionian Sea and Central Mediterranean Sea; MWE=Western Mediterranean Sea

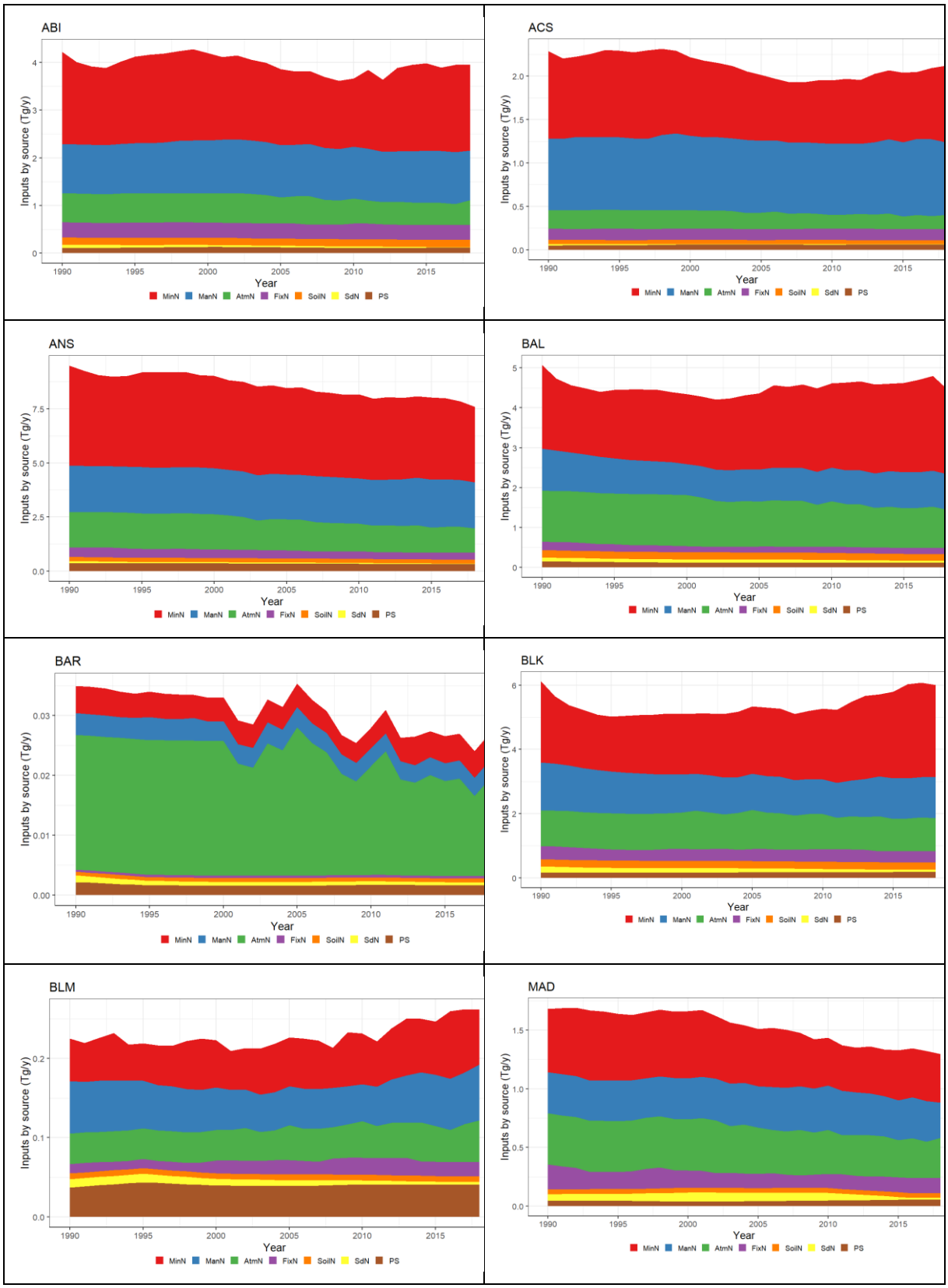

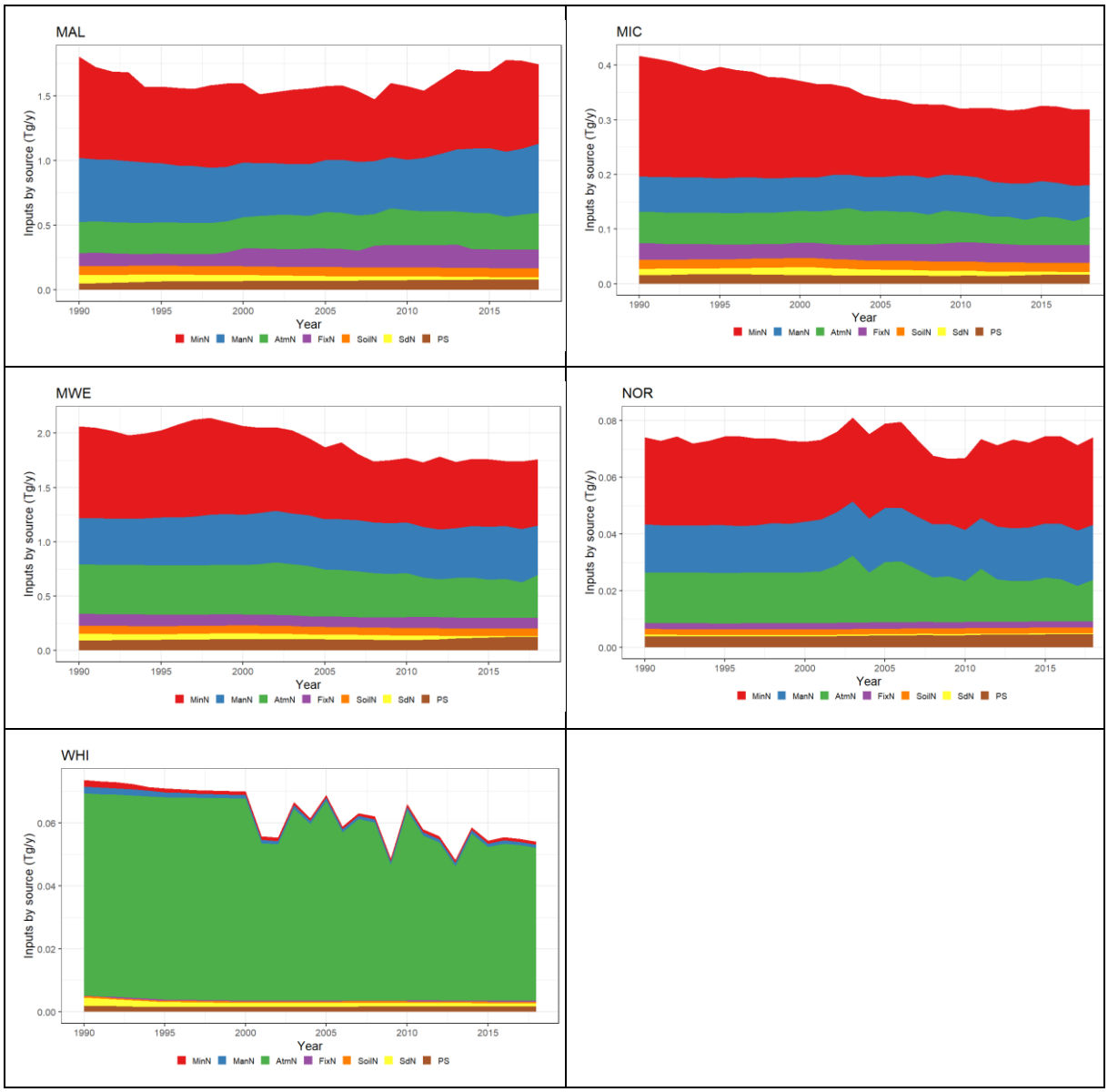

Figure A3.2 Phosphorus inputs to surface waters per marine region. Marine Regions: ABI=Bay of Biscay & Iberian Coast; ACS=Celtic Seas; ANS=Greater North Sea; BAL=Baltic Sea; BLK=Black Sea & Sea of Marmara; MAD=Adriatic Sea; MAL=Aegean Levantine Mediterranean Sea; MIC=Ionian Sea and Central Mediterranean Sea; MWE=Western Mediterranean Sea

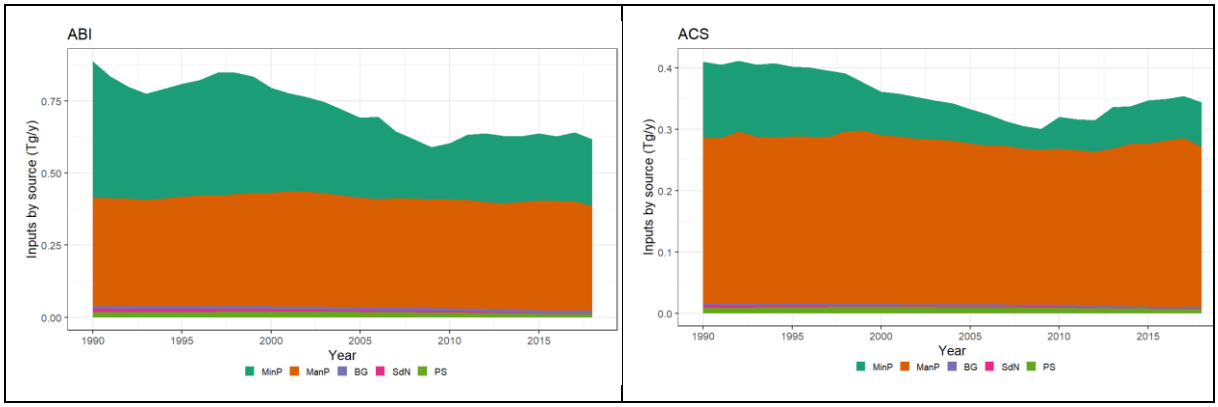

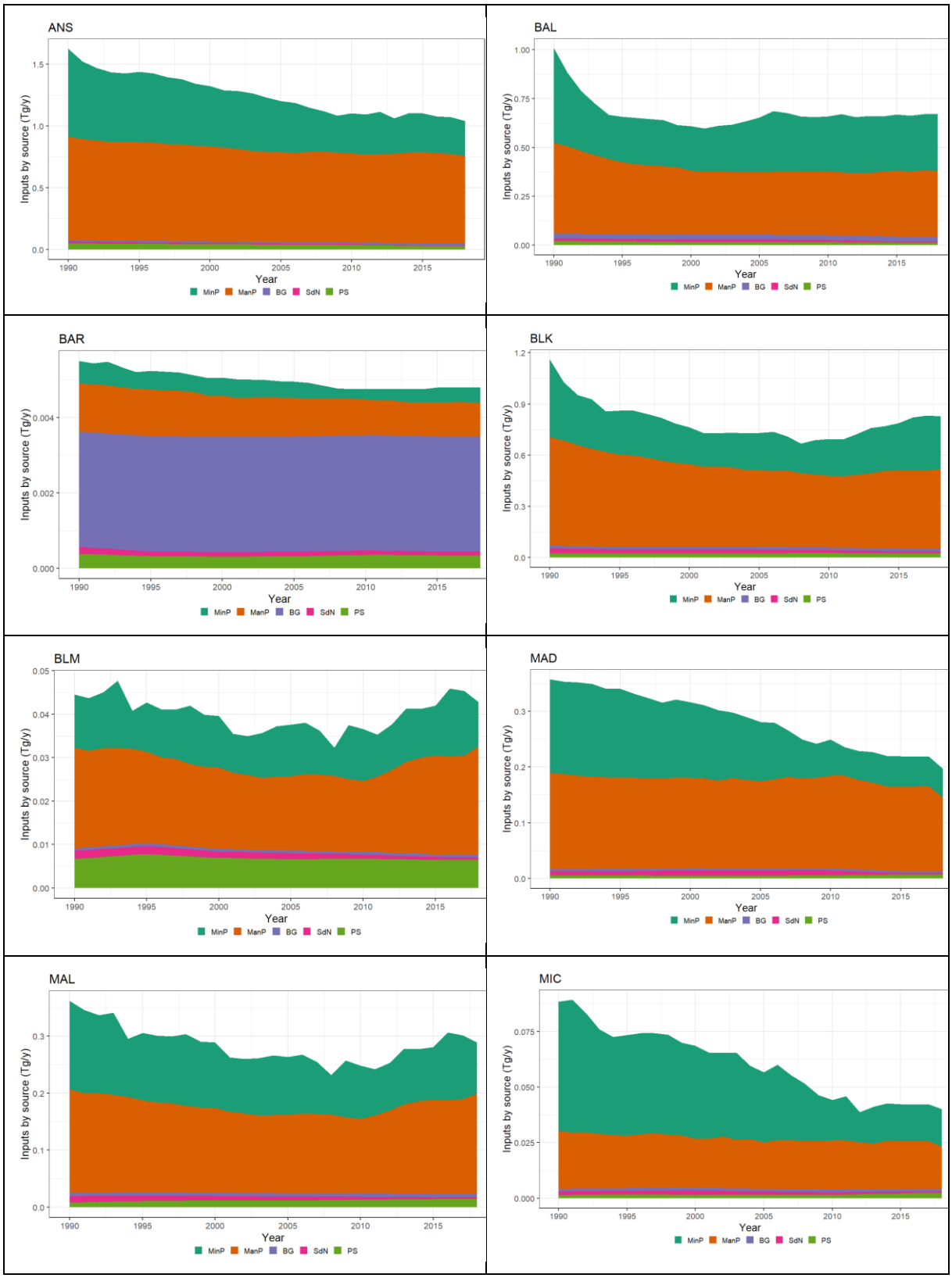
ANS
BAL
BAR
BLK
BLM
MAD
MAL
MIC
Inputs by source (Tg/y)
Year
MinP ManP BG SdN PS

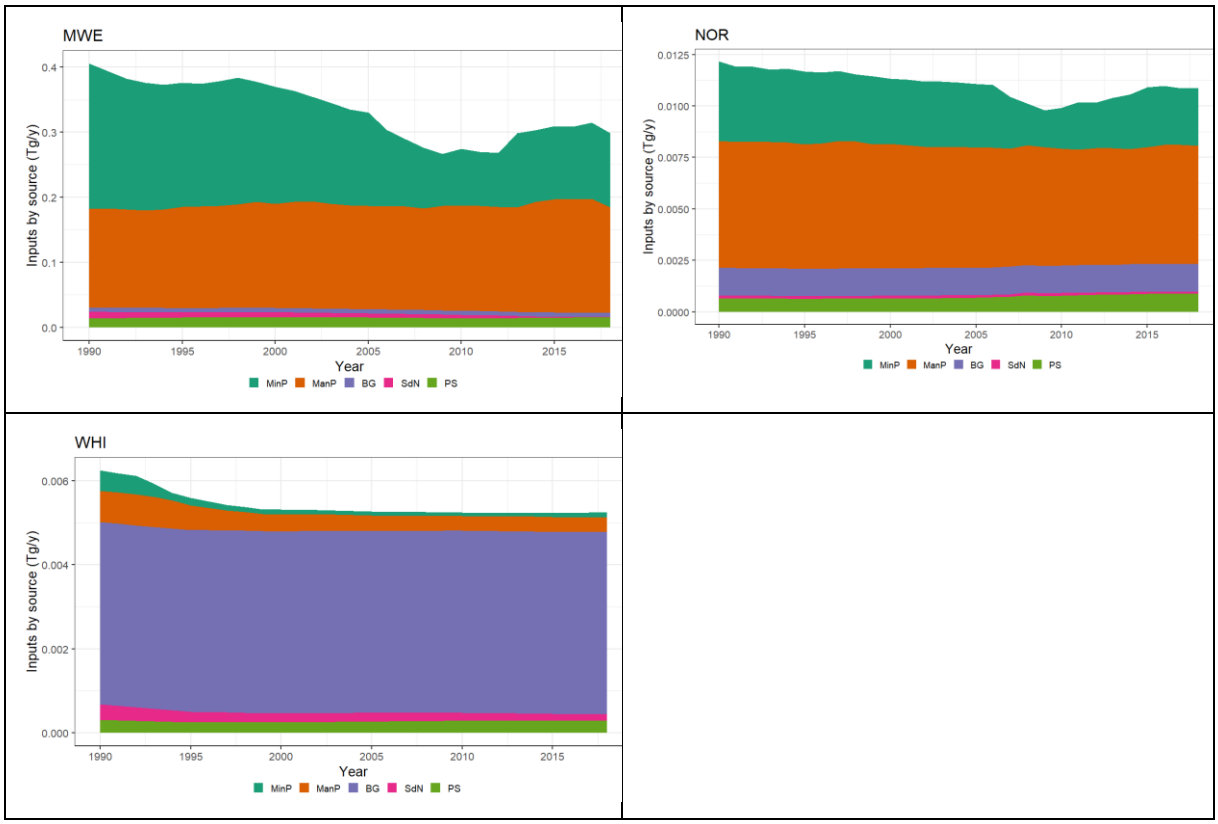

Figure A3.3 Nitrogen outputs to marine regions. Marine Regions: ABI=Bay of Biscay & Iberian Coast; ACS=Celtic Seas; ANS=Greater North Sea; BAL=Baltic Sea; BLK=Black Sea & Sea of Marmara; MAD=Adriatic Sea; MAL=Aegean Levantine Mediterranean Sea; MIC=Ionian Sea and Central Mediterranean Sea; MWE=Western Mediterranean Sea

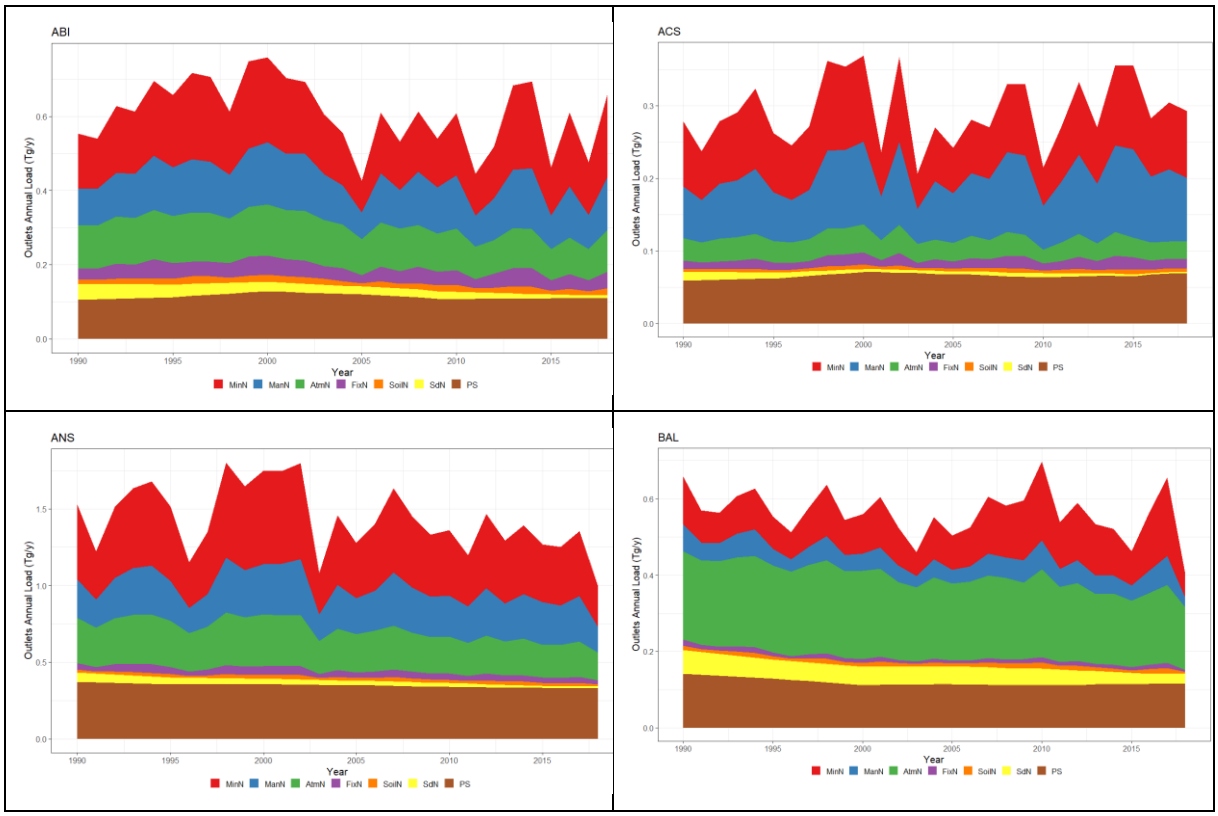

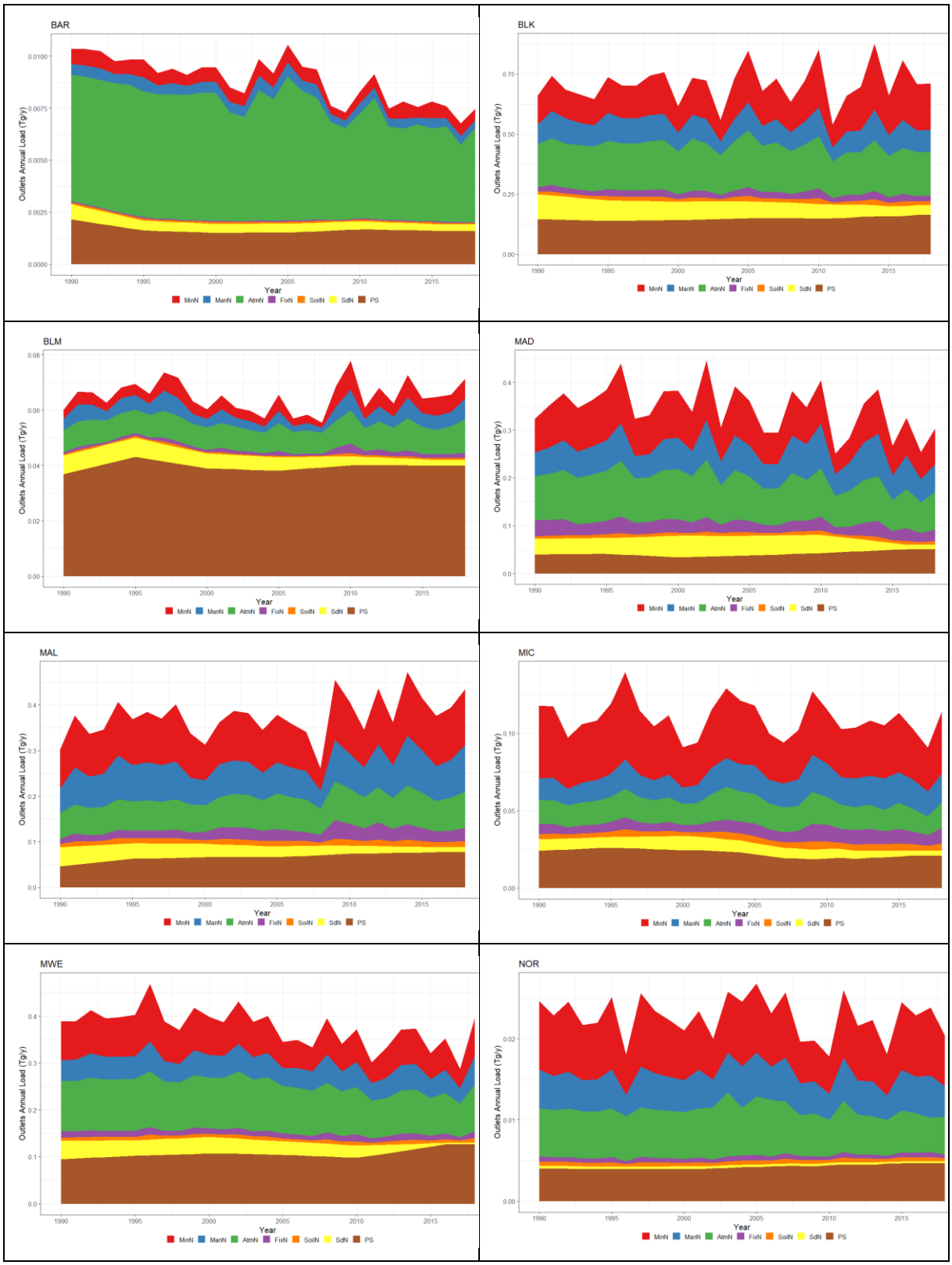
BAR
BLK
BLM
MAD
MAL
MIC
MWE
NOR
Outlets Annual Load (Tg/y)
Year
MinN ManN AtmN FixN SoilN SdN PS

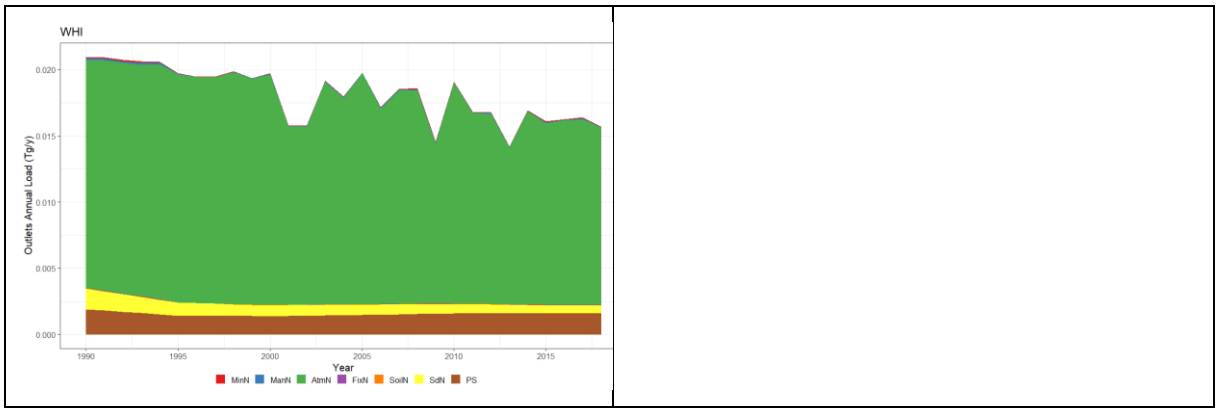

Figure A3.4 Phosphorus outputs to marine regions. Marine Regions: ABI=Bay of Biscay & Iberian Coast; ACS=Celtic Seas; ANS=Greater North Sea; BAL=Baltic Sea; BLK=Black Sea & Sea of Marmara; MAD=Adriatic Sea; MAL=Aegean Levantine Mediterranean Sea; MIC=Ionian Sea and Central Mediterranean Sea; MWE=Western Mediterranean Sea

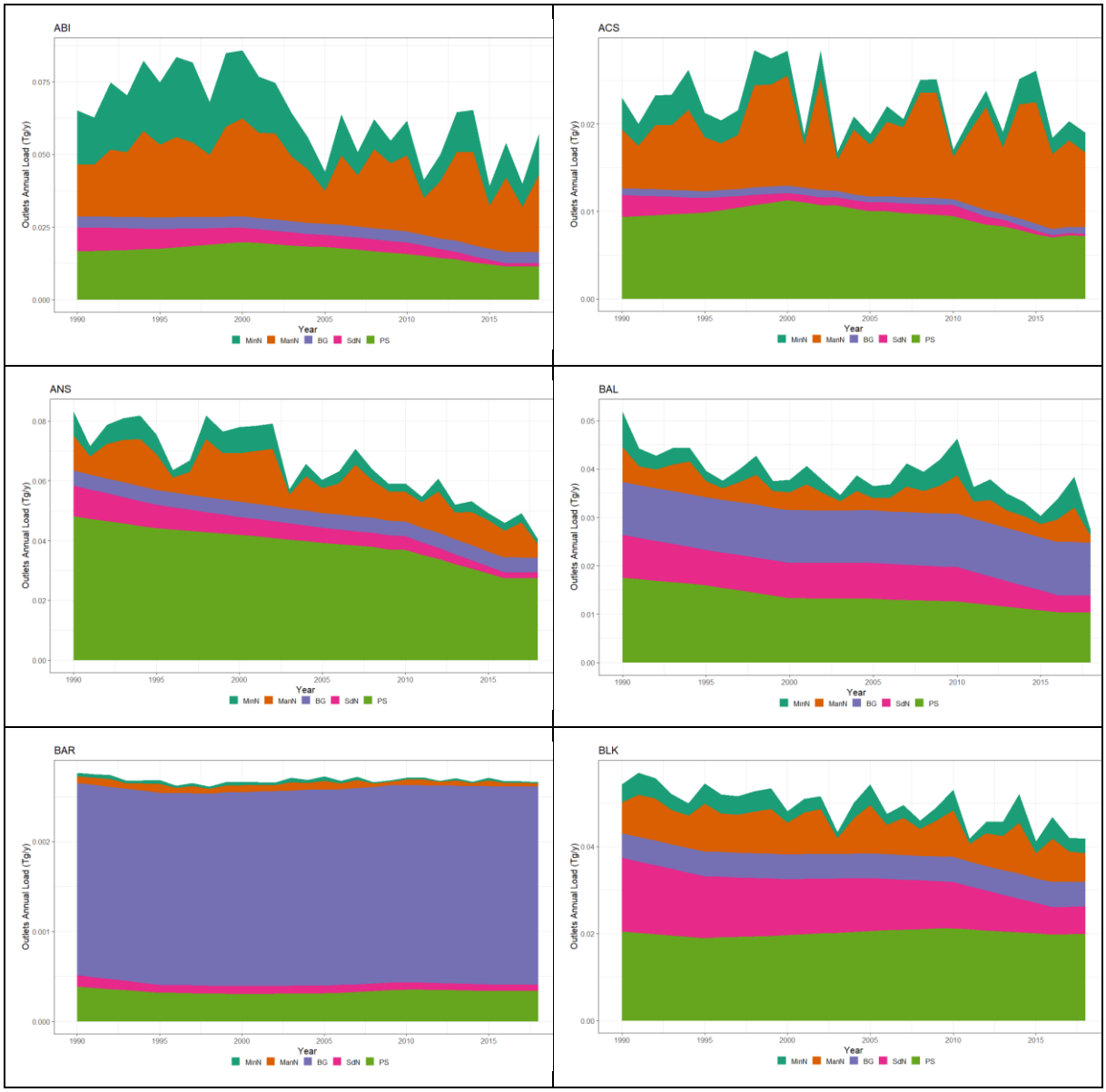

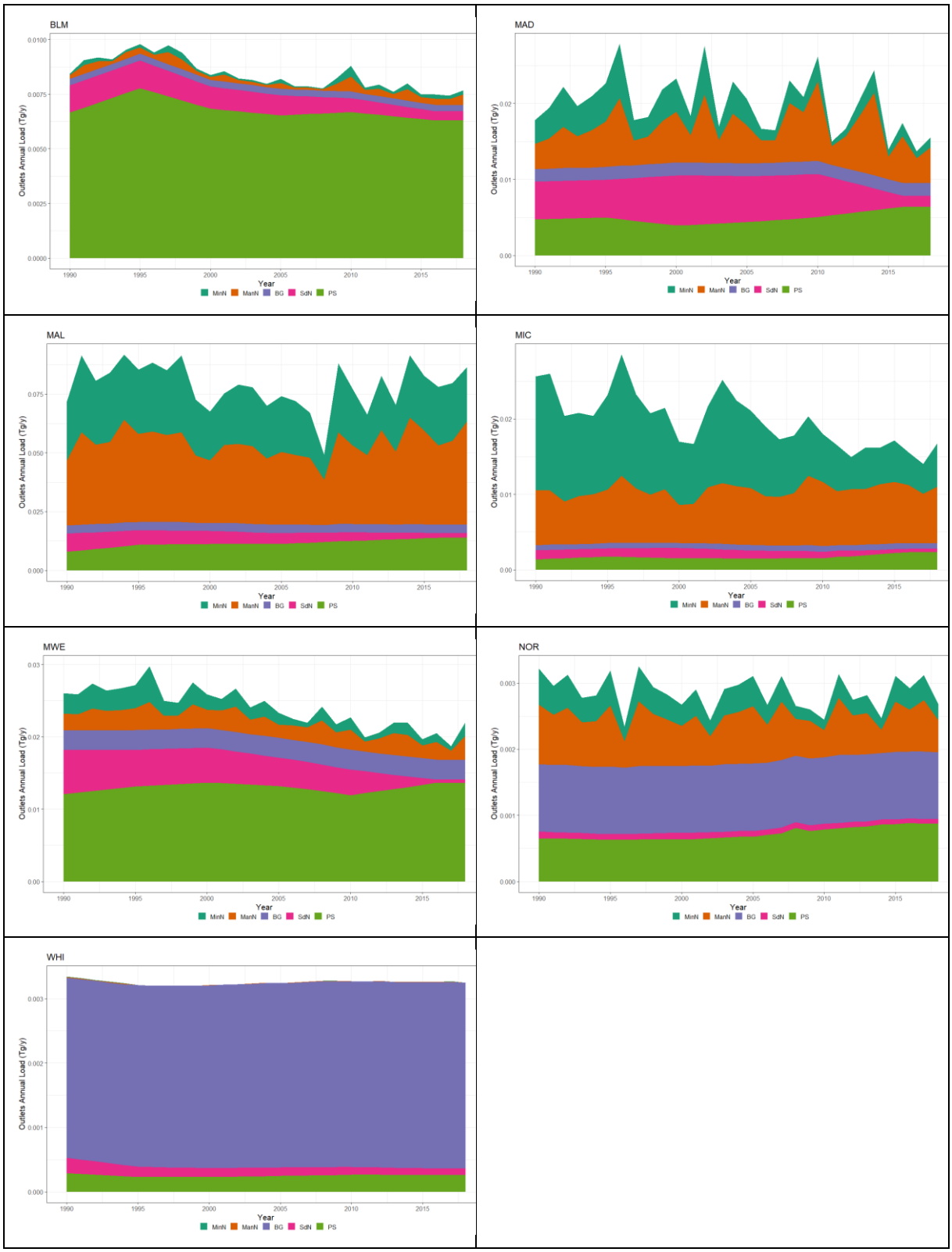
BLM
MAD
MAL
MIC
MWE
NOR
WHI
Outlets Annual Load (Tg/y)
Year
MinN
ManN
BG
SdN
PS

Annex 4. SWAT model - Summary of model inputs

Variable	Description	Source
Subbasins and rivers	Grid-cells and routing river networks	Anna Malagó et al. (2019) A. Malagó et al. (2019) Olivera et al. (2002)
Lakes	HydroLakes database	Messager et al. (2016)
Digital Elevation Model (DEM)	GTOPO30 rescaled at 100x100 m of resolution	LP DAAC (2004)
Landuse/Landcover	GLOBCOVER 2009 map Spatial Production Allocation Model (SPAM)	Arino et al. (2012) You et al. (2014)
Landuse change	Trend analysis of landuse changes	FAOSTAT (2021) Bouraoui and Malagó (2022)
Precipitation	Daily time series from MSWEP dataset at 0.1 degrees resolution. Period 1/1/1979 to 31/12/2019.	Beck et al. (2017)
Other atmospheric forcing variables (temperature, solar radiation, wind speed and relative humidity)	Daily time series from ERA-Interim dataset at 0.1 degrees resolution. Period 1/1/1979 to 31/12/2019.	Dee et al. (2011)
Soils	Soil type and characteristics from the Harmonized World Soil Database	FAO/IIASA/ISRIC/ISSCAS/JRC (2012)
Atmospheric deposition	ISIMIP dataset	Lamarque et al. (2013b, 2013a) Tian et al. (2018)
Mineral fertilizers	Annual time series of N and P mineral fertilizers (kg/ha) in the period 1979-2019 at country level and every 5 years in the SWAT model	IFASTAT (2016) FAOSTAT (2021b)
Manure	Annual time series of N and P manure (kg/ha) in the period 1979-2019 at country level and every 5 years in the SWAT model	Malagò and Bouraoui (2021) GeoNetwork (2007) FAOSTAT (2021c) Bouwman et al. (1997) FAOSTAT (2021d) Sheldrick et al. (2003)
Irrigation quantity and sources (surface, groundwater, lakes)	Annual time series of irrigation by crop in the	AQUASTAT database (2021)

	period 1979-2019 at country level and every 5 years in the SWAT model Definition of grid cell irrigations sources from groundwater, surface water and lakes	Puy et al. (2021) GMIA (2021)
Nitrogen in the aquifer	Predicted nitrate concentrations in the shallow aquifer using a regression analysis based on Nitrates Directive dataset of the reporting period 2012-2015	Bouraoui and Malagó (2020)
Point Sources nutrient emissions	Annual time series of N and P nutrient emissions from point sources in the period 1979-2019	Procedure explained in Malagò and Bouraoui (2021) -For reconstruction of urban and rural population: GHSL datasets (Dijkstra and Poelman, 2014) at resolution of 1 km (Mollweide projection) FAOSTAT urban and rural population dataset for the period 1979-2018 (FAOSTAT, 2021e) CShapes dataset (Schvitz et al., 2021) -For reconstruction of N and P emissions: Jönsson and Vinnerås (2003) Herridge et al. (2008) human and vegetable protein intake taken from the FAO database -For reconstruction of P emissions from detergents: RPA (2006) Schreiber et al. (2003) Kundu *et al* (2015) Chen and Graedel (2016) -For reconstruction of industrial emissions: Morée *et al* (2013) -For reconstruction of connected and unconnected population rates: EUROSTAT (2021) REFIT (2019)

		JMP (2019) GDP (2021)
Water withdrawal by sectors	Annual time series of Water withdrawal by sectors in the period 1979-2019. In the SWAT model the municipal and industrial abstractions were introduced as long term mean of monthly abstraction from deep aquifer	AQUASTAT database (2021) GDP (2021)

GETTING IN TOUCH WITH THE EU

In person

All over the European Union there are hundreds of Europe Direct centres. You can find the address of the centre nearest you online (european-union.europa.eu/contact-eu/meet-us_en).

On the phone or in writing

Europe Direct is a service that answers your questions about the European Union. You can contact this service:

— by freephone: 00 800 6 7 8 9 10 11 (certain operators may charge for these calls),

— at the following standard number: +32 22999696,

— via the following form: european-union.europa.eu/contact-eu/write-us_en.

FINDING INFORMATION ABOUT THE EU

Online

Information about the European Union in all the official languages of the EU is available on the Europa website (european-union.europa.eu).

EU publications

You can view or order EU publications at op.europa.eu/en/publications. Multiple copies of free publications can be obtained by contacting Europe Direct or your local documentation centre (european-union.europa.eu/contact-eu/meet-us_en).

EU law and related documents

For access to legal information from the EU, including all EU law since 1951 in all the official language versions, go to EUR-Lex (eur-lex.europa.eu).

Open data from the EU

The portal data.europa.eu provides access to open datasets from the EU institutions, bodies and agencies. These can be downloaded and reused for free, for both commercial and non-commercial purposes. The portal also provides access to a wealth of datasets from European countries.

The European Commission's science and knowledge service

Joint Research Centre

JRC Mission

As the science and knowledge service of the European Commission, the Joint Research Centre's mission is to support EU policies with independent evidence throughout the whole policy cycle.

EU Science Hub
joint-research-centre.ec.europa.eu

 @EU_ScienceHub

 EU Science Hub - Joint Research Centre

 EU Science, Research and Innovation

 EU Science Hub

 EU Science

Publications Office
of the European Union